Data-Aided Channel Estimation and Monitoring for Coherent Optical Systems

Cuong Cao Do

B.Sc.E.

Submitted in Total Fulfillment of the Requirements of the Degree of

Doctor of Philosophy

July, 2014

Department of Electrical and Electronic Engineering

The University of Melbourne

Victoria 3010

Australia

To my parents

Abstract

The growing demand for high bandwidth internet applications has led to the continuous search for communication systems with higher transport capacity. New generation of optical fibre technology has been able to keep up with this demand by employing coherent detection for higher transmission efficiency in optical networks. Coherent receiver technology enables data transmission with higher efficiency compared to traditional direct detection receiver with on-off keying (OOK) by employing advanced modulation formats such as coherent optical (CO) single carrier (SC) with frequency domain equalisation (FDE) and CO orthogonal frequency division multiplexing (OFDM). The advent of coherent detection has motivated the work in this thesis to develop new transmission techniques and designs for CO networks.

This thesis explores the design of new data-aided (DA) channel estimation (CE) techniques for CO networks, which is a critical component in the digital signal processing (DSP) procedure of optical networks employing coherent receivers. A new technique for chromatic dispersion (CD) estimation is proposed and demonstrated. The technique utilises a block of training sequences (TSs) for estimation of system CD, which is required for subsequent equalisation in CO networks. A new technique for optical signal-to-noise ratio (OSNR) estimation is also demonstrated. The technique also utilises TSs and is designed as an integrated part for CO communication systems employing TSs while achieving fast and accurate estimation performance. Performance of systems employing the same type of TSs for equalisation is also demonstrated. The results indicate a relationship between system performance and overhead ratio. A new frame synchronisation method using TSs is proposed and demonstrated to be able to achieve good synchronisation performance.

This thesis also investigates new channel parameter estimation techniques based on coherent receivers with reduced bandwidth and sampling speed for distributed performance monitoring in optical networks. A new method employing TSs for OSNR

estimation with low-bandwidth coherent receivers is proposed and demonstrated for CO-SC systems. Two methods for estimation of differential group delay (DGD) namely TS-assisted and Stokes vectors blind estimation are demonstrated with good estimation accuracy. While TS-assisted method retains compatibility with both CO-OFDM and CO-SC, the low-bandwidth requirement of the receivers slightly reduces the accuracy of the method. Compared to TS-assisted method, Stokes vectors method is only compatible with CO-OFDM. However, by exploiting specific features of the CO-OFDM format, the method does not require any TSs and provides accurate estimation of DGD for CO-OFDM transmission.

Declaration

This is to certify that:

- The thesis comprises only my original work towards the degree of Doctor of Philosophy except where indicated in the Preface.
- Due acknowledgement has been made in the text to all other material used.
- The thesis is fewer than 100,000 words in length, exclusive of tables, maps, bibliographies and appendices.

Cuong Cao Do

Acknowledgments

I would like to express my deepest gratitude to my principal supervisor, Assoc. Prof. An Vu Tran, for his guidance and encouragement throughout the course of my PhD study. His dedication to excellence and careful attention to details has inspired me throughout this work and I feel very honoured to have had the opportunity to study under his supervision. I would also like to thank Prof. Thas Nirmalathas for his co-supervision during the last year of my candidature. His guidance and encouragement in the final stage of my study have been invaluable.

My sincere thanks to Mr. Don Hewitt for his assistance and discussion on the subject of TS design and SC systems. I wish to thank Mr. Trevor Anderson for the constructive and fruitful discussion on SC systems and the Stokes vectors method. I am grateful to Dr. Simin Chen for his assistance in the study of estimation methods for low-bandwidth receiver. I would like to thank Prof. Arthur Lowery and Dr. Liang Du for supports and guidance in different aspects of the experimental studies.

My thanks go to all staff and students of NICTA Victoria Research Lab and the Photonics Research Lab for providing a very friendly and entertaining working environment. I would also like to thank the Centre for Ultrahigh bandwidth Devices for Optical Systems at Monash University for providing equipments for some of my experimental studies.

On a personal level, I am forever indebted to my parents, Mr. Do Quang Canh and Mrs. Cao Thi Hong Huyen, for their continual understanding and support throughout all my years of study. My special thanks to all of my friends: Ha Nguyen, Chen Zhu, Qi Guo, John Li, and Thanh Nguyen, for their friendship, encouragement, and invaluable support during the hardest times of my study.

Table of Contents

1 Introduction

1.1 Coherent Optical Networks

The great demand for internet-based services has led to the search for higher capacity optical transport networks. More and more internet-based applications are being developed and thus require an upgrade in communication networks. While optical fibre networks with simple direct-detection scheme have been able to keep up with this demand in the past, the continuous growth of bandwidth-hungry applications requires further upgrades beyond the limit of traditional direct-detection optical fibre networks. Recent advancements in optical fibre technology had led to the use of coherent receivers as a replacement for traditional direct-detection systems [1]-[11]. While being more complex, coherent receivers allow both phase and magnitude information of the signal to be captured, and thus allow more efficient data transmission by using more complex modulation formats. The use of coherent receivers also enables a more complex system design and more wireless concepts can be transferred to the optical domain in order to increase system capacity and transmission distance. Figure 1.1 shows the block diagram of a typical polarisation diversity optical coherent receiver. The incoming signal and the local oscillator (LO) signal are both split into two components using polarisation beam splitters (PBSs) and then mixed together using optical hybrid devices. This mixed signal is then demultiplexed using a balanced receiver consisting of photodiodes and electrical sampling devices. The use of coherent receivers is not a new concept and has been investigated since 1990. However, the demand for a greater bandwidth using the same optical fibre, as well as recent advancements in electronic component manufacturing, which enables fast digital signal processing (DSP), had led to the revival of coherent detection in optical communication systems.

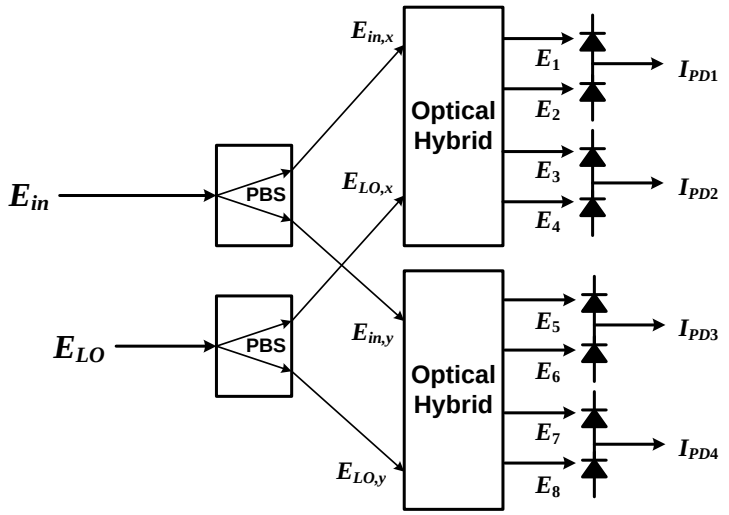

Figure 1.1: Coherent receiver employing polarisation diversity [1].

1.1.1 CO-OFDM versus CO-SC-FDE

Traditional optical fibre communication systems are limited by chromatic dispersion (CD), which severely degrades the signal quality over long transmission distance, especially systems with high baud rate. Traditionally, this limitation must be overcome with the use of dispersion compensated fibres (DCF), which further add to system complexity. With the revival of coherent receivers, since both phase and amplitude of the incoming signal can be captured, it is possible to bring concepts from wireless technology to optical domain in order to overcome the limitation imposed by CD, which can be viewed as similar to the multi-path fading problem in wireless domain. Towards the design of high speed, long-haul optical communication systems using coherent receivers with high CD tolerance, two competing technologies were proposed: coherent optical (CO) orthogonal frequency division multiplexing (OFDM) [2]-[4] and CO single carrier (SC) with frequency domain equalisation (FDE) [6]-[8]. Both of these technologies have been designed to overcome the limitation of CD and polarisation-mode dispersion (PMD), which are major impairments in optical fibre that limit the effective transmission distance. The first proposed technology, CO-OFDM, uses multiple carriers orthogonal to each other to carry information through the channel and is based on wireless OFDM technology. In order to achieve this multicarrier scheme, modulated data are mapped onto subcarriers that are orthogonal to each other as illustrated in Figure 1.2(b). This transformation results in a signal spectrum tightly

packed with multiple orthogonal carriers instead of a few carriers separated by guard bands as in a traditional SC system illustrated in Figure 1.2(a).

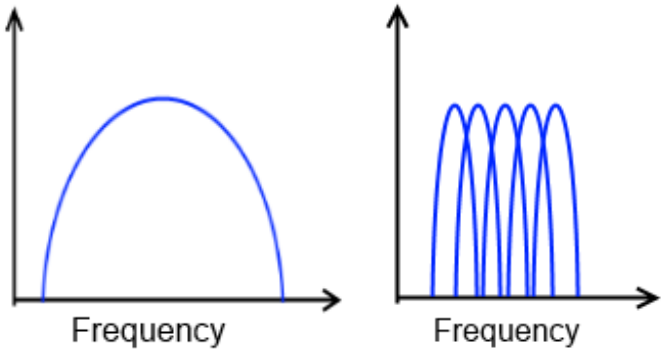

Figure 1.2: Spectrum of (a) SC and (b) OFDM signal [3].

From a mathematical point of view, this mapping is equivalent to taking an Inverse Discrete Fourier Transform (IDFT) operation of the original data and thus in practice OFDM symbols are generated by taking IDFT of blocks of symbols before the modulation stage. From an implementation point of view, OFDM can be viewed as a DFT coded SC transmission scheme with the actual data being an IDFT coded version of the SC scheme, and thus data are designed in frequency domain instead of time domain as in traditional SC system [4]. For optical OFDM, the optical channel model is given by:

For application in high speed long-haul transmission, CO-OFDM format had shown great potential since it exhibits good ability to cope with CD and PMD [2]-[4]. As stated above, in CO-OFDM the modulated blocks of symbols are first transformed into longer symbols that are parallel to each other by means of inverse fast Fourier transform (IFFT) operations before being sent into the optical channel. At the receiver, data are then transformed back from multiple carriers to SC by means of fast Fourier transform (FFT) operations before detection. CO-OFDM, as implemented using DSP technology with IFFT/FFT transform, has the advantage of being simple and fully compatible with optical transmission since all carriers mapping is done using DSP. However, beside the advantages of having multiple subcarriers tightly packed together, CO-OFDM technology exhibits several issues that can limit its popularity in optical systems. As

data are designed in frequency domain and CO-OFDM transformed data into time domain by IFFT, CO-OFDM requires the use of a complex waveform generator at the transmitter in order to generate the CO-OFDM signal since after IFFT the waveform is complex and has many levels. Another potential issue also arising from IFFT transformation of data is the larger peak-to-average power ratio (PAPR) in CO-OFDM compared to CO-SC-FDE systems. However, this difference is only significant in electrical domain. In CO transmission systems, due to the long transmission distance, the PAPR of both systems are expected to be similar [2].

Similar to the adoption of OFDM from the wireless into the optical domain, another wireless transmission scheme is introduced into the optical domain, namely CO-SC-FDE. The main motivation is due to the fact that coherent receivers can capture both signal phase and magnitude, and they allow the use of DSP that can construct filters to reverse the effect of both CD and PMD on the received signal. Thus, the use of DSP makes SC system with CD and PMD equalisation comparable to CO-OFDM in terms of dispersion tolerance. The first implementation of CO-SC receiver's DSP uses time domain equalisation (TDE), resulting in CO-SC-TDE, which can benefit from non-linear equalisation method like least mean square (LMS) and decision feedback equaliser (DFE), although it has been suggested [12] that non-linear method only has a small advantage when polarisation dependent loss is very large and will not present a major improvement in many cases. However, since CD is a very large impairment with long channel impulse response, the use of filters in time domain requires significant computational power and thus is not suitable for equalisation of a large amount of CD. CO-SC system with FDE was proposed [6]-[8] which utilises FFT/IFFT algorithm to perform CD equalisation in frequency domain with significantly less computational effort. In CO-SC-FDE, data at the receiver are first transformed into frequency domain by FFT, and linear channel impairment equalisation is then done in frequency domain using one tap equaliser and then the data are transformed back into time domain by IFFT. This makes CO-SC-FDE superior to CO-SC-TDE in practice and comparable to CO-OFDM in terms of processing efficiency.

Figure 1.3 shows a block diagram comparison between CO-OFDM and CO-SC-FDE. It can be seen that in general, the only difference between CO-SC-FDE and CO-OFDM is

the position of the IFFT block, thus both formats can be employed in CO communication networks.

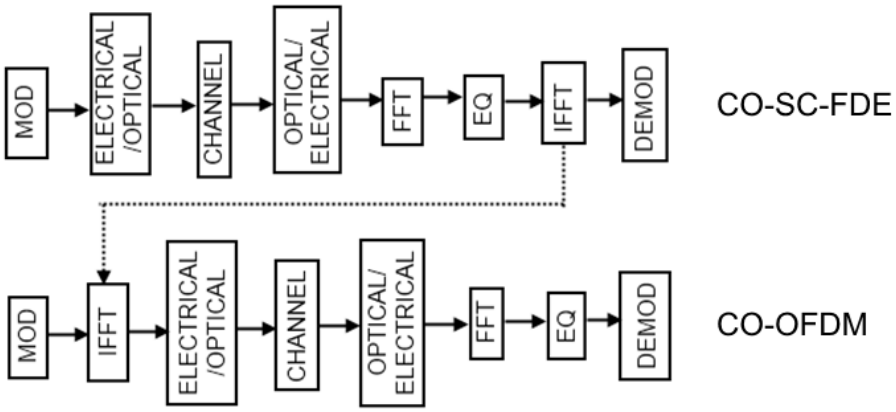

Figure 1.3: Block diagrams of CO-SC-FDE and CO-OFDM.

1.1.2 Data-Aided Channel Estimation and Performance Monitoring

The use of coherent receivers enables full capture of the signal waveform and thus many wireless techniques that rely on full signal waveform can be employed. Since CO-SC-FDE systems rely on frequency domain compensation of CD, the value of the entire transmission link needs to be estimated in order to construct the compensation algorithm. CO-OFDM also benefits from frequency domain CD compensation as this significantly reduces the required guard interval of CO-OFDM. Thus it is very desirable to estimate system CD from the received data at the coherent receiver when the system first starts up [14]-[15]. Traditionally, only a small amount of CD (residual CD) can be estimated by reading the equaliser filter taps [16]-[18], which can be obtained through gradient algorithm or small block of training sequences (TSs). Since CD is a linear channel impairment, techniques employed to estimate channel information can be used to estimate system CD, provided that these can be adapted to the long impulse response requirement. Among these technologies, orthogonal space-time block code (STBC) [19]-[21] or data-aided (DA) channel estimation (CE) is very attractive since it is a simple and robust method for estimation of channel impulse response. Originally designed for CE in CO-OFDM, DA-CE has seen extensive use as an alternative CE method for CO-SC-FDE and has been demonstrated to provide fast and robust

estimation performance with very good tolerance to residual CD. As DA-CE transmits some known symbols for CE, it comes with the cost of reduced transmission efficiency. However, this penalty is more than made up with robust and higher estimation accuracy compared to traditional blind methods. Channel equalisation and polarisation demultiplexing can also benefit from the use of DA-CE, similar to its application in wireless technology and a single technology can be used to estimate system CD as well as subsequent CE for equalisation purposes. The use of DA-CE is not only attractive for CD estimation and channel equalisation, but also for optical performance monitoring (OPM) purposes since the training block is totally transparent to the rest of the data frame. One primary parameter of performance monitoring is the optical signal-to-noise ratio (OSNR), which cannot be estimated by reading channel filter taps and requires separate techniques for estimation. Thus it is very advantageous to use DA-CE technique for OSNR estimation however most research in optical DA-CE has been in the field of utilising DA-CE for equalisation purposes. Beside channel equalisation, It is therefore of great interest to investigate system CD and OSNR estimation techniques based on the training block employed in DA-CE optical systems as this will further utilise the training block, and eliminate the need for any separate data block designed specifically for system CD or OSNR estimation purposes.

1.1.3 Performance Monitoring Using Low-Bandwidth Receivers

Recent advancement in coherent receiver technology has led to great research interest in using coherent receivers for monitoring purposes. While the use of coherent receivers means coherent-based monitoring technologies will be free of extra hardware cost, these techniques will rely on full-speed receivers at the link end for monitoring purposes and are not suitable for distributed monitoring of optical networks. As modern CO networks have evolved from single point-to-point networks to multi path routing with many nodes along a transmission path, it is very desirable to investigate monitoring techniques that utilise low-cost hardware for distributed monitoring of the entire networks. As the cost of coherent receivers continues to be reduced, channel monitoring techniques based on low-bandwidth coherent receivers will be of great interest. As CO-OFDM utilises multiple subcarriers within one given bandwidth, low-bandwidth receiver monitoring will greatly benefit from the use of CO-OFDM format. In principle, data in the subcarriers within the monitoring bandwidth can be fully captured and processed using

DSP for channel monitoring purposes. While CO-SC-FDE does not possess multi carrier characteristics, it is also advantageous to use a low-bandwidth receiver for distributed monitoring of CO-SC systems. Therefore it is of great interest to investigate OPM techniques using low-bandwidth coherent receivers for both CO-SC and CO-OFDM communication systems.

1.2 THESIS OUTLINE

The objective of this thesis is to investigate the design of CE techniques for channel performance monitoring and equalisation in CO communication systems, which is a critical part of designing next generation CO networks. New CE techniques for estimating different optical network parameters are designed, demonstrated and analysed. These techniques are based on DA-CE technology and are fast and robust compared to traditional blind algorithm methods as well as capability of application in both CO-SC-FDE and CO-OFDM systems. New CE algorithms specific for low-bandwidth coherent receivers are also demonstrated and investigated. Unlike traditional full-bandwidth receivers, the use of low-bandwidth receivers requires different techniques for CO-OFDM and CO-SC-FDE systems. While DA-CE can provide a transparent method for OPM under low-bandwidth receivers, CO-OFDM systems can utilise blind techniques and the special carrier structure for OPM purposes.

The thesis begins in Chapter 2 with a literature survey of CE and equalisation techniques for CO systems. General structures of coherent receiver DSP for both equalisation and monitoring are reviewed and possible improvements are discussed. Different techniques for channel monitoring will be reviewed and depending on the required impairment to be monitored, advantages and disadvantages of these techniques are discussed. Different implementations of both traditional blind CE and DA structures are investigated and required new adaptations for CO networks are also discussed.

A new DA system link CD estimation method is presented in Chapter 3. The technique is for full transmission link CD estimation and based on DA-CE technology. Two types of long TSs designed for system link CD estimation are presented and their advantages as well as drawbacks are discussed. The technique can be implemented as single-stage or dual-stage estimation depending on the required accuracy. Simulation and

experimental demonstrations of these CD estimation methods are presented for both single-stage and dual-stage implementations as well as for two modulation formats of polarisation-multiplexed (PM) quadrature phase shift keying (QPSK) and 16-quadrature amplitude modulation (16QAM). The results include estimation error for both PM-QPSK and PM-16QAM modulation formats. Tolerances to different channel impairments are also investigated.

A new DA OSNR estimation technique is presented in Chapter 4. This technique directly utilises the training block for OSNR monitoring purposes and can be adapted for both PM-QPSK and PM-16QAM modulation formats. Two different methods for achieving the estimation technique are investigated. Tolerances of the OSNR estimation technique to difference channel impairments are investigated. Experimental demonstration of the technique is also presented. The results include estimation accuracies for both PM-QPSK and PM-16QAM systems, as well as tolerances to both system transmission and PMD.

Chapter 5 presents a new flexible frame synchronisation structure for DA CO-SC systems. Performance of DA estimation and equalisation for CO systems under different TS lengths, different noise filtering DSP and OSNR impairments is studied. The new synchronisation structure is proposed which enables detection of TS locations as well as TS lengths and thus enables flexible training length in system design. System and frame synchronisation tolerance to different channel impairments are also studied. Simulation and experimental demonstrations of flexible tracking speed CO-SC-FDE systems employing DA-CE are presented.

Chapter 6 presents a new DA OSNR estimation technique designed for low-bandwidth coherent receivers. The technique utilises TSs employed in DA systems, however only a low-bandwidth receiver is required. Simulation and experimental demonstrations are presented. The results include estimation accuracy of the proposed technique as well as receiver bandwidth requirement. Advantages and drawbacks of the technique are discussed.

In Chapter 7, two differential group delay (DGD) monitoring techniques using low-bandwidth coherent receivers are proposed. The first technique is DA and utilises the estimated channel transfer functions. The second technique is designed specifically for

CO-OFDM with low-bandwidth receivers and is non-data-aided (NDA). Compared to SC systems, DGD estimation in CO-OFDM systems using low-bandwidth receivers can be made using blind method due to the specific multi-carrier structures. Two measuring methods for blind estimation of DGD using low-bandwidth receivers in CO-OFDM systems, namely point-to-point estimation and interpolation, are studied. The techniques are demonstrated in both simulations and experiments. Estimation accuracies of the techniques as well as tolerances to different channel impairments are studied.

Chapter 8 gives a summary of the main findings and conclusions of the thesis, and a discussion of possible future works. This final chapter is followed by one appendix containing all acronyms' definition used in the thesis.

1.3 ORIGINAL CONTRIBUTIONS

The original contributions of this thesis are as follows:

- Proposal and demonstration of DA system link CD estimation technique (Chapter 3). Estimation accuracy and channel impairments tolerance are evaluated.

- Proposal and demonstration of a new channel OSNR estimation technique based on the training block of DA CO-SC-FDE system (Chapter 4). Estimation accuracies and performances with respect to channel impairments are studied.

- Design and demonstration of a CO-SC-FDE system employing DA-CE with flexible update speed or overhead ratio (Chapter 5). Performances of CO-SC-FDE systems with respect to update speed and/or aspect ratio are investigated.

- Proposal and demonstration of a new DA channel OSNR estimation technique with low-bandwidth receivers (Chapter 6). The technique utilises the same training block as full speed system. Estimation accuracy and performance with respect to channel impairment are studied.

- Proposal and demonstration of DA DGD estimation technique for CO systems using low-bandwidth receivers (Chapter 7). Estimation performances with respect to different training lengths are studied.

- Proposal and demonstration of a new NDA DGD estimation technique designed for CO-OFDM systems utilising low-bandwidth receivers (Chapter 7). The technique is based on monitoring OFDM subcarriers within the monitoring bandwidth and is NDA. Estimation accuracies and performances with respect to channel impairments are presented.

1.4 LIST OF PUBLICATIONS

1.4.1 Invited Conference Publications

[1] A. V. Tran, C. Zhu, **C. C. Do**, T. Anderson, and E. Skafidas, "Computational-Efficient and Modulation Format-Flexible Training-Aided Single-Carrier Digital Coherent Receiver," invited paper, *International Conference on Optical Internet COIN'2013*, Beijing, China, Oct. 2013.

1.4.2 Conference Publications

[1] **C. Do**, A. V. Tran and D.F. Hewitt, "Chromatic Dispersion Estimation Based on Complementary Golay Sequences for 80 Gb/s QPSK Single-Carrier System with Frequency Domain Equalisation," *Australian Telecommunication Networks and Application Conference ATNAC' 2011*, pp. 1-4, Melbourne, Australia, Jun. 2011.

[2] **C. Do**, C. Zhu, A.V. Tran, S. Chen, T. Anderson, D. Hewitt, and E. Skafidas, "Chromatic Dispersion Estimation in 40 Gb/s Coherent Polarisation-Multiplexed Single Carrier System using Complementary Golay Sequences," *Optical Fibre Communication Conference OFC'2012*, paper OW4G.1, Los Angeles, CA, USA, 2012.

[3] **C. Do**, A. V. Tran, C. Zhu, S. Chen, L. B. Du, T. Anderson, A. J. Lowery, "PMD Monitoring in 16-QAM Coherent Optical System using Golay Sequences," *Opto-Electronics and Communications Conference OECC'2012*, pp. 767-768, Busan, Korea, 2012.

[4] **C. Do**, A. V. Tran, C. Zhu, and E. Skafidas, "Training Sequences in 16-QAM and QPSK Coherent Pol-Mux Single-Carrier Systems," *IEEE Photonics Conference IPC'2012*, pp. 449-450, Burlingame, CA, USA, 2012.

[5] **C. Do**, A. V. Tran, C. Zhu, and E. Skafidas, "Data-Aided Second-Order Polarisation-Mode Dispersion Estimation for QPSK and 16-QAM Coherent Optical Systems," *Opto-Electronics and Communications Conference OECC'2013,* pp. 1-2, Kyoto, Japan, 2013.

[6] A. V. Tran, C. Zhu, **C. Do**, S. Chen, L. B. Du, T. Anderson, D. Hewitt, A. J. Lowery, and E. Skafidas, "Single Carrier QPSK and 16 QAM System Demonstration Using Frequency Domain Equalisation and Training Sequences," *Opto-Electronics and Communications Conference OECC'2012*, pp. 463-464, Busan, Korea, 2012.

[7] C. Zhu, A. V. Tran, S. Chen, L. B. Du, **C. Do**, T. Anderson, A. J. Lowery, and E. Skafidas, "Moments-based OSNR Monitoring for QPSK and QAM Coherent Optical Systems," *Opto-Electronics and Communications Conference OECC'2012*, pp. 747-748, 2012.

1.4.3 Journal Publications

[1] **C. Do**, A. V. Tran, C. Zhu, S. Chen, T. Anderson, D. Hewitt, and E. Skafidas, "Data-Aided Chromatic Dispersion Estimation for Polarisation Multiplexed Optical Systems," *IEEE Photonics Journal*, vol. 4, no. 5, pp. 2037-2049, Oct. 2012.

[2] **C. Do**, A. V. Tran, S. Chen, T. Anderson, D. Hewitt, and E. Skafidas, "Flexible bandwidth DGD estimation for coherent optical OFDM system," *Optics Express*, vol. 21, no. 22, pp.25788-25795, 2013.

[3] **C. Do**, A. V. Tran, C. Zhu, D. Hewitt, and E. Skafidas, "Data-Aided OSNR Estimation for QPSK and 16-QAM Coherent Optical Systems," *IEEE Photonics Journal*, vol.5, no. 5, article 6601609, Oct. 2013.

[4] **C. Do**, C. Zhu and A. V. Tran, "Flexible Tracking Speed Data-Aided Coherent Optical System using Golay Sequences," *IEEE Photonics Journal*, vol.6, no. 3, article 7901409, 2013.

[5] **C. Do**, C. Zhu and A. V. Tran, "Data-Aided OSNR Estimation using Low-Bandwidth Coherent Receivers," *IEEE Photonics Technology Letters*, vol.26, no. 13, pp. 1291-1294, 2014.

[6] A. V. Tran, C. Zhu, **C. Do**, S. Chen, T. Anderson, D. Hewitt, and E. Skafidas, "8×40 Gb/s Optical Coherent Pol-Mux Single Carrier System with Frequency Domain Equalisation and Training Sequences," *IEEE Photonics Technology Letters*, vol. 24, no. 11, pp. 885-887, Jun. 2012.

[7] C. Zhu, A. V. Tran, S. Chen, L. B. Du, **C. Do**, T. Anderson, A. J. Lowery, and E. Skafidas, "Statistical Moments-Based OSNR Monitoring for Coherent Optical Systems," *Optics Express*, vol. 20, no. 16, pp. 17711-17721, Jul. 2012.

1.5 REFERENCES

[1] M. Nakazawa**,** K. Kikuchi, and T. Miyazaki, *High Spectral Density Optical Communication Technologies*, Section 2.1, Springer, Aug. 2010.

[2] W. Shieh, X. Yi, Y. Ma, and Q. Yang, "Coherent optical OFDM: has its time come?'' *Journal of Optical Networking*, vol. 7, no. 3, pp. 234-255, 2008.

[3] Y. Tang, Y. Ma, and W. Shieh, "107 Gb/s CO-OFDM transmission with inline chromatic dispersion compensation," *Optical Fibre Communication Conference OFC'2009*, paper OWW3, San Diego, CA, USA, Mar. 2009.

[4] J. Armstrong, "OFDM for optical communications," *Journal of Lightwave Technology*, vol. 27, no. 3, pp. 189–204, Feb. 2009.

[5] S. J. Savory, "Digital filters for coherent optical receivers," *Optics Express*, vol. 16, no. 2, pp. 804-817, Jan. 2008.

[6] R. Kudo, T. Kobayashi, K. Ishihara, Y. Takatori, A. Sano, and Y. Miyamoto, "Coherent Optical Single Carrier Transmission Using Overlap Frequrency Domain Equalisation for Long-Haul Optical Systems," *Journal of Lightwave Technology*, vol. 27, no. 16, pp. 3721–3728, Aug. 2009.

[7] K. Ishihara et al., "Frequency-domain equalisation for optical transmission systems," *Electronics Letters*, vol. 44, no. 14, pp. 870-872, Jul. 2008.

[8] K. Ishihara et al., "Frequency-domain equalisation without guard interval for optical transmission systems," *Electronics Letters*, vol. 44, no. 25, pp. 1480-1482, Dec. 2008.

[9] R. Kudo, T. Kobayashi, K. Ishihara, Y. Takatori, A. Sano, E. Yamada, H. Masuda, and Y. Miyamoto, "PMD compensation in optical coherent single carrier transmission using frequency-domain equalisation," *Electronic Letters*, vol. 45, no. 2, pp. 124-125, Jan. 2009.

[10] J. Li, C. Zhao, S. Zhang, F. Zhang, and Z. Chen, "Experimental Demonstration of 120-Gb/s PDM CO-SCFDE Transmission Over 317-km SSMF," *IEEE Photonics Technology Letters*, vol.

22, no. 24, pp. 1814-1816, Dec. 2010.

[11] M. Kuschnerov, F.N. Hause, K. Piyawanno, B. Spinnler, M.S. Alfiad, A. Napoli, and B. Lankl, "DSP for coherent single-carrier receivers," *Journal of Lightwave Technology*, vol. 27, no. 16, pp. 3614-3622, Aug. 2009.

[12] M. Kuschnerov, M. Chouayakh, K. Piyawanno, B. Spinnler, E. de Man, P. Kainzmaier, M. S. Alfiad, A. Napoli, and B. Lankl, "Data-aided versus blind single carrier coherent receivers," *IEEE Photonics Journal*, vol. 2, no. 3, pp.387-403, Jun. 2010.

[13] L. Sun, X. Wang, and S. Zhang: "A Novel Frequency Domain Equalisation Algorithm for SC-FDE System," *Pacific-Asia Conference on Knowledge Engineering and Software Engineering KESE*, pp. 132-135, Shenzhen, China, Dec. 2009.

[14] F. N. Hauske, C. Xie, Z. Zhang, C. Li, L. Li, and Q. Xiong, "Frequency domain chromatic dispersion estimation" , *Optical Fibre Communication conference OFC'2010*, paper JThA11, San Diego, CA, USA, Mar. 2010.

[15] F. N. Hauske, Z. Zhang, C. Li, C. Xie, and Q. Xiong, "Precise, robust and least complexity CD estimation," *Optical Fibre Communication Conference OFC'2011*, paper JWA032, San Diego, CA, Mar. 2011.

[16] R. A. Soriano, F. N. Hauske, N. G. Gonzalez, and I. T. Monroy, "Chromatic dispersion estimation in digital coherent receivers," *Journal of Lightwave Technology*, vol. 29, no. 11, pp. 1627–1637, Jun. 2011.

[17] F. Pittala, F. N. Hauske, Y. Yabin, N. G. Gonzalez, and I. T. Monroy, "Fast and robust CD and DGD estimation based on data-aided channel estimation," *International Conference on Transparent Optical Networks ICTON 2011*, paper We.D1.5, Stockholm, Sweden, Jun. 2011.

[18] F. Pittalà, F. N. Hauske, Y. Yabin, N. G. Gonzalez, and I. T. Monroy, "Combined CD and DGD Monitoring Based on Data-Aided Channel Estimation," *Signal Processing in Photonic Communications SPPCom'2011*, pp. SPTuC3, Toronto, Canada, Jun. 2011.

[19] S. Alamouti, "A simple transmit diversity technique for wireless communications," *IEEE Journal on Communication*, vol. 16, no. 8, pp. 1451-1458, Oct. 1998.

[20] S. D. Howard, A. R. Calderbank, and W. Moran, "A simple signal processing architecture for instantaneous radar polarimetry," *IEEE Transactions on Information Theory*, vol. 53, no. 4, pp 1282-1289, Apr. 2007.

[21] V. Tarokh, H. Jafarkhani, and A. R. Calderbank, "Space-Time Block Codes from Orthogonal Designs," *IEEE Transactions on Information Theory*, vol. 45, no. 5, pp 1456-1467, Jul. 1999.

2 Literature Survey

2.1 INTRODUCTION

In coherent optical (CO) systems, data can be modulated using single carrier (SC) or orthogonal frequency division multiplexing (OFDM) formats as mentioned in Chapter 1. Both formats employ many different designs of receiver's digital signal processing (DSP) for data equalisation as well as channel impairment estimation and optical performance monitoring (OPM). While there are some differences between the DSP structures of CO-SC and CO-OFDM, both of these formats benefit from system link chromatic dispersion (CD) estimation and compensation, channel equalisation and OPM. This chapter provides a review of key DSP techniques for CO-SC and CO-OFDM transmission structures. Techniques for data transmission and receiver equalisation [1]-[36], which are essential for coherent receiver operation, will be reviewed. Techniques for estimation of system CD will also be presented [37]-[56]. System CD estimation is the very first essential component of the receiver's DSP since CD is a large impairment and will significantly affect system performance if left uncompensated. Techniques for receiver's DSP after CD compensation will also be presented [57]-[87]. Finally, channel parameter estimation techniques for OPM in optical communication systems will also be reviewed and discussed [84]-[138].

2.2 RECEIVER'S DSP FOR COHERENT OPTICAL SYSTEMS

Besides enabling higher and more complex transmission formats, the use of coherent receivers enables DSP techniques to compensate for channel impairments and to recover the original signal constellations. Many techniques can be used for the purpose of channel equalisation and a combination of these techniques can be used at the

receiver depending on the system's modulation format as well as the carrier format. This section describes key DSP techniques that are typically employed for both CO-SC and CO-OFDM transmission formats.

2.2.1 CO-SC and CO-OFDM

Coherent receivers support decoding of both phases and magnitudes of the optical signals and thus different complex transmission schemes can be used. At the base carrier level, two transmission schemes were proposed, namely CO-OFDM [1]-[17] and CO-SC [18]-[36]. Conventional CO-OFDM systems operate by sending data through multiple subcarriers that are orthogonal to each other. The equivalent of having data on multiple orthogonal slow-speed subcarriers is to design data in frequency domain and then convert these data blocks into time domain, using inverse fast Fourier transform (IFFT) [1]-[17]. The optical channel model for CO-OFDM signals can be given by [1]:

$$c'_{ki} = e^{j(\phi_i)} \cdot c_{ki} \cdot e^{j\Phi_D(k)} + n_{ki} \tag{2.1}$$

$$\phi D(k) = \phi_0 + 2\pi\tau_0 \cdot f_k + \frac{\pi \cdot c}{f^2_{LD1}} D_t \cdot f_k{}^2 \tag{2.2}$$

Where c_{ki},c'_{ki} are the ith transmitted and received symbols in the kth OFDM subcarrier, ϕ_i is the transmitter and receiver phase noise, $\Phi_D(k)$ is the CD-induced subcarrier phase and n_{ki} is the ASE noise. At the receiver, data are transformed back into frequency domain by fast Fourier transform (FFT) before demodulation. It can be seen that, due to data designed in frequency domain, the effect of CD on CO-OFDM symbols is that of a phase rotation for different subcarrier and thus can be tolerated by CO-OFDM structure. In CO-SC scheme, data are designed in time domain and transmitted using traditional SC method. At the receiver, data are equalised using either time domain equalisation (TDE) or frequency domain equalisation (FDE) to compensate for linear impairments accumulated during transmission. This results in two variations of CO-SC systems namely CO-SC with TDE and CO-SC with FDE, respectively. Since CO-SC-FDE scheme utilises FFT to transform blocks of data into frequency domain for equalisation and then transforms equalised data back into time domain by IFFT, the structure of this scheme as well as its DSP complexity is very similar to CO-OFDM scheme. As illustrated in Chapter 1, the major difference between CO-SC-FDE and CO-OFDM is the location of the IFFT block, which has been relocated from the transmitter to the

receiver between CO-OFDM and CO-SC-FDE. Both schemes are designed to cope with degradations generated by system CD in order to achieve significant transmission distance in uncompensated links. For traditional CO-OFDM, CD is tolerated by the use of cyclic prefix (CP) blocks and multiple slow-speed subcarriers, while in CO-SC, dispersion is typically compensated for using either TDE or FDE.

Traditionally, CO-SC systems had employed TDE for channel equalisation [18]-[28]. Li et al. demonstrated the use of CO-SC-FDE systems in [29]-[30]. The system's DSP consisted of frequency domain channel estimation (CE) by pilot symbols and signal equalisation using FDE. The bit rate was 120 Gb/s and modulation format was polarisation-multiplexed (PM) quadrature phase shift keying (QPSK). The transmission distance was 317 km using standard single-mode fibre (SSMF). The design of CO-SC-FDE by Li et al. is very similar to the traditional CO-OFDM design and CP blocks were inserted into CO-SC-FDE blocks of symbols to avoid inter-block interference (IBI) during transmission, and the receiver utilises a similar DSP structure compared to CO-OFDM. The receiver's DSP structure can be summarised as follows: at the receiver, channel transfer functions are estimated using pilot symbols and the CP blocks in each FDE data block are removed. Each data block is then transformed into frequency domain and all impairments are compensated in frequency domain using estimated channel information from pilot symbols. As such it is expected that the lengths of the CP blocks used will be proportional to the transmission distance similar to traditional CO-OFDM systems. The number of CP symbols used for each CO-SC-FDE symbol was not given in the paper.

While CP blocks have been employed in traditional design of CO-SC-FDE and CO-OFDM systems to combat CD, such usage will decrease the system's efficiency at long transmission distance due to the amount of CP symbols required. A separate CD compensation technique is much more preferred in order to achieve long distance transmission without inline compensation. Recent advancements in coherent receiver's DSP technology have made separate CD compensation using DSP possible for both CO-SC and CO-OFDM systems, resulting in much more similar DSP structures for both transmission schemes. Figure 2.1 illustrates a generic DSP structure for both CO-SC and CO-OFDM systems. After capturing the transmitted signal by coherent detection,

system CD is compensated in a separate CD compensation stage using DSP. If there is offset between the local oscillator's (LO) and the signal's frequency, a separate frequency offset (FO) compensation stage is also required for both CO-SC-FDE and CO-OFDM to compensate for the offset between the signal's and the LO frequency. Frame synchronisation is performed to identify the OFDM block in CO-OFDM systems and in case of CO-SC systems that utilise pilot symbols, frame synchronisation is needed to identify the pilot symbols. CE and equalisation are then performed to equalise the remaining impairments in the signal. As an extra product of coherent detection, channel impairments such as differential group delay (DGD) and optical signal-to-noise ratio (OSNR), can also be estimated for OPM purposes.

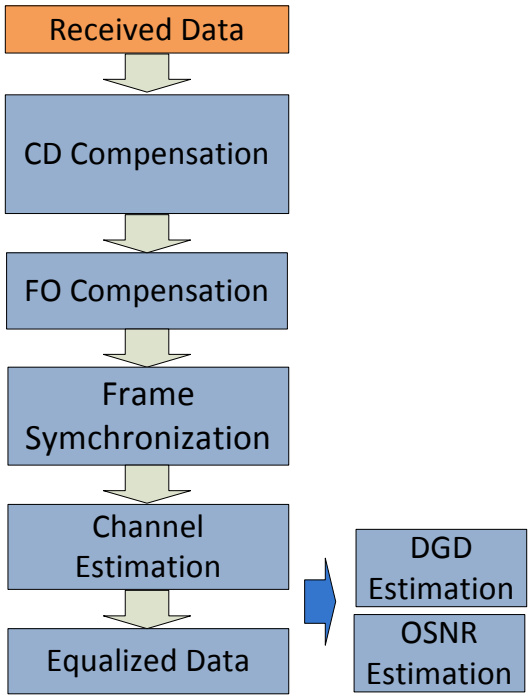

Figure 2.1: DSP block diagram for CO systems.

It can be seen that system CD compensation is the very first block for CO systems' DSP design. For modern design of CO-OFDM and CO-SC systems, system CD compensation is necessary to eliminate the need for long CP blocks at long transmission distance. The CD compensation techniques are described in the next section.

2.2.2 CD Compensation in CO-SC and CO-OFDM Systems

2.2.2.1 CO-SC with Time-Domain CD Compensation

CD represents the largest impairment for CO systems which scales linearly with transmission distance. CD is also proportional to the square of system baud rate and thus higher baud rate systems are significantly more sensitive to CD which in turn limits the possible uncompensated transmission distance for high bit rate optical communication systems. While signal loss can be compensated by Erbium-doped fibre amplifiers (EDFA), CD will degrade the signal and thus limit the reach of uncompensated optical signal before the effect of dispersion makes the signal unrecoverable. Before the introduction of coherent receivers, dispersion was a primary limiting factor for transmission distance and needed to be compensated by means of dispersion compensation fibre (DCF) module. Such fibre reverses the effect of CD and the amount of compensation is matched to the transmission distance. Thus after travelling through the DCF the effect of CD will be compensated and the signal can be recovered. However, while CD is a large impairment, the effect due to CD is simple and linear and with coherent receivers being capable of capturing both the magnitude and phase of the optical signal, compensation of CD using DSP is possible using coherent receivers. The first-generation implementation of CD compensation DSP techniques for CO-SC systems is based on implementing a set of time domain filters which reverses the effect of CD from the captured signal using DSP. Savory et al. proposed the design of time domain digital filters for CD compensation in [21]-[24]. The technique can be described as follows: in time domain, the effect of CD on a pulse can be described by the partial differential equation [21]:

$$\frac{\partial A(z,t)}{\partial z} = j\frac{D\lambda^2}{4\pi c}\frac{\partial^2 A(z,t)}{\partial t^2} \tag{2.3}$$

where z is the transmission distance, t is a time variable, λ is the wavelength of the light, c is the speed of light, D is the dispersion coefficient of the fibre, and $\partial(.)$ represents the partial derivative operation. Based on Equation 2.3, a time domain finite impulse response (FIR) filter can be constructed to reverse the effect of CD using electronic DSP. The filter-tap's values are given as:

$$a_k = \sqrt{\frac{jcT^2}{D\lambda^2 z}} \exp\left(-j\frac{\pi cT^2}{D\lambda^2 z}k^2\right) \text{ with } -\left\lfloor\frac{L}{2}\right\rfloor \le k \le \left\lfloor\frac{L}{2}\right\rfloor \text{ and } L = 2\left\lfloor\frac{|D|\lambda z^2}{2cT^2}\right\rfloor + 1 \qquad (2.4)$$

where a_k is the k[th] tap of the FIR filter, T is the system sampling speed, and L is the number of taps required for CD compensation. Utilising Equation 2.4, it can be calculated that for a 10 Gbaud system transmitting over 4,000 km SSMF with fibre dispersion parameter of D = 17ps/nm.km, the CD compensation filter will require no more than 250 taps. The technique was investigated using numerical simulations for comparison at different OSNR levels between 0 km transmission and 40,000 km transmission using digital CD compensation. The results indicated that the CD accumulated after transmission can be compensated using time domain digital filters and assuming fibre model consists of CD only, system performance after 40,000 km transmission with CD compensation is similar to the performance in the back-to-back case. Transmission of CO-SC systems with time domain CD equalisation was demonstrated in experiments by Savory et al. in [24] using 42.8-Gb/s PM-QPSK transmission over 6400-km SSMF. Similar demonstration of CD compensation in time domain was reported by Fludger et al. in [25] and Duthel et al. in [26]. Curri et al. reported on the benefits of using DSP-based CD compensation in [27], in which the system tolerance to nonlinear effect was improved compared to using optical CD compensation (by means of DCF). A similar demonstration on the benefits of DSP-based CD compensation compared to DCF was also reported by Alfiad et al. in [28].

2.2.2.2 CO-SC with Frequency-Domain CD Compensation

Section 2.2.2.1 described CD compensation technique for CO-SC systems using time-domain FIR filters. While the use of FIR filters can perfectly compensate for CD, using FIR filters is computationally intensive in general and thus a reduced-complexity CD compensation DSP technique is desirable. A different DSP scheme for CD compensation was proposed by Ishihara et al. in [31]-[33] which utilises FDE for CD compensation. The scheme can be described as follows: assuming a transmitted signal $s[n]$ in time domain, after transmission with only CD in the system, the received signal in frequency domain can be expressed as:

$$r[k] = H_{CD}[k]s[k] \qquad (2.5)$$

where $H_{CD}[k]$ denotes the discrete frequency domain CD transfer function, $r[k]$ and $s[k]$ denote the FFT of the received signal and original transmitted signal respectively. Assuming $H_{CD}[k]$ is known, the original signal $s[k]$ can then easily be obtained from $r[k]$ by dividing $r[k]$ with the CD transfer function. The CD transfer function can be presented in frequency domain from Equation 2.3 by taking the Fourier transform and solving for the frequency domain CD transfer function $H_{CD}(f)$ as:

$$H_{CD}(f) = \exp\left(-j\frac{D\lambda^2\pi}{c}f^2\right) \tag{2.6}$$

where f is the frequency in Hz.

Equation 2.6 describes an all-pass filter with phase rotation in frequency domain and it can be seen that the effect of CD depends on the transmission distance and thus will be very large at long uncompensated links. The frequency domain compensation filters, derived in sampled block format, can be expressed as:

$$H_{CDcomp}[k] = \left(H_{CD}[k]\right)^{-1} = \exp\left(j\frac{D\lambda^2\pi}{c}k^2\right) \text{ where } -\frac{R_s}{2} \le k \le \frac{R_s}{2} \tag{2.7}$$

with $H_{CDcomp}[k]$ being the discrete CD compensating function, k is the discrete frequency index and R_s is the signal sampling rate. While in time domain the effect of CD is a convolution of the CD transfer function with the original signal, in frequency domain this effect is reduced to multiplying the data spectrum with the CD transfer function and thus compensation is less computationally intensive.

In order for Equation 2.5 to be valid (and thus making compensation using Equation 2.7 possible), CP blocks need to be inserted before the transmitted data blocks to prevent IBI when taking the FFT/IFFT operations. Thus, CP blocks are used with every block of data that needs to be transformed into frequency domain for equalisation by Ishihara et al. in [31]. The bit rate before coding was 25 Gb/s with CP amount of 6.2% or 3.1% resulting in final bit rates of 21.7 Gb/s or 22.4 Gb/s, respectively. The use of FDE results in CO-SC-FDE systems with significant reduction in DSP complexity as CD compensation using FIR filter is a computationally intensive technique and makes CO-SC-FDE systems similar to CO-OFDM systems in terms of complexity and CD tolerance. While the use of FFT/IFFT significantly reduces the equalisation complexity

for both CO-OFDM and CO-SC-FDE systems, the need for CP blocks with lengths proportional to transmission distance for every block of data indicates a trade-off between transmission distance and the actual transmission efficiency.

An improved design for FDE was proposed by Ishihara et al. in [32]-[33] and Kudo et al. in [34]-[36], namely overlap-FDE (OFDE). The use of OFDE is demonstrated in Figure 2.2.

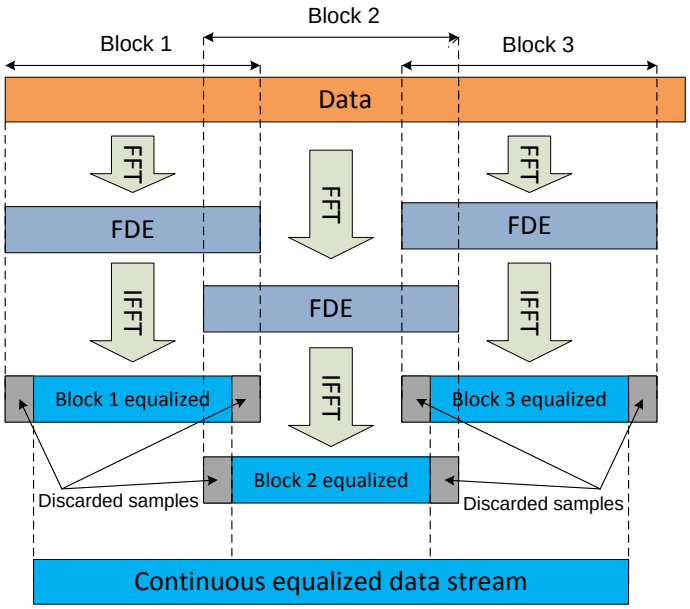

Figure 2.2: Overlap FDE (OFDE) [32].

The operating principle of OFDE can be described as follows: In OFDE, the CP blocks are no longer needed to be inserted between each data block, resulting in a continuous data stream. Initially, equalisation of this stream using FDE leads to IBI of the compensated data blocks. Nevertheless, these affected symbols only appear at the beginning and the end of the equalised data blocks. The effect of IBI thus can be easily removed by discarding the affected symbols. The next data block to be equalised then contains the symbols discarded by the previous block and new symbols to be equalised. After the equalisation, polluted symbols are then removed before repeating the process. The amount of symbols to be discarded is equal to the required amount of CP symbols and the overlap lengths between blocks are simply chosen to be twice the amount of symbols to be discarded.

The use of OFDE results in a CD compensation scheme having slightly higher computing complexity compared to CP-FDE. However, the removal of CP requirement greatly enhances bandwidth efficiency, making OFDE a superior method for CD compensation. An SC system was used for OFDE demonstration [32] resulting in demonstration of CO-SC-FDE with no guard interval and high bandwidth efficiency. Compared to the CO-SC-FDE scheme demonstrated by Li et al. in [29], the use of a separate CD compensation stage for CO-SC-FDE by Ishihara et al. in [32] results in significantly more transmission distance and removes the need for splitting data stream into FDE blocks guarded by CP blocks. As CD compensation represents the biggest use of FDE in general, CO-SC systems with CD compensation using OFDE are denoted as CO-SC-FDE systems for the rest of the thesis.

2.2.2.3 CO-OFDM with CD Compensation

Sections 2.2.2.1 and 2.2.2.2 described CD compensation using coherent receiver's DSP for CO-SC systems. The implementation of OFDE for CD compensation greatly enhances the transmission capability of CO-SC systems as the dominant impairment can now be effectively compensated without any significant penalty. At first, this presents an advantage for CO-SC systems over traditional CO-OFDM systems since the traditional design of CO-OFDM relies on CP blocks to resist CD instead. While the use of CP blocks simplifies DSP for CO-OFDM, the amount of CP symbols needed in each CP block is proportional to the transmission distance. This in turn results in CO-OFDM systems requiring a large amount of CP symbols for long distance transmission and reduces the effective bit rate of CO-OFDM scheme at long transmission distance. However, it can be easily seen that CD compensation using OFDE is totally transparent to the type of transmission scheme used. Therefore it is also possible to use CD compensation (with OFDE) for CO-OFDM systems and compensate for the majority of accumulated CD in the captured signal. The motivation for CO-OFDM with CD compensation is primarily to reduce the amount of CP symbols needed at long transmission distance while still maintain the benefits of CO-OFDM multicarrier structure.

Liu et al. proposed the application of CD compensation using OFDE for CO-OFDM systems [11]-[12]. The use of OFDE for CD compensation significantly reduces the

amount of CP symbols used in designing CO-OFDM systems for long transmission. This brings about the design of reduced guard interval (RGI) CO-OFDM, where only a small amount of CP symbols are needed for long distance CO-OFDM transmission, in order to tolerate the remaining inter-symbol-interference (ISI) after first stage CD compensation using OFDE.

An improved design based on two-stage equalisation was proposed by Sano et al. in [13]-[14], Miyamoto in [15] and Chandrasekhar et al. in [16], where the first stage also includes CD compensation. After CD compensation, the second stage includes transforming data back into frequency domain and compensating for residual impairments using adaptive blind channel equalisation with constant modulus algorithm (CMA). This results in no-guard-interval (NGI) CO-OFDM which approaches the bandwidth efficiency of CO-SC-FDE using OFDE.

A variation of the two-stage equalisation approach was proposed by Chen et al. in [17], that is zero-guard-interval (ZGI) CO-OFDM. The approach also includes first stage CD equalisation. However, the second stage performs CE using training sequences (TSs), as well as equalises the captured CO-OFDM signal using estimated channel transfer functions before transforming the equalised data back into frequency domain. This also results in CO-OFDM systems having no guard interval in the data streams, yet a small portion of the bandwidth is used for the TS required for CE. The difference between DA-CE and non-data-aided (NDA) CE schemes will be discussed in Section 2.2.3.

Regardless of the transmission schemes used, it can be seen that most modern designs of CO systems employ CD compensation in the first stage so as to realise long transmission distances with realistic overhead ratios. CD compensation using OFDE can also be regarded as a superior method compared to CP-FDE or TDE due to its bandwidth and computation efficiency. Therefore, the first stage CD compensation using OFDE is a mandatory part in realising high efficiency transmission for both CO-SC-FDE and CO-OFDM transmission schemes. As CD compensation using OFDE requires knowledge of total accumulated CD, estimation of system CD becomes an essential part of coherent receiver's DSP. Furthermore, as CD compensation leaves some residual amount of CD to be compensated in the second stage equalisation,

estimation of residual CD also gained research interests. The techniques for system CD and residual estimation are described in the next section.

2.2.3 CD Estimation Techniques

As outlined in the previous section, CD can be compensated using either FIR filters or frequency domain compensation using OFDE method and thus with the introduction of coherent receivers, signal degradation by CD can be mitigated at the receiver based entirely on DSP and no extra DCF are required. However, CD compensation requires the knowledge of the total transmission CD parameter and thus estimation of transmission link CD is of great interest as the receiver requires this information for the CD compensation procedure. Furthermore, as estimation techniques of this parameter are not entirely accurate, compensation of CD based on estimation will leave some residual CD for subsequent compensation during data equalisation. This requires the design of receiver's DSP for data equalisation to be capable of tolerance to residual CD. Because of this reason, monitoring of residual CD also gained great research interest as this value needs to also be within the system tolerance limit and high value residual CD can potentially cause problems for receiver's DSP procedures.

For estimation of system CD, techniques are primarily based on scanning and compensating a wide range of CD values in order to maximise a pre-defined signal parameter [37]-[45], or examining the entire captured signal's spectrum properties [46]-[48]. Estimation techniques for residual CD however, are primarily based on estimated channel transfer functions obtained during equalisation [49]-[56]. The next section will present a review of techniques for estimation of both system CD and residual CD in CO systems.

2.2.3.1 CD Estimation based on Step Size Scanning

Since CD can be compensated in frequency domain, the most traditional method for CD estimation using coherent receivers is to rely on scanning through a wide range of CD values with variable step sizes [37]-[45]. At each step, the captured signal is compensated for CD and the quality of the compensated signal is then examined in various ways for a cost function that maximises when the correct CD value is reached. The step size for CD estimation will depend on the maximum amount of the system CD

needed to be estimated, as using small step size will require high computational effort while large step size will result in high estimation errors.

Soriano et al. proposed a blind CD estimation technique based on best match search using the step size scanning principle described above in [37]. The method works by constructing different CD compensation filters, each with a different CD value. The captured signal is then evaluated using these filters for compensation and the compensated signal is then equalised using CMA algorithm. Based on the equalised signal, a cost function can then be calculated based on the clock tone recovery's ability of the CMA algorithm. The best matched CD value within the scanning range will leave the smallest residual amount of CD in the compensated signal and thus enable clock tone recovery to be performed at maximum magnitude. The magnitude of CT is then used to determine the best match of CD value through a cost function. The step size of the proposed method was 200 ps/nm, and the maximum amount of CD to be estimated was 30,000 ps/nm, which is approximately 1764 km of SSMF at a dispersion value of 17 ps.nm/km. It can be easily calculated from these numbers that the maximum number of steps used are 150. At each step, approximately 6200 symbols are examined to calculate the CMA clock tone function. The computational requirement of the method was not discussed.

Kuschnerov et al. proposed a similar design of the step size scanning approach for CD estimation in [38]-[39]. Here the same approach of scanning multiple CD values with step size of 200 ps/nm is applied. At each CD value, the signal is also compensated similar to the approach proposed by Sorinano in [37]. The compensated signal is then also evaluated for a minimum error criterion that only appears when the best matched CD value is applied to the signal. Compensation of CD is employed in frequency domain and the error criterion is also based on CMA blind equalisation algorithm. The design of step size scanning CD estimation is improved by using a two-stage design approach: the first stage compensates for system CD using large step size (200 ps/nm) and a wide range of system CD values. When the matched CD value for the first stage estimation is found, the second stage is performed using smaller step size of 20 ps/nm and a smaller range of CD values. Thus, the method's accuracy is improved to approximately 24 ps/nm estimation error, which is a very high degree of accuracy for system CD estimation. The estimation range demonstrated was up to 24,000 ps/nm,

equivalent to 1411 km transmission using SSMF with a dispersion value of 17 ps/nm.km.

Wang et al. reported a different CD estimation technique based on step size scanning approach in [40]. The signal is compensated using a CD compensation filter with different values defined by CD range and step size. After blind CD equalisation, delay tap pairs from the compensated signal are selected for CD estimation. The cost function to be minimised is the standard deviation of the distance between the delay tap pairs and the diagonal of the delay tap plots. The iteration is calculated in step size of 1000 ps/nm.km, which is a significant improvement compared to 200 ps/nm.km step size, and the process will stop as soon as the correct CD value is found instead of scanning the entire pre-defined CD range. Because such method is considered to be adaptive, depending on the amount of accumulated CD in the system, a large or small number of scanning steps will be used. Estimation accuracy was demonstrated to be 25 ps/nm with a range of CD up to 24,000 ps/nm. Up to 95,200 symbols were used for CD estimation.

Many other techniques for CD estimation are also based on the same concept of scanning through a wide range of CD values and compensate the signal through the pre-defined CD values, then evaluate a cost function to find a minimum value that matches the system CD. Theories and demonstrations of these approaches had been published in a few papers [41]-[45].

2.2.3.2 CD Estimation based on Signal Spectrum

Signal spectrum CD estimation method typically relies on the effect of CD on the signal pulse propagating through the optical fibre. A method for system CD estimation was proposed by Sui et al. [46]-[47], called CD estimation by auto-correlation of the signal power waveform (ACSPW). As the name suggested, this technique utilises the auto-correlation of the signal power waveform to estimate the total amount of CD. The operation of this algorithm can be summarised as follows: let $y[n] = s[n]^2$ be the power of the received signal $s[n]$, the auto-correlation function $R_{yy}(\tau)$ of $y[n]$ will yield a peak with peak location related to CD as illustrated in Figure 2.3 [46]. Therefore, by examining the auto-correlation function $R_{yy}(\tau)$, the value of system CD can be estimated. In order to increase the power of the peak used in ACSPW, high pass filter DSP implementation is typically used [46]-[48].

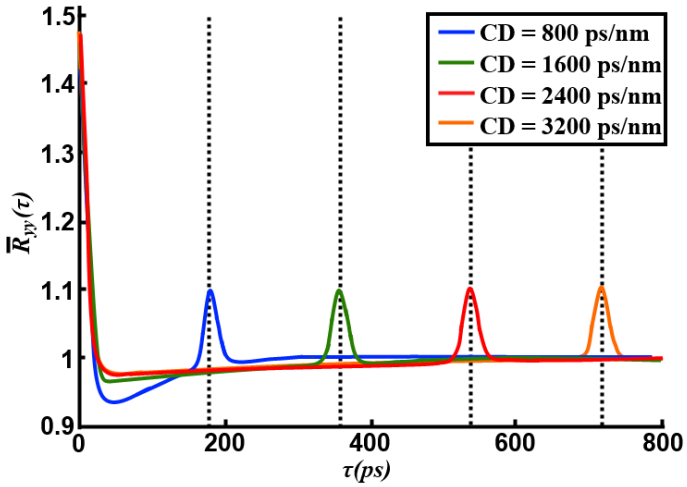

Figure 2.3: Demonstration of ACSPW: different values of CD yield different peaks on the auto-correlation function [46].

ACSPW can estimate CD based on analysing the signal power of incoming random data, and thus can be classified as a blind estimation technique since no TSs need to be used. A primary disadvantage of ACSPW, however, is that the technique is very computationally intensive and requires large blocks of FFT/IFFT for CD estimation from the incoming signal data [48]. In order to perform ACSPW, large blocks of FFT/IFFT to transform the signal into frequency domain need to be employed, which indicates a significant requirement in terms of hardware implementation. For CD estimation, ACSPW requires approximately 8192 symbols to calculate the auto-correlation function. It is noted that after CD estimation, CD compensation requires significantly smaller blocks of FFT/IFFT. A second minor problem is that ACSPW yields inaccurate results for small amount of CD, which can be solved by adding a known amount of CD to the signal before performing ACSPW. This additional CD value will ensure that the estimated CD value will be higher than the required minimum amount for ACSPW. After estimation, the added value can then be subtracted to reveal the correct CD value as explained by Pereira et al. in [48].

2.2.3.3 CD Estimation based on Estimated Channel Transfer Function

Since system CD estimation typically yields some errors, estimation of a small amount of CD (residual CD) for subsequent equalisation of transmitted data is also of great

importance. Techniques for estimation of residual CD are primarily based on analysing the estimated channel transfer functions. The inverses of transfer functions, which are also named equaliser filter taps, can be used for estimation of channel residual CD. The general approach for these techniques relies on the CD transfer function in frequency domain, which is a quadratic phase function as demonstrated in Equation 2.6. In the absence of nonlinear elements, optical channel can be modelled as a transfer function $H(f)$ with the complex transmitted signal $s(f)$, received signal $r(f)$ and noise $n(f)$ in frequency domain as:

$$r(f) = H(f)s(f) + n(f) \tag{2.8}$$

where $H(f)$ is the channel transfer matrix and consists of polarisation dependent components such as polarisation-mode dispersion (PMD) and polarisation independent components such as residual CD. As PMD is a unitary matrix, the residual CD transfer function $H_{CD,residual}(f)$ can be estimated from the determinant of $H(f)$ [49]. The residual CD value is estimated from this transfer function using quadratic fit. The main variations of equaliser filter taps based CD estimation do not lie in the estimation of CD itself, but in the approaches in which channel transfer matrix can be obtained. Traditionally, this channel transfer matrix can be obtained by blind gradient algorithm, which is based on searching for the filter coefficients that maximise a cost function. Such approach was demonstrated in [49]-[54]. The approach works reasonably well for a small amount of residual CD and requires a large amount of symbols to be analysed before the channel transfer matrix can be found. Once this matrix is correctly estimated, however, CD can be easily estimated by manipulating the estimated channel transfer functions to eliminate the PMD matrix, leaving only the residual CD transfer function. Details of quadratic fit implementation for CD estimation were not given in these papers.

However, a primary problem of using blind CE for CD estimation purpose is that the signal needed to be equalised first with all linear impairments compensated, before the monitoring matrix can be found. Thus, this approach assumes that residual CD or any other impairment are within the tolerance of the blind CE algorithm and can be compensated. Since the signal is already compensated, the amount of CD is already within the receiver's tolerance limit and as CD does not change over time, monitoring

of residual CD is not necessary for blind CE method.

A different approach to CD estimation based on CE was proposed by Pittala et al. [55]-[56] which is similar to the CE approach proposed by Li et al. in [29] and utilises TSs for CE purpose and can be classified as DA-CE. By using four orthogonal TSs, a simple and fast estimation of the channel transfer matrix can be performed before any data need to be equalised. The types of TSs used for demonstration of CE vary with different papers. Li et al. [29] used a pair of m-sequence and zero sequence where Pittala et al. used the design of two orthogonal constant amplitude zero autocorrelation (CAZAC) sequences [55]-[56]. It is noted that the use of TSs solves the singularity stability problem which occurs in the traditional blind estimation method, where the outputs on both polarisation transfer functions converge to one single value. This makes using TSs a highly robust and attractive technique for channel transfer functions estimation purpose. Since DA-CE does not require equalisation of data using gradient algorithm for CE purpose, the range of residual CD tolerance is only limited by the design of TSs used for DA-CE in theory. Residual CD estimation range was chosen at up to 500 ps/nm in [55]. After CD transfer function estimation, quadratic fit CD estimation was implemented using a search structure, where multiple CD transfer functions were constructed, the CD value that produces a transfer function that matches the estimated CD function with minimal error was then chosen as the estimated CD value. The step size for the proposed method is 50 ps/nm. Thus, error for the proposed method can be expected to be within half of the chosen step size. The maximum range of DA CD estimation method was not provided in the paper.

In general, residual CD estimation is primarily based on manipulating the estimated channel transfer coefficients to reveal the CD transfer function. The main variations in this approach are the different methods to acquire the channel transfer functions. There are two types of method for CE as described above: blind method using gradient algorithm, such as CMA, and DA method using TSs. Theoretical study and demonstration of the above methods for residual CD estimation have been published in a few papers [49]-[56]. The primary limitation of blind methods is the limited tolerance to CD, where a slightly large CD value will potentially cause blind estimation to fail. Since the tolerance range of blind estimation is small and CD needs to be compensated before estimation, this limitation makes estimation of residual CD using blind method

an unnecessary process. DA-CE has the potential to overcome these limitations with a small trade-off in bandwidth efficiency due to the TSs. However, the main limitation of DA-CE method proposed in [55]-[56] is the limited channel impulse response captured by CE. While this method is significantly more robust than the traditional blind method and requires much less computational complexity, DA-CE using short TSs is not suitable for system CD estimation. In order to estimate system CD, significantly different CE structure will be needed. The subject of DA system CD estimation will be investigated in details in Chapter 3.

2.2.4 Timing Recovery, Frequency Offset Compensation and Frame Synchronisation

2.2.4.1 Timing Recovery and Frequency Offset Compensation

Section 2.2.3 described estimation and compensation techniques for system CD. Compensation of CD reduces the amount of CP symbols required for CO-OFDM and enables CO-SC transmission without DCF. After CD compensation, the next steps in coherent receiver's DSP structure typically include timing recovery, FO compensation and frame synchronisation. The task of timing recovery is to compensate for the difference in timing phase between the transmitted and received signals and can be employed using the square timing recovery method [57] and can be described as follows. After applying a square filter, the timing error can be detected using a pre-defined algorithm and averaged out in a post filter stage. Kuschnerov et al. demonstrated the method in [39], [58] and the accuracy of the method was found to be directly related to the amount of CD, indicating a need for CD compensation in the first stage.

Since CO transmission uses LO to detect the signal, the received signal is prone to FO and FO needs to be compensated. FO estimation using DSP typically relies on the symmetry of the signal power spectrum for identification of FO. Typically, the signal power spectrum without FO is symmetric around the carrier and thus this property of the signal's spectrum can be utilised for estimation of FO [59]-[60]. An FO estimation technique based on RF pilot tone and spectrum symmetry was reported in [61] by Zhou et al. and can be described as follows: the captured signal blocks are transformed into frequency domain by FFT and the carrier RF tone is identified as the peak in the signal

spectrum. In a signal without FO then the carrier peak is located in the middle of the spectrum and thus the offset between estimated and ideal peaks can be calculated. The signal can then be compensated by multiplying the data stream with the inverse amount of offset resulting in FO-compensated signal. Figure 2.4 illustrates the concept of FO compensation using carrier peak in CO-OFDM systems. The peak is located in the centre of the spectrum in case of no FO and is shifted due to FO as illustrated in Figure 2.4. The location of the peak can then be used for FO estimation and compensation.

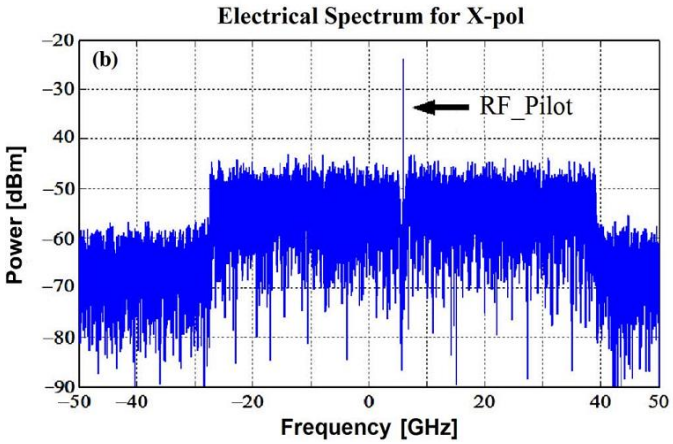

Figure 2.4: RF pilot tone shifted due to FO [61].

2.2.4.2 Frame Synchronisation

Since CO-OFDM format converts multiple subcarriers into blocks in time domain, frame synchronisation is required for CO-OFDM in order to recover the positions of the OFDM frames. Frame synchronisation is also required by CO-SC-FDE systems that utilise pilot symbols for CE as the pilot symbols' locations need to be estimated. Typically, frame synchronisation consists of sending a separate synchronisation header containing known data. At the receiver, the received signal is compared with the known synchronisation header utilising autocorrelation algorithm and the peak in the timing index will identify the location of the timing header. The structure of the timing header can also be customised for different purposes and different header structures had been proposed [62]-[65].

One of the headers for frame synchronisation was reported by Cox and Schmild [62] and the method had been shown to be robust against CD. As traditional design of CO-OFDM does not have any CD compensation capability, the method is very suitable for CO-OFDM systems. However, the method has large uncertainty due to the plateau in the frame synchronisation metric. Minn et al. proposed a different method [63] with improved frame synchronisation uncertainty with triangle-shaped metric. While both of these methods are robust against CD, the introduction of CD compensation technique has made CD tolerance a much less needed feature of frame synchronisation method. An example of frame synchronisation using header is illustrated in Figure 2.5. The index area has a triangle shape and the peak indicates the header's location. The data blocks' locations can then be easily calculated based on the header's location.

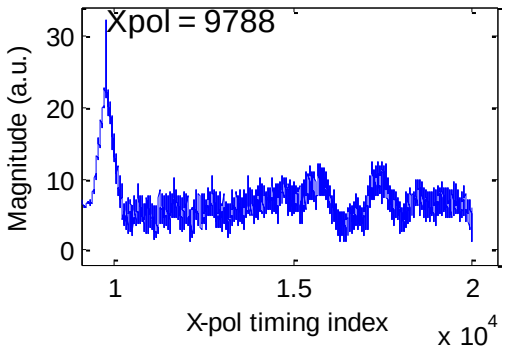

Figure 2.5: Timing synchronisation with triangle-shaped timing metric.

Huang et al. proposed a modified frame synchronisation scheme with single impulse shaped metric in [65]. While the header design is not robust to CD, stable and correct frame synchronisation can be achieved with CD compensation. With CD tolerance no longer a requirement for frame synchronisation in CO systems, it can be expected that a special header is no longer needed. For systems employing pilot symbols for CE the pilot symbols can also be used for frame synchronisation as well. The use of pilot symbols for CE and frame synchronisation will be investigated in Chapter 5.

2.2.5 Channel Estimation

After CD compensation, the received data need to be compensated for residual impairments, which include residual CD (caused by imperfection in the first stage compensation) and PMD. The second stage compensation is typically performed by

means of CE, where the remaining channel transfer matrix is estimated and the data signal is equalised using the estimated channel information. There are typically two approaches to CE: blind approach, which employs gradient algorithms for the estimation of channel transfer functions, and DA approach, which utilises blocks of known symbols for CE. These two approaches will be presented and discussed in the next section, along with their advantages and disadvantages.

2.2.5.1 Blind Channel Estimation

Savory et al. proposed the use of CMA for data equalisation in PM CO-SC systems in [24]. The CMA algorithm [66]-[67] is based on the fact that PM-QPSK signals only have constant amplitudes and different phases. Therefore, an adaptive algorithm can be used to solve a transfer function that minimises the variation in the equalised signals' amplitudes. The DSP procedure at the receiver consists of two-stage equaliser, where the first stage is a FIR equaliser used to compensate for CD in a TDE approach. The second stage of equalisation employs four adaptive filters with very short taps to equalise the data using CMA algorithm. The channel transfer matrix is adaptively estimated by examining the data signals and adapting the filter coefficients. This is done so that the output signals' amplitudes will have only one value with minimal variations according to CMA algorithm. The maximum transmission distance for the experiment was 6400 km using two-stage equalisation approach. The complexity of CMA and the stability of the adaptive algorithm were not discussed. The CMA can also be employed for PM-16QAM modulation format and demonstrations on blind equalisation using CMA for PM-16QAM had been reported by Winzer et al. in [68], Gnauck et al. in [69] and Yamanaka et al. in [70].

Kikuchi et al. [71] analysed the CMA algorithm and showed that beside a long convergence time, blind equalisation also suffers from some stability issues, such as the singularity problem. This problem occurs when the outputs of both polarisations' transfer functions converge to a single value resulting in the algorithm failing to demultiplex the data signal. The problem is especially severe when there is polarisation dependent loss (PDL) in the transmission system, thus leads to the signals having different powers on different polarisation tributaries. A method to overcome the

singularity problem of CMA was proposed by Liu et al. in [72]. By pre-configuring the CMA filter, Liu et al. demonstrated that the singularity problem can be avoided.

In the design of CO-OFDM systems, after the introduction of frequency domain CD compensation for reducing the amount of CP symbols used in a single CO-OFDM block, the use of adaptive blind equalisation was also introduced to CO-OFDM systems to remove the training symbols used for CE. This approach was demonstrated by Sano et al. in [14], in which an overhead-free CO-OFDM system was demonstrated without any CP blocks or training symbols. As previously described, the DSP procedure consists of first stage CD equalisation using fixed size CD compensation based on OFDE. As the conventional CO-OFDM modulates the data symbol in frequency domain; in the second stage, the signal is transformed into frequency domain by means of FFT, and equalisation is performed using blind adaptive CMA algorithm. This approach allows a large amount of CD compensation and residual impairment compensation, instead of relying on CP blocks for CD and PMD tolerance as in the traditional CO-OFDM approach. A transmission distance of 3600 km was demonstrated for overhead-free CO-OFDM using adaptive blind channel equalisation based on CMA.

2.2.5.2 Data-Aided Channel Estimation and Equalisation

Following the introduction of blind CE for demultiplexing of CO-SC systems, DA-CE was demonstrated using TSs for CE and equalisation [29]-[30], [55]-[56], [73]. The TSs, also called pilot symbols, are used for CE and subsequent equalisation of data can be performed based on CE provided by TSs. The method typically works as follow: first two orthogonal sequences S_1 and S_2 are chosen, and then four TSs are designed in a space-time structure similar to the wireless techniques proposed in [74]-[76]. The structure is illustrated in Figure 2.6:

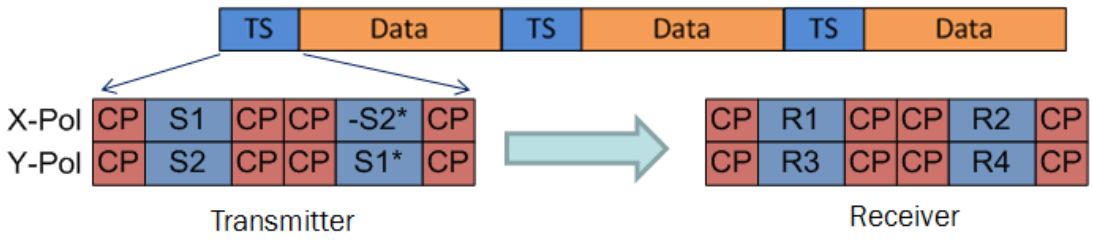

Figure 2.6: TS structure for DA-CE.

where S_1 and S_2 are the two original TSs, R_1-R_4 denote the copies of the TSs at the receiver after transmission and $(.)^*$ denotes the complex conjugate of the sequence (.). Typically small CP blocks are added between TSs within a block to prevent interferences between TSs due to residual impairments. After CD compensation, the location of the TSs can be identified using the timing method described in Section 2.2.4.2 and the TSs can be extracted. In frequency domain, the received TSs can be viewed as a multiplication of the original TS matrix with the channel transfer function as:

$$\begin{pmatrix} R_1[k] & R_2[k] \\ R_3[k] & R_4[k] \end{pmatrix} = \begin{pmatrix} H_{xx}[k] & H_{yx}[k] \\ H_{xy}[k] & H_{yy}[k] \end{pmatrix} \begin{pmatrix} S_1[k] & -S_2[k]^* \\ S_2[k] & S_1[k]^* \end{pmatrix} + \begin{pmatrix} N_x[k] \\ N_y[k] \end{pmatrix} \tag{2.9}$$

Using Equation 2.9, the channel transfer matrix can be estimated as:

$$H[k] = \begin{pmatrix} H_{xx}[k] & H_{yx}[k] \\ H_{xy}[k] & H_{yy}[k] \end{pmatrix} \approx \begin{pmatrix} R_1[k] & R_2[k] \\ R_3[k] & R_4[k] \end{pmatrix} \begin{pmatrix} S_1[k] & -S_2[k]^* \\ S_2[k] & S_1[k]^* \end{pmatrix}^{-1} \tag{2.10}$$

where $R_1[k]$-$R_4[k]$ are the FFTs of the received sequences; $N_x[k]$ and $N_y[k]$ are noise components in frequency domain and $H_{xx}[k]$, $H_{yy}[k]$, $H_{yx}[k]$, $H_{xy}[k]$ are the discrete frequency domain channel transfer functions.

Kuschnerov et al. [73] analysed the difference between different blind estimation algorithms and DA-CE methods. The CAZAC sequences were used in DA-CE in conjunction with different detection algorithms. The paper found that traditional blind estimation method typically has slow convergence speed and a small performance penalty compared to DA-CE in conjunction with minimum mean squared error (MMSE) detection method. The OSNR penalty for using blind estimation method is approximately 0.7 dB higher compared to DA-CE with MMSE. Parallelisation of CMA significantly reduces the number of symbols used for CMA convergence however it is demonstrated that OSNR penalty is higher when CMA is used with parallelisation. The paper also suggested that, in order to achieve a reasonable overhead ratio of DA-CE, prior CD compensation is necessary. This can be easily explained as DA-CE also has a limited amount of memory to cover the channel impulse response. Thus CD needs to be first compensated as a large amount of CD will generate a long channel impulse

response exceeding the estimation capability of either DA or blind CE. The overhead ratio for DA-CE and the respective estimation performance was not discussed in the paper. In general, it can be seen that traditional blind equalisation typically suffers from high complexity and slow convergence speed, as well as low equalisation performance. For data-aided equalisation, while there is a small trade-off in term of bandwidth efficiency, this is made up by higher equalisation performance compared to blind methods.

A widely used approach for enhancing DA-CE is to repeat the TSs multiple times to obtain an estimated channel transfer function based on averaging multiple estimations. Elschner et al. demonstrated DA-CE in [77] using an average of 10 blocks of 16-symbol CAZAC sequences. This approach improves estimation performance at the cost of increasing overhead ratio and thus is not desirable for practical implementation of DA-CE. Spinnler et al. [78] demonstrated a DSP approach for improving CE performance by performing moving average filter (MAF) operation over estimated channel transfer functions. The main drawback of using MAF is that the method will also average out the residual channel impairments contained in the estimated channel transfer function, thus these need to be removed before filtering and added back after. The TSs used were CAZAC sequences and different performances based on different TS lengths are demonstrated. For a single block of TS, a longer block with longer TS length gives better performance at the cost of increasing overhead ratio. Thus there is a trade-off between equalisation performance of DA CO systems and the required overhead ratio. The subject of overhead ratio and equalisation performance will be investigated in details in Chapter 5.

While the concept of DA-CE was introduced to CO-SC-FDE system after the demonstration of traditional blind adaptive algorithms such as CMA, for CO-OFDM systems, the process is inverted when traditional CO-OFDM systems are designed with training symbols for CE and blind adaptive algorithms were introduced after traditional DA-CE methods. Regardless of the approaches used for CE, the data can be equalised using the estimated channel transfer functions and the carrier phase can then be recovered using the popular m^{th} power feed-forward carrier recovery method [79]-[81]. The m^{th} power carrier recovery scheme can be described as follows: the method first removes data modulation by raising the signal to m^{th} power (with m being a number

depending on the modulation format) and the remaining carrier phase can then be estimated. It can be seen that this method is best suited for phase shift keying (PSK) signal and the modulation can be removed without using any pilot symbols [81]. A different method for carrier phase recovery, namely data-aided maximum likelihood (DAML) carrier recovery, was also proposed by Kam in [82] and utilise pilot symbols for initialisation of a maximum-likelihood estimation scheme for carrier phase recovery. Since the scheme relies on pilot symbols, it is more suitable for systems with DA-CE as the TSs can be employed as pilot symbols. An advantage of DAML is that the scheme does not rely on the modulation format of the signal, and can be employed for any arbitrary modulation formats.

2.2.5.3 Training Sequences for Data-Aided Channel Estimation

Section 2.2.5.2 reviewed the use of TSs for CE in CO systems. In theory, sequences with flat power spectrum will provide the best estimation performance and as such are widely used in many CE schemes. However, in CO-SC-FDE transmission, due to the transmitter data consisting of only binary modulation, sequences with binary structures are also desirable as the sequences can be generated by binary modulators instead of high resolution digital to analogue converters (DACs).

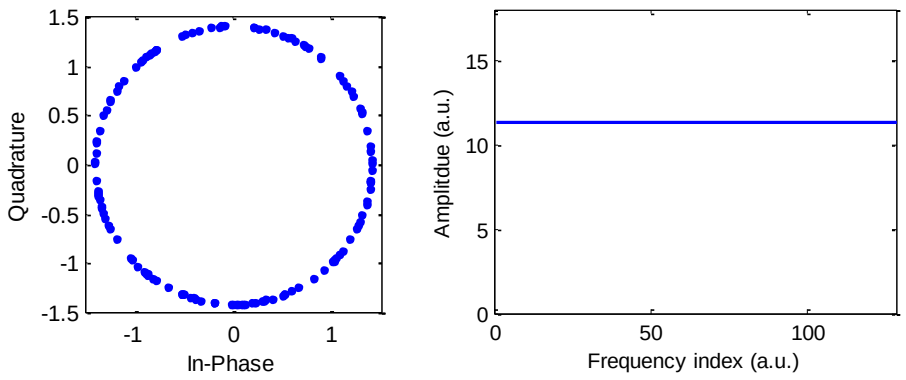

(a) *(b)*

Figure 2.7: (*a*) *Chu sequence constellation and* (*b*) *Chu sequence spectrum*

CAZAC sequences had been proposed for CE in CO-SC-FDE system [55]-[56] and also in CO-OFDM [3] systems, where the Chu sequence [83]-[84], a well-known CAZAC sequence, had been employed for CE. Chu sequence has ideal spectrum property: its

spectrum is constant in frequency domain and thus is ideal for CE purpose. However, Chu sequence had very complex constellation as illustrated in Figure 2.7(a) in time domain and a high resolution DAC is required for the generation of Chu sequence.
The spectrum of Chu sequence is shown in Figure 2.7(b) and it can be seen that the spectrum is flat in frequency domain, enabling accurate CE. For DA-CE estimation, a Chu sequence can be used as the S_1 sequence and the S_2 sequence is generated by shifting the original S_1 sequence as demonstrated in [55], resulting in a new Chu sequence orthogonal to the original sequence. However, the complex constellation of Chu sequence is an unattractive feature for implementation in CO-SC-FDE systems, where simple signal constellation in the transmitter is normally an advantage. Pittala et al. proposed the use of minimum-phase CAZAC (MP-CAZAC) sequences with 16-symbol length in [55]. Compared to the standard Chu sequence, the MP-CAZAC sequence has QPSK constellation when the sequence is 16-symbol long. While this design solved the complex constellation problem, its drawback is the restriction of the TSs being very short in terms of length and potentially limits CE and equalisation performance of DA-CE method. The relationship between total CD tolerance, system performance and TS lengths will be investigated in Chapter 3 and Chapter 5 respectively.

Li et al. reported the use of m-sequence for demonstration of CO-SC-FDE transmission in [29]. M-sequence possesses special "near ideal" spectrum property: the sequence spectrum is flat at all frequencies except at DC. The training structure used by Li et al. is demonstrated in Figure 2.8 and can be generalised for DA-CE using single TS. It can be seen that compared to the general training structure, an m-sequence is used as S_1 and a zero sequence is used as S_2. However, m-sequence can only be generated at odd length of 2^n-1 and thus does not match the use of FDE where the FFT size is normally at even length of 2^n. Due to this reason an interpolation step is required to translate the estimated channel resolution from 2^n-1 to 2^n. Li et al. mentioned the advantage of m-sequence: the sequence is binary and thus can be generated by pulse pattern generator instead of high resolution DAC. The m-sequence length used in the paper was 127 symbols.

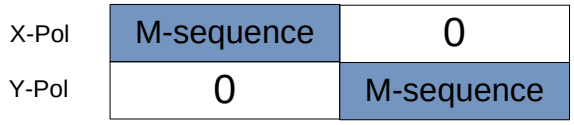

Figure 2.8: Training structure using m-sequence.

Another type of sequences that can be used for CE is Golay sequences [85]-[86]. Golay sequences are two sequences that form one complementary pair as proposed by Golay in [85]. The complementary property of Golay sequences can be expressed as follows: let *xcorr*(*a*[*n*]) denotes the autocorrelation function (ACF) of sequence *a*[*n*] then:

$$xcorr(a[n]) + xcorr(b[n]) = 2N_{ts}\delta(n) \tag{2.11}$$

where $\delta(n)$ is the Dirac delta function; *a*[*n*] and *b*[*n*] are the two Golay sequences and N_{ts} is the sequence length.

Equation 2.11 illustrates that the sum of the autocorrelation of *a*[*n*] and *b*[*n*] is an impulse function. By taking the discrete Fourier transform (DFT) of Equation 2.11, Golay property can be derived in frequency domain as having complementary power spectra:

$$|A[k]|^2 + |B[k]|^2 = 2N_{ts} \tag{2.12}$$

where *A*[*k*] and *B*[*k*] are the FFTs of *a*[*n*] and *b*[*n*].

Figure 2.9 demonstrates the property of Golay sequences. The autocorrelation of each sequence is shown in Figure 2.9(a) and the sum of their autocorrelation is shown in Figure 2.9(b). It can be seen that in the case of individual ACFs, each sequence yields a high peak in the middle of ACF and opposite ACF components outside the peak. This results in a combination of one single peak in the middle of the combined ACF and zero everywhere else when the ACFs are combined. Golay property in frequency domain is shown in Figures 2.9(c) and (d). In the case of individual power spectrum, at every spectral component, the PS of one sequence is symmetric to the PS of the other sequence over a linear line. This makes the sum of the PSs of "*a*" and "*b*" Golay sequences become a linear flat power spectrum in frequency domain. Golay sequences can be generated recursively for any arbitrary 2^n length and still maintain binary

constellation. However the seed sequence in [85] is of binary phase shift keying (BPSK) format and is not suitable for PM-QPSK or PM-16QAM in CO systems. Holzmann et al. outlined a few special properties used to construct different Golay pairs from original pair in [86]. By applying these properties, it can be seen that if S_1 and S_2 are two Golay sequences, then S_1^* and S_2, S_1 and $-S_2^*$, S_1^* and $-S_2^*$ also form three complementary Golay pairs. The format used in the paper was complex Golay sequences in which each symbol takes either real values without imaginary components or complex values without any real components.

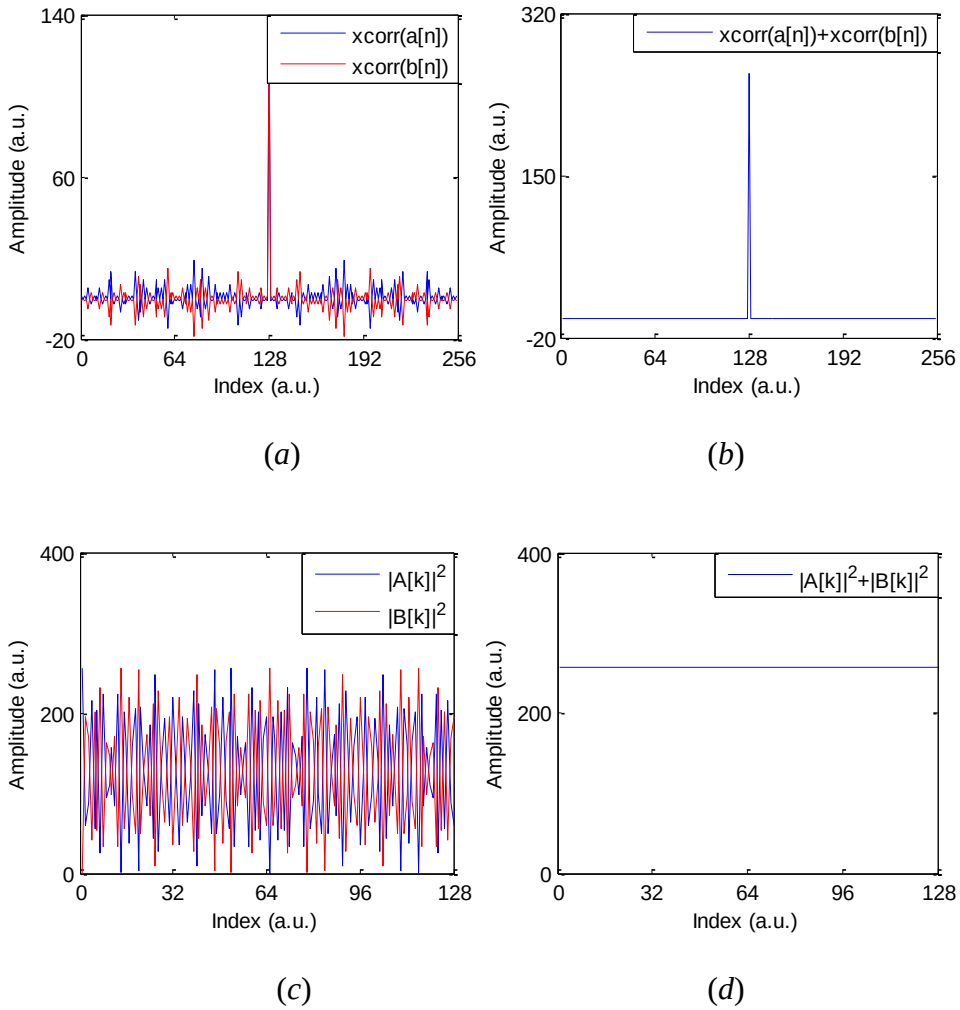

Figure 2.9: (*a*) *Autocorrelation of Golay "a" and "b" sequence;* (*b*) *Sum of their autocorrelation;* (*c*) *Power spectrum of Golay "a" and "b" sequence;* (*d*) *Sum of their power spectrum.*

Zoltowshi et al. [87] proposed the use of Golay sequence CE in a 2x2 multiple-input

multiple-output (MIMO) OFDM wireless system. The design of the CE matrix is similar to the one illustrated in Figure 2.6 with S_1 and S_2 being the two complementary Golay sequences. The paper also noted the formation of four Golay pairs when arranging two Golay sequences according to the structure in Figure 2.6 due to Golay properties as explained above. As Golay sequences possess both length-independent constellation and special spectrum property, it is more advantageous than CAZAC sequences when using long sequences for CE in a CO system, and the sequence can also be customised to fit PM-QPSK and PM-16QAM modulation formats for easy integration into commercial modulators. The design of Golay sequences for DA-CE in CO systems will be discussed in Chapters 3, 4 and 5 of this thesis.

2.3 OPTICAL PERFORMANCE MONITORING

OPM is also an important part of future CO network designs. As the signal travels through the optical channel and acquires different channel impairments, the quality of the signal and the amount of impairments accumulated during transmission need to be monitored for network quality and fault detection. There are typically a few parameters that need to be monitored in optical transmission. The first key parameter is OSNR, which represents the amount of noise accumulated in the signal and thus defines the received signal quality. As there is no known method for compensation of accumulated noise in the signal after transmission, monitoring of OSNR will likely be a critical part of OPM in the near future and monitoring of this parameter has also gained many research interests [88]-[126]. While residual CD is a static impairment that does not change over time, DGD is a fast varying impairment and thus monitoring of DGD is very desirable to ensure network stability [127]-[138]. Recent proposed techniques for estimation of these two parameters will be presented in the next section.

2.3.1 Optical Signal-to-Noise Ratio Estimation

Many techniques can be employed for OSNR estimation. These include techniques based on linear interpolation [88], polarisation nulling [89]-[94], Stokes vectors [95]-[98], non-linear optical effects [99]-[101], interferometer [102]-[105], beat noise analysis [106]-[118], optical amplifiers' conditions [119]-[120], or analysing the signal-

to-noise ratio (SNR) using coherent receiver for OSNR estimation [121]-[126]. These techniques are presented in the next section.

2.3.1.1 Non-coherent OSNR Estimation Techniques

OSNR estimation technique using linear interpolation is demonstrated in Figure 2.10 [88]. The technique estimates the power of the signal and the noise power based on the optical spectrum. The OSNR can be calculated from the noise level and the signal level measured from the optical spectrum.

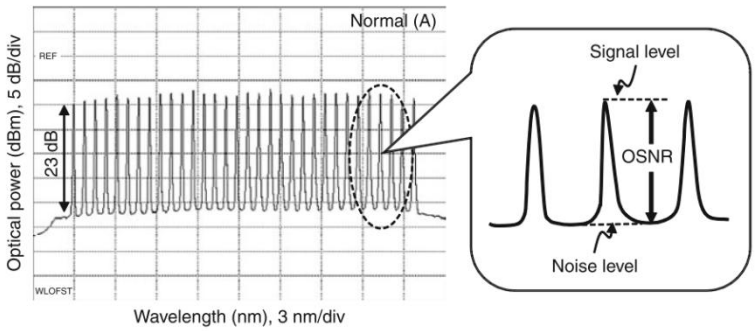

Figure 2.10: Principle of OSNR measurement using linear interpolation [*88*].

Linear interpolation technique can be explained as follows. Assuming the ASE noise having a uniform spectrum across all frequency, then the noise level does not need to be measured at the in-band signal wavelength but can be measured at an out-of-band different wavelength. The result OSNR can still be calculated from the measured in-band signal level and the out-of-band noise level. A primary potential problem of linear interpolation technique is when different channels in a wavelength division multiplexed (WDM) network generate different noise level, thus causing false OSNR estimation using out-of-band interpolation technique. For accurate OSNR estimation, measuring the in-band noise at each channel is necessary [88].

Techniques based on polarisation nulling utilise the fact that the optical noise has an even power distribution in both polarisations while the optical signal is concentrated on one polarisation [89]-[94]. Thus, in principle, if signals on both polarisations are separated then one polarisation will contain both the signal and noise power while the other polarisation will only contain noise power.

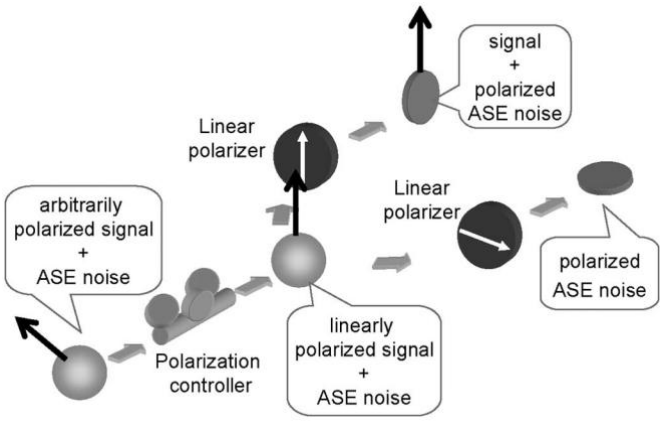

Figure 2.11: Principle of OSNR estimation using polarisation-nulling technique [*89*].

Figure 2.11 demonstrates the principle of OSNR estimation using polarisation nulling techniques. The signal is passed through a polarisation controller to become linearly polarised with signal plus noise on one polarisation and only noise on the orthogonal polarisation. The signal is then split into two components by two orthogonal linear polarisers. It can be shown that:

$$OSNR = \frac{P_x - P_y}{2P_y}\left(\frac{B_n}{B_r}\right) \tag{2.13}$$

where P_x and P_y are the power of the signal plus noise polarisation component and the noise only polarisation component, respectively. B_n is the noise equivalent bandwidth while B_r is the resolution bandwidth. Since OSNR is derived from the noise within the channel, the technique can measure the actual OSNR within the channel bandwidth (in-band OSNR). However, as polarisation nulling utilises two polarisation components of the signal for OSNR estimation, the drawbacks of the technique include degradation due to PMD and polarisation-dependent loss (PDL). Lee et al. proposed an improved method for polarisation nulling technique in [91]. The technique was designed to provide extra calibration in the case of signal leak from P_x into P_y due to PMD by using an additional optical band-pass filter (OBPF). The technique can be explained as follow: since P_y now contains noise with some signal power, the signal is further split into two equal parts, denoted P_{y1} and P_{y2}. The P_{y2} component is then fed into an OBPF to reduce the noise bandwidth thus produce a calibration point for correctly estimating the amount

of signal leaked into the P_y component. The OSNR can then be estimated from P_x, P_{y1} and P_{y2}.

Although the improved technique in [91] can accurately measure OSNR in the event of signal leak from one polarisation to another, it requires precise alignment of two tunable filters [93]. Cheung et al. proposed a different improved technique based on polarisation nulling using only one OBPF [94]. The technique measures two polarisation components at different frequencies within the entire signal spectrum: at the centre and at the slope of the entire signal spectrum. This technique provides another method for calibrating the amount of power transferred between two polarisation components that caused degradation in OSNR measurement. The technique was demonstrated in [94] to be able to estimate OSNR with an estimation error of 1.5 dB, where the conventional polarisation nulling technique obtained an error of 3 dB [90].

While polarisation-nulling technique provides an accurate way for estimation of OSNR, the technique heavily relies on the fact that signal's power is concentrated on one polarisation while the other polarisation only contains noise. This makes the technique not applicable to modern CO systems which utilise polarisation multiplexing for signal transmission on both polarisation components. For in-band OSNR estimation for high-order modulation formats such as PM-QPSK and PM-16QAM, different techniques need to be employed.

Another group of techniques for OSNR estimation based on polarisation is by utilising Stokes parameters [95]-[98]. The method was proposed by Peterson et al. in [95]-[96] and utilised degree of polarisation (DOP), one of the Stokes parameters, for OSNR estimation. The OSNR can be estimated as:

$$OSNR = \frac{DOP}{1 - DOP}\left(\frac{B_n}{B_r}\right) \tag{2.14}$$

where B_n and B_r are the noise-equivalent and resolution bandwidth, respectively. Since Stokes parameters can reveal the polarisation state of the signal, technique based on Stokes parameters can identify the degradation effects caused by PMD. Skold et al. proposed a method for accurate measurement of OSNR using DOP based on measuring the amount of DOP caused by PMD using spectral state of polarisation (SOP) in [97].

After estimation of DOP caused by PMD, the DOP caused by OSNR can be estimated and the correct OSNR value can be calculated in the presence of PMD. However, the accuracy of OSNR estimation based on DOP becomes more sensitive to DOP estimation error as the OSNR increases. Thus, accurate estimation of DOP is required for OSNR estimation techniques based on DOP [88]. Lu et al. proposed an enhancement for OSNR estimation based on DOP in the presence of high OSNR using off-centre filtering [98]. The technique can be described as follow: by filtering an off-centre part of the entire signal spectrum, the signal power will be significantly smaller while the noise power stays the same. A different calibration factor from DOP to OSNR is then used resulting in OSNR estimations that are less sensitive to DOP estimation error in the high OSNR region. The technique was demonstrated in experiments to be able to improve sensitivity by 0.63%/dB for 10-Gb/s return-to-zero on-off keying (RZ-OOK) optical systems and 3.14 %/dB for 40-Gb/s RZ-OOK systems.

OSNR estimation can also be based on non-linear optical effects and such techniques depend on the relationship between the non-linear effect and OSNR [99]-[101]. These techniques typically employ extra fibres or optical components to generate non-linear effects associated with OSNR for the purpose of OSNR estimation.

Chen et al. proposed an OSNR monitoring technique based on cascaded four wave mixing (FWM) non-linear effects produced by OSNR in [99]. The technique employs a non-linear optical loop mirror (NOLM) as illustrated in Figure 2.12:

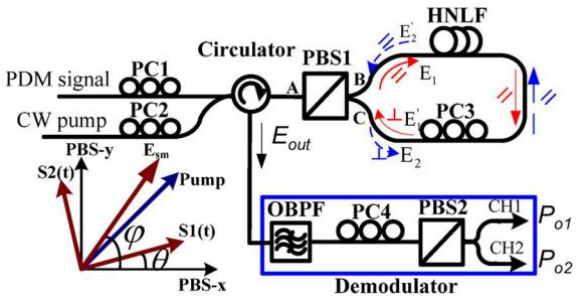

Figure 2.12: OSNR monitoring using non-linear loop mirror [*99*].

The incoming signal is passed through a polarisation beam splitter (PBS) and propagated in different directions inside the loop mirror. A highly non-linear fibre

(HLNF) is used to provide the cascaded FWM process. The output signal after FWM contains OSNR related power information and can be processed for OSNR estimation.

A similar technique was proposed by Adams et al. [100]. The technique also employs NOLM at the output port of the optical signal similar to the one in Figure 2.12. However the non-linear phenomenon used for OSNR estimation is cross phase modulation (XPM). Another different non-linear based technique was reported by Ng et al. in [101] and utilised an optical parametric amplifier together with FWM for estimation of OSNR.

A different group of techniques for OSNR estimation are techniques based on interferometer [102]-[105]. The technique is primarily based on a Mach-Zehnder delay interferometer consisting of two optical paths. The incoming optical signal is split into two paths at the interferometer and one path has an optical delay and a phase adjuster. The delay and phase of the optical signal in one path are adjusted so that the signals from two paths are combined in a destructive or constructive manner at the end of the interferometer device and a power meter is used for reading the combined signals' powers. Since the signal is assumed to be highly coherent, constructive combination will allow measurement of the signal plus noise's power at the power meter while destructive combination will allow measurement of only the noise power. The OSNR can then be calculated and the technique was found to be CD-tolerant and insensitive to polarisation effects [105].

Besides the above mentioned OSNR estimation techniques, there are many other techniques that are not based on SNR. These include beat noise analysis techniques [106]-[118], which utilise the beat noises detected at the receiver for OSNR estimation. Another group of techniques for OSNR estimation are techniques based on the operating condition of optical amplifiers [119], [120]. Since the optical noises are typically generated at the optical amplifiers, analysing the amplifiers can provide a method for estimating the total system OSNR.

With the advent of coherent receivers however, it is also possible to estimate the signal's OSNR based entirely on the receiver's DSP and captured signal's SNR. Techniques for estimation of OSNR based on coherent receiver's DSP will be presented in the next section.

2.3.1.2 OSNR Estimation Based on Coherent Receivers

Due to the ability of coherent receivers to capture both the magnitude and phase of the optical signal, a linear translation between optical and electrical domain can be obtained. Since the introduction of coherent receivers to optical communication systems, using coherent receivers for OSNR estimation has seen great research interest [121]-[126]. Since coherent receivers can only capture the electrical signal after photo detection, OSNR estimation technique based on coherent receivers needs to rely on the captured signal's SNR.

Ives et al. proposed an OSNR estimation technique based on equalised PM-QPSK signal constellation for coherent receivers in [121]. The technique consists of first equalising the received signal using CMA. The signal constellation before phase noise correction is shown in Figure 2.13(a) while the signal constellation after phase noise correction is shown in Figure 2.13(b). The technique works by estimating the width of the signal constellation ring before phase noise correction using statistics of the equalised signal. Thus only the constellation before carrier phase recovery is needed.

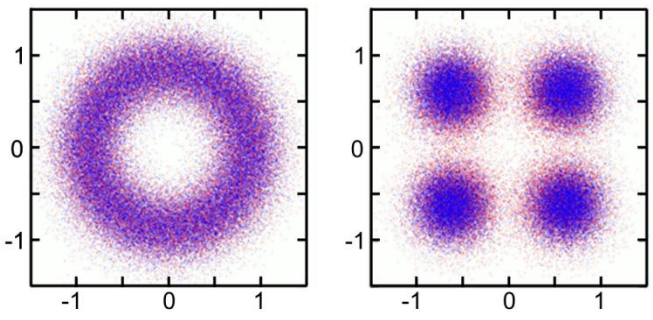

(a) *(b)*

Figure 2.13: (*a*) *Equalised signal constellation before phase correction and* (*b*) *after phase correction* [*121*].

In an ideal noise-free receiver, SNR of the equalised signal is directly related to the OSNR. The OSNR can then be estimated from the SNR by taking a reference bandwidth and system bit rate into account. Experimental demonstration showed that the receiver added extra noise into the signal. Thus, the estimated OSNR values were lower than the actual OSNR values measured by an independent optical spectrum

analyser (OSA). As a result of this, receiver noise correction for the estimated result was employed. Receiver's noise correction can be achieved by measuring SNR at a calibration point and subtracting the receiver noise from the estimated SNR before converting into OSNR. The results, after corrections, were accurate. However, the primary limitation of the method proposed by Ives et al. is that the statistical methods used will only work with PM-QPSK modulation format. This limitation is imposed by the statistical method proposed by Ives et al., which assumes that the transmitted signal is in PM-QPSK format [121]. A similar technique was also demonstrated by Pittala et al. in [122] and Faruk et al. in [123].

Zhu et al. proposed an improved design of the statistical method proposed by Ives et al. in [124]. The basic concept for OSNR estimation based on receiver SNR remains the same. However, the improved statistical method can estimate SNR in both PM-QPSK and PM-16QAM modulation formats by measuring the width of multiple rings generated by the equalised signal. The method was demonstrated for PM-QPSK and PM-16QAM modulation formats with an accuracy of 0.5 dB. The same receiver noise calibration technique was also employed for OSNR estimation. Both DA-CE and blind approaches for signal equalisation are demonstrated. The estimation performances are similar between the two approaches.

Schmogrow et al. proposed a different version of OSNR estimation based on SNR in [125]. The technique can be summarised as follow: assuming all impairments are compensated, the received signal's constellation consists of the signal with added noise components. The distance between the actual received signal constellation points versus the ideal constellation points are generated by noise and can be used as a tool for OSNR estimation. The error vector magnitude (EVM), a quantity used to estimate the average distance between the equalised symbols versus the ideal symbols, is dependent on the signal's OSNR and can be used for OSNR estimation similar to the ring width measurement (statistical method) approach proposed by Ives et al. in [121]. Compared to statistical methods, EVM method requires phase noise compensation. However, EVM method provides a single estimation approach that works with all modulation formats. Dong et al. proposed an improved version for OSNR estimation using coherent detection in [126] with non-linearity tolerance, the first stage estimation still utilised SNR and EVM. However, the non-linear noise is correlated to each other due to the fact

that they are induced by CD during transmission, thus the non-linear noise can be calibrated according to the transmission characteristics. The technique was demonstrated to be able to estimate OSNR accurately in the event of non-linear noise provided that the transmission configuration is known.

All OSNR estimation approaches for coherent receivers exhibit similar design pattern: the captured signal is first equalised, either by DA or NDA equaliser and the SNR is estimated from the signal constellation before phase noise correction using statistical methods, or after phase noise correction using EVM. One drawback of these approaches, however, is the requirement of the data signal to be equalised first. Due to this, the choice of equaliser used for actual data equalisation and noise-aware equaliser is limited. While the noise information must be known for computing, the equaliser coefficients cannot be employed for systems with OSNR estimation capability without some types of feedback loop, in which the estimated SNR information is fed back to the equaliser for second time equalisation. A separate OSNR estimation block will solve this problem resulting in DA OSNR estimation for coherent receivers. The subject of DA OSNR estimation is investigated in Chapters 4 and 6 of this thesis.

2.3.2 Differential Group Delay Estimation

DGD is characterised by the delay between signals travelling on two polarisation axes. DGD causes PMD and is a dynamic effect that changes with time. This contradicts to CD, which is a static effect that only depends on transmission length. Since DGD is a time-variant impairment, estimation of this parameter needs to be done at a repeated frequency during transmission, and monitoring of this parameter from coherent receivers is also considered important for OPM. Various techniques for DGD estimation have also been proposed [52]-[56], [127]-[138]. These include techniques based on channel transfer functions [52]-[56], [127], OFDM's spectrum property [128], RF tones [129]-[134], eye pattern monitoring [135]-[137], and frequency resolved SOP rotation [138]. Techniques based on coherent receivers have received the most research interest as the estimation can be carried out purely using DSP from the captured signal.

2.3.2.1 DGD Estimation Based on Coherent Receiver's DSP

Hauske et al. proposed the technique for DGD estimation using coherent receivers and captured signal in [52], [127]. The technique is designed as an integrated part of the receiver's DSP and utilises the estimated channel transfer functions. Assuming the channel transfer function is successfully estimated from the captured signal, then after CD estimation, the DGD matrix can be obtained by dividing the channel transfer matrix with the estimated CD transfer function. After CD separation, the DGD matrix can be expressed as [120]:

$$H_{DGD}(f) = \begin{bmatrix} u^*(f) & -v(f) \\ v^*(f) & u(f) \end{bmatrix} \tag{2.15}$$

where $H_{DGD}(f)$ denotes the DGD matrix and $u(f)$, $v(f)$ are the components inside the DGD matrix. The DGD transfer function in frequency domain can be estimated as:

$$\tau(f) = 2\sqrt{u_f(f)u^*{}_f(f) + v_f(f)v^*{}_f(f)} \tag{2.16}$$

where $\tau(f)$ denotes the DGD transfer function and the subscripted index f denotes the derivation with respect to frequency. The value of DGD can then be estimated from integration over the DGD transfer function and the estimation region is limited to the central region of $\tau(f)$ for the best accuracy. The accuracy of the technique is demonstrated to be approximately 8 ps of estimation error.

Faruk et al. also demonstrated the same approach for DGD estimation from CE using coherent receivers [53]-[54]. The residual CD described in the paper was slightly large and thus training mode was first performed using TSs for residual CD estimation. This is done to prevent singularity problem from the CE using CMA. Estimation of DGD follows the design proposed by Hauske et al. as follow: small residual CD is estimated and subtracted, and DGD is estimated from the derivative of the DGD transfer matrix.

Pittala et al. proposed a variation of the DGD estimation technique based on CE in [55]-[56]. Here, CE is performed using TSs as previously described. While there is some bandwidth efficiency trade-off associated with the DA-CE approach, this approach effectively solved the singularity problem observed in the traditional blind approach while allowing a much greater tolerance to residual CD. The approach has also

improved the resolution of the estimated channel transfer matrix. DGD is estimated from the same DSP procedure proposed by Hauske et al. The estimation accuracy is shown in simulation to be approximately 8 ps.

For CO-OFDM systems, DGD estimation was demonstrated by Yi et al. in [128]. Since CO-OFDM signal is designed in frequency domain, DGD estimation is performed using the principle of frequency response amplitude change in CO-OFDM subcarriers, which is an effect caused by DGD. A 900-ps DGD emulator was used for DGD estimation demonstration. Relative error is estimated to be approximately 1%, which is equivalent to 90 ps of DGD.

In general, DGD estimation for coherent receivers is typically based on the estimated channel transfer function for coherent receivers, which leads to most research on DGD estimation method for coherent receivers based on CO-SC-FDE systems due to the ready availability of the blind CMA algorithm. However, this also indicates that DGD first needs to be compensated before being estimated. DA-CE solves this problem by providing a transparent CE solution that works with both CO-SC-FDE and CO-OFDM systems. However, blind DGD estimation using the special carrier structure of CO-OFDM systems is still not widely studied. The subject of blind DGD estimation for CO-OFDM systems will be investigated in Chapter 7 of this thesis.

2.3.2.2 Other DGD Estimation Techniques

Other techniques can be used for DGD estimation such as RF tones technique [129]-[134]. RF-based techniques typically depend on the effects of DGD on the power of the signal at a given frequency. Ishikawa et al. demonstrated the approach in [131] and the technique can be summarised as follows. By using an OBPF to filter one frequency of the electrical signal, the power of a single frequency component can be measured and this power is proportional to the amount of DGD and thus can be used for DGD estimation. Nezam et al. proposed a different technique for non-return-to-zero (NRZ) signals based on the concept of examining the RF tones for DGD estimation [132]. As an NRZ signal spectrum has no clock tones without CD, the technique utilised fibre Bragg grating to generate CD and clock tones at the receiver for DGD monitoring, the amplitude of the clock tones generated is proportional to DGD as illustrated in Figure 2.14:

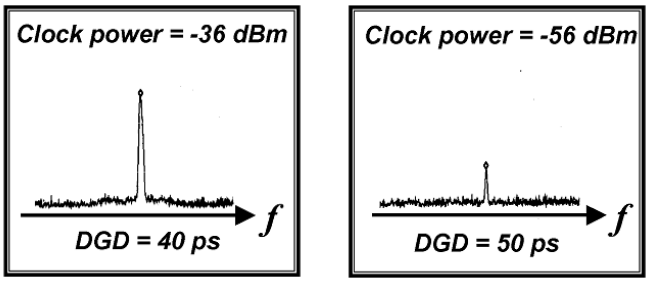

(*a*) (*b*)

Figure 2.14: DGD estimation using RF clock tone: clock power with (*a*) *DGD = 40 ps and* (*b*) *DGD = 50 ps.*

The techniques proposed in [131] and [132] both showed a periodic relationship between power (clock or frequency component) and DGD. DGD reduces the power of the RF signal up to a certain point then starts to increase the RF signal's power. This characteristic limits the estimation range of these techniques to approximately 50 ps.

Yu et al. [133] and Yang et al. [134], [135] proposed DGD estimation based on RF spectrum by utilising an FBG notch filter. The technique utilised FBG notch filter located 10 GHz away from the carrier. The FBG notch filter generates minimum power at different point in the signal's spectra and the power of these points can be used for estimation of DGD. The estimation range is shown to be up to 50 ps with different modulation formats. The accuracies of the techniques were not discussed in the papers.

Beside RF tone techniques, other techniques that are not based on channel transfer functions can also be used for estimation of DGD in optical systems. This includes eye diagram [136]-[138], and frequency resolved SOP rotation [139].

2.4 CONCLUSIONS

This chapter presented a survey of key DSP technologies for CO communication systems. Design approaches for both CO-SC-FDE and CO-OFDM systems typically include a two-stage approach where the system CD is compensated in the first stage and various DSP processes are used for the second stage compensation. In order to perform the first stage CD compensation, the system CD value must be known, thus various techniques for estimation of system CD are presented and discussed in terms of concept,

performance and complexity. A comparison of two types of techniques for second stage CE, namely NDA and DA, was presented. Compared to NDA technique, DA scheme imposes a small trade-off in terms of bandwidth efficiency. Nonetheless, this trade-off is made up with various advantages of DA technique, including fast, accurate and robust performance in CE. The use of DA technique for CE is very attractive in the design of future high speed CO communication networks.

This chapter also presented a review of OPM schemes for optical networks, including OSNR and DGD monitoring. For OSNR estimation, schemes that are based on coherent receivers typically rely on the estimation of equalised signal's SNR. The approach of each scheme was discussed to show the differences and enhancements between each technique. For DGD estimation, most schemes based on coherent receivers follow the same approach where DGD is estimated from the estimated channel transfer matrix and is primarily designed for CO-SC-FDE systems. Very little research focus had been given to DGD estimation for CO-OFDM systems, and DGD estimation for CO-OFDM are primarily based on analysing subcarrier's amplitude in frequency domain.

2.5 REFERENCES

[1] W. Shieh, and C. Athaudage, "Coherent optical orthogonal frequency division multiplexing," *Electronics Letters*, vol. 42, no. 10, pp. 587–589, May 2006.

[2] W. Shieh, W. Chen, and R. S. Tucker, "Polarisation mode dispersion mitigation in coherent optical orthogonal frequency division multiplexed systems," *Electronics Letters*, vol. 42, no. 17, pp. 996–997, 2006.

[3] W. Shieh, X. Yi, Y. Ma, and Q. Yang, "Coherent optical OFDM: has its time come?" *Journal of Optical Networking*, vol. 7, no. 3, pp. 234-253, Mar. 2008.

[4] W. Shieh, X. Yi, and Y. Tang, "Transmission experiment of multi-gigabit coherent optical OFDM systems over 1000 km SSMF fibre," *Electronics Letters*, vol. 43, 183–185, Feb. 2007.

[5] W. Shieh, H. Bao, and Y. Tang, "Coherent optical OFDM: theory and design," *Optics Express*, vol.16, no.2, pp. 841-859, Jan. 2008.

[6] Y. Tang, Y. Ma, and W. Shieh, "107 Gb/s CO-OFDM transmission with inline chromatic dispersion compensation," *Optical Fibre Communication Conference OFC'09*, paper OWW3, San Diego, CA, USA, Mar. 2009.

[7] S. L. Jansen, I. Morita, N. Takeda, and H. Tanaka, "20-Gb/s OFDM transmission over 4,160-km SSMF enabled by RF-pilot tone phase noise compensation," *Optical Fibre Communication Conference OFC* 2007, paper PDP15, Anaheim, CA, USA 2007.

[8] I.B. Djordjevic, and B. Vasic, "Orthogonal frequency division multiplexing for high speed optical transmission," *Optics Express*, vol. 14, no. 9, pp. 3767-3775, May 2006.

[9] J. Armstrong, "OFDM for Optical Communications," *Journal of Lightwave Technology*, vol. 27, no. 3, pp. 189-204, Feb. 2009.

[10] A. J. Lowery, L. Du, and J. Arnstrong , "Orthogonal frequency division multiplexing for adaptive dispersion compensation in long haul WDM systems," *Optical Fibre Communication Conference OFC* 2006, paper PDP39, Anaheim, California, USA, Mar. 2006.

[11] X. Liu, S. Chandrasekhar, B. Zhu, P. J. Winzer, A. H. Gnauck, and D. W. Peckham, "Transmission of a 448-Gb/s reduced-guard-interval CO-OFDM signal with a 60-GHz optical bandwidth over 2000 km of ULAF and five 80-GHz-grid ROADMs," *Optical Fibre Communication Conference OFC'2010*, paper PDPC2, San Diego, CA, USA, 2010.

[12] X. Liu, S. Chandrasekhar, B. Zhu, P. J. Winzer, A. H. Gnauck, D. W. Peckham, "448-Gb/s Reduced-Guard-Interval CO-OFDM Transmission Over 2000 km of Ultra-Large-Area Fibre and Five 80-GHz-Grid ROADMs," *Journal of Lightwave Technology*, vol. 29, no. 4, Feb. 2010.

[13] A.Sano, Y. Takatori, and Y. Miyamoto, "No-guard-interval coherent optical OFDM for 100-Gb/s/ch long-haul transmission systems," *Optical Fibre Communication Conference OFC'09*, paper OTuO3, San Diego, USA, 2009.

[14] A. Sano et al., "No-guard-interval coherent optical OFDM for 100-Gb/s long-haul WDM transmission (invited)," *Journal of Lightwave Technology*, vol. 27, no. 16, pp. 3705-3713, Aug. 2009.

[15] Y. Miyamoto and S. Suzuki, "Advanced optical modulation and multiplexing technologies for high-capacity OTN based on 100 Gb/s channel and beyond," *IEEE Communication Magazine*, vol. 48, no. 3, pp. 65-72, Mar. 2010.

[16] S. Chandrasekhar, X. Liu, B. Zhu, and D. W. Peckham, "Transmission of 1.2-Tb/s 24-carrier no-guard-interval coherent OFDM superchannel over 7200-km of ultra-large-area fibre," *European Conference on Optical Communication ECOC'09*, paper PD2.6, Vienna, Austria, 2009.

[17] C. Chen, Q. Zhuge, and D. Plant, "Zero-guard-interval coherent optical OFDM with overlap frequency-domain CD and PMD equalisation," *Optics Express*, vol. 19, no. 8, pp. 7451-7467, Apr. 2011.

[18] H. Sun, K.-T. Wu, and K. Roberts, "Real-time measurements of a 40 Gb/s coherent system," *Optics Express*, vol. 16, no. 2, pp.873 -879, Jan. 2008.

[19] O. B. Pardo , J. Renaudier , H. Mardoyan , P. Tran , G. Charlet, and S. Bigo, "Investigation of design options for overlaying 40 Gb/s coherent PDM-QPSK channels over a 10 Gb/s system infrastructure," *Optical Fibre Communication Conference OFC'2008*, pp. 1-3, San Diego, CA, USA, 2008.

[20] T. J. Xia, G. Wellbrock, D. Peterson, W. Lee, M. Pollock, B. Basch, D. Chen, M. Freiberger, M. Alfiad, H. de Waardt, M. Kuschnerov, B. Lankl, T. Wuth, E. D. Schmidt, B. Spinnler, C. J. Weiske, E. de Man, C. Xie, D. van den Borne, M. Finkenzeller, S. Spaelter, M. Rehman, J. Behel, M. Chbat, and J. Stachowiak, "Multi-rate (111-Gb/s, 2x43-Gb/s, and 8x10.7-Gb/s) transmission at 50- GHz channel spacing over 1040-km field-deployed fibre," *European Conference on Optical Communication ECOC'2008*, pp. 1-4, Brussels, Belgium, 2008.

[21] S. J. Savory, "Digital filters for coherent optical receivers," *Optics Express*, vol. 16, no. 2, pp. 804-817, Jan. 2008.

[22] S. J. Savory, G. Gavioli, R. I. Killey, and P. Bayvel, "Electronic compensation of chromatic dispersion using a digital coherent receiver," *Optics Express*, vol. 15, no. 5, 2120–2126, Mar. 2007.

[23] S. J. Savory, “Compensation of fibre impairments in digital coherent systems,” *European Conference on Optical Communication ECOC'2008*, paper Mo.3.D.1, Brussels, Belgium, 2008.

[24] S. J. Savory, G. Gavioli, R.I. Killey, P. Bayvel, "Transmission of 42.8Gbit/s Polarisation Multiplexed NRZ-QPSK over 6400km of Standard Fibre with no Optical Dispersion Compensation," *Optical Fibre Communication Conference OFC'*2007, paper OTuA1, Anaheim, CA, USA, 2007.

[25] C. R. S. Fludger, T. Duthel , D. van den Borne , C. Schulien , E.-D. Schmidt, T. Wuth , J. Geyer , E. De Man , G.-D. Khoe, and H. de Waardt, "Coherent equalisation and POLMUX-RZ-DQPSK for robust 100-GE transmission,” *Journal of Lightwave Technology*, vol. 26, no. 1, pp.64 -72, Jan. 2008.

[26] T. Duthel , C. Fludger , C. Schulien , D. van den Borne , G.-D. Khoe , H. d. Waardt , E.-D. Schmidt , E. d. Man and T. Wuth "Impairment tolerance of 111 Gbit/s POLMUX-RZ-DQPSK using a reduced complexity coherent receiver with a T-spaced equaliser,” *European Conference on Optical Communication ECOC’2007*, pp.53 -54, Berlin, Germany, 2007.

[27] V. Curri , P. Poggiolini , A. Carena, and F. Forghieri, "Dispersion compensation and mitigation of nonlinear effects in 111-Gb/s WDM coherent PM-QPSK systems," *IEEE Photonics Technology Letters*, vol. 20, no. 17, pp.1473 -1475, Sep. 2008.

[28] M. S. Alfiad , D. van den Borne , S. Jansen , T. Wuth , M. Kuschnerov , A. Napoli, and H. de Waardt, “111-Gb/s POLMUX-RZ-DQPSK Transmission over LEAF: Optical Versus Electrical Dispersion Compensation,” *Optical Fibre Communication Conference OFC’2009*, pp. 1-3, San Diego, CA, USA, 2009.

[29] J. Li, C. Zhao, S. Zhang, F. Zhang, and Z. Chen, "Experimental Demonstration of 120-Gb/s PDM CO-SCFDE Transmission Over 317-km SSMF,” *IEEE Photonics Technology Letters*, vol. 22, no. 24, pp. 1814-1816, Dec. 2010.

[30] J. Li , S. Zhang , F. Zhang and Z. Chen, "Comparison of transmission performances for CO-SCFDE and CO-OFDM systems,” *IEEE Photonics Technology Letters*, vol. 22, no. 14, pp. 1054-1056, Jul. 2010.

[31] K. Ishihara, T. Kobayashi, R. Kudo, Y. Takatori, A. Sano, E. Yamada, H. Masuda, and Y. Miyamoto, “Frequency-domain equalisation for optical transmission systems,” *Electronics Letters*, vol. 44, no. 14, pp. 870-872, Jul. 2008.

[32] K. Ishihara, T. Kobayashi, R. Kudo, Y. Takatori, A. Sano, E. Yamada, H. Masuda, M. Matsui, M. Mizoguchi, and Y. Miyamoto, “Frequency-domain equalisation without guard interval for optical transmission systems,” *Electronics Letters*, vol. 44, no. 25, pp. 1480-1482, Dec. 2008.

[33] K. Ishihara, T. Kobayashi, R. Kudo, Y. Takatori, A. Sano, and Y. Miyamoto, “Frequency-domain equalisation for coherent optical single-carrier transmission systems,” *IEICE Transactions on Communications*, vol. E92-B, no.12, pp. 3736-3743, Dec. 2009.

[34] R. Kudo, T. Kobayashi, K. Ishihara, Y. Takatori, A. Sano, E. Yamada, H. Masuda, Y. Miyamoto, and M. Mizoguchi, “Single carrier transmission with two-stage overlap frequency domain equalisation for long-haul optical systems,” *Electronics Letters*, vol. 45, no. 3, pp. 135-191, Jan. 2009.

[35] R. Kudo, T. Kobayashi, K. Ishihara, Y. Takatori, A. Sano, E. Yamada, H. Masuda, Y. Miyamoto, and M. Mizoguchi, “Two-stage overlap frequency domain equalisation for long-haul optical systems,” *Optical Fibre Communication Conference OFC’09*, paper OMT3, San Diego, CA, USA, Mar. 2009.

[36] R. Kudo, T. Kobayashi, K. Ishihara, Y. Takatori, A. Sano, and Y. Miyamoto, "Coherent Optical

Single Carrier Transmission Using Overlap Frequrency Domain Equalisation for Long-Haul Optical Systems," *Journal of Lightwave Technology*, vol. 27, no. 16, pp. 3721–3728, Aug. 2009.

[37] R. A. Soriano, F. N. Hauske, N. G. Gonzalez, and I. T. Monroy, "Chromatic dispersion estimation in digital coherent receivers," *Journal of Lightwave Technology*, vol. 29, no. 11, pp. 1627–1637, Jun. 2011.

[38] M. Kuschnerov, F. N. Hauske, K. Piyawanno, B. Spinnler, A. Napoli, and B. Lankl, "Adaptive chromatic dispersion equalisation for non-dispersion managed coherent systems," *Optical Fibre Communication Conference OFC'2009*, San Diego, CA, USA, paper OMT1, 2009.

[39] M. Kuschnerov, F. N. Hauske, K. Piyawanno, B. Spinnler, M. S. Alfiad, A. Napoli, and B. Lankl, "DSP for Coherent Single-Carrier Receivers," *Journal of Lightwave Technology*, vol. 27, no. 16, pp. 3614-3622, Aug. 2009.

[40] D. Wang, C. Lu, A. P. T. Lau, and S. He, "Adaptive chromatic dispersion compensation for coherent communication systems using delay-tap sampling technique," *IEEE Photonics Technology Letters*, vol. 23, no. 14, pp. 1016–1018, Jul. 2011.

[41] R. Borkowski, X. Zhang, D. Zibar, R. Younce, and I. T. Monroy, "Experimental demonstration of adaptive digital monitoring and compensation of chromatic dispersion for coherent DP-QPSK receiver," *Optics Express*, vol. 19, no. 26, pp. 728–735, Dec. 2011.

[42] S. M. Ranzini, E. C. Magalhães, V. B. Ribeiro, V. V. Nascimento, and J. C. R. F. Oliveira, "Accurate blind chromatic dispersion estimation in long-haul 112 Gbit/s PM-QPSK WDM coherent systems," *OSA Signal Processing in Photonics Communications SPPCom 2012*, paper SpTh2B.3, Toronto, Canada, 2012.

[43] H. Wymeersch and P. Johannisson, "Maximum-likelihood-based blind dispersion estimation for coherent optical communication," *Journal of Lightwave Technology*, vol. 30, no. 18, pp. 2976–2982, Sep. 2012.

[44] F. N. Hauske, C. Xie, Z. Zhang, C. Li, L. Li, and Q. Xiong, "Frequency domain chromatic dispersion estimation," *Optical Fibre Communication Conference OFC'2010*, paper JThA11, San Diego, CA, USA, May 2010.

[45] F. N. Hauske, Z. Zhang, C. Li, C. Xie, and Q. Xiong, "Precise, robust and least complexity CD estimation," *Optical Fibre Communication Conference OFC'2011*, paper JWA032, San Diego, CA, Mar. 2011.

[46] Q. Sui, A P. T. Lau, and C. Lu, "Fast and Robust Chromatic Dispersion Estimation Using Auto-Correlation of Signal Power Waveform for DSP-based Coherent Systems," *Optical Fibre Communication Conference OFC'2012*, pp 1-3, Los Angeles, CA, USA, Mar. 2012.

[47] Q. Sui, A. P. T. Lau, and C. Lu, "Fast and robust blind chromatic dispersion estimation using auto-correlation of signal power waveform for digital coherent systems," *Journal of Lightwave Technology*, vol. 31, no. 2, pp. 306–312, Jan. 2013.

[48] F. C. Pereira, V. N. Rozental, M. Camera, G. Bruno, and D. A. A. Mello, "Experimental Analysis of the Power Auto-Correlation-Based Chromatic Dispersion Estimation Method," *IEEE Photonics Journal*, vol. 5, no. 4, pp. 7901608, Jul. 2013.

[49] F. N. Hauske, J. Geyer, M. Kuschnerov, K. Piyawanno, T. Duthel, C. Fludger, D. van den Borne, E. Schmidt, B. Spinnler, H. de Waardt, and B. Lankl, "Optical performance monitoring from FIR filter coefficients in coherent receivers," *Optical Fibre Communication Conference OFC'2008* , paper OThW2, San Diego, CA, USA, 2008.

[50] J. C. Geyer, F. N. Hauske, C. R. S. Fludger, T. Duthel, C. Schulien, M. Kuschnerov, K.

Piyawanno, D. van den Borne, E. D. Schmidt, B. Spinnler, B. Lankl, and B. Schmauss, "Channel parameter estimation for polarisation diverse coherent receives," *IEEE Photonics Technology Letters*, vol. 20, no. 10, pp. 776–778, May. 2008.

[51] J. C. Geyer, C. R. S. Fludger, T.Duthel, C.Schulien, and B.Schmauss, "Performance monitoring using coherent receiver," *Optical Fibre Communication Conference OFC 2008*, paper OThH5, San Diego, CA, USA, 2009.

[52] F. N. Hauske, M.Kuschnerov, B.Spinnler, and B.Lankl, "Optical performance monitoring in digital coherent receivers," *Journal of Lightwave Technology*, vol. 27, no. 16, pp. 3623–3631, Jun. 2009.

[53] M. S. Faruk, Y. Mori, C. Zhang, K. Igarashi, and K. Kikuchi, "Multi-impairment monitoring from adaptive finite-impulse-response filters in a digital coherent receiver," *Optics Express*, vol. 18, no. 26, pp. 26929-26936, Dec. 2010.

[54] Md. S. Faruk, Y. Mori, C. Zhang, K. Igarashi, and K. Kikuchi, "Multi-impairments monitoring from the equaliser in a digital coherent optical receiver," *European Conference and Exhibition on Optical Communication ECOC'2010*, pp. 1-3, Torino, Italia, 2010.

[55] F. Pittala, F. N. Hauske, Y. Yabin, N. G. Gonzalez, and I. T. Monroy, "Fast and robust CD and DGD estimation based on data-aided channel estimation," *International Conference on Transparent Optical Networks ICTON'2011*, paper We.D1.5, Brussels, Stockholm, Jun. 2011.

[56] F. Pittalà, F. N. Hauske, Y. Yabin, N. G. Gonzalez, and I. T. Monroy, "Combined CD and DGD Monitoring Based on Data-Aided Channel Estimation," *Signal Processing in Photonic Communications SPPCom*'2011, pp. SPTuC3, Toronto, Canada, 2011.

[57] M. Oerder, and H. Meyr, "Digital filter and square timing recovery," *IEEE Transactions on Communications*, vol. COMM-36, no. 5, pp. 605 -612, May 1988.

[58] M. Kuschnerov , F. N. Hauske , K. Piyawanno , B. Spinnler , E.-D. Schmidt, and B. Lankl, "Joint equalisation and timing recovery for coherent fibre optic receivers," *European Conference on Optical Communication ECOC'2008*, pp. 1-2, Brussels, Belgium, 2008.

[59] M. Morelli and U. Mengali, "Feedforward frequency estimation for PSK - A tutorial review," *European Transactions on Telecommunication*, vol 9, no. 2, pp. 103-116, Mar. 1998.

[60] J. C. M. Diniz, J. C. R. F. de Oliveira, E. S. Rosa, V. B. Ribeiro, V. E. S. Parahyba, R. da Silva, E. P. da Silva, L. H. H. de Carvalho, A. F. Herbster, and A. C. Bordonalli, "Simple feed-forward wide-range frequency offset estimator for optical coherent receivers," *Optics Express*, vol. 19, no.26, pp. B323-B328, Dec. 2011.

[61] X, Zhou, X. Yang, R. Li, and K. Long, "Efficient Joint Carrier Frequency Offset and Phase Noise Compensation Scheme for High-Speed Coherent Optical OFDM Systems," *Journal of Lightwave Technology*, vol. 31, no. 11, pp. 1755–1761, Jun. 2013.

[62] T. M. Schmidl and D. C. Cox, "Robust frequency and timing synchronisation for OFDM, " *IEEE Transactions on Communications*, vol. 45,no. 12, pp. 1613 – 1621, Dec. 1997.

[63] H. Minn, V. K. Bhargava, and K. B. Letaief, " A robust timing and frequency synchronisation for OFDM systems, " *IEEE Transactions Wireless Communication*, vol. 2, no. 4, pp. 822 – 839, Jul. 2003.

[64] B. Park, H. Cheon, and C. Kang, " A novel timing estimation method for OFDM systems," *IEEE Communication Letters*, vol. 7, no. 5, pp. 239 – 241, May 2003.

[65] Y. Huang, X. Zhang, and L. Xi, "Modified Synchronisation Scheme for Coherent Optical OFDM

Systems," *Journal of Optical Communications and Networking*, vol. 5, no. 6, pp. 584-592, Jun. 2013.

[66] C. B. Papadias, and A. Paulraj, "A space-time constant modulus algorithm for SDMA systems," *IEEE 46th Vehicular Technology Conference VTS'1996*, pp. 86 -90, Atlanta, GA, USA, 1996.

[67] A. J. Paulraj, and C. B. Papadias, "Space-time processing for wireless communications," *IEEE Signal Processing Magazine*, vol. 14, no. 6, pp.49 -83, Nov. 1997.

[68] P. J. Winzer and A. H. Gnauck, "112-Gb/s polarisation-multiplexed 16-QAM on a 25-GHz WDM grid," *European Conference on Optical Communication ECOC'2008*, paper Th.3.E.5, Brussels, Belgium, 2008.

[69] A. H. Gnauck, P. J. Winzer, C. R. Doerr, and L. L. Buhl, "10 × 112-Gb/s PDM 16-QAM transmission over 630 km of fibre with 6.2-b/s/Hz spectral efficiency," *Optical Fibre Communication Conference OFC'2009*, paper PDPB8, San Diego, CA, USA, 2009.

[70] S. Yamanaka, T. Kobayashi, A. Sano, H. Masuda, E. Yoshida, Y. Miyamoto, T. Nakagawa, M. Nagatani, and H. Nosaka, "11 × 117 Gb/s PDM 16-QAM Transmission over 1440 km with a spectral efficiency of 6.4 b/s/Hz using high-speed DAC," *European Conference on Optical Communication ECOC'2010*, paper We.8.C.1, Torino, Italia, 2010.

[71] K. Kikuchi, "Performance analyses of polarisation demultiplexing based on constant-modulus algorithm in digital coherent optical receivers," *Optics Express*, vol. 19, no. 10, pp. 9868-9880, May 2011.

[72] L. Liu , Z. Tao , W. Yan , S. Oda , T. Hoshida and J. C. Rasmussen "Initial tap setup of constant modulus algorithm for polarisation de-multiplexing in optical coherent receivers," *Optical Fibre Communication Conference OFC'2009*, pp. 1-3, San Diego, CA, USA, 2009.

[73] M. Kuschnerov, M. Chouayakh, K. Piyawanno, B. Spinnler, E. de Man, P. Kainzmaier, M. S. Alfiad, A. Napoli, and B. Lankl, "Data-aided versus blind single carrier coherent receivers," *IEEE Photonics Journal*, vol. 2, no. 3, pp.387-403, Jun. 2010.

[74] S. Alamouti, "A simple transmit diversity technique for wireless communications," *IEEE Journal on Communication*, vol. 16, no. 8, pp. 1451-1458, Oct. 1998.

[75] S. D. Howard, A. R. Calderbank, and W. Moran, "A simple signal processing architecture for instantaneous radar polarimetry," *IEEE Transactions on Information Theory*, vol. 53, no. 4, pp 1282-1289, Mar. 2007.

[76] V. Tarokh, H. Jafarkhani, and A. R. Calderbank, "Space-Time Block Codes from Orthogonal Designs," *IEEE Transactions on Information Theory*, vol. 45, no. 5, pp 1456-1467, Jul. 1999.

[77] R. Elschner, F. Frey, C. Meuer, J. K. Fischer, S. Alreesh, C. Schmidt-Langhorst, L. Molle, T. Tanimura, and C. Schubert, "Experimental demonstration of a format-flexible single-carrier coherent receiver using data-aided digital signal processing," *Optics Express*, vol. 20, no. 27, pp. 28786-28791, Dec. 2012.

[78] B. Spinnler, S. Calabro, and M. Kuschnerov, "Pilot-assisted channel estimation methods for coherent receivers," *Optical Fibre Communication Conference OFC'2013*, pp 1-3, paper OW4B-3, Mar. 2013.

[79] A. J. Viterbi, and A. M. Viterbi, "Nonlinear estimation of PSK-modulated carrier phase with applications to burst digital transmission," *IEEE Transactions on Information Theory*, vol. IT-29, no. 4, pp.543 -551, Jul. 1983.

[80] E. Ip, and J. M. Kahn, "Feedforward carrier recovery for coherent optical communications,"

Journal of Lightwave Technology, vol. 25, no. 9, pp. 2675-2692, Sep. 2007.

[81] M. Kuschnerov , D. van den Borne , K. Piyawanno , F. N. Hauske , C. R. S. Fludger , T. Duthel , T. Wuth , J. C. Geyer , C. Schulien , B. Spinnler , E.-D. Schmidt, and B. Lankl, "Joint-polarisation carrier phase estimation for XPM-limited coherent polarisation-multiplexed QPSK transmission with OOK-neighbors," *European Conference on Optical Communication ECOC'2008*, pp. 1-2, Brussels, Belgium, 2008.

[82] P. Y. Kam, "Maximum likelihood carrier phase recovery for linear suppressed-carrier digital data modulations," *IEEE Transactions in Communications*, vol.34, no. 6, pp. 522–527, Jun. 1986.

[83] C. Chu, "Polyphase codes with good periodic correlation properties," *IEEE Transactions on Information Theory*, vol. 18, no. 4, pp. 531-532, Jul. 1972.

[84] J. S. Pereira, "Generalized Chu polyphase sequences," *International Conference on Telecommunications ICT*, pp. 47-52, May 2009.

[85] M. J. Golay, "Complementary series," *IRE Transactions on Information Theory*, vol. 7, no. 2, 82-87, Apr. 1961.

[86] W. H. Holzmann and H. Kharaghani, "A computer search for complex Golay sequences," *Australasian Journal of Combinatorics*, vol. 10, pp. 251-258, Apr. 1994.

[87] M. Zoltowshi, T. Qreshi, and R. Calderbank, "Complementary codes based channel estimation for MIMO-OFDM systems," *46th Annual Allerton Conference on Communication, Control, and Computing*, pp. 133-138, USA, Sept. 2008.

[88] C. K. Chan, *"Optical Performance Monitoring,"* Section 2.2, pp. 22-26, Academic Press, 2010.

[89] M. Rasztovits-Wiech, M. Danner, and W. R. Leeb, "Optical signal-to-noise ratio measurement in WDM networks using polarisation extinction," *European Conference on Optical Communication ECOC'98*, pp. 549–550, Madrid, Spain, 1998.

[90] D. K. Jung, C. H. Kim, and Y. C. Chung, "OSNR monitoring technique using polarisation-nulling method," *Optical Fibre Communication Confernce OFC'2000*, paper WK4, Baltimore, MD, 2000.

[91] J. H. Lee, D. K. Jung, C. H. Kim, and Y. C. Chung, "OSNR monitoring technique using polarisation-nulling method," *IEEE Photonics Technology Letters*, vol. 13, no. 1, pp. 88–90, Jan. 2001.

[92] J. H. Lee and Y. C. Chung, "Improved OSNR monitoring technique based on polarisation-nulling method," *Electronics Letters*, vol. 37, no. 15, pp. 972–973, Jul. 2001.

[93] J. H. Lee, H. Y. Choi, S. K. Shin, and Y. C. Chung, "A Review of the Polarisation-Nulling Technique for Monitoring Optical-Signal-to-Noise Ratio in Dynamic WDM Networks," *Journal of Lightwave Technology*, vol. 24, no. 11, pp. 4162-4171, Nov. 2006.

[94] M.-H. Cheung, L.-K. Chen, and C.-K. Chan, "A PMD-insensitive OSNR monitoring scheme based on polarisation nulling with off-center narrow-band filtering," *Optical Fibre Communication Conference OFC'2004*, paper FF2, Los Angeles, CA, USA, 2004.

[95] M. Petersson, H. Sunnerud, B. Olsson, and M. Karlsson, "Optical performance monitoring using degree of polarisation in presence of polarisation-mode dispersion," *European Conference on Optical Communication ECOC'2004*, paper Tu3.6.2, Stockholm, Sweden, 2004.

[96] M. Peterson, H. Sunnerud, M. Karlsson, B. E. Olsson, "Performance monitoring in optical

networks using Stokes parameters," *IEEE Photonics Technology Letters*, vol. 16, no. 2, pp. 686-688, Feb. 2004.

[97] M. Sköld, B-E. Olsson, H. Sunnerud, and M. Karlsson, "PMD-Insensitive DOP-Based OSNR Monitoring by Spectral SOP Measurements," *Optical Fibre Communication Conference OFC'2005*, paper OThH3, Anaheim,CA, USA, 2005.

[98] G. Lu and L. Chen, "Enhancing the monitoring sensitivity of DOP-based OSNR monitors in high OSNR region using off-center narrow-band optical filtering," *Optics Express*, vol. 15, no. 3, pp. 823-828, Feb. 2007.

[99] Z. Chen, L. Yan, A. Yi, W. Pan, and B. Luo, "Simultaneous OSNR monitoring for two polarisation tributaries of a PDM signal using a polarisation-diversity nonlinear loop mirror based on FWM," *Journal of Lightwave Technology*, vol. 30, no. 14, pp. 2376-2381, Jul. 2012.

[100] R. Adams, M. Rochette, T. T. Ng, and B. J. Eggleton, "All optical in band OSNR monitoring at 40Gb/s using nonlinear optical loop mirror," *IEEE Photonics Technology Letters*, vol. 18, no. 3, pp. 469–471, Feb. 2006.

[101] T. T. Ng, J. L. Blows, M. Rochette, J. A. Bolger, I. Littler, and B. J.Eggleton, "In band OSNR monitoring and chromatic dispersion monitoring using a fibre optical parametric amplier," *Optics Express*, vol. 13, pp. 5542–5552, Jul. 2005.

[102] Z. Tao, Z. Chen, L. Fu, D. Wu, and A. Xu, "A novel method to monitor OSNR using a Mach-Zehnder interferometer," *The 4th Pacific Rim Conference on Lasers and Electro-Optics CLEO/Pacific Rim 2001*, paper ThB2-4, Chiba, Japan, 2001.

[103] X. Lin, and L. Yan, "Multiple-channel OSNR monitoring with a single detector," *IEEE Photonics Technology Letters*, vol. 16, no. 12, pp. 2637-2639, Nov. 2004.

[104] Y-C. Ku, C.-K. Chan, and L.-K. Chen, "A novel robust OSNR monitoring technique with 40-dB dynamic range using phase modulator embedded fibre loop mirror," *Optical Fibre Communication Conference OFC'2006*, paper OWN6, Anaheim, CA, USA, 2006.

[105] X. Liu, Y.-H. Kao, S. Chandrasekhar, I. Kang, S. Cabot, and L. L. Buhl, "OSNR Monitoring Method for OOK and DPSK Based on Optical Delay Interferometer," *IEEE Photonics Technology Letters*, vol. 19, no. 15, pp. 1172-1174, Aug. 2007.

[106] S. K. Shin, K. J. Park, and Y. C. Chung, "A novel optical signal-to-noise ratio monitoring technique for WDIM networks," *Optical Fibre Communication Conference OFC'2000*, paper WK6, Baltimore, 2000.

[107] C. Dorrer, and X. Liu, "Noise monitoring of optical signals using RF spectrum analysis and its application to phase-shift-keyed signals," *IEEE Photonics Technology Letters*, vol. 16, no. 7, pp. 1781-1783, Jul. 2004.

[108] H. Y. Choi, Y. Takushima, and Y. C. Chung, "OSNR monitoring technique for DPSK/QPSK signals based on self-heterodyne detection," *IEEE Photonics Technology Letters*, vol. 20, no. 13, pp. 1124-1126, Jul. 2008.

[109] J. H. Lee, N. Yoshikane, T. Tsuritani, and T. Otani, "Dynamic monitoring of physical link performance for path computation in transparent optical networks," *Opto-Electronics and Communications Conference OECC'2008*, paper weK4, Sydney, Australia, 2008.

[110] C. J. Youn, S. K. Shin, K. J. Park, and Y. C. Chung, "OSNR monitoring technique using high-frequency," *Asia-pacific optical and wireless communications APOC'2001*, pp. 4584-4603, Beijing, China, 2001

[111] S. D. Dods, and T. B. Anderson, "In-band optical signal-to-noise monitoring technique using polarisation diversity," *The 18th annual meeting of the IEEE lasers and electro-optics society*, paper WEE2, Sydney, Australia, 2005.

[112] T. B. Anderson, K. Clarke, S. D. Dods, and M. Bakaul, "Robust, low cost, in-band optical signal-to-noise ratio monitoring using polarisation diversity," *Optical Fibre Communication Conference OFC'2007*, paper OMM3, Anaheim, CA, 2007.

[113] C. J. Youn, K. J. Park, J. H. Lee, and Y. C. Chung, "OSNR monitoring technique based on orthogonal delayed-homodyne method," *IEEE Photonics Technology Letters*, vol. 14, no. 10, pp. 1469-1471, Oct. 2002.

[114] G. Ishikawa, and H. Ooi, "Polarisation-mode dispersion sensitivity and monitoring in 40-Gbit/s OTDM and 10-Gbit/s NRZ transmission experiments," *Optical Fibre Communication Conference OFC'1998*, paper WC5, San Jose, CA, USA, 1998.

[115] W. Chen, R. S. Tucker, X. Yi, W. Shieh, and J. S. Evans, "Optical signal-to-noise ratio monitoring using uncorrelated beat noise measurement," *IEEE Photonics Technology Letters*, vol. 17, no. 11, pp. 2484-2486, Nov. 2005.

[116] M. Bakaul, "Low-cost PMD-insensitive and dispersion tolerant in-band OSNR monitor based on uncorrelated beat noise measurement," *IEEE Photonics Technology Letters*, vol. 20, no. 11, pp. 906-908, Jun. 2008.

[117] C. Xie, D. C. Kipler, L. Moller, and R. Ryf, "Orthogonal-polarisation heterodyne OSNR monitoring insensitive to polarisation-mode dispersion and nonlinear polarisation scattering," *Journal of Lightwave Technology*, vol. 25, no. 1, pp. 177–183, Jan. 2007.

[118] X. Tian, Y. Su, W. Hu, L. Leng, P. Hu, L. Yi, Y. Dong, and H. He, "Nonlinearity-tolerant in-band OSNR monitoring for synchronous traffic using gated-signal RF spectral analysis," *Optical Fibre Communication Conference OFC'2006*, paper OThP1, Anaheim, CA, 1998.

[119] J. H. Lee, N. Yoshikane, T. Tsuritani, and T. Otani, "In-band OSNR monitoring technique based on link-by-link estimation for dynamic transparent optical networks," *Journal of Lightwave Technology*, vol. 26, no. 10, pp. 1217–1225, May 2008.

[120] J. H. Lee, H. Guo, T. Tsuritani, N. Yoshikane, and T. Otani, "Field trial of all-optical networking controlled by intelligent control plane with assistance of optical performance monitors," *Journal of Lightwave Technology*, vol. 27, no. 2, pp. 94–100, Jan. 2009.

[121] D. J. Ives, B. C. Thomasen, R. Maher, and S. Savory, "Estimating OSNR of equalised QPSK signals," *European Conference and Exhibition on Optical Communication ECOC'2011*, paper OThH5, Geneva, Switzerland, 2011.

[122] F. Pittala, F. N. Hauske, Y. Ye, N. G. Gonzalez, and I. T. Monroy, "Joint PDL and in-band OSNR monitoring supported by data-aided channel estimation," *Optical Fibre Communication Conference OFC'2012*, paper OW4G, Los Angeles, CA, USA, 2012.

[123] M. S. Faruk and K. Kikuchi, "Monitoring of optical signal-to-noise ratio using statistical moments of adaptive-equaliser output in coherent optical receivers," *Opto-Electronics and Communications Conference OECC'2011*, pp. 233–234, Kaosiung, China, 2011.

[124] Zhu, A. V. Tran, S. Chen, L. Du, C. Do, T. Anderson, A. Lowery, and E. Skafidas, "Statistical moments-based OSNR monitoring for coherent optical systems," *Optics Express*, vol. 20, no. 16, pp. 17711-17721, Jul. 2012.

[125] R. Schmogrow, B. Nebendahl, M. Winter, A. Josten, D. Hillerkuss, S. Koenig, J. Meyer, M. Dreschmann, M. Huebner, C. Koos, J. Becker, W. Freude, and J. Leuthold, "Error vector

magnitude as a performance measure for advanced modulation formats," *IEEE Photonics Technology Letters*, vol. 24, no. 1, pp. 61-63, Jan. 2012.

[126] Z. Dong, A. Lau and C. Lu, "OSNR monitoring for QPSK and 16-QAM systems in presence of fibre nonlinearities for digital coherent receivers," *Optics Express*, vol 20, no. 17, pp. 19520-19534, Aug. 2012.

[127] F. N. Hauske, M. Kuschnerov, K. Piyawanno, B. Spinnler, E. D. Schmidt, and B. Lankl, "DGD estimation from FIR filter taps in presence of higher order PMD," *European Conference on Optical Communication ECOC'2008*, pp. 1-2, Sep. 2008.

[128] X. Yi, W. Shieh, Y. Ma, Y. Tang, and G. J. Pendock, "Experimental demonstration of optical performance monitoring in coherent optical OFDM systems," *Optical Fibre Communication Conference OFC'2008*, paper OThW3, San Diego, USA, 2008.

[129] D.C. Kilper, R. Bach, D. J. Blumenthal, D. Einstein, T. Landolsi, L. Ostar, M. Preiss, and A.E. Willner, "Optical performance monitoring," *Journal of Lightwave Technology*, vol. 22, no. 1, pp. 294–304, Jan. 2004.

[130] Y. C. Chung, "Optical performance monitoring techniques; current status and future challenge," *European Conference on Optical Communication ECOC'2008*, paper W.E.1.D.1, Brussels, Belgium, 2008.

[131] G. Ishikawa and H. Ooi, "Polarisation-mode dispersion sensitivity and monitoring in 40-Gbit/s OTDM and 10-Gbit/s NRZ transmission experiments," *Optical Fibre Communication Conference OFC'1998*, pp. 117–119, San Jose, CA, USA, 1998.

[132] S. M. R. M. Nezam, Y.-W. Song, C. Yu, J. E. McGeehan, A. B. Sahin, and A. E. Willner, "First-Order PMD Monitoring for NRZ Data Using RF Clock Regeneration Techniques," *Journal of Lightwave Technology*, vol. 22, no. 4, pp. 1086-1093, May 2004.

[133] C. Yu, Y. Wang, T. Luo, Z. Pan, S.M.R. Motaghian Nezam, A. B. Sahin, and A. E. Willner, "Chromatic-Dispersion-Insensitive PMD Monitoring for NRZ Data Based on Clock Power Measurement Using a Narrowband FBG Notch Filter," *European Conference on Optical Communications ECOC'2003*, paper Tu4.2.3, Rimini, Italia, 2003.

[134] J. Yang, K. W. L. Chee, and C. Yu, "CD Insensitive PMD Monitoring for Different Modulation Formats Based on RF Tone Power MEasurement Using an FBG Notch Filter," *International Conference on Information, Communications and Signal Processing ICICS' 2009*, pp. 1-5, Macau, 2009.

[135] J. Yang, C. Yu, L. Cheng, Z. Li, C. Lu, A. P. T. Lau, H. Tam, and P. K. A. Wai, ""CD-insensitive PMD monitoring based on RF power measurement," *Optics Express*, vol. 19, no. 2, pp. 1354-1359, Jan. 2011.

[136] F. Buchali, S. Lanne, J.P. Thiery, W. Baumert, and H. Bulow, "Fast eye monitoring for 10 Gbit/s and its application for optical PMD compensation," *Optical Fibre Communication Conference OFC'2001*, paper TuP5, Anaheim, CA, USA, 2001.

[137] F. Buchali, W. Baumert, H. Bulow, and J. Poirrier, "A 40 Gb/s eye monitor and its application to adaptive PMD compensation," *Optical Fibre Communication Conference OFC'2002*, pp. 202-203, Anaheim, CA, USA, 2002.

[138] F. Buchali, W. Baumert, H. Bulow, U. Feiste, R. Ludwig, and H. G. Weber, "Eye monitoring in a 160 Gbit/s RZ field transmission system," *European Conference on Optical Communication ECOC'2001*, pp. 288-289, Amsterdam, Netherlands, 2001.

[139] G. W. Lu, C. Xie, Y. C. Ku, L. K. Chen, and C. K. Chan, "Enhanced PMD monitoring with

frequency-resolved SOP rotation by self phase modulation," *IEEE Photonics Technology Letters*, vol. 16, no. 9, pp. 2180–2182, Sep. 2004.

3 Data-Aided Chromatic Dispersion Estimation

3.1 INTRODUCTION

In Chapter 2, a survey of chromatic dispersion (CD) estimation techniques for coherent optical (CO) single carrier (SC) systems was presented. System link CD estimation is a very critical component in CO systems and is essential for subsequent timing recovery and frequency offset (FO) compensation. However previous methods of estimating CD transfer function typically depend on gradient algorithms that compensate for a range of CD values in order to maximize a cost function [1]-[8] or using autocorrelation of signal power waveform (ACSPW) [9]-[10], both of which tend to require high DSP complexity. Techniques that are based on estimating channel transfer functions are very attractive as CD is a linear impairment and is contained inside the channel transfer matrix [11]-[15]. However, CD estimation techniques that are based on blind channel estimation (CE) [11]-[13], or data-aided (DA) CE using short training sequences (TSs) [14]-[16], are typically limited in terms of channel impulse response, which in turn lead to a very limited range in CD estimation and as thus are more suitable for residual CD monitoring instead of system link CD estimation. Since DA approach can provide higher estimation resolution than what is possible with blind estimation by expanding on the TS lengths, it is a very attractive technology for system CD estimation. However, one of the primary challenges of expanding to longer TS block is to keep the TS constellations compatible with the modulation format of the entire frame while still provide optimal estimation performance. It is therefore desirable to investigate CD estimation technique that is capable of estimating the entire transmission link CD based on DA-CE technology which utilises long TS block.

In this chapter, full transmission link CD estimation using DA-CE method for both polarisation-multiplexed (PM) quadrature phase shift keying (QPSK) and 16-quadrature amplitude modulation (16QAM) systems is presented [17]. New modulation-format specific TSs namely Golay sequences and quantised Chu sequences aided by quadratic fit interpolation to achieve full channel CD estimation are investigated. Modulation-format specific sequences will ensure easy integration into PM-QPSK and PM-16QAM commercial modulators without the need for high resolution digital-to-analogue converter (DAC) unlike the case with the ideal full-level constant amplitude zero autocorrelation (CAZAC) sequences. Theory on DA channel response estimation and CD estimation is presented in Section 3.2. Sequence designs that are suitable for the proposed technique while still providing good performance are investigated in Section 3.3. Section 3.4 describes the simulation analysis on the proposed method performance and tolerance to various impairments. Section 3.5 presents experimental demonstration of the proposed CD estimation technique whose estimation performance is shown to be accurate and robust to other channel impairments. Finally the chapter is concluded in Section 3.6.

3.2 DATA-AIDED CHROMATIC DISPERSION ESTIMATION

With optical coherent receivers, both the in-phase and quadrature components of incoming optical signals can be captured. Hence it is possible to use traditional wireless technology such as space-time block code (STBC) to estimate the channel transfer functions and compensate for most linear impairments. System CD is a linear channel component and can be modelled as a linear all-pass filter with a very long impulse response as presented in Chapter 2. Thus, CE will need to be capable of capturing all impulse responses generated by system CD. However, system CD, while being a very large channel impairment, is only needed to be estimated once and subsequence CD compensation can be performed based on this estimation as CD is static and does not change overtime. While the relationship between the total amount of CD and channel impulse response in time domain is known, such relationship between the lengths of TSs used for CD estimation and the range of CD to be estimated has not been demonstrated in the literature. This chapter demonstrates that, for system CD estimation, a block of long TSs is required. While flat-spectrum CAZAC sequences provide ideal performance for CE, their complex constellations make it difficult for the

implementation of full channel CD estimation using DA-CE as the long CAZAC sequences will require a very high-resolution DAC to generate the optical signals that contains the sequences.

The CD estimation technique presented in this chapter is based on DA-CE technique and utilises two types of TSs with either QPSK or 16QAM constellation. By utilising these types of TSs, long TSs can be generated to match the long impulse response generated by system CD and thus DA system's CD estimation can be implemented without any high-resolution DAC. Low-complexity estimation is performed with single stage quadratic interpolation, which yields accurate estimation with one single step instead of step size scanning estimation algorithm. Estimation accuracy enhancement using a two-stage approach will also be demonstrated and the results can be generalized into multiple stage feedback structure where the number of stages can be implemented depending on the amount of accumulated CD in the signal.

3.2.1 Channel Estimation

Modern CO-SC systems are normally PM in order to allow data transmission on both the X- and Y- polarisation tributaries of the optical signal. As proposed in [18], optical channel in PM systems can be modelled as a 2×2 multiple-input multiple-output (MIMO) transmission channel and wireless techniques for estimating the MIMO channel can be used. For PM-CO systems, the channel transfer matrix $H(f)$ is modelled as the 2x2 matrix:

$$H(f) = \begin{pmatrix} H_{xx}(f) & H_{yx}(f) \\ H_{xy}(f) & H_{yy}(f) \end{pmatrix} \tag{3.1}$$

where H_{xx} and H_{yy} correspond to the transfer function in the X and Y-polarisation, respectively; and H_{xy} and H_{yx} correspond to the cross-coupling between these two polarisation tributaries, respectively. As coherent PM optical is similar to a 2x2 MIMO wireless channel, estimation of $H(f)$ can be performed using STBC with Alamouti's arrangement [19]-[21] where the transmission matrix $S[k]$ in frequency domain is scheduled as:

$$S[k]=\begin{pmatrix} S_1[k] & -S_2^{*}[k] \\ S_2[k] & S_1^{*}[k] \end{pmatrix} \tag{3.2}$$

where $S_1[k]$ and $S_2[k]$ are the discrete Fourier transforms (DFTs) of two orthogonal sequences. Using Fourier transform properties, the training matrix in Equation 3.2 can be scheduled in time domain as:

$$S[n]=\begin{pmatrix} S_1[n] & -S_2^{*}[-n] \\ S_2[n] & S_1^{*}[-n] \end{pmatrix} \tag{3.3}$$

where $S_1[n]$ and $S_2[n]$ are the time domain form of two orthogonal sequences and $S[-n]$ indicates a left-to-right flipped (time-inversed) sequence compared to the original sequence $S[n]$. The TSs are inserted into the data stream for both polarisations using the space-time scheduling format presented in Section 2.2.5.2 of Chapter 2. Assuming a standard linear optical channel model, after transmission, an estimation of the channel transfer matrix $H[k]$ can be obtained by multiplying the received signal with the inverse of the original training matrix. The estimated matrix $H[k]$ contains all linear channel impairments. Assuming the length of $H[k]$ is sufficient, system CD can be estimated from $H[k]$ using the method outlined in the next section.

3.2.2 System Chromatic Dispersion Estimation

In systems with weak nonlinearities, a linear optical channel model mainly consists of two parts: polarisation-independent components such as CD and amplitude filters, and polarisation-dependent components such as polarisation-mode dispersion (PMD). The linear optical channel model in Equation 3.1 can be expressed in terms of CD transfer function and PMD matrix as [11]-[15]:

$$\begin{pmatrix} H_{xx}(f) & H_{yx}(f) \\ H_{xy}(f) & H_{yy}(f) \end{pmatrix} = G(f)\begin{pmatrix} u(f) & v(f) \\ -v^{*}(f) & u^{*}(f) \end{pmatrix} \tag{3.4}$$

where $G(f)$ is the CD transfer function; PMD elements are contained in the 2x2 matrix $\begin{pmatrix} u(f) & v(f) \\ -v^{*}(f) & u^{*}(f) \end{pmatrix}$ with $|u(f)|^2+|v(f)|^2=1$. Since the PMD matrix is unitary, the CD transfer function $G(f)$ can be estimated from the determinant of the transfer matrix $H(f)$ as:

$$G(f) = \sqrt{H_{xx}(f)H_{yy}(f) - H_{yx}(f)H_{xy}(f)} \tag{3.5}$$

The CD transfer function $G(f)$ is a complex function with the phase component being a quadratic function as illustrated in Chapter 2. If an estimated sample of this quadratic function is known, then CD can be estimated by performing quadratic fit on the sampled estimated function.

While CE in [15] is based on DA method, the CD estimation method proposed in [15] is based on knowing approximately the total amount of CD to be estimated and reconstructing multiple theoretical CD curves around this value and choosing the curve that best fits the estimated value. This approach can be viewed as similar to the step size scanning approach in traditional CD estimation methods except channel transfer functions are estimated using DA method with limited range. While this does not require any extra processing on the estimated CD curve, this approach is limited to measuring a small amount of CD (residual CD) since large CD values require longer sequences and a large amount of estimation operations before the best fit is found. It is trivial that since CD is a quadratic phase rotation, a quadratic interpolation approach will yield estimated value in one single step with good accuracy and is a more feasible approach for estimating the entire system CD. In the proposed approach, the entire system transfer matrix is first estimated using a block of long TSs and then the system CD transfer function is estimated according to Equations 3.5. The estimated CD transfer function phase response $\psi(f)$ is then used for system CD estimation using least square quadratic interpolation. However, due to the square root operation of Equation 3.5, the phase response $\psi(f)$ of the CD transfer function $G(f)$ is clipped with the condition of $-\pi/2 \leq \psi(f) \leq \pi/2$ as illustrated in Figure 3.1(a) which makes it difficult to unwrap the phase response and reconstruct the CD curve for estimation by interpolation as the threshold needs to be set lower than the standard $\pi \leq \psi(f) \leq \pi$. Since only the phase response of $G(f)$ is of importance, the CD phase response curve $\psi(f)$ is instead estimated from $G(f)^2$ as:

$$2\psi(f) = \arg\left[G(f)^2\right] = \arg\left[H_{xx}(f)H_{yy}(f) - H_{yx}(f)H_{xy}(f)\right] \tag{3.6}$$

where *arg*(.) denotes the phase component of complex number (.). The phase function $2\psi(f)$ is then converted to a single quadratic curve by unwrapping the phase of the CD

transfer function. Since $2\psi(f)$ has phase threshold condition of $-\pi \leq \psi(f) \leq \pi$, standard unwrap operation can be employed to convert the phase response to one single quadratic function. The final $\psi(f)$ can be obtained by dividing $2\ \psi(f)$ by 2 after unwrapping and the CD curve is illustrated in Figure 3.1(b).

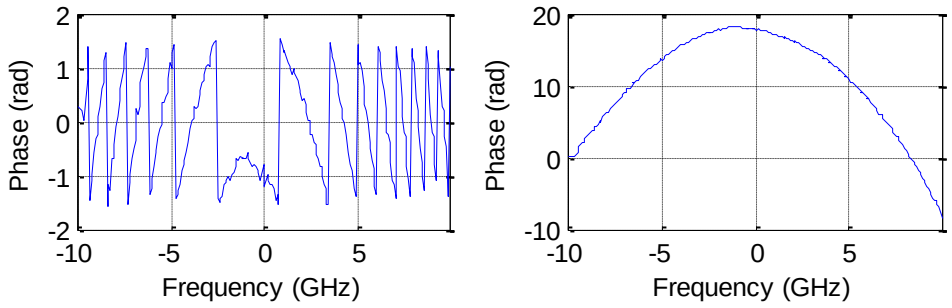

(a) *(b)*

Figure 3.1: (a) Estimated CD transfer function and (b) Unwrapped phase response.

Since the unwrapped curve represents a noisy quadratic function, a parabolic interpolation is fitted to this curve using least square quadratic fit method and the coefficients of this parabola are extracted. The raw estimated quadratic function contains three coefficients in standard form. Of the three quadratic fit coefficients, only the first value contains the CD transfer function and total system CD parameter is then extracted from this parameter. Figure 3.2 illustrates all steps to estimate CD from the original channel transfer matrix and it can be seen that no gradient or recursive algorithm is needed. The estimated system CD value can be stored in the receiver's memory for subsequent blind CD compensation.

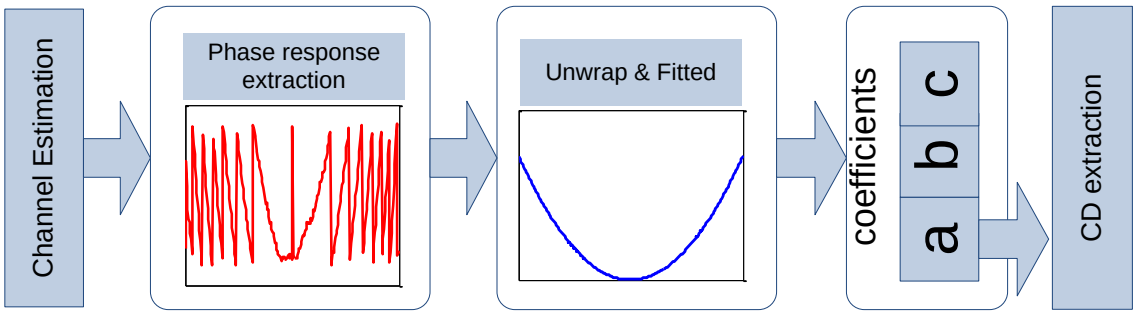

Figure 3.2: Quadratic fit CD estimation block diagram.

3.2.3 Required Sequence Length Analysis

In order to estimate system CD using the above method, TSs sent through the channel have to be of sufficient lengths to cover the long channel memory imposed by the system CD. An expression for the minimum required sequence lengths for CD estimation can be obtained by noting that in the case of time domain CD compensation using an FIR filter as illustrated in [22], the maximum number of required taps are given by:

$$L_h = \frac{Dz\lambda^2}{cT^2} \tag{3.7}$$

where L_h represents the channel memory length or the number of taps, λ is the laser wavelength, D is the dispersion factor, z is the transmission length, c is the speed of light and T is the receiver's sampling period. Equation 3.7 expresses the minimum required FIR filter length for CD compensation and can be used to calculate the required TS lengths for a given maximum amount of CD to be estimated. Since the received signal is sampled at the receiver for further processing, if S_p represents the samples per symbol then by extending the expression in [16] and combining with Equation 3.7 the required sequence length is:

$$N_{ts,req} = \frac{L_h N_t}{S_p} = \frac{Dz\lambda^2 B^2 N_t S_p}{c} \tag{3.8}$$

where B is the system baud rate and $N_t = 2$ for coherent PM systems. Since Equation 3.8 only depends on system baud rate and transmission length, both PM-QPSK and PM-16QAM modulation formats will have the same required sequence lengths with respect to system baud rate and transmission. The sampling speed S_p however, is inversely proportional to $N_{ts,req}$ and will have a significant impact on the required TS length $N_{ts,req}$ for CD estimation. For proper capture of transmitted signals, $S_p \geq 2$ is required at the sampling device. However, to reduce the amount of training symbols used for CD estimation, $S_p = 1$ is more desirable. This condition can be easily achieved by first capturing the received TSs with $S_p \geq 2$, then applying a resampling and anti-aliasing process to reduce the captured signal to $S_p = 1$. This process ensures that the signals are properly captured with $S_p = 1$ for CD estimation.

Using Equation 3.8 with S_p = 1, TSs with lengths of N_{ts} = 64 symbols are required to accurately estimate CD for around 2000-km fibre transmission in 40-Gb/s PM-QPSK or 80-Gb/s PM-16QAM-modulated CO systems. Assuming a 25-Gbaud system with a maximum CD compensation capability of 50,000 ps/nm (approximately 3000 km), a TS block with TS lengths of 512 symbols is sufficient to estimate the entire system CD.

3.3 LONG TRAINING SEQUENCE DESIGN

For DA CD estimation in PM systems, two types of TSs, both designed for the specific system modulation formats such as PM-QPSK and PM-16QAM, are proposed. The first type, called quantised CAZAC-Chu sequence (Q-Chu), is a modified design based on the original CAZAC-Chu sequence [23]-[24] while the second type is derived from Golay complementary sequences. Their design and spectral properties are presented in the next section.

3.3.1 CAZAC-based QPSK and 16QAM Sequences

The first type of sequence proposed in this chapter is quantised quadriphase Chu (Q-Chu) sequences [24]. Q-Chu sequences are derived directly from the original CAZAC-Chu sequence [23] by first generating orthogonal Chu sequences at a desired length. In the second phase of quantisation, the sequences are passed through a slicer to obtain QPSK sequences with good frequency response comparable to the original Chu sequences as shown in Figure 3.3(a). The slicer can be mathematically formulated as:

$$C_k = \mathrm{sgn}(real(Z_k)) + j \times \mathrm{sgn}(imag(Z_k)) \tag{3.9}$$

where Z_k is the original Chu sequence, sgn(x) equals to 1 when $x > 0$ and equals to -1 otherwise. This transformation offers a relatively flat frequency spectrum which is slightly worse than that of the ideal Chu sequence, which has a flat spectrum.

Figure 3.3(b) shows the frequency spectrum of a single Q-Chu sequence (blue line) compared to the spectrum of an ideal Chu sequence (pink line) and it can be seen that the transformation has a negative effect on Q-Chu sequence's frequency spectrum. However, no null point is observed over the entire frequency spectrum of the Q-Chu sequence, thus the degradation in estimation accuracy is expected to be small for using the Q-Chu sequence.

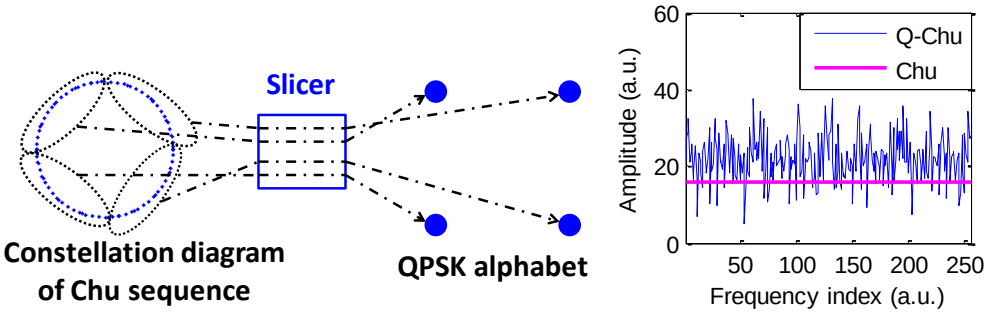

(a) *(b)*

Figure 3.3: (a) Generation of Q-Chu sequence and (b) Frequency spectrum of Q-Chu-sequence compared to that of ideal Chu sequence.

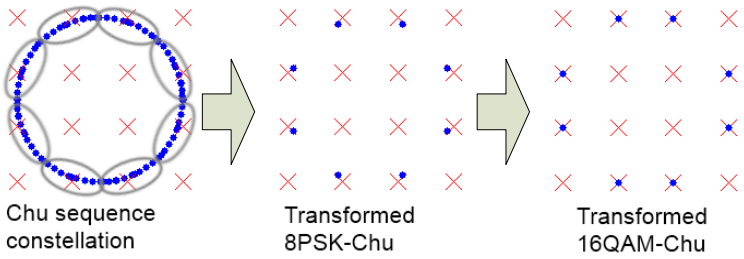

(a)

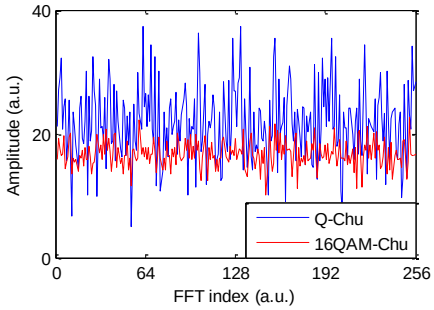

(b)

Figure 3.4: (a) Generation of 16QAM-Chu sequences and (b) Frequency spectrum of Q-Chu and 16QAM-Chu sequences.

For PM-16QAM systems, the design of Chu-based 16QAM sequence (16QAM-Chu) can be employed by modifying the method used to generate the Q-Chu sequences described above. To differentiate the new sequence from the original Q-Chu sequence,

the new sequence obtained by this method is termed 16QAM-Chu. In order to obtain a 16QAM-Chu sequence, an original Chu sequence is passed through an 8-phase shift keying (8PSK) slicer with a design similar to the slicer described in Figure 3.3(a) above. After the polyphases to 8-phases transformation, an 8PSK-Chu sequence is obtained. The 8-PSK sequence is then adjusted to fill in the square 16QAM constellation in order to form the final Chu-based 16QAM sequence. The process of transforming a Chu sequence to a 16QAM-Chu sequence is shown in Figure 3.4(a) while Figure 3.4(b) shows the frequency spectrum of the 16QAM-Chu sequence compared to the Q-Chu sequence. It can be seen that the 16QAM-Chu sequence has slightly better frequency spectrum compared to the Q-Chu sequence. This is expected as the 8PSK slicer induces less loss in spectral property compared to the original quadriphase slicer.

3.3.2 Golay Sequences

As described in Chapter 2, Golay sequences consist of $a[n]$ and $b[n]$ sequences that satisfy Golay property [25]-[28]. Golay sequences are orthogonal to each other and can be generated using many techniques for different required sequence lengths. In CD estimation using DA-CE technique, the lengths of the sequences are preferred to be in powers of 2 in order to match the FFT/IFFT operations and the sequence constellations are preferred to match the constellation of the modulation format at any 2^n lengths. Thus the simplest way for generation of Golay sequences used for DA-CE is by employing the recursive generation technique using "seed sequences" [25]. The seed sequences can then be chosen to match the transmission modulation format constellation and any Golay pair of length 2^n can be generated from the seed sequences using recursive construction. In order to employ Golay sequences for DA-CE in CO systems, the sequences are arranged in space-time using the following matrix:

$$S[n] = \begin{pmatrix} S_1[n] & -S_2^*[-n] \\ S_2[n] & S_1^*[-n] \end{pmatrix} = \begin{pmatrix} a[n] & -b^*[-n] \\ b[n] & a^*[-n] \end{pmatrix} \tag{3.10}$$

where $S_1[n]$ and $S_2[n]$ are the two discrete sequences arranged in space-time and $a[n]$, $b[n]$ are the two Golay sequences. It can be seen that $a[n]$ and $-b^*[-n]$ also form one orthogonal Golay pair, as well as the two pairs $\{a^*[-n], b[n]\}$ and $\{-b^*[-n], a^*[-n]\}$ [21]. Using Equation 3.10 four orthogonal Golay pairs can be arranged to fit with Alamouti's STBC arrangement. For channel estimation using the space-time structure in Equation

3.10, the condition for achieving minimum mean squared error channel estimation (MMSE-CE) is given by [29]:

$$\left|S_1[n]\right|^2 + \left|S_2[n]\right|^2 = c \tag{3.11}$$

where c is a constant and it can be seen that Equation 3.11 can be satisfied by choosing S_1[n] and S_2[n] as the two complementary Golay sequences. The use of complex conjugate indicates the need for complex-valued sequences while it can also be seen that systems with PM-QPSK, PM-16QAM, or higher-order modulation formats will benefit from TSs that fits the modulated data constellation. Since Golay sequences are generated by recursive construction, constellation property of long Golay sequences only depends on the seed pair, which makes Golay sequences are ideal for CD estimation purposes as the sequences can be generated with any arbitrary lengths and still maintain desired constellations. For the seed sequences, instead of using real-valued binary phase shift keying (BPSK) Golay seed sequences [25], complementary QPSK seed sequences $a[n]$ = [1+j 1-j] and $b[n]$ = [1+j -1+j] are used for Golay sequence construction. It can be easily shown that the two seed sequences satisfy Golay autocorrelation property and sequences of 2^n length can be generated using the recursive construction method to form QPSK Golay sequences or any arbitrary length of 2^n.

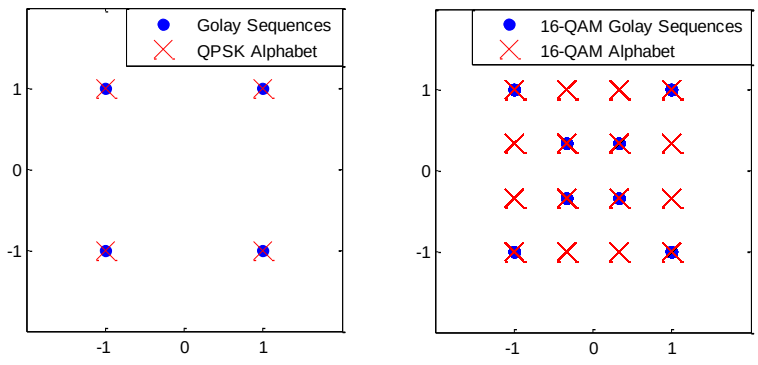

(a) *(b)*

Figure 3.5: Constellation of (a) QPSK Golay sequences and (b) 16QAM Golay sequences.

For PM-16QAM systems, 16QAM format Golay seed sequences can be constructed from seed QPSK sequences as [28]: $s[n] = 2a[n] + b[n]$ and $t[n] = -2b[n] + a[n]$, where $s[n]$

and $t[n]$ are the 16QAM Golay pair and $a[n]$ and $b[n]$ are the QPSK Golay pair, respectively. The constellation of the original QPSK Golay sequences and normalised 16QAM Golay sequences can be seen in Figure 3.5 and it can be seen that both the QPSK and 16QAM Golay sequences fit their corresponding constellations. While QPSK Golay sequences can be used in PM-16QAM system by mapping the four QPSK constellation points to 16QAM, it can be seen that the 16QAM Golay sequences have average power similar to that of a 16QAM data signal.

3.4 SIMULATION ANALYSIS

3.4.1 Simulation Setup

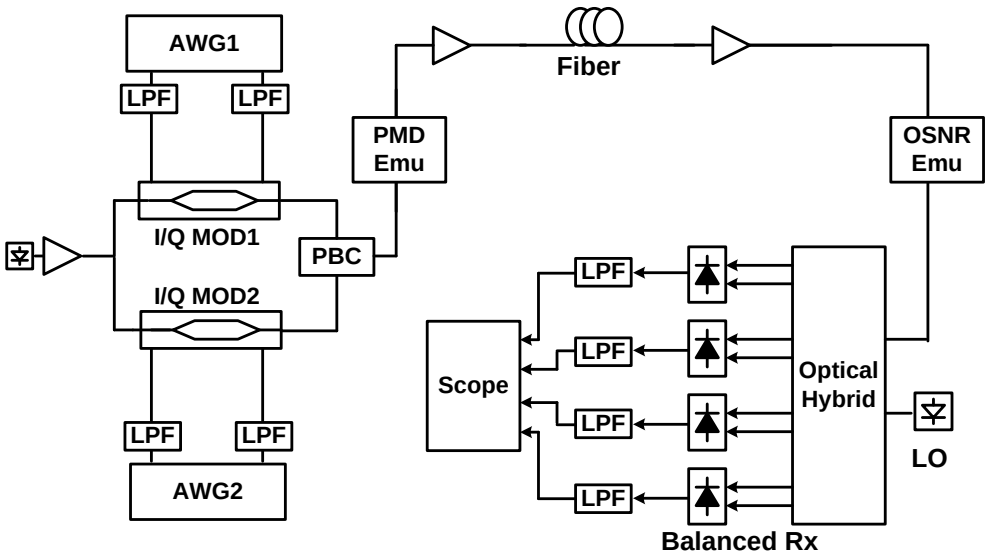

Figure 3.6: Simulation setup.

Simulations are carried out with *VPI TransmissionMaker 8.6* and the simulation setup is shown in Figure 3.6. TSs are added to the randomly generated data and the combined frames are sent through an arbitrary waveform generator (AWG) model to convert data into electrical signals at a baud rate of 10 Gbaud and then to I/Q modulators to convert into optical signals for each polarisation tributary. Optical signals on X- and Y-polarisations are then combined using polarisation beam combiner (PBC) to form the PM optical signal. As described in Section 3.2.3, a sequence length of only 64 symbols is required for 2000-km transmission. However, longer lengths of 128 symbols and 256 symbols are also used to investigate estimation performance. Fibre model consists of

multiple spans with amplifiers to compensate for fibre loss and a value of 16.8 ps/nm.km is set as the dispersion parameter for the fibre model. A second-order PMD emulator and optical signal-to-noise ratio (OSNR) emulator are added at the beginning and end of the fibre model to investigate the estimation performance against various levels of PMD and OSNR. The receiver model consists of standard balanced receiver using optical hybrids and photodiodes. Output data are sampled at 2 samples per symbol and stored for further receiver DSP processing using MATLAB.

3.4.2 Effect of Cyclic Prefix Length

Cyclic prefix (CP) blocks are normally added at the beginning and end of the TSs to serve as guard intervals and prevent inter-symbol interferences from the previous symbol to the next TS block. While CP blocks are traditionally associated with CO-OFDM, CP blocks can also be included in CO-SC systems between TSs to resist interferences caused by channel impairments. Since DA-CE can also be used for channel equalisation, in order for the CP blocks to be effective, the length of each CP block N_{cp} needs to be sufficiently long to cover the entire channel impulse response and in the case of using CP blocks for CE, $N_{cp} = N_{ts}/4$ [16] where N_{ts} is the length of a single sequence in the training block. However, as CD estimation only utilises the phase response information from frequency domain CE, this impairment normally dominates other effects caused by having insufficient amount of CP symbols and using frequency domain estimation should give robust CD estimation performance with only a small amount of CP symbols. Figure 3.7 shows the reconstructed CD curve using estimated value for 3800-km transmission for 40-Gb/s PM-QPSK system with two CP length values of $N_{cp} = 32$ and $N_{cp} = 4$. Using Equation 3.8 it can be seen that a core sequence length value of $N_{ts} = 128$ will cover the entire channel impulse response for 3800-km 10-Gbaud transmission and $N_{cp} = 32$ is the required amount of CP symbols. However, it can be seen that for $N_{cp} = 4$ the majority of CD curve can still be reconstructed with outside edges of the curve being polluted by inter-block interference (IBI). In such a situation, the estimation range can be reduced to the "clean" area of the curve for accurate CD estimation with minimal performance degradation. For the CD curve in Figure 3.7(a), the area used for CD estimation after 3800-km transmission with $N_{cp} = 4$ is 90.6% of the original CD curve (fully recovered in Figure 3.7(b)), where the outermost 6 samples from each side had been discarded. While it is preferable to guard

the TSs with sufficient CP blocks and preventing IBI, in the event of insufficient CP lengths, system CD can still be estimated with very small degradation in estimation performance.

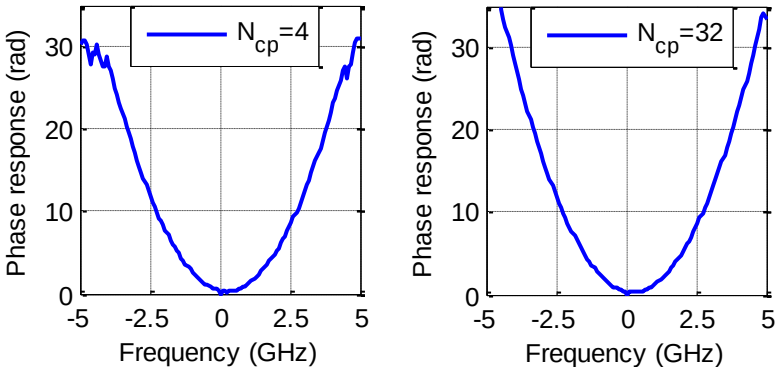

(a) *(b)*

Figure 3.7: CD estimation curve for N_{ts} = 128 with (a) N_{cp} = 4 and (b) N_{cp} = 32.

3.4.3 Impairment Tolerance Analysis

CD is estimated using the method described in Section 3.2.2 and compared to the actual CD value as set by the dispersion parameter and transmission distance. The errors are calculated in root mean squared (RMS) error percentage as:

$$E_{RMS} = 100\frac{\sqrt{(CD_E - CD_A)^2}}{CD_A} \tag{3.12}$$

where E_{RMS} is the RMS error value, CD_E is the estimated CD value and CD_A is the actual CD value. Figure 3.8(a) shows the estimation performance in RMS error percentage for different transmission distances with no PMD at an OSNR value of 26 dB for the PM-QPSK system for all three types of sequence (Chu, Q-Chu and Golay) with different sequence length N_{ts}. It can be seen that Golay sequences perform similarly to the CAZAC sequences for all transmission distances and both achieve high accuracy with low error percentage while the Q-Chu sequence has slightly worse performance as the degraded signal spectrum has a degradation effect in CE and in turn affecting CD estimation accuracy. Also it can be seen that the error percentage slightly

decreases as the transmission distance increases since the total CD increases linearly with distance but the estimation error does not, which in most cases results in slightly higher accuracy at longer distances. Finally, longer sequence improves the estimation performance since this increases the resolution of the estimated channel information and provides the quadratic interpolation with more data for more accurate results. Results for the PM-16QAM system are shown in Figure 3.8(b) with similar trends compared to the PM-QPSK system but with slightly higher overall error since compared to the PM-QPSK system, the PM-16QAM system has been scaled down to fit inside the modulator range and this results in a loss of power to the TS block as the TSs also have average power similar to the PM-16QAM system. Using QPSK sequence for the PM-16QAM system will result in improved estimation performance. However, this comes with the trade-off of some potential system instability. Also since the 16QAM-Chu sequence has an improved frequency spectrum, performance gap between the 16QAM-Chu, Golay and ideal Chu sequences is smaller. Simulation results for both PM-QPSK and PM-16QAM systems show that both Golay and quantised-Chu sequences attain similar estimation performances compared to the ideal Chu sequence and these sequences are a good candidate for system CD estimation based on DA-CE in CO-SC systems utilising PM-QPSK and PM-16QAM modulation formats.

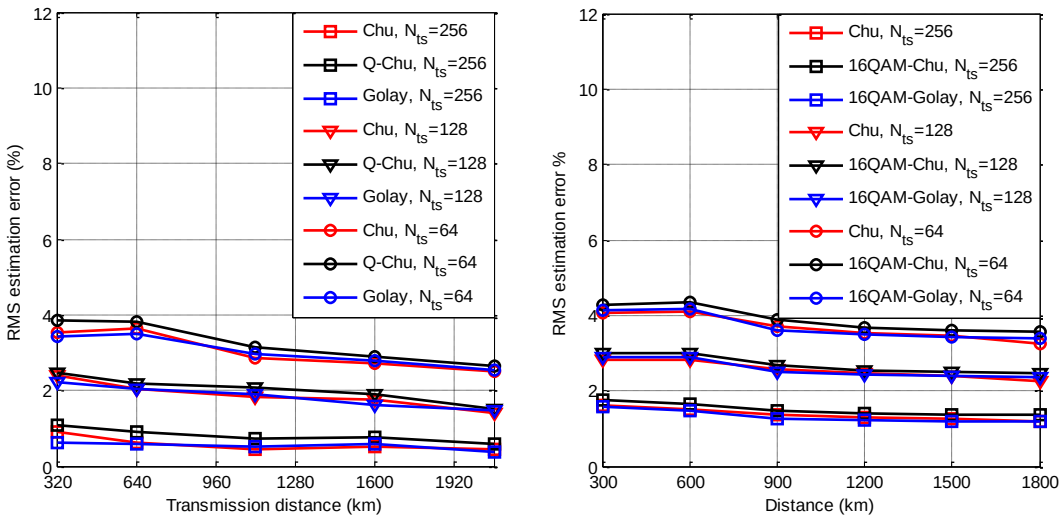

(a) *(b)*

Figure 3.8: RMS error at various fibre lengths for (a) PM-QPSK system and (b) PM-16QAM system.

Figure 3.9(a) shows the CD estimation error for the PM-QPSK system using Chu, Q-Chu and Golay sequences at 2080-km transmission distance against different PMD values (represented by mean differential group delay - DGD) using the PMD emulator with second-order PMD and sequence length N_{ts} = 256 symbols. It can be seen that with the addition of PMD, the estimation performance degrades slightly at very high DGD values and overall still achieves very high accuracy of less than 3% RMS error. In all cases both the Chu and Golay sequences perform similarly. The Q-Chu sequences have slightly worse performance but still within 0.2% error of the Chu sequence. Results for estimation error in PM-16QAM system are shown in Figure 3.9(b) for Chu, 16QAM-Chu and 16QAM-Golay sequences and similar trends can be observed compared to those of the PM-QPSK system.

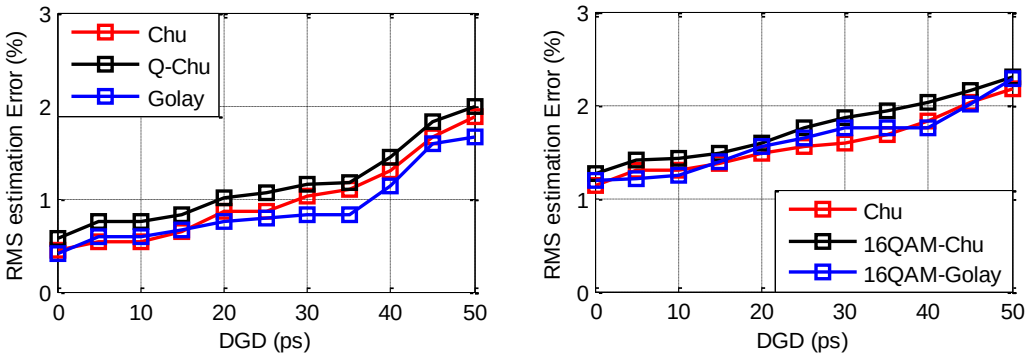

(a) *(b)*

Figure 3.9: RMS error against PMD for (a) PM-QPSK system and (b) PM-16QAM system.

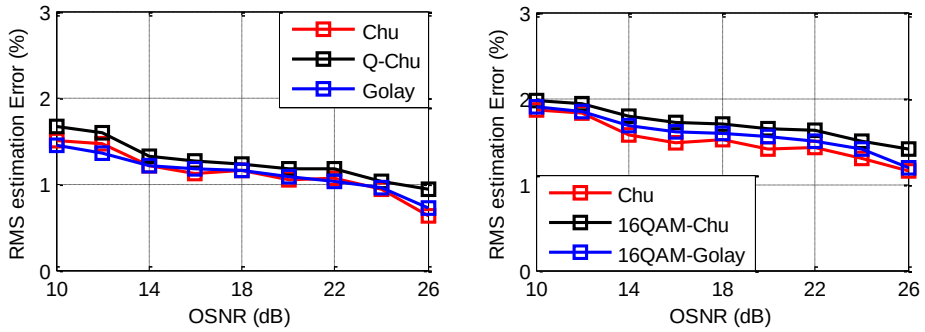

(a) *(b)*

Figure 3.10: RMS error against OSNR for (a) PM-QPSK system and (b) PM-16QAM system.

Figure 3.10 shows simulation results for CD estimation performance against different levels of OSNR for both PM-QPSK and PM-16QAM systems using the proposed TSs. It can be seen that lower OSNR has slightly negative impact on the estimation performance. This effect can be explained as the additional noise generated by low OSNR level will cause noisy CE and noisy CD curves which slightly degrade estimation accuracy as a result. Since CD is still dominant, the effect of additional noise is small and the technique is considered to be robust against different levels of OSNR. Furthermore, it can be seen that the technique utilises only the phase response of the determinant function and as thus can be expected to be robust against PDL, which is a magnitude function as demonstrated in [30].

Overall it can be seen that the CD estimation performance using the proposed Golay and Chu-based TSs is accurate and comparable to the ideal Chu sequence for both PM-QPSK and PM-16QAM systems. The use of longer sequences improves the estimation performance compared to using shorter sequences as expected for estimation using interpolation such as quadratic fit. While the constellation of the Chu sequence becomes much more complex at longer length, all other sequences have length-independent constellation and can be generated at longer length using PM-QPSK/PM-16QAM modulators. It can also be seen that both PMD and OSNR slightly affect the estimation performances however the effect is quite small and the residual error can be left as residual CD is compensated during system equalisation. For different transmission distances, using the minimum required sequence length of N_{ts} = 64 results in the RMS estimation errors of around 5%. Increasing the length to 256 symbols reduces the estimation error to less than 2% for both PM-QPSK and PM-16QAM systems.

3.4.4 Dual-Stage Data-Aided Chromatic Dispersion Estimation

The previous section describes the DA CD estimation technique which utilises single-stage quadratic fit interpolation on the estimated channel response for CD estimation. The technique is low in complexity and the obtained errors are within a fraction of the true CD value due to quadratic fit. For normal to medium length transmission distance, it can be seen that the residual CD due to estimation error is small and can be compensated by subsequent channel equalisation based on either blind or DA method.

However, since CD can be compensated by using pre-defined values it is also possible to enhance the accuracy of the proposed method by performing a second stage of estimating residual CD and adding this value to the previously estimated CD value to further reduce the estimation error of the proposed DA CD estimation method. Figure 3.11 shows the block diagram of dual-stage DA CD estimation. In the first stage CD is estimated with TSs using quadratic fit method described in Section 3.2.2. This estimated value is then used to compensate for CD in the TSs using overlap frequency domain equalisation (OFDE) method to produce partially CD-compensated TS block. In order to limit the effect of estimation error, the amount of CD to be compensated is limited to 90% of that of the estimated CD value. The CD-compensated TS block is then fed to the second stage of CD estimation, which utilises the exact DSP procedure of the first stage CD estimation to estimate the residual CD component. The two estimated CD values are then added together to form the total system CD parameter.

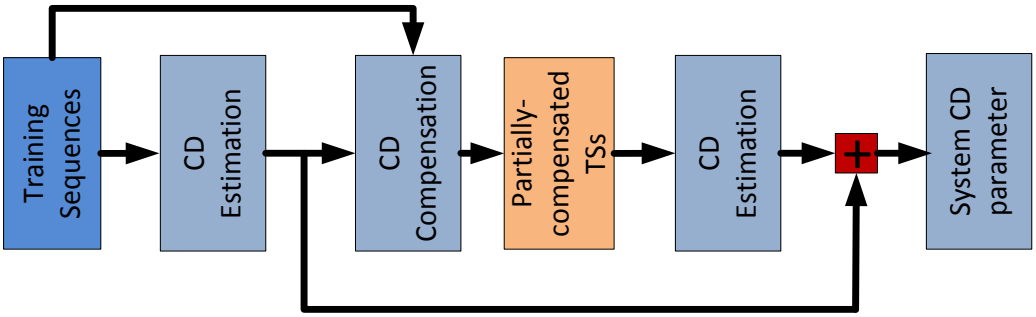

Figure 3.11: Dual-stage CD estimation block diagram.

Figure 3.12 shows the RMS error in simulations using two-stage DA CD estimation for different transmission distance using a 10-Gbaud PM-QPSK CO-SC system with TS length N_{ts} = 256 symbols and it can be seen that by adding a second stage, significant improvement in estimation error can be achieved. The two-stage method is most effective with long transmission distance as the residual CD is larger and, in terms of relative error percentage, can be estimated more accurately compared to short transmission distance where the residual CD is already small. This leads to a smaller estimation error percentage at long distance and larger error percentage at short distance similar to first stage estimation error. Depending on the transmission distance, second

stage CD estimation may not be necessary as the residual CD in the first stage is already small for short transmission distance. For an adaptive CD estimation method based on DA-CE, the estimated value during the first stage estimation can be used to determine whether a second stage estimation is necessary.

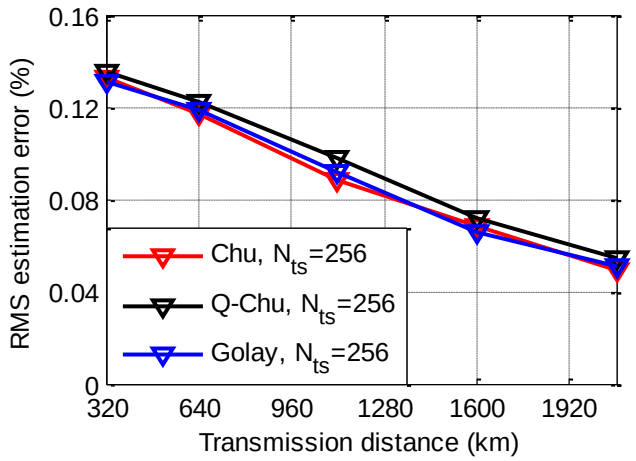

Figure 3.12: RMS estimation error for dual-stage CD estimation for PM-QPSK system with N_{ts} = 256 in simulation.

3.5 EXPERIMENTAL DEMONSTRATION

3.5.1 Experimental Setup

Figure 3.13(a) shows the experimental setup to demonstrate the CD estimation technique using PM-QPSK and PM-16QAM systems. The TSs are generated by two AWGs at 10 Gsymbol/s. Chu and Q-Chu sequence pairs are generated using shift orthogonal method and Golay sequences are generated using recursive construction and QPSK seed pairs. While sequences with minimal length of 64 symbols are required from Equation 3.8, each TS in the experimental demonstration has been chosen to have length N_{ts} = 256 symbols in order to enhance the estimation accuracy with CP lengths N_{cp} = 64 as illustrated in Figure 3.14(a). The TS block, consisting of four TSs plus CP blocks, is inserted into the randomly generated data frame at a code rate of 1.5% overhead ratio. The sequences are then modulated using two I/Q optical modulators to generate optical signals on X and Y- polarisations, respectively. The two data signals are then multiplexed through the PBC to form final PM-QPSK signal. A 160-km long

recirculating loop with standard single-mode fibre (SSMF) is used as a fibre channel with loop timing determining the total transmission length.

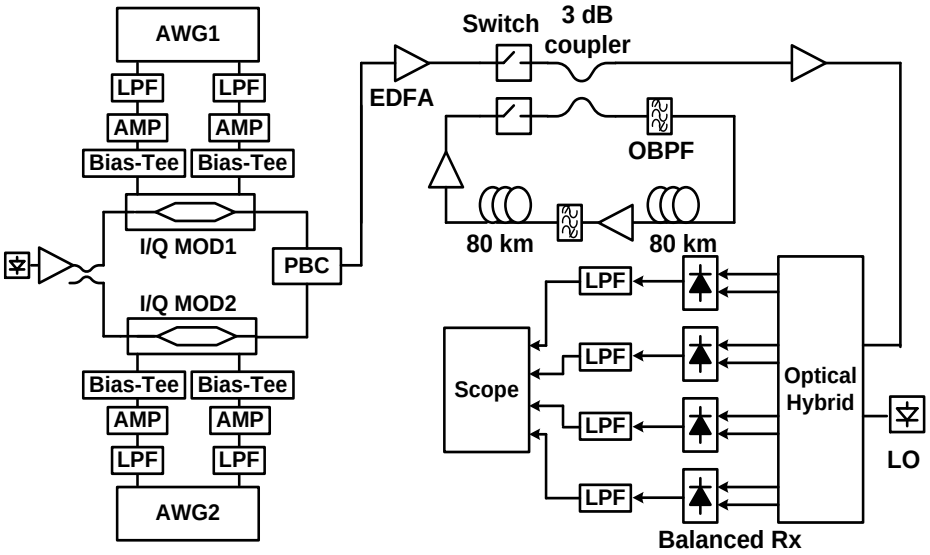

(a)

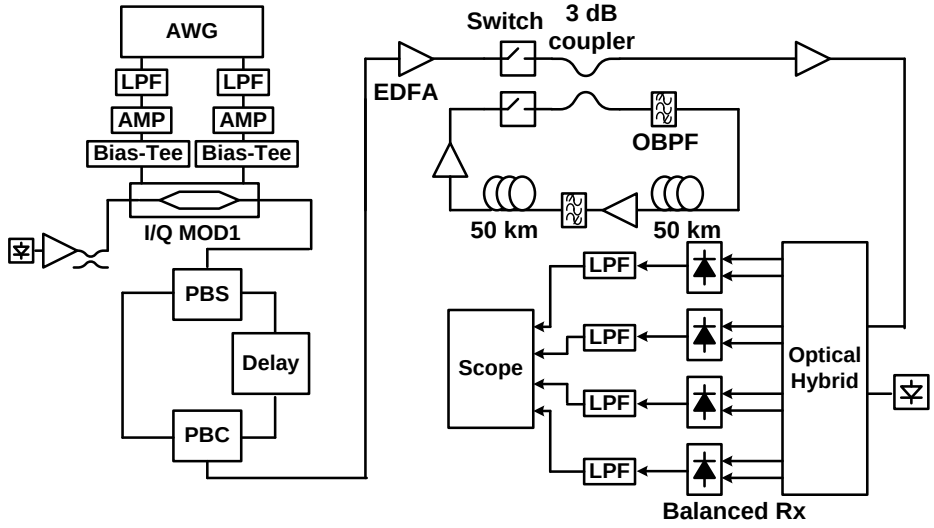

(b)

Figure 3.13: Experimental setup for (a) PM-QPSK system and (b) PM-16QAM system.

For PM-16QAM experiments, due to the unavailability of the original setup, the transmitter side consists of only one AWG to generate data on the X-polarisation and a delay line to emulate the Y-polarisation with delay time of 27.2 ns as shown in Figure 3.13(b). The recirculating loop is 100-km long and due to the different setup, the

structure of the TSs is modified and shown in Figure 3.14(b) for the PM-16QAM system. The receiver setup for both PM-QPSK and PM-16QAM systems is the same, where the signals are first filtered by an optical band-pass filter (OBPF) before being fed into an optical hybrid followed by 18-GHz balanced receivers. The signals are then captured in a 20-GHz 50-Gsamples/s oscilloscope for offline processing.

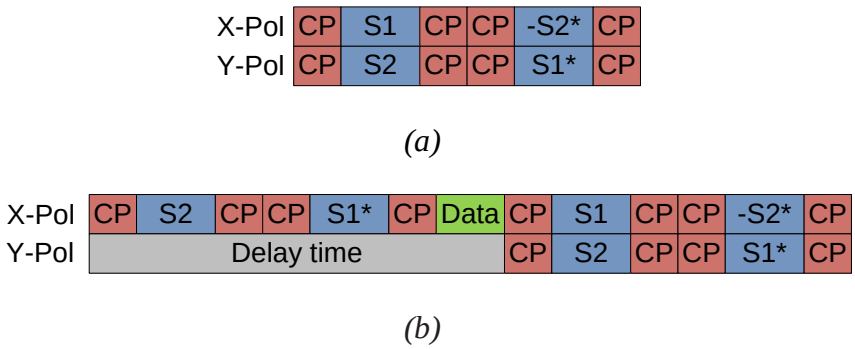

Figure 3.14: Structure of training frame for (a) PM-QPSK system and (b) PM-16QAM system.

Both FO compensation and frame synchronisation are carried out by DA algorithms [29]. After FO compensation and frame synchronisation, CD transfer function is estimated using the method described in Section 3.2.2 above.

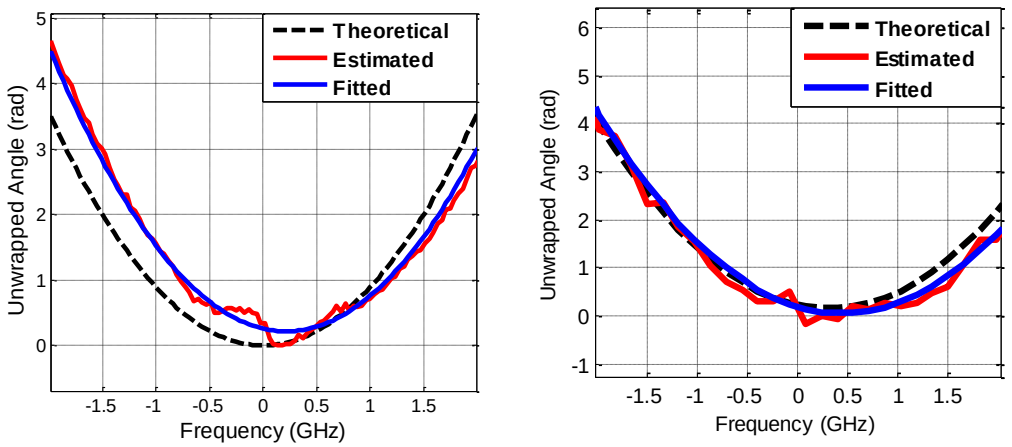

Figure 3.15: CD estimation phase curves for (a) 40-Gb/s PM-QPSK system after 2080 km and (b) 80-Gb/s PM-16QAM system after 1800 km.

The phase responses of the CD transfer function are shown in Figure 3.15(a) for PM-QPSK 2080-km transmission and Figure 3.15(b) for PM-16QAM 1800-km transmission, respectively. The red curve indicates the extracted estimated phase response, the black curve is the theoretical value, and the blue curve is the least square quadratic fit. It can be seen that both the estimated and quadratic fit CD curves are shifted due to extra impairments in the systems. However the CD estimation is extracted from the curvature of the phase plots and is immune to this shift.

3.5.2 Experimental Results

3.5.2.1 Single-Stage CD Estimation

Distance (km)	**Real CD (ps/nm)**	**RMS error % (Golay)**	**RMS error % (Chu)**	**RMS error % (Q-Chu)**	**RMS error % (Random)**
320	5376	0.4	1.5	1.7	1.2
640	10752	1.2	1.0	1.3	0.9
1120	18816	0.9	0.9	1.0	14.0
1600	26880	0.5	0.6	0.8	5.5
2080	34944	0.9	0.7	1.1	8.0

Table 3.1: Experimental results for PM-QPSK system.

Experimental results for PM-QPSK system transmission are summarised in Table 3.1. In order to measure RMS errors, the real CD parameter for the fibre is measured using the baseband amplitude-modulation response method in [31] and is found to be 16.8 ps/nm.km with 0.1% accuracy. It can be seen that the estimation is accurate with low RMS error percentage with a maximum error of 1.5% for the Chu sequence and 1.2% for the Golay sequences while it can also be seen that the Q-Chu sequence has slightly worse performance with maximum error of 1.7%. When random QPSK data sequences are used as TSs, significant higher estimation errors are obtained at long distances.

Figure 3.16 shows the estimation error percentage using the Chu, Q-Chu and Golay sequences at different transmission fibre lengths while results using random PM-QPSK

sequence are omitted due to having much higher error (above 5% for transmission distance beyond 640 km). It can be seen that the Golay sequences achieve very similar performance compared to the full-level Chu sequence whereas the Q-Chu sequence has slightly worse performance. However, the performance of the Q-Chu sequence is still within 0.5% error of the ideal Chu sequence. Overall, experimental results for PM-QPSK system are accurate and consistent with the simulation results.

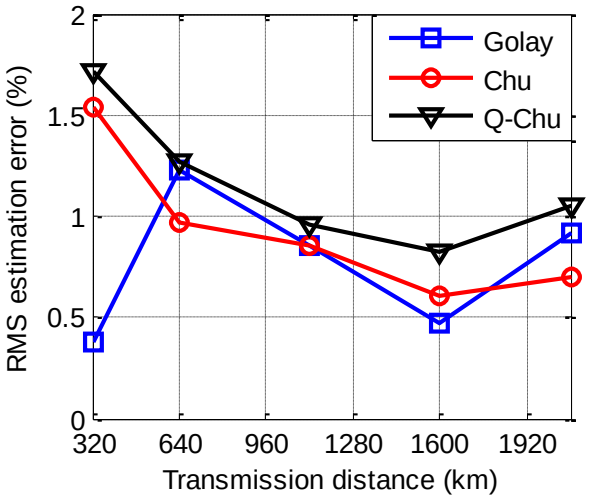

Figure 3.16: RMS estimation error at different transmission distances for PM-QPSK system.

For PM-16QAM system experiments, due to the unavailability of a second AWG, data on the Y-polarisation are emulated by delaying data on the X-polarisation with a delay time of 27.2 ns, which corresponds to 272 symbols for 10-Gbaud system. This delay time setup limits the maximum length of the TSs to 128 symbols per sequence and the maximum CP length is limited to N_{cp} = 4 symbols in the case N_{ts} = 128. While this length is enough for channel memory requirements according to Equation 3.8 and as shown in the simulation, the estimation performance is less accurate compared to using 256-symbol sequences. The lack of CP symbols is also tolerated by reducing the estimation area as demonstrated in Section 3.4.2 and thus a small estimation penalty is added as a result. Tables 3.2 and 3.3 show the experimental results for the PM-16QAM system with both sequence length of N_{ts} = 128 and N_{ts} = 64, respectively. The CD parameter of the fibre used in this experiment had been independently measured using the method in [31] to be 16 ps/nm.km with 0.1% accuracy. It can be seen that for N_{ts} =

128, maximum errors for Chu, 16QAM-Golay and 16QAM-Chu sequences are 3.04%, 2.9%, and 3.05 %, respectively. For N_{ts} = 64, maximum errors for Chu, 16QAM Golay, and 16QAM-Chu sequences are 4.3%, 4.4% and 4.5%, respectively.

Distance (km)	**Real CD (ps/nm)**	**RMS error % (16QAM-Golay)**	**RMS error % (Chu)**	**RMS error % (16QAM-Chu)**
300	4800	2.76	2.96	2.65
600	9600	2.90	2.80	2.91
900	14400	2.84	3.04	3.05
1200	19200	2.70	2.64	2.60
1500	24000	2.60	2.47	2.79
1800	28800	2.63	2.80	2.74

Table 3.2: Experimental results summary for PM-16QAM system with N_{ts} = 128.

Distance (km)	**Real CD (ps/nm)**	**RMS error % (16QAM-Golay)**	**RMS error % (Chu)**	**RMS error % (16QAM-Chu)**
300	4800	4.35	4.25	4.46
600	9600	4.15	4.15	4.45
900	14400	4.29	4.01	4.25
1200	19200	4.20	4.25	4.4
1500	24000	3.96	4.28	4.36
1800	28800	4.05	3.98	4.05

Table 3.3: Experimental results summary for PM-16QAM system with N_{ts} = 64.

Figure 3.17 shows the combined data from Tables 3.2 and 3.3 and it can be seen that all 3 types of sequences perform very similarly to each other and the maximum errors are consistent with the simulation results. While 256-symbol sequences are not used, the relationship between sequence length and their performance for 128-symbol and 64-symbol sequences is verified and is consistent with the simulation results. Overall it can be seen that for both PM-QPSK and PM-16QAM systems, Golay pairs and Chu-based

sequences provide very similar performance compared to the ideal Chu sequence, while offering advantage of length-independent constellation which make them suitable for large CD estimation using DA-CE aided by quadratic fit curve interpolation.

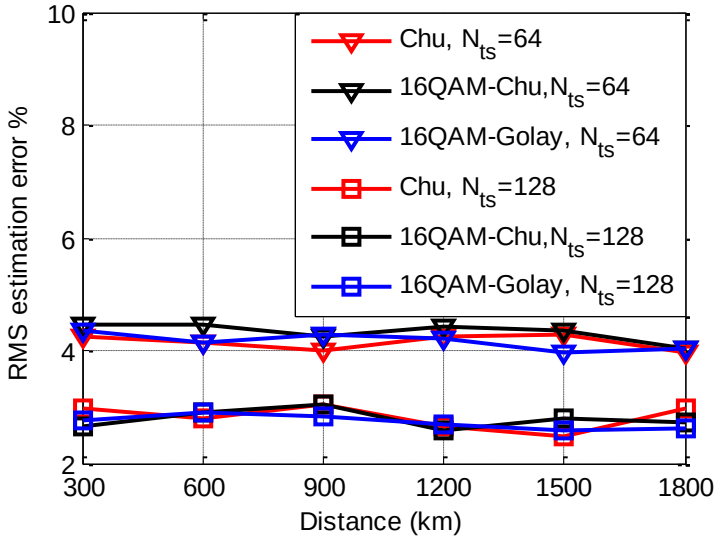

Figure 3.17: Estimation performance of Golay, 16QAM Golay, Chu and 16QAM-Chu sequences for PM-16QAM system.

3.5.2.2 Dual-Stage CD Estimation

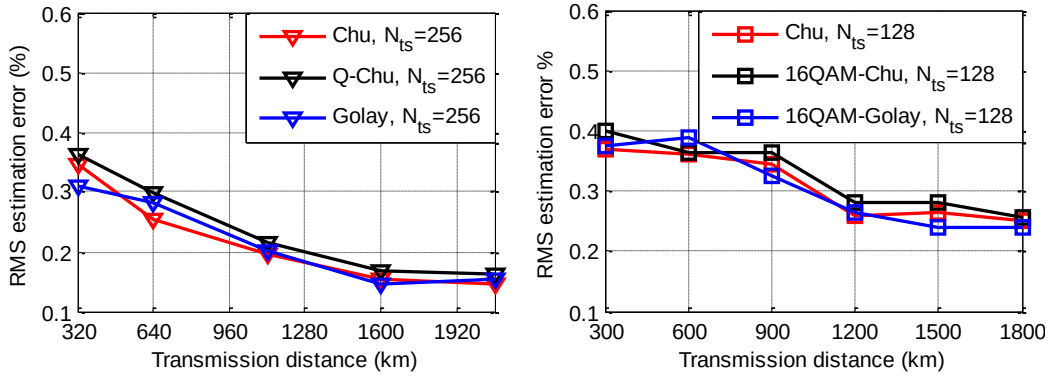

(a) *(b)*

Figure 3.18: RMS error for dual-stage CD Estimation in (a) PM-QPSK system and (b) PM-16QAM system.

Figure 3.18 shows the RMS errors for CD estimation using dual-stage method described

in Section 3.4.4 for both 40-Gb/s PM-QPSK and 80-Gb/s PM-16QAM systems with variable transmission distances with training length of N_{ts} = 256 for PM-QPSK system and N_{ts} = 128 for PM-16QAM system. It can be seen that estimation performance increases across the entire transmission range and the most improvement is at long transmission distance as predicted for dual-stage CD estimation using least square quadratic fit. For a very small transmission distance, a medium improvement in estimation accuracy is observed while a slightly larger improvement in estimation error is observed at a long transmission distance compared to a single stage estimation. This observation can be explained as follows: for short distance the residual CD is already very small and causes larger error in the second stage of estimation, which in turn results in smaller relative improvement compared to a long transmission distance, where the residual CD is larger. Overall it can be seen that estimation of CD is accurate with small percentage of errors and depends on the transmission length as estimated by the single-stage CD estimation, single-stage or dual-stage estimations can be employed. It is also possible to implement a third stage of estimation to further reduce the estimation error using the above concept. However for most CO systems with realistic transmission distances and sophisticated receiver DSP, single-stage or dual-stage DA estimations are sufficient to estimate the entire system CD with required accuracy. Assuming subsequent equalisation techniques, either blind or data-aided, are capable of compensating up to 30-km transmission in a 25GBaud system, then it can be seen that the proposed CD estimation technique can be used for total transmission link of up to 10000 km using dual-stage CD estimation before the signal needs to be regenerated.

3.6 CONCLUSIONS

This chapter presented a DA transmission link CD estimation technique based on the use of STBC for CE and quadratic interpolation for CD estimation. The technique can be employed as simple single-stage estimation or more complex dual stage estimation depending on the required estimation accuracy. The use of long TSs for DA-CE technique enables fast and simple full channel impulse response estimation at the receiver. The relationship between channel CD, system baud rate and required sequence length was also investigated. While CAZAC sequences provide ideal CE performance due to their flat frequency spectra, the complex constellations make it impossible to use long CAZAC sequences in practice for CD estimation purposes. Two types of TSs

designed for practical use of long TSs are proposed, namely Golay sequences and quantised CAZAC sequences and had been demonstrated to offer similar performance to ideal CAZAC-Chu sequences. Moreover, both Golay sequences and Chu-based sequences can be customized in PM-QPSK and PM-16QAM formats for any arbitrary lengths which allow easy integration into commercial 100-Gb/s PM-QPSK systems and also those that employ higher order modulators such as PM-16QAM modulators and beyond. Through simulation, it was confirmed that the proposed CD estimation method is robust against various levels of PMD and OSNR and in general longer sequences give more accurate results. This can be explained as longer sequences give higher estimation resolution in frequency domain and thus provide the estimation algorithm with more samples to interpolate, which in turn results in better accuracy.

For higher estimation accuracy, the use of dual-stage CD estimation was also demonstrated alongside single-stage estimation and it can be seen that with a small trade-off in computational complexity, the estimation accuracy can be improved significantly. The use of dual-stage CD estimation is most effective with longer transmission distances as the second stage only estimates the residual CD and this parameter is also proportional to the total transmission distance. For short distances, the residual CD due to estimation error is small and the use of second stage is not required in practice as most coherent receiver DSPs are capable of some tolerance to residual CD. The use of single or dual-stage estimation can be determined by the estimated CD value in the first stage, which roughly estimates the system CD and the receiver can use this parameter to determine if a second stage estimation is required.

The combined techniques were experimentally demonstrated through 40-Gb/s coherent PM-QPSK system for up to 2080-km transmission distance and 80-Gb/s PM-16QAM system for up to 1800-km distance. Both single-stage and dual-stage estimation techniques were demonstrated with high accuracies and the results were consistent with theory and simulation.

The study of using DA method for system CD estimation had led to the design of TSs with length-independent constellation and channel CD estimation method based on least square interpolation. These techniques can be used for OSNR estimation purpose, as well as timing synchronisation for DA-CE and equalisation, which will be presented in

Chapters 4 and 5, respectively.

3.7 REFERENCES

[1] M. Kuschnerov, F. N. Hauske, K. Piyawanno, B. Spinnler, A. Napoli, and B. Lankl, "Adaptive chromatic dispersion equalisation for non-dispersion managed coherent systems," *Optical Fibre Communication Conference OFC'2009*, San Diego, CA, USA, paper OMT1, 2009.

[2] F. N. Hauske, C. Xie, Z. Zhang, C. Li, L. Li, and Q. Xiong, "Frequency domain chromatic dispersion estimation," *Optical Fibre Communication Conference OFC'2010*, paper JThA11, San Diego, CA, USA, May 2010.

[3] D. Wang, C. Lu, A. P. T. Lau, and S. He, "Adaptive chromatic dispersion compensation for coherent communication systems using delay-tap sampling technique," *IEEE Photonics Technology Letters*, vol. 23, no. 14, pp. 1016–1018, Jul. 2011.

[4] R. Borkowski, X. Zhang, D. Zibar, R. Younce, and I. T. Monroy, "Experimental demonstration of adaptive digital monitoring and compensation of chromatic dispersion for coherent DP-QPSK receiver," *Optics Express*, vol. 19, no. 26, pp. 728–735, Dec. 2011.

[5] S. M. Ranzini, E. C. Magalhães, V. B. Ribeiro, V. V. Nascimento, and J. C. R. F. Oliveira, "Accurate blind chromatic dispersion estimation in long-haul 112 Gbit/s PM-QPSK WDM coherent systems," *OSA Signal Processing in Photonics Communications (SPPCom)*, paper SpTh2B.3, Toronto, Canada, 2012.

[6] H. Wymeersch and P. Johannisson, "Maximum-likelihood-based blind dispersion estimation for coherent optical communication," *Journal of Lightwave Technology*, vol. 30, no. 18, pp. 2976–2982, Sep. 2012.

[7] R. A. Soriano, F. N. Hauske, N. G. Gonzalez, and I. T. Monroy, "Chromatic dispersion estimation in digital coherent receivers," *Journal of Lightwave Technology*, vol. 29, no. 11, pp. 1627–1637, Jun. 2011.

[8] M. Kuschnerov, F.N. Hause, K. Piyawanno, B. Spinnler, M.S. Alfiad, A. Napoli, and B. Lankl, "DSP for coherent single-carrier receivers," *Journal of Lightwave Technology*, vol. 27, no. 16, 3614-3622, Aug. 2009.

[9] Q. Sui, A P. T. Lau, and C. Lu, "Fast and Robust Chromatic Dispersion Estimation Using Auto-Correlation of Signal Power Waveform for DSP-based Coherent Systems," *Optical Fibre Communication Conference OFC'2012*, pp 1-3, Los Angeles, CA, USA, 2012.

[10] Q. Sui, A. P. T. Lau, and C. Lu, "Fast and robust blind chromatic dispersion estimation using auto-correlation of signal power waveform for digital coherent systems," *Journal of Lightwave Technology*, vol. 31, no. 2, pp. 306–312, Jan. 2013.

[11] J. C. Geyer, F. N. Hauske, C. R. S. Fludger, T. Duthel, C. Schulien, M. Kuschnerov, K. Piyawanno, D. van den Borne, E. D. Schmidt, B. Spinnler, B. Lankl, and B. Schmauss, "Channel parameter estimation for polarisation diverse coherent receives," *IEEE Photonics Technology Letters*, vol. 20, no. 10, pp. 776–778, May. 2008.

[12] F. N. Hauske, J. Geyer, M. Kuschnerov, K. Piyawanno, T. Duthel, C. Fludger, D. van den Borne, E. Schmidt, B. Spinnler, H. de Waardt, and B. Lankl, "Optical performance monitoring from FIR filter coefficients in coherent receivers," *Optical Fibre Communication Conference OFC'2008* , paper OThW2, San Diego, CA, USA, 2008.

[13] F. N. Hauske, M. Kuschnerov, B. Spinnler, and B. Lankl, "Optical Performance Monitoring in Digital Coherent Receivers," *Journal of Lightwave Technology*, vol. 27, no. 16,pp. 3623-3631, Aug. 2009.

[14] F. Pittalà, F. N. Hauske, Y. Yabin, N. G. Gonzalez, and I. T. Monroy, "Combined CD and DGD Monitoring Based on Data-Aided Channel Estimation," *Signal Processing in Photonic Communications SPPCom*'2011, pp. SPTuC3, Toronto, Canada, 2011.

[15] F. Pittala, F. N. Hauske, Y. Yabin, N. G. Gonzalez, and I. T. Monroy, "Fast and robust CD and

DGD estimation based on data-aided channel estimation," *International Conference on Transparent Optical Networks ICTON'2011*, paper We.D1.5, Brussels, Stockholm, Jun. 2011.

[16] M. Kuschnerov, M. Chouayakh, K. Piyawanno, B. Spinnler, E. de Man, P. Kainzmaier, M. S. Alfiad, A. Napoli, and B. Lankl, "Data-aided versus blind single carrier coherent receivers," *IEEE Photonics Journal*, vol. 2, no. 3, pp.387-403, Jun. 2010.

[17] C. Do, A. V. Tran, C. Zhu, S. Chen, T. Anderson, D. Hewitt and E. Skafidas, "Data-Aided Chromatic Dispersion Estimation for Polarisation Multiplexed Optical Systems," *IEEE Photonics Journal* , vol 4, no. 5, pp. 2037–2049, Oct. 2012.

[18] Y. Han and G. Li, "Coherent optical communication using polarisation multiple-input-multiple-output," *Optics Express*, vol. 13, no. 19, pp. 7527-7534, Sep. 2005.

[19] S. Alamouti, "A simple transmit diversity technique for wireless communications," *IEEE Journal on Communication*, vol. 16, no. 8, pp. 1451-1458, Oct. 1998.

[20] S. D. Howard, A. R. Calderbank, and W. Moran, "A simple signal processing architecture for instantaneous radar polarimetry," *IEEE Transactions on Information Theory*, vol. 53, no. 4, pp 1282-1289, Mar. 2007.

[21] V. Tarokh, H. Jafarkhani, and A. R. Calderbank, "Space-Time Block Codes from Orthogonal Designs," *IEEE Transactions on Information Theory*, vol. 45, no. 5, pp 1456-1467, Jul. 1999.

[22] S. J. Savory, "Compensation of fibre impairments in digital coherent systems," *European Conference on Optical Communication ECOC'2008*, paper Mo.3.D.1, Brussels, Belgium, 2008.

[23] C. Chu, "Polyphase codes with good periodic correlation properties," *IEEE Transactions on Information Theory*, vol. 18, no. 4, pp. 531-532, Jul. 1972.

[24] J. S. Pereira, "Generalized Chu polyphase sequences," *International Conference on Telecommunications ICT*, pp. 47-52, May 2009.

[25] M. J. Golay, "Complementary series," *IRE Transactions on Information Theory*, vol. 7, no. 2, 82-87, Apr. 1961.

[26] W. H. Holzmann and H. Kharaghani, "A computer search for complex Golay sequences," *Australasian Journal of Combinatorics*, vol. 10, pp. 251-258, Apr. 1994.

[27] R. Craigen, W. H. Holzmann and H. Kharaghani, "Complex Golay sequences: structure and applications," *Discrete mathematics*, vol. 252, no. 1, pp. 73-89, May 2002.

[28] C. Chong et al, "Two construction of 16-QAM Golay complementary sequences," *IEEE International Symposium on Information Theory ISIT 2002*, pp. 240, 2002

[29] C. Zhu, A. V. Tran, C. C. Do, F. Pittala, F. N. Hauske, S. Chen, T. Anderson and E. Skafidas, "Digital Signal Processing for Training-Aided Coherent Optical Single-Carrier Frequency-Domain Equalisation Systems" accepted in *Journal of Lightwave Technology*.

[30] M. S. Faruk, Y. Mori, C. Zhang, K. Igarashi, and K. Kikuchi, "Multi-impairment monitoring from adaptive finite-impulse-response filters in a digital coherent receiver," *Optics Express*, vol. 18, no. 26, pp. 26929-26936, Dec. 2010.

[31] D. Derickson, *Fibre Optic Test and Measurement*, Section 12.3, pp. 486-487, Prentice Hall 1998.

4 Data-Aided OSNR Estimation for Coherent Optical Systems

4.1 INTRODUCTION

Coherent receivers enable a linear translation between the optical signals and the captured electrical signals and thus, besides enabling digital signal processing (DSP), the use of coherent receivers for optical communication networks has also enabled a whole new level of optical performance monitoring (OPM) techniques for monitoring signal quality and estimation of channel impairments. Based on the captured signals at the coherent receivers, estimation of chromatic dispersion (CD), polarisation-mode dispersion (PMD) and polarisation-dependent loss (PDL) had been demonstrated [1]-[4]. Optical signal-to-noise ratio (OSNR) is also a very important parameter in monitoring network performance and is directly related to the network quality, and estimation of this parameter has seen intensive research interests [5]-[23]. Unlike CD, PMD and PDL, OSNR cannot be estimated from the acquired channel transfer matrix and also cannot be compensated using DSP in electrical domain. Thus, estimation of this parameter has become a critical component in designing OPM for high-speed optical communication networks. As demonstrated in Chapter 2, OSNR estimation technologies can be based on optical signal spectrum [5], polarisation nulling [6]-[11], signal's degree of polarisation (DOP) [12]-[15], non-linear optical effects [16]-[18], or signal-to-noise ratio (SNR) of the received signals based on coherent receivers [19]-[25]. Among the proposed techniques, those based on received signals' SNR are very attractive as the implementation of these techniques will utilise the same receiver used for signal equalisation and no extra hardware is involved. While it is well-known that the equalised signal constellation can provide an easy path for OSNR estimation, the implementation of SNR-based techniques typically utilises the actual received data

signals equalised from zero-forcing method, and analyses the constellation of the received signals [20]-[25]. While these techniques provide accurate estimation of OSNR utilising coherent receivers, as well as the capability to work with both blind and data-aided (DA) systems, the requirement for use of zero-forcing equaliser means that these techniques cannot be implemented in systems with more sophisticated data equalisers such as minimum mean square error (MMSE) equalisation method. Furthermore, for coherent optical (CO) systems employing DA channel estimation (CE), the general trend is to utilise DA-CE for initial acquisition of channel transfer matrix and subsequently improving equalisation performance through complex adaptive algorithms [25], which could lead to inaccuracies in OSNR estimation using equalised data constellation. Thus, there are advantages of designing OSNR estimation techniques for coherent receivers that do not require equalisation of the actual data frame. Since DA-CE had been demonstrated as being able to provide fast and robust CE [25]-[29], it is very likely that the future implementation of CO single carrier (SC) systems will implement some forms of DA-CE and it is desirable to investigate OSNR estimation technique based on DA-CE method. As the training sequences (TSs) are only used for CE in CO systems with DA-CE, it is desirable to investigate methods that utilise the training blocks for OSNR and SNR estimation purposes for this would make the estimation transparent to the actual data and enable the use of SNR-aware equalisers such as MMSE as well as more sophisticated data equalisation methods.

In this chapter, an SNR and OSNR estimation technique for CO systems with DA-CE based on complementary Golay sequences is presented [30]. The technique utilises TSs for CE and also equalises the TSs for OSNR estimation through filtered CE. The use of long sequences enables fast and robust CE. This also allows OSNR estimation right at the beginning of the data frame with the additional advantage that SNR estimation is transparent to the data frame plus the entire data frame does not need to be equalised before updating SNR and OSNR information. The technique is verified through simulations and experiments to be able to accurately estimate a wide range of OSNR with an estimation error of around 0.7 dB and is robust against channel impairments.

4.2 SNR AND OSNR ESTIMATION USING COHERENT RECEIVERS

4.2.1 Data-Aided SNR Estimation

As previously presented in Chapter 3, coherent polarisation-multiplexed (PM) optical channel can be modelled as a 2x2 multiple-input multiple-output (MIMO) transmission link similar to a wireless MIMO channel. Based on this model, DA-CE and equalisation using least square estimation can then be performed [26]. After the channel transfer matrix is acquired, equalisation of the following data frame can be executed based on either zero-forcing (ZF) or MMSE criteria with the latter requiring information about SNR. Equalisation can be performed based on the fractionally-spaced equaliser [27] with ZF method and the equalised data information can be used for channel SNR estimation [22]. In order to estimate SNR from the TSs, we first consider an equalised data sequence in time domain with noise information expressed as:

$$r[n] = s[n] + w[n] \tag{4.1}$$

where $r[n]$ is the equalised sequence, $s[n]$ is the original sequence and $w[n]$ represents the added noise. We further assume that the noise is Gaussian with a mean of 0 and a variance of $2\sigma^2$.

From Equation 4.1 it can be observed that if the signal or its constellation is known, then the noise parameters can be estimated. In case the entire signal is known, then the noise parameters can be directly subtracted from the received signal, whereas in case the signal constellation is known, statistical method can be used to estimate the SNR [21]-[22]. Since the TSs are known, it is possible to estimate the noise parameters from the TSs by using the noise subtraction method. The entire frame does not need to be equalised first and the SNR information can be used for subsequent data equalisation using noise-aware MMSE method while the OSNR information can be further processed from SNR for OPM purpose. Thus the use of training-based SNR estimation technique leaves flexibility in choosing receiver data equalisation method as only the TSs need to be equalised using zero-forcing criteria.

However, a limitation of using the TSs for SNR estimation mainly comes from the use of TSs as a method for CE. SNR estimation by noise subtraction from the TSs is only possible if the received sequences have been successfully equalised using a noise-free

CE. If the TSs are self-equalised using raw CE and overlap frequency domain equalisation (OFDE), then the results obtained will be an approximate version of the original sequences without any noise components since the noise is also "equalised". In order to treat the TSs as regular data and to equalise the TSs using DA-CE, a noise-suppressed estimated channel transfer matrix needs to be used for the equalisation of the TSs. A standard approach to estimate a noise-suppressed channel transfer matrix is to repeat the TSs multiple times and to use averaged estimation over multiple training blocks as the estimated channel transfer matrix. This will ensure an accurate estimation since the noise in CE will be averaged out. However, it can be seen that using multiple training blocks will significantly increase the overhead ratio. A different method that can be applied to achieve enhanced CE is the use of digital noise filters on the raw estimated channel transfer functions. In this case only a single training block is required and the use of noise filtering can help to achieve an enhanced estimation from the initial least square estimation using TSs.

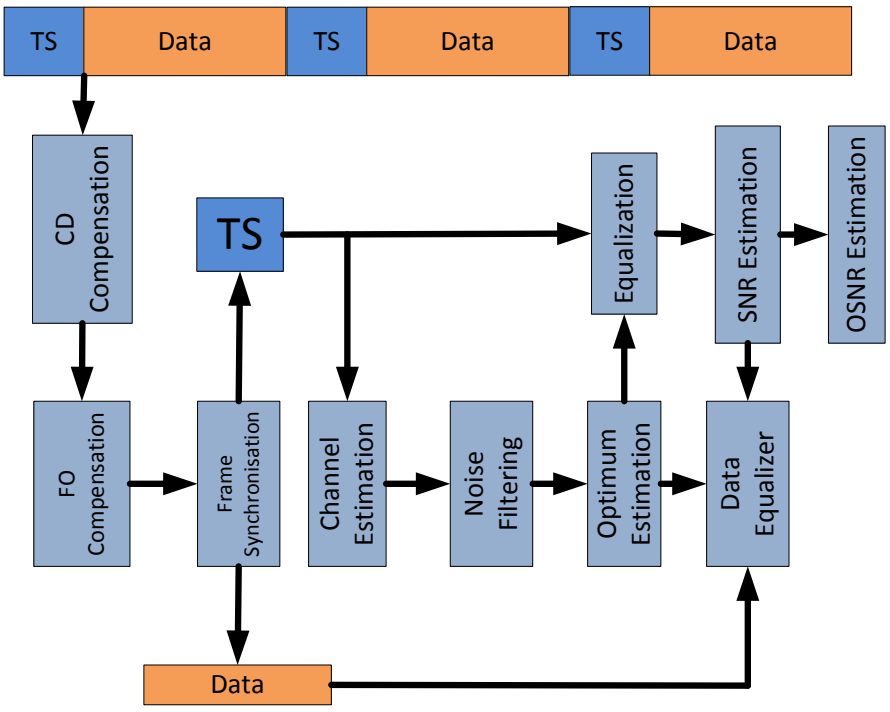

Figure 4.1: Block diagram of receiver's DSP for DA-CE with OSNR estimation.

Figure 4.1 illustrates a block diagram of the receiver's DSP for CO-SC systems using DA-CE with OSNR estimation. The training blocks are frequently inserted into the

actual data frame for CE purpose with each frame consisting of one training block and the actual transmitted data. At the receiver, CD is estimated using the method presented in Chapter 3 and is compensated in the frequency domain using OFDE. After frequency offset (FO) compensation and frame synchronisation, the training blocks can be separated from the data frame for CE. This estimation is passed through a noise filter to remove all noise components and the resultant "optimal" estimation is used at that point for the equalisation of the TS. SNR and OSNR information can then be estimated for channel monitoring purposes while the SNR information can also be relayed back to the equaliser for data equalisation using noise-aware equaliser like MMSE.

The main requirement for this scheme is the aforementioned implementation of the noise-free CE procedure as described in Figure 4.1. A few methods have been suggested in order to enhance CE from the initial DA raw estimation. A moving average filter (MAF) can be employed to average out the noise in CE or the time domain nulling filter (TDNF), can be used [25]. A primary characteristic of using filters for the enhancement of CE is that the estimated channel transfer function has to be of reasonably high resolution, regardless of the actual channel impulse response. Thus, a desirable approach for utilising the TS as "OSNR-header" would be to utilise long sequences and noise filtering method for the enhancement of CE.

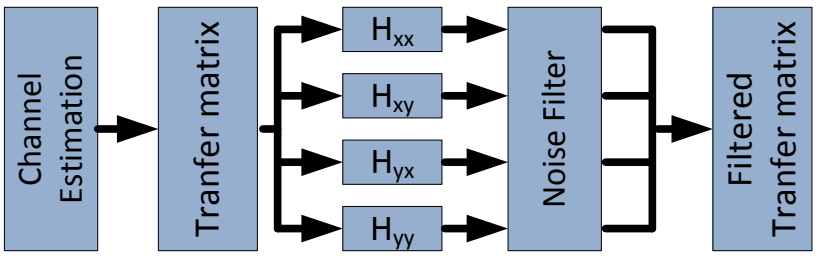

Figure 4.2: CE with noise filtering.

Figure 4.2 illustrates the steps for OSNR estimation using the proposed self-equalised TSs method. The raw channel transfer matrix is first estimated using DA method as described in Chapter 3. The channel transfer matrix is 2x2 in dimension whereas typically employed digital noise filters are only one-dimensional. Because of that, each element of this matrix is separated in a single one-dimensional vector before passing through the noise filters. The resulting filtered transfer function is then rearranged back

to form the filtered channel transfer matrix. By suppressing noise during CE, the equalised TS will contain noise samples in their equalised signal constellation, which can be used for OSNR estimation purpose.

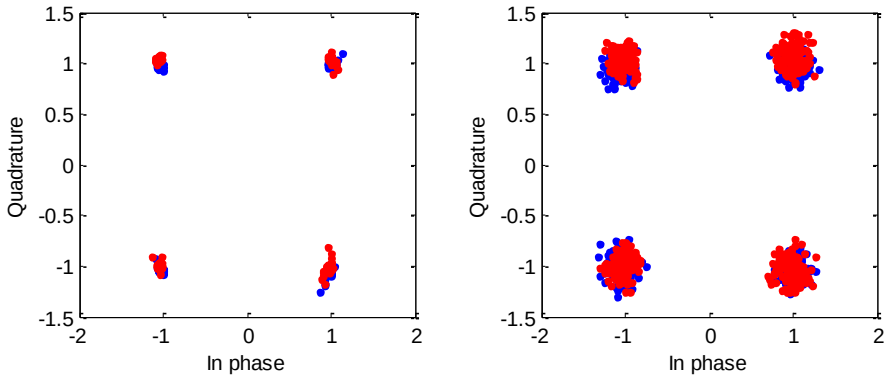

(a) *(b)*

Figure 4.3: Constellations of equalised TS for PM-QPSK with (a) no filtering in channel transfer function, and (b) filtering in channel transfer function.

Figure 4.3 shows constellation plots of the equalised TSs for PM quadrature phase shift keying (QPSK) systems before and after channel filtering using MAF and Golay sequences with length N_{ts} = 256 symbols and OSNR = 22 dB. Golay sequences can be generated with any arbitrary length and can be employed for CE with optimal estimation performance. Here the same Golay sequences are also employed for the proposed SNR and OSNR estimation method based on TS self-equalisation technique. In the case of no channel filtering, the TSs are first used for CE and this raw estimation is then used for the equalisation of the training blocks. As illustrated in Figure 4.3(a), it can be seen that most of the original "perfect" signal constellation is received with only small variations in the equalised TSs. Since the estimated channel matrix is estimated from the TS while the TS is equalised using this estimation and OFDE method, this variation is a result of the misalignment between the overlap-cut equaliser and the training block, in comparison to having the "perfect equalisation". On the other hand, it can also be seen in Figure 4.3(b) that with DA-CE and noise filtering, the TSs are equalised using the filtered channel transfer matrix and the noise is preserved in the final constellation. This in turn results in an equalised training block with added noise and this training block can be used for system SNR estimation and subsequent system OSNR estimation.

After equalisation of TSs using the estimated channel information with filtering, the added noise can then be subtracted from the signal and the SNR is measured as:

$$SNR = \frac{1}{N}\sum_{k=1}^{N}\frac{s[k]^2}{w[k]^2} \tag{4.2}$$

where $s[k]$ represents the sampled signal and $w[k]$ represents the sampled noise. Once system SNR has been estimated, further steps can be employed to derive system OSNR from system SNR. It had been demonstrated that system OSNR and system SNR are linearly related through a calibration factor related to the receiver's noise [20]. In general, system SNR can be viewed as channel OSNR plus the receiver's noise. Therefore, the OSNR can be estimated first by measuring the electrical RF noise SNR_{RF} at a reference OSNR point [21]-[22] and subtracting this noise parameter from the estimated system SNR. This is done by measuring the reference point in back-to-back configuration without any added amplified spontaneous emission (ASE) noise, and then calculates the OSNR as:

$$OSNR_{dB} = 10\log_{10}\left(\frac{R_s}{B_{ref}}\right) - 10\log_{10}(SNR^{-1} - SNR_{RF}{}^{-1}) \tag{4.3}$$

where B_{ref} and R_s are the reference bandwidth and system baud rate, respectively, and SNR_{RF} is the measured system SNR without any added ASE noise.

4.2.2 Filter Types

The previous section described the method for SNR and OSNR estimation using self-equalised TSs. It can be observed that many filter types can be employed to achieve noise free CE for the purpose of SNR and OSNR estimation. Since the estimated channel transfer matrix is split into four separate vectors before passing to the noise filter, only one dimensional filter is required. This section hence describes two noise filtering techniques employed for channel SNR estimation using DA-CE and TS self-equalisation technique.

4.2.2.1 Moving Average Filter

A simple yet effective filter for noise removal is the MAF. This is a single-stage feed-forward noise filter operating directly on the sampled channel transfer function. With respect to the channel transfer matrix, the MAF function can be defined as:

$$W_{i,j}[n] = \frac{1}{N_{sample,avg}} \sum_{k=0}^{N_{sample,avg}-1} H_{i,j}[n+k] \tag{4.4}$$

where $W_{i,j}[n]$ is the filter channel transfer function; $H_{i,j}[n]$ is the original transfer function; i, j indicate the position of the function inside the frequency domain 2x2 transmission matrix and $N_{sample,avg}$ is the number of averaged samples to be used with MAF. The filter parameter to be optimised for OSNR estimation L_{maf} is defined as:

$$L_{maf} = \frac{N_{sample,avg}}{S_p N_{ts}} \tag{4.5}$$

where S_p is the number of samples per symbol and N_{ts} is the length of each TS. MAF is an optimal filter used to remove noise in time domain signals. Here, in consideration of frequency domain channel transfer functions as time domain signals, this approach will eliminate most of the noise in the CE, which in term ensures that this information is preserved in the final equalised signal for SNR estimation purpose.

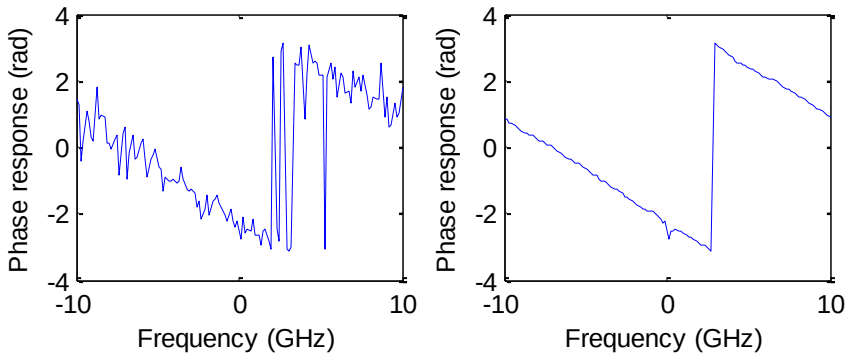

(a) *(b)*

Figure 4.4: Phase response of Hxx with (a) no noise filtering and (b) MAF

Figure 4.4 shows a simulation demonstration of the phase response of the H_{xx} transfer function before and after noise filtering using MAF filter with L_{maf} = 0.125 and N_{ts}=64 in back-to-back transmission with OSNR = 15 dB. It can be seen that the noise in estimation is successfully filtered out and the transfer function is essentially noise free,

which enables self-equalisation of the TSs and preserves the noise information for OSNR estimation purpose.

Nonetheless, it is well-known that MAF has the worst frequency response compared to other filters [31] and will also filter out signal information together with noise. As a consequence, one drawback of using MAF is that if the channel transfer function contains medium to large CD value, then MAF method will significantly degrade CE performance because the CD in CE is also averaged together with the noise component. Also, since MAF operates by averaging over multiple samples in the channel transfer matrix, higher resolution estimation will provide more samples over the total channel bandwidth, which in turn enables better performance for MAF.

4.2.2.2 Time Domain Nulling Filter

Another method to remove noise from CE is also proposed in [27] by utilising a TDNF. This is a noise removal technique designed to enhance frequency domain raw channel transfer functions estimated by DA-CE technique and can be described as follows. First, the method performs a high resolution estimation of the channel transfer matrix in frequency domain, with the estimated transfer functions' resolution being many times higher than required by the channel impulse response. The filtering is then applied by converting these transfer functions into time domain by means of inverse Fourier transforms (IFFTs). Consequently, this operation results in an impulse response function with many taps containing only noise due to high resolution estimation. Noise components that are outside of the actual channel impulse response are suppressed and the final impulse response function is converted back into frequency domain using fast Fourier transforms (FFTs), creating a filtered channel transfer matrix. The filter parameter, L_{tdnf} is defined as:

$$L_{tdwf} = \frac{N_{sample,nulled}}{S_p N_{ts}} \qquad \text{with} \qquad N_{sample,nulled} = S_p N_{ts} - L_h \tag{4.6}$$

where $N_{sample,nulled}$ is the number of samples to be nulled using TDNF, L_h is the total channel impulse response; S_p and N_{ts} are the samples per symbol and the length of each TS, respectively.

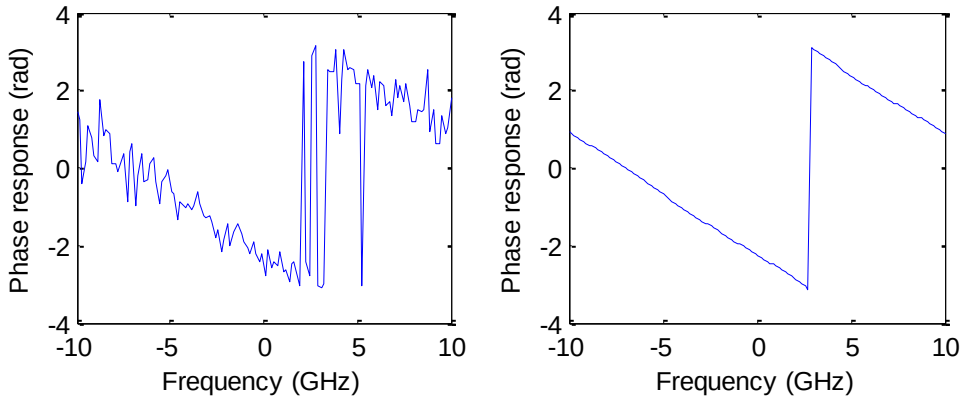

(a) *(b)*

Figure 4.5: Phase response of Hxx with (a) no noise filtering and (b) TDNF

Figure 4.5 shows a simulation demonstration of the phase response of the H_{xx} transfer function before and after noise filtering using TDNF with L_{tdnf} = 0.97 and N_{ts}=64 in back-to-back transmission with OSNR = 15 dB. It can be seen that compared to MAF, TDNF is slightly less aggressive in filtering out channel information causing small ripples in the phase response however the entire filtered response is also slightly smoother compared to MAF. Nonetheless, these differences are very small and should not cause any significant differences between equalisation performances of the two methods. In theory, if the channel impulse response length in time domain is equal to the resolution of the CE in frequency domain, then no noise filtering will be performed since $L_h = N_{ts}$. It can be seen that performing CE with a large CD value will result in a longer channel impulse response, leaving fewer noise-only taps if both conditions in Equation 4.6 are to be satisfied. For CE, it is trivial that this method provides a trade-off between CD tolerance and noise enhancement performance.

From a channel enhancement perspective, both MAF and TDNF methods are subject to degradation due to CD with TDNF providing a trade-off between CD tolerance and noise filtering performance. Another similarity is that both methods require high resolution estimation of the frequency domain channel transfer matrix. This condition can be achieved without difficulty by using a training block with long TSs for CE purpose.

4.3 SIMULATION ANALYSIS

The previous section presented theory on the proposed DA SNR and OSNR estimation technique, which utilises only the training blocks for estimation purpose based on self-equalised TSs using noise-filtered CE. In this section, computer simulations are used to investigate performances as well as different characteristics of the proposed technique versus different channel impairments.

4.3.1 Simulation Setup

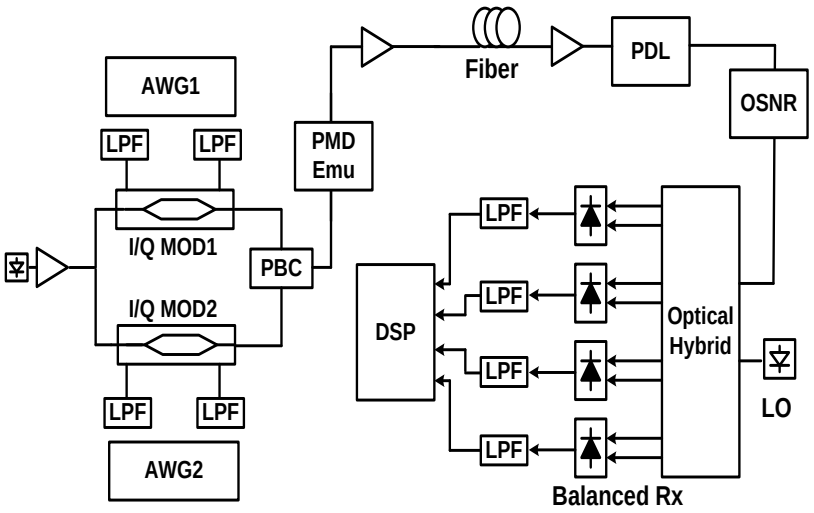

Figure 4.6: Simulation setup for DA OSNR estimation.

Figure 4.6 shows the simulation setup to investigate the proposed DA OSNR estimation technique. Since Golay sequences can be generated with arbitrary sequence length while at the same time still maintaining simple constellation and optimal CE performance, they are selected as the TSs of choice for designing the training blocks. Golay TSs are generated with both QPSK and 16-quadrature amplitude modulation (16QAM) constellations using the method described in Chapter 3 by two arbitrary waveform generators (AWGs) at 25 Gsymbol/s resulting in 100 Gb/s and 200 Gb/s effective bit rates for PM-QPSK and PM-16QAM systems, respectively. The sequences are then modulated and multiplexed through a polarisation beam combiner (PBC) to form the optical PM signal. First-order PMD emulator is added at the beginning of a transmission line to simulate a given amount of differential group delay (DGD). The transmission

line is modelled using standard single-mode fibre (SSMF) with a dispersion parameter of 16.8 ps/nm.km. At the receiver end, PDL and OSNR emulators are used to generate PDL and OSNR, respectively. The PDL emulator is modelled by the use of the lumped model described in [30] while OSNR is emulated by adding polarisation-independent noise to the signal and the incoming signal is assumed to be noise-free. The receiver part consists of a standard balanced polarisation-diversity coherent receiver using optical hybrids and photodiodes. Data after photo detection are saved at a rate of 2 samples per symbol for offline DSP using MATLAB.

Since CD plays a critical role in the performance of the proposed technique, system CD estimation is first performed using the DA CD estimation technique proposed in Chapter 3 and then CD compensation is performed in frequency domain using OFDE method. System CD compensation does not need to compensate for the exact CD value as the remaining CD is compensated during the next stages of receiver's DSP and thus only a rough estimation of CD is needed. Since CO system with DA-CE relies on estimating channel response using TSs, frame synchronisation is essential to extract the TS from the CD-compensated signal frame for CE. For that reason, after CD compensation, frame synchronisation, using sampled auto correlation algorithm as described in Section 2.2.4.2 of Chapter 2, is carried out to find the TSs. The peak location in the autocorrelation index indicates the position of the synchronisation header and from this peak the location of the training block can be calculated. To further optimise system efficiency, instead of using another separate header for frame synchronisation, the Golay "*a*" sequence is used as the synchronisation header. Channel transfer matrix is estimated by multiplying the received TS with an inverse copy of the original matrix, as described in Chapter 3, before the matrix is decomposed into four standalone vectors for noise filtering.

4.3.2 Filter Optimisation

With the aim of utilising noise filtering technique for DA OSNR estimation, the parameters of the filters need to be optimised. The optimisations of the two proposed filters in Section 4.2.2 are necessary as too much noise removal will also remove critical channel information and could bring about the degradation of equalisation performance and defeat noise filtering purpose. On the other hand, if too little noise filtering is

applied then the resultant CE will still be noisy, resulting in poor equalisation performance and in turn poor estimation accuracy. In order to simplify the process of filter optimisation, we optimise the filter parameters based on back-to-back transmission in simulation. This is done so that performance degradation by CD and other channel impairments is not involved. A block of TSs is sent through the OSNR emulator with various levels of OSNR, and the core sequence length is set at N_{ts} = 256 for high accuracy while still taking into account the realistic implementation of the technique. Three different levels of OSNR ranging from 8 to 24 dB are used for parameter optimisation to study the effect of filter optimisation over a wide range of OSNR, as well as to determine whether different optimisations at different levels of OSNR are necessary. Since MAF is a one-dimensional feed-forward noise filter, its only parameter is the filter average size L_{maf}, which indicates the amount of samples used for the averaging process. Consequently, the optimisation of this parameter is carried out by applying the filtering process described in Section 4.2.2 using MAF with different L_{maf} to filter out the noise in the estimated channel transfer functions. For each frame, the training block is self-equalised using the filtered CE with variable filter sizes, and the OSNR is estimated from the equalised TSs. The estimated OSNR values are then compared to the true OSNR values as set by the OSNR emulator and the estimation errors are used to optimise MAF parameter.

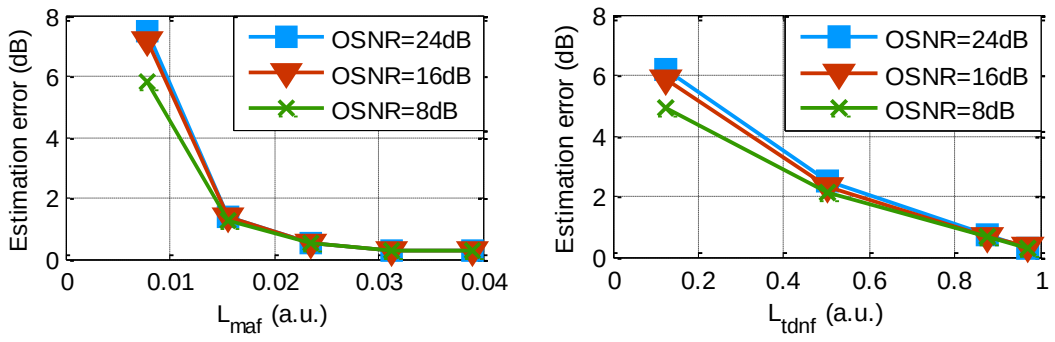

(a) *(b)*

Figure 4.7: Estimation error as function of filter size with N_{ts} = 256 for (a) MAF using L_{maf} and (b) TDNF using L_{tdnf}.

Figure 4.7(a) shows a plot of estimated OSNR errors as a function of L_{maf} using MAF for a QPSK system with core sequence length N_{ts} = 256. It can be seen that if the size L_{maf} is set too low then there is almost no difference compared to the case of not using any noise filtering and errors in OSNR estimation are very large. An average L_{maf} significantly improves the channel OSNR estimation performance and it can be seen that, at L_{maf} = 0.0313 the filter has reached optimised size and errors in estimation are very low (less than 0.5 dB). It can also be seen that while under no filtering, different OSNR levels produce different estimation errors. Estimation performances of all 3 OSNR levels converge at one single filter size and thus only a single filter size is needed for estimation of a wide range of OSNR. Beyond L_{maf} = 0.0313 there is almost no improvement in estimation performance of OSNR thus it can be concluded that for OSNR estimation using self-equalised TS with MAF, optimal filter size for core length of N_{ts} = 256 can be chosen to be L_{maf} = 0.0313.

In order to employ TDNF for OSNR estimation purpose, the filter also needs to be optimised, similar to using MAF described above. The optimisation of TDNF is performed using a process similar to the optimisation of MAF. Figure 4.7(b) shows a plot of the estimated OSNR errors as a function of the number of zeroed taps L_{tdnf} using the TDNF method. From this, it can be seen that, similar to the case of MAF, performance increases with the increased amount of zeroed taps. However, since increasing L_{tdnf} will decrease the filter tolerance to residual impairments, some taps must be left for residual impairments when using TDNF such that $L_{tdnf} < 1$. The optimised parameter for the TDNF method is chosen to be L_{tdnf} = 0.97.

4.3.3 CD Tolerance Analysis

Noise filtering techniques are essential for SNR and OSNR estimation from the TSs. However, the use of noise filtering DSP is subject to CD tolerance as in theory high CD transfer function is also averaged out during the filtering process. Performance degradation due to noise filtering will depend on the amount of CD contained in the transfer functions, as well as the filtering method used. It is therefore necessary to investigate CD tolerance of the proposed OSNR estimation method.

CD tolerance of using noise filter for noise-free CE is investigated using computer simulations. The training blocks are sent through the transmission line model consisting of SSMF as described in the simulation setup (Figure 4.4) with transmission length determining the total CD value. Different values of OSNR are set at the receiver and the captured data are then processed to determine estimation errors with respect to CD. QPSK Golay sequences with length N_{ts} = 256 symbols are used for CE and OSNR estimation. MAF parameter is set at the optimised value of L_{maf} = 0.0313 while TDNF parameter is set at the optimised value of L_{tdnf} = 0.97.

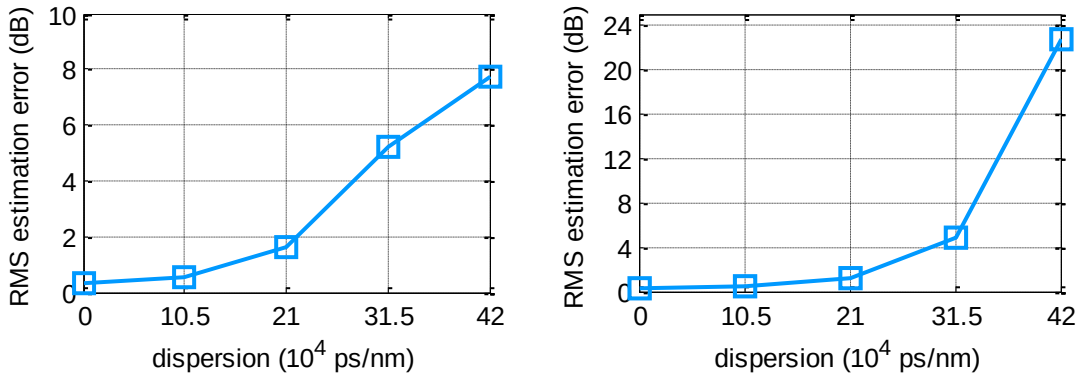

(a) *(b)*

Figure 4.8: Estimation error versus uncompensated dispersion for (a) MAF and (b) TDNF.

Figure 4.8(a) shows estimation errors with respect to different CD values for the proposed OSNR estimation technique using MAF with an OSNR value of 22 dB. It can be seen that for a small amount of CD then the noise filtering DSP technique is CD tolerance and almost no degradation is observed. Up to 10000 ps/nm of residual CD, equivalent to 600 km of uncompensated transmission, noise filtering method can tolerate only around 0.2-dB penalty in estimation accuracy. However, increasing residual CD to 42000 ps/nm causes a 7.5 dB loss in estimation accuracy. It can be seen that estimation performance degradation starts with relatively large CD values and this degradation increases with residual CD values. This effect is expected as large CD causes the channel transfer function to change rapidly with respect to frequency, then the MAF will average out these changes, resulting in a highly inaccurate CE. Therefore, if residual CD is left in the transfer function, a high value of residual CD can affect

equalisation performance and SNR estimation accuracy using self-equalised TSs. Figure 4.8(b) shows the estimation error with regard to different CD values for TDNF. It can be seen that tolerance for up to 600-km transmission is similar to MAF. However, when CD value exceeds certain limitation, in this case uncompensated 600-km transmission, performance of TDNF degrades significantly. The unusual rise in estimation error is the result of a total system failure for CE and equalisation. Since the TDNF has been optimised for OSNR estimation purpose, its tolerance to CD is minimised. As a result, failure condition is achieved when CD generates an impulse response longer than the maximum length allowed by the optimised TDNF. Under such a condition, the exceeding taps will be nulled by TDNF bringing about inaccurate CE. In general, it can be concluded that both MAF and TDNF are tolerable to a small amount of CD, and large CD in the transfer matrix will lead to high estimation inaccuracies for both MAF and TDNF, which in turn lead to degradation in OSNR estimation performance.

As described in Chapter 3, CD is an all pass transfer function that is polarisation independent. Since residual CD can be estimated using CE, the effect of residual CD can be mitigated by estimating the residual CD first, subtracting this function from the estimated channel transfer matrix, and then adding it back after noise filtering [24]. Residual CD estimation is performed using the same procedure used for the estimation of system CD as demonstrated in Chapter 3 and subtracted from the channel transfer functions before noise filtering.

4.3.4 Timing Offset Analysis

As a result of the specific requirement of having polarisation-diversity TSs for CO systems with DA-CE, the TSs are expected to be aligned in time on both polarisation tributaries. In practice, different timing on each polarisation signal before PBC makes the TSs subject to timing offset (TO), which is defined as the difference in time between the start location of the TSs on the X-polarisation and the start location of the TSs on the Y-polarisation. Under an ideal condition this difference is minimal and the TSs are viewed as perfectly aligned. Nevertheless, in practice, some offsets will be observed. Figure 4.9 illustrates the principle of TO for CO systems with DA-CE, where the Y-polarisation signal is delayed by a certain amount of time instead of perfectly synchronised to the X-polarisation signal.

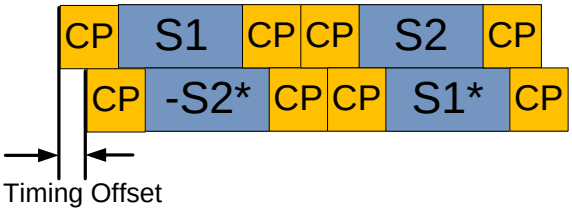

Figure 4.9: Timing offset in DA-CE.

The effect of TO in frequency domain can be viewed as a linear phase response similar to CD, which is also a quadratic phase response in frequency domain. As the TSs are guarded with cyclic prefix (CP) blocks, in a standard equalisation scheme the equalisation performance will be robust to this offset since this information is contained in the CE and can be inverted during the equalisation process.

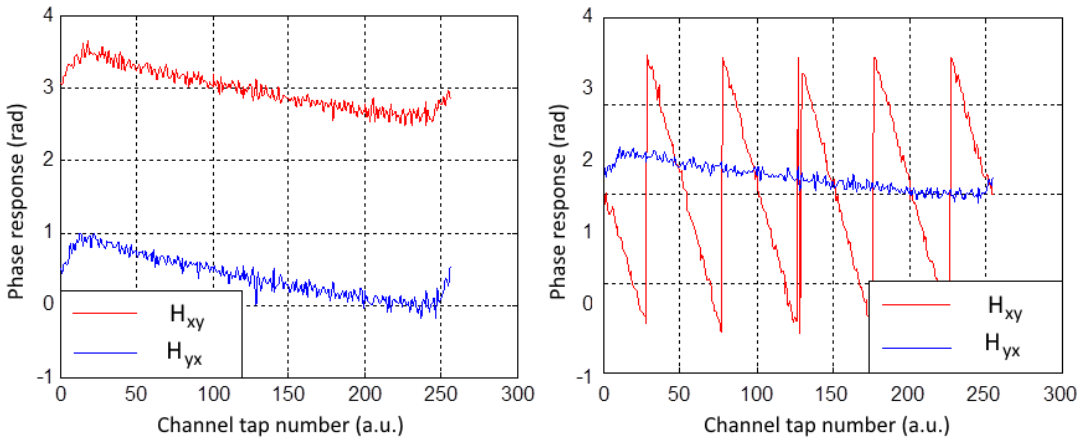

(a) *(b)*

Figure 4.10: H_{xy} and H_{yx} phase response with (a) TO = 0 ps and (b) TO = 200 ps.

Figure 4.10 illustrates the effect of TO on the channel transfer function phase response of the H_{xy} and H_{yx} components, while the H_{xx} and H_{yy} components of the transfer matrix have been omitted for clarity purpose. It can be seen that with zero TO, as illustrated in Figure 4.10(a), the phase response is almost linear and does not change a lot with frequency. Whereas, with a TO of 200 ps, a linear phase response that changes with frequency can be observed on the H_{xy} component of the transfer matrix in Figure 4.10(b). By applying noise filtering DSP, the transfer functions of TO can be averaged out by the filter similar to the case with CD that leads to performance degradation. The

effect of TO, however, can be generalised as a linear phase response and thus can be removed before noise filtering and added back later on using the approach for CD removal described in Section 4.3.3. However, as estimation of TO is not entirely accurate, it is desirable to first evaluate the proposed method's tolerance to TO.

Figure 4.11 shows the estimation error on OSNR estimation with different TO values. Here the noise filtering is applied directly to the transfer matrix without removing the TO first. From that it can be observed that a large value of TO has a small degradation effect on OSNR estimation due to noise filtering DSP averaging out channel information. For 200-ps timing delay between two polarisations, which is equivalent to 2 symbol period for system with baud rate of 10 Gsymbols/s, a total degradation of 0.45 dB in estimation accuracy can be observed. This degradation can be removed similar to the case with residual CD by subtracting TO from the transfer matrix. Since TO can be viewed as a linear phase response in frequency domain, single stage least square interpolation can be used to estimate the amount of TO. Furthermore, since the phase response is different for each component of the transfer matrix, after the matrix to vector decomposition, TO for each vector representing one matrix component is estimated independently and subtracted by the estimated value before noise filtering. These TO values are added back after noise filtering to form the filtered channel transfer matrix.

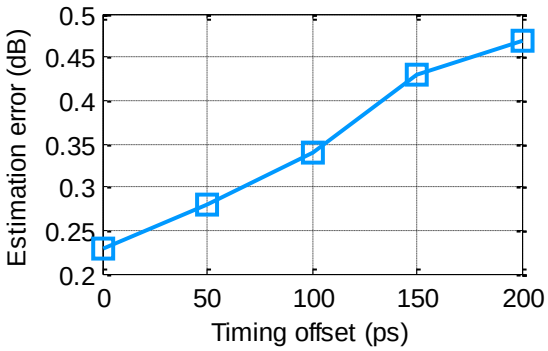

Figure 4.11: Estimation error vs. TO.

4.3.5 Polarisation Dependent Loss (PDL) Tolerance

Polarisation dependent loss (PDL) is another important impairment in optical communication system. The general effect of PDL is to cause different losses on different polarisation tributaries, resulting in an optical signal with different power on the X-polarisation and Y-polarisation, and in turn create an optical signal with different OSNR values on each polarisation tributary. PDL also causes polarisation depolarisation as a result of unequal signals on both polarisations, and this will affect the system OSNR [32]. In order to study the effect of PDL on the proposed OSNR estimation method, a PDL simulation model is built using the lumped model suggested in [32]. The PDL model assumes the Y-polarisation signal is the one with greater loss and consists of a polarisation rotation device which rotates the incoming signal by a given angle, defined as the PDL angle. The rotated signal is then split into two independent signals on each polarisation by means of PBC and then the Y-polarisation signal is passed through an attenuator which attenuates signal on the Y-polarisation by a given amount defined as PDL value. The two polarisation signals are then combined using PBC before rotated back using polarisation rotator. Since the OSNR emulator emulates OSNR by adding non-polarised noise to the incoming signal, PDL emulator is placed in front of the OSNR emulator in order to simulate the PDL effect under different OSNRs. Placement of PDL module after the OSNR emulator will cause the signal to have similar OSNR level on both polarisation signals and the effect of PDL cannot be studied. Two parameters are used to control the PDL emulator which is the rotation angle (PDL angle) and the loss on the Y-polarisation signal (PDL level). The effect of PDL angle on OSNR estimation is studied by first passing the signal through the PDL emulator with variable angle and the captured signal at the receiver is then used to estimate OSNR on both the X- and Y-polarisation tributaries. For the purpose of studying estimation performance with different PDL angles, a small amount of PDL (weak PDL) is assumed. For clarity purpose, a reference value is selected as the OSNR value in the case of no PDL. For different PDL angles with a constant amount of PDL level, OSNR value on each polarisation signal is then estimated. The estimation error with respect to PDL angle is then calculated as the difference between the estimated OSNR values on each polarisation versus the reference OSNR value.

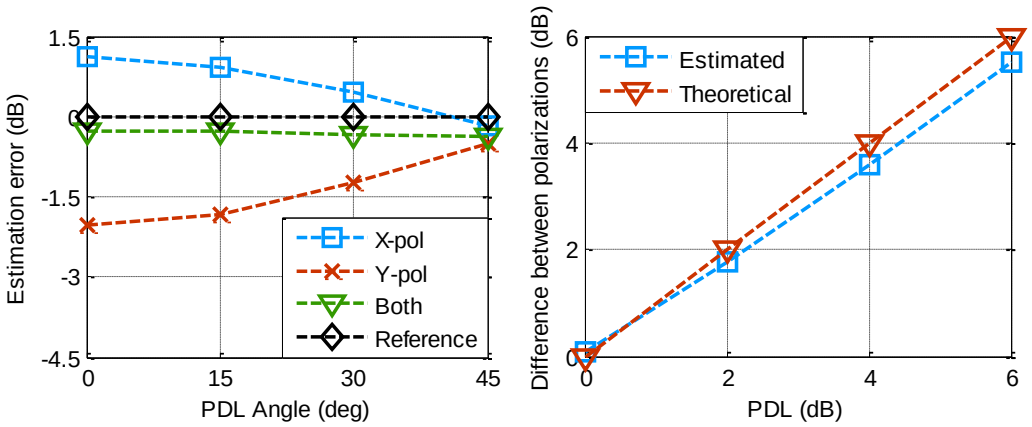

Figure 4.12: Estimation difference between X- and Y-polarisations under (a) PDL = 3 dB with different PDL angles and (b) different PDL levels under worst case PDL.

Figure 4.12(a) shows the OSNR estimation error on each of the X- and Y-polarisations for OSNR = 19 dB under the effect of weak PDL (PDL = 3 dB) and different PDL angles. It can be seen that due to the interaction with PDL, the estimated OSNR on X- and Y-polarisations are not the same and the overall OSNR estimation is different compared to the case with no PDL (reference line, normalised to 0 dB). As the PDL model assumes signal loss on the Y-polarisation, for all PDL angles except at 45 degree, X-polarisation signals give higher OSNR than the reference case while Y-polarisation signals give lower OSNR than the reference case. This behaviour is expected as the OSNR emulator assumes the signal is noise free while the estimated results are a combination of both OSNR emulator and OSNR degradation due to PDL. The difference between OSNR on each polarisation signal is related to PDL value as expected. The difference of around 0.4 dB at the PDL angle of 45° (best case PDL) is consistent with the proposed theory [30] and both polarisation signals give similar OSNR estimation results in case of the best case PDL. The effect of different PDL levels is investigated for the worst case PDL by keeping the PDL angle constant at 0° and varying the attenuation on the Y-polarisation signal to create different PDL levels. Figure 4.12(b) shows that, for the worst case PDL (PDL angle = 0°), differences in the estimated OSNR on X- and Y-polarisations are linearly related to different PDL levels. This difference in estimated OSNR values is expected and is consistent with the theory of PDL model. For very high PDL then it can be seen that there is a small degradation

in estimation performance compared to the theoretical value; although for low to medium values, the proposed technique has good performance with respect to PDL. This shows that the proposed technique is able to estimate OSNR of the X- and Y-polarisation tributaries independently and reflect OSNR differences caused by PDL, which is a desirable characteristic for OSNR monitoring in polarisation-multiplexed (PM) coherent CO systems.

4.3.6 Estimation Error

Figure 4.13 shows the root mean squared (RMS) estimation error for different OSNR for back-to-back transmission, using 256-symbol Golay sequences. Since it is very difficult to measure high OSNR value in practice due to the noise from the receiver, the measured range of OSNR in simulation was set to between 10 – 22 dB for both QPSK and 16QAM systems. It can be seen that estimations for both QPSK and 16QAM systems are accurate with a maximum error of around 0.25 dB for 256-symbol TSs. It can also be seen that with optimised filter parameters, both MAF and TDNF techniques have very similar performance for OSNR estimation. While TDNF method can provide a trade-off in accuracy and channel impairment tolerance, in order to measure SNR using the proposed scheme, both MAF and TDNF techniques require these impairments to be estimated for the highest SNR estimation accuracy. Thus, MAF can be considered as a simpler method to implement as no IFFT/FFT operations are needed.

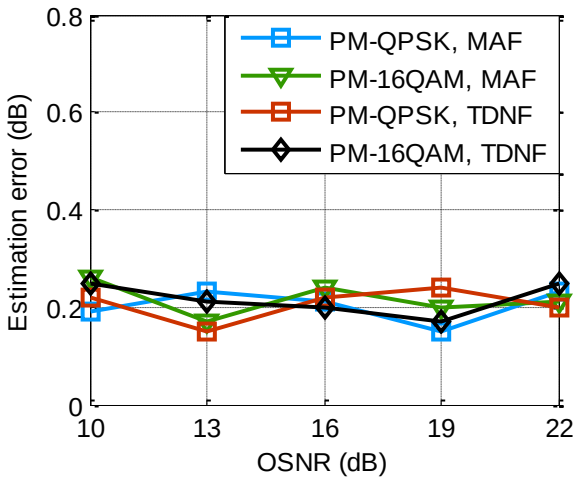

Figure 4.13: Estimation error vs. different OSNR in simulation for QPSK and 16QAM systems with MAF and TDNF.

4.4 EXPERIMENTAL DEMONSTRATION

Figure 4.14 shows the experimental setup to verify the proposed technique. The transmitter consists of two I/Q modulators and the TSs are generated using two AWGs at rate of 10 Gsymbol/s. The TSs are followed by randomly generated data to form one data frame and signals on both polarisation tributaries are combined using PBC to form PM signals. This translates into 40 Gb/s and 80 Gb/s effective bit rates for PM-QPSK and PM-16QAM, respectively. The system is assumed to operate at optimal launched power to minimise non-linear noise as this degrades estimation performance [21]. The transmission line consists of one single 400-km SSMF with amplifiers. At the receiver a first order PMD emulator is added to generate a known amount of DGD. The PMD emulator used is Fibrepro PE4200 and the range of DGD is set to be between 0-30 ps. An ASE source is added using two cascaded optical amplifiers. Since it is very difficult to estimate high OSNR due to other noise sources independent of ASE noise and high OSNR is unrealistic for most systems, the OSNR range to be monitored is set to 10 - 22 dB. The signal is then split into two paths using a coupler with a ratio of 9:1. The 10% path is then fed into an optical spectrum analyser (OSA) for independent measurement of the OSNR while the other path is sent into balanced coherent receivers. The data are then captured using 40 GHz sampling scope for offline DSP.

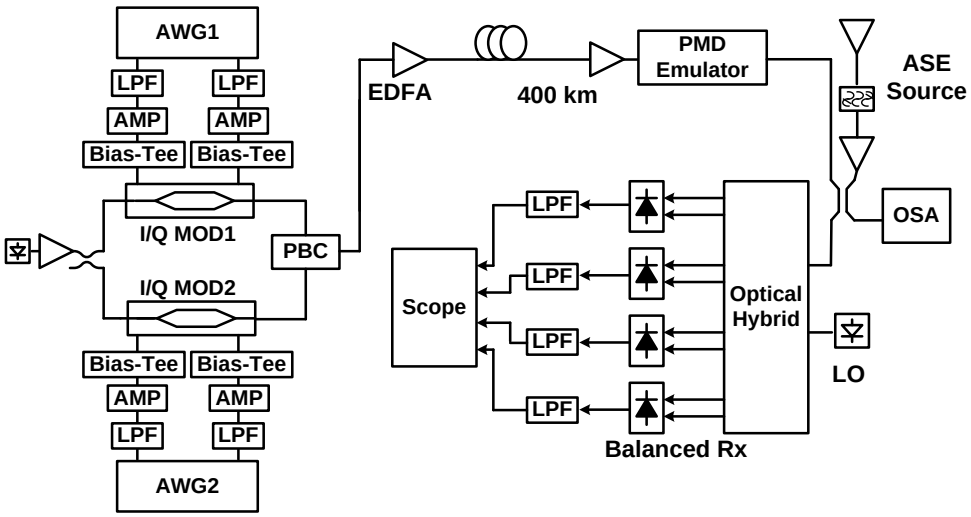

Figure 4.14: Experimental setup.

Since residual CD and TO will affect performance of noise filtering, these parameters are estimated using least square interpolation method presented in Sections 4.3.3 and 4.3.4 and then subtract them from the channel transfer matrix. These impairments are subtracted before noise filtering and then added back at the end. Residual CD is estimated using LS quadratic fit while TO is estimated using LS linear fit on the channel transfer functions. These residual impairments are only needed to be roughly estimated once as the remaining impairments due to estimation errors are small and are tolerated by the noise filters. The extracted TSs are then equalised using filtered CE and DA maximum likelihood (DAML) phase noise compensation [33]. As the equalised TSs utilise some CP symbols for guarding against inter-block interference (IBI), these CP symbols are also equalised and utilised for initialisation of DAML.

Figure 4.15 shows the measured RMS estimation error in experiments for QPSK and 16QAM systems using 256-symbol long TSs after back-to-back and 400-km transmission using SSMF. It can be seen that estimation is accurate with a maximum error of around 0.75 dB for both QPSK and 16QAM systems with 16QAM systems having slightly higher maximum error. Both MAF and TDNF methods have similar estimation performances. Overall, estimation for both systems achieves a maximum error of around 0.7 dB and is consistent with other SNR-based estimation technique [21]-[22], which verifies that the proposed method is able to estimate OSNR with high accuracy.

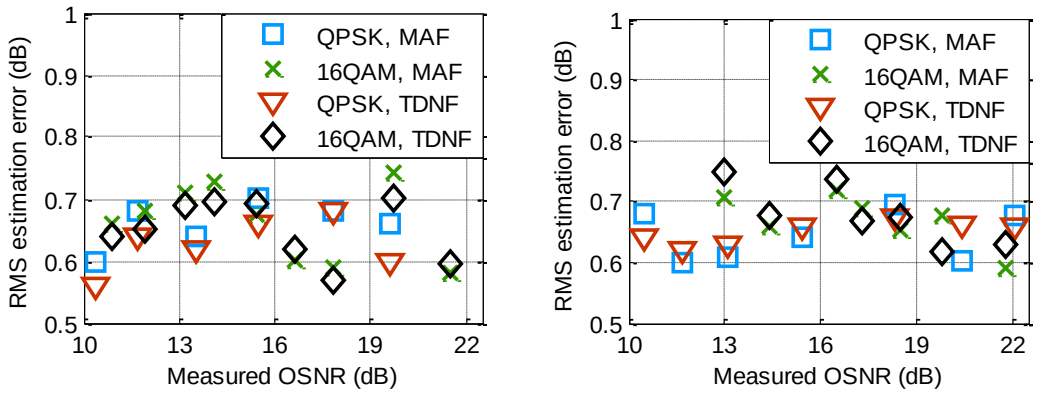

(a) *(b)*

Figure 4.15: Measured estimation error with (a) back-to-back and (b) after 400-km transmission.

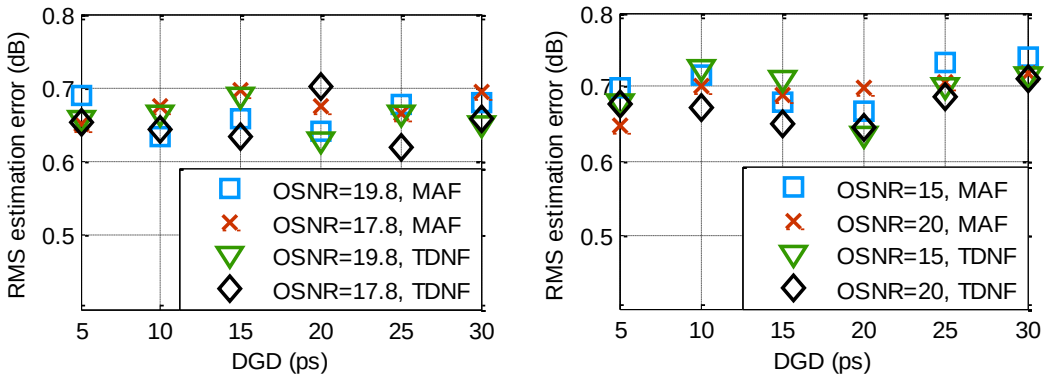

Figure 4.16: Measured estimation error against DGD with (a) back-to-back and (b) after 400-km transmission.

Figure 4.16 shows the estimation error against DGD for QPSK systems using a first-order PMD emulator for back-to-back and 400-km SSMF transmissions. It can be seen that for a wide DGD range of 0-30 ps there is almost no degradation in the estimation performance. This shows that the proposed technique is also robust against DGD. Overall, it can be concluded that the proposed OSNR estimation technique is accurate and robust against channel linear impairments.

4.5 CONCLUSIONS

This chapter presented an in-band OSNR estimation technique based on TSs for CE and self-equalisation of the training blocks. The training blocks are inserted as part of the design for CO systems with DA-CE; and by utilising the same training blocks, SNR and OSNR can be estimated without utilising any extra overhead. The use of training blocks instead of regular data frame also enables the technique to be transparent to the equalisation algorithm in the receiver. As a consequence, data can be equalised using complex receiver instead of having to rely on simple zero forcing method.

The proposed method is outlined in Section 4.2 and consists of self-equalisation of the training blocks using time domain noise filtering for estimated channel transfer function. Two filters are employed for the noise filtering stage namely MAF and TDNF. Characteristics of these two filters for OSNR estimation are tested in computer simulations and the results showed that the two filters have similar performances. Each

filter gives similar tolerance to residual CD with the exception that TDNF has significant degradation at CD exceeding the filter optimised design in comparison to MAF. Nevertheless, the required residual CD amount to cause this degradation is very large and thus is unlikely to be encountered in practice, since such a large residual CD value will cause significant problem in frame synchronisation stability. For a normal range of residual CD, combining with CD subtraction before noise filtering, both filters are robust against residual CD. The same conclusion can be drawn for tolerance with respect to TO, as this impairment will generate linear phase response in frequency domain and can be removed before noise filtering and added back to the filtered transfer matrix.

The proposed method is tested against PDL in simulation to verify estimation accuracy. Results showed that with PDL, two different OSNR values on each polarisation signal can be estimated and the difference between the two reflects the amount of PDL in the system. This behaviour is consistent with the effect of PDL on system OSNR and showed that the proposed estimation scheme is robust against PDL. The proposed OSNR estimation scheme is verified in experiments with 40-Gb/s QPSK and 80-Gb/s 16QAM CO-SC systems with up to 400-km transmission. The results show that estimation is accurate with an RMS error of around 0.7 dB. While this error is slightly larger than other coherent receiver-based OSNR estimation methods, the number of symbols used is significantly lower. Therefore, a small increase in estimation error is a good trade-off between estimation speed, receiver flexibility and estimation accuracy.

The OSNR estimation technique presented in this chapter is based on utilising noise filtering methods for achieving enhanced CE. While these noise filtering methods only require one block of TS for CE, the trade-off in using noise filtering techniques is the requirement of long TS lengths for high resolution CE. The relationship between TS lengths and estimation performances is therefore of great interest and will be investigated further in Chapter 5.

4.6 REFERENCES

[1] C. Do, A. V. Tran, C. Zhu, S. Chen, T. Anderson, D. Hewitt and E. Skafidas, "Data-Aided Chromatic Dispersion Estimation for Polarisation Multiplexed Optical Systems," *IEEE Photonics Journal*, vol. 4, no. 5, pp. 2037–2049, Oct. 2012.

[2] F. N. Hauske, J. Geyer, M. Kuschnerov, K. Piyawanno, T. Duthel, C. Fludger, D. van den Borne,

E. Schmidt, B. Spinnler, H. de Waardt, and B. Lankl, "Optical performance monitoring from FIR filter coefficients in coherent receivers," *Optical Fibre Communication Conference OFC'2008* , paper OThW2, San Diego, CA, USA, 2008.

[3] F. Pittala, F. N. Hauske, Y. Yabin, N. G. Gonzalez, and I. T. Monroy, "Fast and robust CD and DGD estimation based on data-aided channel estimation," *International Conference on Transparent Optical Networks ICTON'2011*, paper We.D1.5, Brussels, Stockholm, Jun. 2011.

[4] M. S. Faruk, Y. Mori, C. Zhang, K. Igarashi, and K. Kikuchi, "Multi-impairment monitoring from adaptive finite-impulse-response filters in a digital coherent receiver," *Optics Express*, vol 18, no. 26, Dec. 2010.

[5] C. K. Chan, *Optical Performance Monitoring*, Section 2.2, pp. 22-26, Academic Press, 2010.

[6] M. Rasztovits-Wiech, M. Danner, and W. R. Leeb, "Optical signal-to-noise ratio measurement in WDM networks using polarisation extinction," *European Conference on Optical Communication ECOC'98*, pp. 549–550, Madrid, Spain, 1998.

[7] D. K. Jung, C. H. Kim, and Y. C. Chung, "OSNR monitoring technique using polarisation-nulling method," *Optical Fibre Communication Confernce OFC'2000*, paper WK4, Baltimore, MD, 2000.

[8] J. H. Lee, D. K. Jung, C. H. Kim, and Y. C. Chung, "OSNR monitoring technique using polarisation-nulling method," *IEEE Photonics Technology Letters*, vol. 13, no. 1, pp. 88–90, Jan. 2001.

[9] J. H. Lee and Y. C. Chung, "Improved OSNR monitoring technique based on polarisation-nulling method," *Electronics Letters*, vol. 37, no. 15, pp. 972–973, Jul. 2001.

[10] M.-H. Cheung, L.-K. Chen, and C.-K. Chan, "A PMD-insensitive OSNR monitoring scheme based on polarisation nulling with off-centre narrow-band filtering," *Optical Fibre Communication Conference OFC'2004*, paper FF2, Los Angeles, CA, 2004.

[11] J. H. Lee, H. Y. Choi, S. K. Shin, and Y. C. Chung, "A Review of the Polarisation-Nulling Technique for Monitoring Optical-Signal-to-Noise Ratio in Dynamic WDM Networks," *Journal of Lightwave Technology*, vol. 24, no. 11, pp. 4162-4171, Nov. 2006.

[12] M. Petersson, H. Sunnerud, B. Olsson, and M. Karlsson, "Optical performance monitoring using degree of polarisation in presence of polarisation-mode dispersion," *European Conference on Optical Communication ECOC'2004*, paper Tu3.6.2, Stockholm, Sweden, 2004.

[13] M. Peterson, H. Sunnerud, M. Karlsson, B. E. Olsson, "Performance monitoring in optical networks using Stokes parameters," *IEEE Photonics Technology Letters*, vol. 16, no. 2, pp. 686-688, Feb. 2004.

[14] M. Sköld, B-E. Olsson, H. Sunnerud, and M. Karlsson, " PMD-Insensitive DOP-Based OSNR Monitoring by Spectral SOP Measurements," *Optical Fibre Communication Conference OFC 2005*, paper OThH3, Anaheim,CA, USA, 2005.

[15] G. Lu and L. Chen, " Enhancing the monitoring sensitivity of DOP-based OSNR monitors in high OSNR region using off-centre narrow-band optical filtering," *Optics Express*, vol. 15, no. 3, pp. 823-828, 2007.

[16] Z. Chen, L. Yan, A. Yi, W. Pan, and B. Luo, "Simultaneous OSNR monitoring for two polarisation tributaries of a PDM signal using a polarisation-diversity nonlinear loop mirror based on FWM," *Journal of Lightwave Technology*, vol. 30, no. 14, pp. 2376-2381, Jul. 2012.

[17] R. Adams, M. Rochette, T. T. Ng, and B. J. Eggleton, "All optical in band OSNR monitoring at 40Gb/s using nonlinear optical loop mirror," *IEEE Photonics Technology Letters*, vol. 18, no. 3, pp. 469–471, Feb. 2006.

[18] T. T. Ng, J. L. Blows, M. Rochette, J. A. Bolger, I. Littler, and B. J.Eggleton, "In band OSNR monitoring and chromatic dispersion monitoring using a fibre optical parametric amplier," *Optics Express*, vol. 13, pp. 5542–5552, Jul. 2005.

[19] W. Shieh, R. S. Tucker, W. Chen, X. Yi, and G. Pendock, "Optical performance monitoring in coherent optical OFDM systems," *Optics Express*, vol. 15, no. 2, pp. 350-356, Jan. 2007.

[20] M. S. Faruk, Y. Mori, and K. Kikuchi, "In-Band Estimation of Optical Signal-to-Noise Ratio From Equalised Signals in Digital Coherent Receivers," *IEEE Photonics Journal*, vol 6, no. 1, pp. 7800109, Feb. 2014.

[21] M. S. Faruk and K. Kikuchi, "Monitoring of optical signal-to-noise ratio using statistical moments of adaptive-equaliser output in coherent optical receivers," *Opto-Electronics and Communications Conference OECC'2011*, pp. 233–234, Kaosiung, China, 2011.

[22] D. J. Ives, B. C. Thomasen, R. Maher, and S. Savory, "Estimating OSNR of equalised QPSK signals," *European Conference and Exhibition on Optical Communication ECOC'2011*, paper OThH5, Geneva, Switzerland, 2011.

[23] C. Zhu, A. V. Tran, S. Chen, L. Du, C. Do, T. Anderson, A. Lowery, and E. Skafidas, "Statistical moments-based OSNR monitoring for coherent optical systems," *Optics Express*, vol. 20, no. 16, pp. 17711-17721, Jul. 2012.

[24] R. Schmogrow, B. Nebendahl, M. Winter, A. Josten, D. Hillerkuss, S. Koenig, J. Meyer, M. Dreschmann, M. Huebner, C. Koos, J. Becker, W. Freude, and J. Leuthold, "Error vector magnitude as a performance measure for advanced modulation formats," *IEEE Photonics Technology Letters*, vol. 24, no. 1, pp. 61-63, Jan. 2012.

[25] F. Pittala, F. N. Hauske, Y. Ye, N. G. Gonzalez, and I. T. Monroy, "Joint PDL and in-band OSNR monitoring supported by data-aided channel estimation," *Optical Fibre Communication Conference OFC'2012*, paper OW4G, Los Angeles, CA, USA, 2012.

[26] B. Spinnler, S. Calabro, and M. Kuschnerov, "Pilot-assisted channel estimation methods for coherent receivers," *Optical Fibre Communication Conference OFC'2013,* pp 1-3, paper OW4B-3, Mar. 2013.

[27] C. Zhu, A. Tran, F. Hauske, S. Chen, T. Anderson, and E. Skafidas, "Low-Complexity Fractionally-Spaced Frequency Domain Equalisation with Improved Channel Estimation for Long-Haul Coherent Optical Systems". *Optical Fibre Communication Conference OFC'2013*, pp. OW4B.5, Anaheim, CA, USA, 2013.

[28] A. V. Tran, C. Zhu, C. C. Do, S. Chen, T. Anderson, D. Hewitt, and E. Skafidas, "8×40-Gb/s optical coherent pol-mux single carrier system with frequency domain equalisation and training sequences," *IEEE Photonics Technology Letters*, vol. 24, no. 11, pp. 885–887, Mar. 2012.

[29] A. V. Tran, C. Zhu, C. C. Do, S. Chen, L. Du, T. Anderson, D. Hewitt, A. Lowery and E. Skafidas, "Single carrier QPSK and 16 QAM system demonstration using frequency domain equalisation and training sequences," *Opto-Electronics and Communications Conference OECC'2012*, paper 5B3-4, Busan, Korea, 2012.

[30] C. Do, A. Tran, C. Zhu, D. Hewitt, and E. Skafidas, "Data-Aided OSNR Estimation for QPSK and 16QAM Coherent Optical System," *IEEE Photonics Journal*, vol 5, no. 5, Oct. 2013.

[31] S. W. Smith, *The Scientist and Engineer's Guide to Digital Signal Processing*, Section 15.1, pp. 277-284, California Technical Publishing, 1997.

[32] T. Duthel, C.R.S. Fludger, J. Geyer, and C. Schulien, 'Impact of Polarisation Dependent Loss on Coherent POLMUX-NRZ-DQPSK" *Optical Fibre Communication Conference OFC'2008*, paper OThU5, San Diego, CA, USA, 2008.

[33] P. Y. Kam, "Maximum likelihood carrier phase recovery for linear suppressed-carrier digital data modulations," *IEEE Transactions in Communications*, vol.34, no. 6, pp. 522–527, Jun. 1986.

5 Data-Aided Channel Estimation with Flexible Overheads

5.1 INTRODUCTION

Chapter 2 presented a survey of channel equalisation methods for coherent optical (CO) single carrier (SC) systems. Chromatic dispersion (CD) is typically compensated in the first stage using digital filters [1]-[4] and the remaining impairments are compensated in the second stage using either blind or data-aided (DA) channel estimation (CE) methods [5]-[9]. Among these methods, the use of DA-CE and equalisation is of great interest as the channel is estimated using training sequences (TSs) and not gradient algorithm which results in fast and robust CE performance [7]-[9]. Another added advantage of using DA-CE is that it allows for the design of format-flexible CO systems where a single digital signal processing (DSP) structure can be used for both polarisation-multiplexed (PM) quadrature phase shift keying (QPSK) and 16-quadrature amplitude modulation (16QAM) instead of having to utilise different gradient algorithms for different modulation formats as in the case with blind equalisations [9]-[11]. However, due to the long impulse response generated by system CD, the use of only TSs for CE and equalisation will result in the requirement of very long TSs which is not practical as the overhead ratio will likely be high as a consequence. As indicated in Chapter 3, the use of TSs for the estimation of the entire system transfer functions, including CD, will result in the need for long sequences with lengths that scale up with transmission distance and this is also true for using TSs for the estimation of channel transfer matrix in a single stage equalisation structure. Two-stage approach where system CD is compensated in the first stage and residual impairments are compensated in the second stage is a much more favourable approach as TSs are only utilised in the second stage resulting in a reduced requirement of the TS length. Since the second stage only needs to equalise the remaining channel impairments, short TSs can be used. The minimum-phase (MP) constant amplitude zero autocorrelation (CAZAC) sequences [12]-[13] are

ideal for short sequence implementation since the 16-symbol MP-CAZAC sequences have constellations that match QPSK constellations. Golay sequences [14]-[17], with length independent constellations, can also be used and the performance of Golay sequences had been demonstrated to be similar to the ideal CAZAC sequence for CO systems [9]. While only short TSs, with length just enough to cover the remaining channel impulse response, are required for second stage equalisation, the use of long TSs is still relevant as longer sequences provide better CE in theory [18] and could result in better equalisation compared to short TSs. The use of noise filtering techniques on the estimated channel transfer matrix further adds more complexity to the relationship between TS lengths and performances as these techniques operate directly on the estimated channel transfer matrix and thus will be dependent on the TS lengths. A flexible DA system, where the TS lengths can be altered depending on the condition of the optical channel, is therefore very desirable in practice.

Since CO-SC systems employing DA-CE rely on TSs for channel acquisition, frame synchronisation to locate the TSs is critical for the operation of DA-CE. However, most designs of CO-SC systems with DA-CE depend on known TSs with fixed length or techniques that utilise a separate frame synchronisation block [10]. The separate frame synchronisation techniques are typically found in coherent orthogonal frequency division multiplexing (OFDM) systems [19]-[22] and are adapted for CO-SC-FDE systems with DA-CE. It is thus desirable to investigate the performance of TSs, under different lengths and types, with respect to channel equalisation performance as well as the design of DA receiver's DSP that can detect the TS lengths in order to allow a flexible training structure in the transmitted signal.

In this chapter, the relationship between different sequence lengths and their equalisation performances is investigated using Golay sequences. A new frame synchronisation structure based on utilising smaller core Golay sequences is presented. This frame synchronisation method can detect both the TS location, as well as its length and allow for a flexible TS length structure in the transmitted signal. Section 5.2 presents the relationship between TS lengths and the overall system tracking speed, as well as the noise filtering techniques used in a two-stage CO-SC-FDE. Section 5.3 presents simulation comparison between different TS lengths and performances, taking overhead optimisation and noise filtering into account and the results show that a

flexible TS length system is desirable in order to optimise between performance and overhead penalty. Section 5.4 presents the frame synchronisation method based on Golay sequences for detecting both TS lengths as well as TS locations. This method allows for flexible overhead ratio and tracking speed in the system, where the length of the TSs can be changed depending on the channel condition. Finally the chapter is concluded in Section 5.5.

5.2 CHANNEL ESTIMATION USING TRAINING SEQUENCES

For CO-SC-FDE systems employing either DA-CE or non-data-aided (NDA) CE, CD is typically compensated in the first stage. DA CD estimation, as presented in Chapter 3 can be used to estimate system CD for blind compensation purpose. Regardless of the method used for system bulk CD estimation, after CD compensation, the remaining channel transfer function consists of only a small amount of residual impairments to be compensated in the second stage. For DA-CE, these impairments are estimated using TSs. As CE is affected by noise, the use of noise filtering DSP will be of benefit to CE and ensure optimal equalisation performance. There are typically two methods for achieving enhanced noise-free CE namely averaging over multiple estimations [10] and noise filtering [8]. As presented in Chapter 4, noise filtering methods can be used to provide optimal CE for signal-to-noise ratio (SNR) and optical signal-to-noise ratio (OSNR) estimation using self-equalised TSs. It can be seen that the approach can also be utilised for equalisation of the actual data frame in CO communication systems. At first noise filtering techniques seem to imply less overhead penalty compared to sending multiple TS blocks for averaging. However the requirement of long TSs further adds complications to the comparison of these methods. For the same time slot, multiple blocks of short TSs can be sent for averaging, or a long block of TSs can be sent for CE with noise filtering. However, a comparison between noise filtering and using multiple blocks of TS for channel equalisation has not been considered. This section presents the principles as well as effects on system overhead ratio of the two methods for achieving enhanced CE.

5.2.1 Enhanced Channel Estimation

As described in Chapter 3, DA-CE operates by sending TSs together with the data frame. At the receiver the TSs are used for CE and the actual data are equalised based

on the estimated channel transfer functions. Under a single TS block structure, system performance is expected to be proportional to the length of the TS block [18] as a longer block will give higher CE accuracy and in theory will lead to better equalisation performance. However, as estimation by DA-CE is affected by noise, it is necessary to reduce this impairment in order to obtain noise-free CE. Enhanced CE can be achieved by averaging multiple estimations, or by using noise filtering techniques.

5.2.1.1 Averaging Multiple Estimations

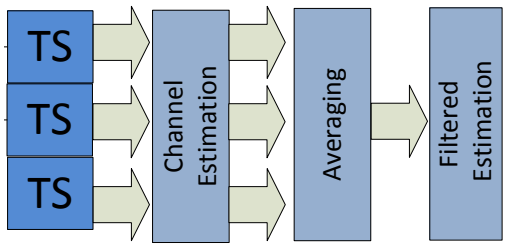

Figure 5.1: Enhanced CE by means of averaging multiple blocks of TSs.

A simple method to achieve enhanced CE is by repeating the TS block multiple times before sending in the actual data frame. Figure 5.1 describes the steps for CE using the average of multiple blocks where the training blocks are repeated 3 times. At the receiver, these blocks are separated and multiple CEs are performed. The final estimated channel transfer matrix is obtained as the average over multiple estimations. As the noise is randomly distributed throughout the TSs, averaging multiple CEs will remove the effect of noise while keeping the channel transfer functions intact. However, it can be seen that using this method will directly increase the system overhead ratio, as an average of 10 blocks will increase the overhead ratio by 10 times compared to using a single block. If the overhead ratio is to be kept constant, then in order to increase the amount of training blocks used for CE, these blocks need to be sent less regularly which results in a reduced system update speed, defined as:

$$T = \frac{B\mu}{N_{total}} \tag{5.1}$$

where T is the system update speed, B is the system baud rate, μ is the system coding ratio and $N_{total} = 2N_{ts} + 4N_{cp}$ is the total number of training symbols used; N_{ts} and N_{cp} are

the core sequence length and the CP block length respectively. Here the update speed is defined as the interval between sending the TSs and it is trivial from Equation 5.1 that the system update speed is inversely proportional to the amount of TS blocks used for CE. As the amount of blocks used is proportional to the clarity of the estimated channel transfer functions in theory, there is a trade-off between system performance and update speed for a constant overhead ratio using multiple block averaging for CE.

5.2.1.2 Channel Estimation with Noise Filtering

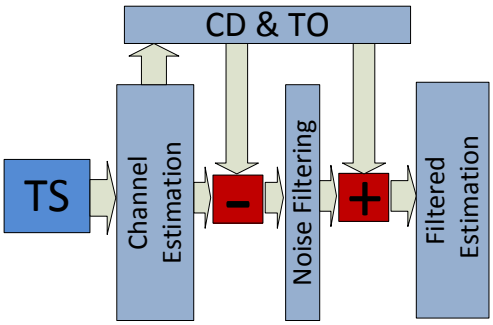

Figure 5.2: Block diagram of enhanced CE with noise filtering DSP.

Noise filtering techniques for CE are also proposed in [8], which operate by applying a noise filter on the received TS block and provide enhanced CE. In theory, this enhancement comes without the penalty of increasing the overall overhead ratio as only a single TS block is needed and DA CO-SC systems can operate at maximum efficiency using DA-CE with noise filtering DSP. Figure 5.2 shows the block diagram of noise filtering DSP used for enhancing CE, where the channel transfer matrix is first estimated from the received TSs. Since residual linear components including CD and timing offset (TO) will affect noise filtering performance, these components are estimated using least square interpolation method similar to the CD estimation technique proposed in Chapter 3 and subtracted from the channel transfer matrix. After CD and TO subtraction, the digital noise filter is applied to the channel transfer matrix and residual linear components are then added back to form the filtered transfer matrix used for equalisation. By using noise filtering, only one block of TS is needed for enhanced estimation performance. While noise filtering is a very attractive method for enhancing CE, this method comes with the trade-off of less tolerance to linear channel

impairments compared to multiple block averaging method. The total enhancement using noise filtering is also dependent on the lengths of the TSs used and the method is most suited for training blocks with medium to long TSs.

5.3 SEQUENCE LENGTH AND PERFORMANCE

Section 5.2 describes the two methods for achieving noise-free CE for CO-SC systems with DA-CE. While both methods had been independently demonstrated, a comparison between performances of these two methods, in the context of signal equalisation using DA-CE, has not been made. Since overhead ratio presents a penalty for CO-SC systems utilising DA-CE, it is of great interest to investigate the performance of these two methods with respect to channel impairments and overhead ratio penalty. This section investigates the performance of these two enhanced CE methods using computer simulations. The merits and drawbacks of both methods are discussed.

5.3.1 Simulation Setup

Simulations are carried out using *VPI TransmissionMaker 8.7* to evaluate the performance of CO systems with DA-CE using different sequence lengths and the setup is shown in Figure 5.3. Each training block consists of four Golay sequences arranged in space-time block code (STBC) structure as described in Section 2.2.5.2 of Chapter 2 with each sequence having the same length N_{ts} with N_{ts} = 32, 64, or 128 symbols. Cyclic prefixes (CP) blocks of 4-symbol long are inserted between sequences to resist residual CD and an overhead ratio of 1% is set for all systems which results in systems with update speed of 367.65 - 1250 KHz. The electrical signals are converted to optical signals by means of in phase/quadrature modulator and the final PM optical signal is formed by combining signals on both X-polarisation and Y-polarisation through polarisation beam combiner (PBC). System baud rate is set at 25 Gbaud which results in 100-Gb/s PM-QPSK and 200-Gb/s PM-16QAM effective bit rate, respectively. Transmission distance is 1000 km using standard single-mode fibre (SSMF) and an optical signal-to-noise ratio (OSNR) emulator is used to emulate a given value of OSNR. The receiver consists of standard balanced coherent receivers and the received data are stored and processed offline using MATLAB.

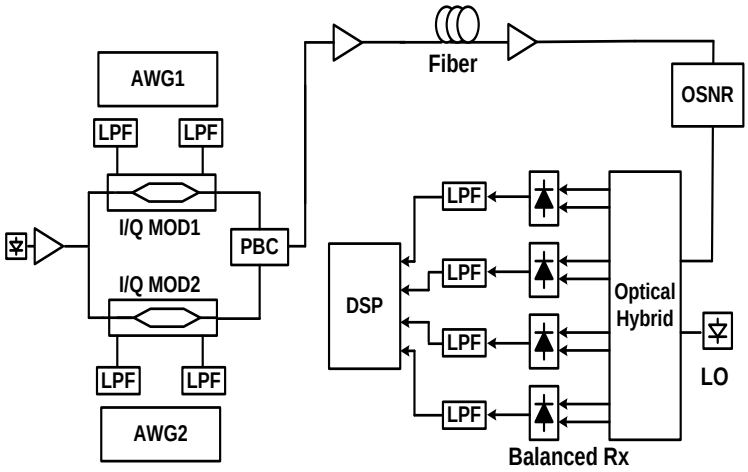

Figure 5.3: Simulation setup.

5.3.2 Performance of Noise Filtering DSP

While using multiple blocks of TSs is a simple technique and performance simply improves with the number of blocks used for CE, as demonstrated in Chapter 4 noise filtering techniques can also be used for enhancing CE performance. Noise filtering using moving average filter (MAF) depends on the filter size and also the resolution of the estimated channel transfer matrix. A small filter size will essentially provide minimal performance enhancement to the system while a large filter size could potentially degrade estimation performance due to the strong effect of averaging. As such, optimisation of noise filtering method is needed. Since the optimised values for OSNR estimation provided in Chapter 4 assume that only the TSs are equalised, this value is only sufficient for equalisation of the TSs and a different optimised filter size is needed for the case of actual data equalisation using DA-CE with noise filtering. Furthermore, assuming a constant channel transfer matrix with small impulse response in time domain, it can be seen that the resolution of the estimated transfer matrix is proportional to the length of the TS N_{ts} and thus the maximum filter size can be expected to be proportional to N_{ts} as well. Figure 5.4 shows the estimated signal Q values (derived from the signal constellations) for the simulated PM-QPSK system with different MAF's filter size L_{maf} expressed in terms of fractions of TS length N_{ts} for PM-QPSK systems with OSNR = 24dB. CD and TO are assumed to be zero for simplicity and the signals are equalised using fractionally-spaced equaliser [11]. It can be seen that

all TS lengths achieve optimal performance with MAF's filter size of L_{maf} = 0.25 while a larger filter size of L_{maf} = 0.5 gives some degradation in performance as expected as too much averaging on the channel transfer function has a degradation effect on the estimation performance. As the optimal L_{maf} is constant across all values of N_{ts}, increasing N_{ts} will increase the performance of both CE and noise filtering and in turn increase the equalisation performance. However, it can also be seen that the importance of filter size decreases with increasing sequence lengths and almost no difference in terms of performance can be observed for different filter size when the TSs are 128-symbol long. Thus using a longer sequence length could result in both an increase in performance and a reduced requirement for MAF filter size, which helps minimize the possible degradation caused by MAF due to channel information being averaged out.

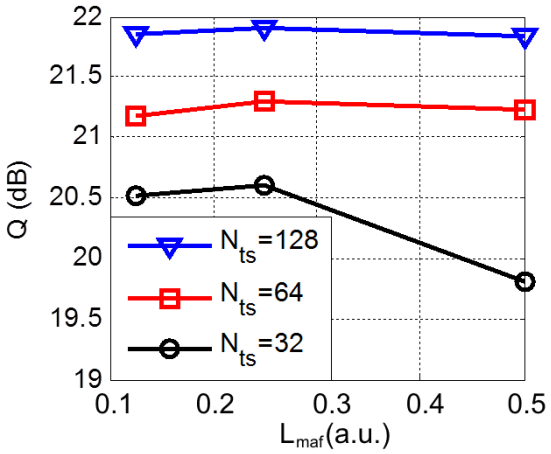

Figure 5.4: Equalised signal SNR as a function of MAF's filter size for QPSK systems.

5.3.3 Dispersion Tolerance Analysis of Noise Filtering Techniques

While the majority of CD can be compensated via overlap frequency domain compensation (OFDE), imperfections in CD estimation will leave residual CD in the estimated channel transfer matrix. If this residual CD value exceeds the tolerance of the system, significant degradation in equalisation performance will be observed. It is therefore necessary to investigate CD tolerance of both averaging and noise filtering methods. In order to investigate the CD tolerance of DA-CE, training blocks are inserted regularly into modulated data frame for CE purpose. Each training block

consists of four TSs with different core lengths N_{ts}. In order to evaluate the performance of using the average of multiple training blocks with respect to CD tolerance, multiple training blocks are placed next to each other before the actual data frame. Different values of residual CD are simulated using a transmission line model with dispersion parameter of 16.8 ps.nm/km and different transmission distances are set to represent various CD values. At the receiver, these blocks are used for CE and a non-weighted average of these estimations obtained from the training blocks is used for channel equalisation. For CE using single block with noise filtering, only one block is used for CE and equalisation, and the remaining blocks are discarded.

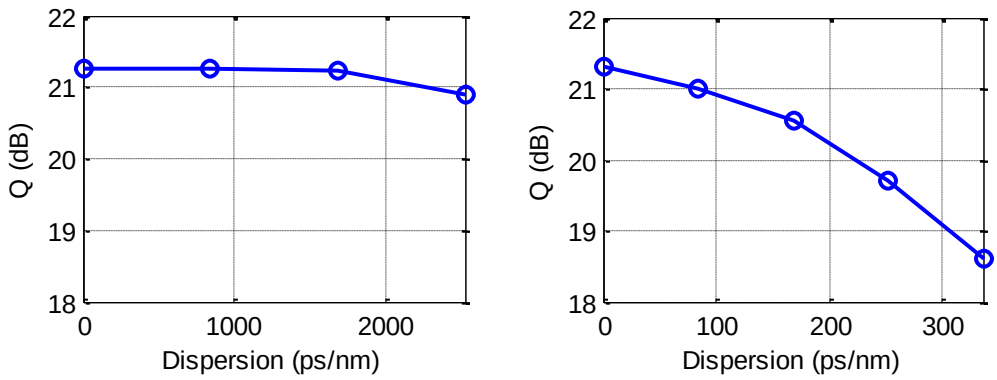

(a) *(b)*

Figure 5.5: CD tolerance for N_{ts} = 64, with (a) averaging and (b) noise filtering.

Figure 5.5 shows the Q value of the equalised signal constellation with respect to different residual CD values using DA-CE with a TS length of N_{ts} = 64 symbols. It can be seen that both techniques suffer from residual CD and degradation happens when CD is increased. Since averaging multiple blocks does not degrade the channel transfer function compared to noise filtering, the maximum CD tolerance of TS block with N_{ts} = 64 is 5880 ps/nm. However it can be seen from Figure 5.5(a) that degradation in equalisation performance happens before maximum tolerance is reached. This degradation is small and is only noticeable for a very large amount of residual CD. For using a single block of TS with noise filtering, performance degradation is much more severe with an increasing amount of CD as the CD transfer function gets averaged out. Thus CD needs to be estimated and removed before noise filtering. It can be concluded

that both methods are subject to degradation with a large residual amount of CD. However this degradation is more severe for noise filtering method and thus residual CD removal before noise filtering is mandatory for CE employing single TS block and noise filtering. When multiple TS blocks are used to obtain the averaged CE, equalisation tolerance to residual CD degrades slightly with an increasing amount of CD when this amount is within the CD tolerance limit.

5.3.4 Overhead Ratio and Equalisation Performance

Overhead ratio is one of the most critical factors in designing DA DSP for CO-SC systems. While previous demonstrations of DA-CE in CO-SC systems use many training blocks for CE [5], [10], optimisation of overhead ratio is critical for practical implementation purposes. However the use of different noise removal techniques and different TS types and lengths make it difficult for designing optimal DA system for equalisation purposes. In theory, sequences with flat spectrum property provide best CE as the signal power is flat across the entire frequency spectrum ensuring optimal estimation of all frequency components. The CAZAC sequences, while having flat signal spectrum and are ideal for CE, are difficult to implement in practice due to complex constellations that change with different sequence lengths. This leads to the search for alternative sequences with modulation format specific constellations for CE purpose. Among these, Golay sequences have been demonstrated to give estimation performance similar to ideal CAZAC sequences while still maintaining simple constellation for implementation purpose. The only drawback is that the sequences need to be designed as a pair and thus is not suitable for any implementations that utilise only one sequence. However, since a typical CO system is implemented as a 2x2 PM multiple-in-multiple-out (MIMO) system, this problem is solved by arranging Golay sequences in a typical STBC arrangement. Thus for CO systems employing DA-CE, Golay sequences present an attractive alternative choice compared to the ideal CAZAC sequence.

Beside the problem of having different sequence types for DA-CE, designing choice for noise filtering types and sequence lengths also needs to be optimised in terms of channel equalisation performance and the time slot needed to send the required training blocks. As demonstrated in Section 5.3.3, assuming residual CDs are left to be compensated

using the TSs alone, averaging multiple TSs provides better tolerance to CD compared to using noise filtering. However, this advantage is largely mitigated by estimating and subtracting residual CD first before performing noise filtering. For the same time slot used to send TSs, this leads to the choice of either sending multiple blocks of short TSs or a single block of long TSs for CE. Figure 5.6 illustrates the implementation of two types of training design in the same time slot. For the same time slot, a single block of long TSs can be used for CE. If the TS core length N_{ts} is cut by half, then two blocks of TSs can be used. However, estimation performance of using the average two training blocks with core length N_{ts} might not necessary be equivalent to having one block of length $2N_{ts}$ and utilising noise filtering to remove noise in CE. Thus it is very desirable to investigate the performance of sequence length and the amount of repeated blocks to be used for a given time slot for sending TSs.

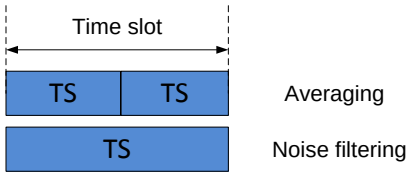

Figure 5.6: Averaging vs. noise filtering for the same time slot in DA-CE.

Simulations are carried out in order to investigate the relationship between TS lengths, number of averaging blocks and channel equalisation performances. A time slot of 384 symbols is used for sending the TSs. While the experimental system is only capable of 10 Gb/s, system baud rate is set to 25 Gbaud to further evaluate the effect of DA-CE in high speed systems. Modulation format is set to either PM-QPSK or PM-16QAM resulting in 100-Gb/s PM-QPSK and 200-Gb/s PM-16QAM CO-SC systems, respectively. Golay sequences are used to fill the TS time slot with different core length of 32, 64, and 128 symbols resulting in one, two and four blocks of TS, respectively.

Figure 5.7(a) shows the Q value of the received data using TS block with different lengths after 1000-km transmission. System CD is compensated in frequency domain during first stage equalisation and TSs are used for second-stage equalisation to compensate the remaining impairments. Regardless of core sequence lengths, only one block of TSs is used and CE is enhanced by noise filtering using MAF as described in

Section 5.2.1. The MAF parameter is set at L_{maf} = 0.25. It can be seen that TSs with longer lengths in general produce better estimation accuracy and equalisation performance compared to shorter TSs and the trade-off between performance and update speed/overhead ratio is clear. Changing the sequence lengths from N_{ts} = 32 to N_{ts} = 64 gives an average increase of around 0.9 dB in Q value across the entire OSNR range while increasing N_{ts} from N_{ts} = 64 to N_{ts} = 128 gives an increase of around 0.6 dB in Q value.

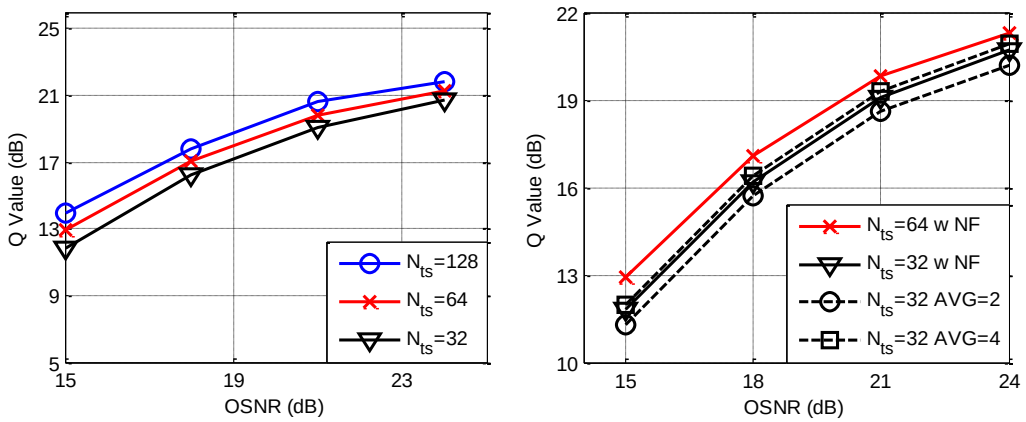

(a) *(b)*

Figure 5.7: Simulated Q value of equalised QPSK data for (a) different sequence lengths using noise filtering and (b) different noise removal techniques.

Figure 5.7(b) shows a comparison between using multiple short sequences and suppressing the noise in estimation by averaging the results compared to using a longer sequence with noise filtering DSP. TSs with core length of 32 symbols are used and the number of repeated blocks is set to either 2 or 4 resulting in a total time slot of 128 and 256 symbols, respectively. It can be seen that for N_{ts} = 32 the receiver needs around 4 averages (AVG = 4) to match the performance of noise filtering DSP, and using a single sequence of twice the length (N_{ts} = 64) with noise filtering improves the estimation performance beyond what can be achieved with 4 training blocks with core length N_{ts} = 32. A single training block with core length of N_{ts} = 64 symbols also results in less total overhead ratio compared to 4 blocks of TS with length N_{ts} = 32 and is an overall superior method for CE with noise removal. Overall, for the same time slot, a single long sequence with noise filtering DSP will provide better performance compared to

multiple short sequences. Similar to CAZAC sequences in [8], longer Golay sequences provide slightly better estimation and equalisation as a result of better CE accuracy and better noise filtering performance. While doubling the sequence length will increase the system performance, this comes with a trade-off of halving the update speed if the overhead ratio is to be kept constant, or increasing the system overhead ratio for keeping a constant update speed.

5.4 FLEXIBLE FRAME SYNCHRONISATION USING GOLAY SEQUENCES

Section 5.3 described the investigation of TS lengths and performances for CO-SC systems with DA-CE using Golay sequences. With the addition of noise filtering, the use of a single block of TSs and noise filtering DSP is a preferable method as the technique gives better performance in the same time slot compared to averaging multiple blocks of TSs. However, there is also a trade-off between TS core length and total system equalisation performance even in the case of using noise filtering techniques. In general a TS block with longer core sequence length gives better equalisation performance with the trade-off of increasing system overhead ratio or reducing update speed. Thus it is very desirable to design DA CO-SC systems with flexible overhead ratio where the TS core length N_{ts} can be changed depending on the channel condition. However, as CO-SC systems with DA-CE are sensitive to frame synchronisation, different frame synchronisation methods need to be developed if a system with flexible overhead ratio is to be used. The traditional frame synchronisation method for DA-CE systems, assuming CD compensation in the first stage, is to utilise autocorrelation similar to the Schmild's format proposed in OFDM systems [19]. The frame synchronisation algorithm compares the incoming signal with a known sequence to determine the sequence location. In the case of DA-CE, the header sequence used is the first sequence S_1. However, as the receiver's DSP depends on knowing the exact TS to perform frame synchronisation, changing TS length will cause failure in the receiver's frame synchronisation.

In this section, a new frame synchronisation for DA receiver DSP based on the minimum TS length for Golay sequences is presented. The frame synchronisation method does not depend on the knowledge of the entire TS and instead only depends on

the minimum designed TS length for frame synchronisation and TS length detection by exploiting Golay sequences recursive generation property.

5.4.1 Flexible Sequence Length Frame Synchronisation

As demonstrated in Section 5.3.4, the TS length is related to system equalisation performance. Depending on channel condition, the transmitter may need to alter the TS length to optimise the system performance and tracking penalty and the receiver's DSP must be able to detect this change. If the location of the first TS and its length is known, then the rest of the TS lengths and location can be obtained through calculations. Traditional methods for frame synchronisation typically involve a separate header block. At the receiver the block location is estimated based on autocorrelation metrics and the TS locations can be found. Since the TSs used for CE are known, it is possible to also utilise the TSs as the frame synchronisation block and the first TS that appears in time (the S_1 sequence) can be used for frame synchronisation using autocorrelation. Thus the problem is simplified to detecting length and location of the first sequence S_1 in the TS block in case the length of S_1 is not known. The proposed flexible frame synchronisation method in this chapter is based on using Golay sequences as the TSs. Assuming a Golay pair of length N_{ts} generated by recursive construction [14]. The "*a*" and "*b*" sequences can be written as:

$$\begin{aligned} a_n &= \left[a_{n-1} \quad b_{n-1} \right] = \left[a_{n-2} \quad b_{n-2} \quad a_{n-2} \quad -b_{n-2} \right] \\ &= \left[a_{n-i} \quad b_{n-i} \quad a_{n-i} \quad b_{n-i} \quad \ldots \quad a_{n-i} \quad b_{n-i} \right] \end{aligned} \tag{5.2}$$

$$\begin{aligned} b_n &= \left[a_{n-1} \quad -b_{n-1} \right] = \left[a_{n-2} \quad b_{n-2} \quad -a_{n-2} \quad b_{n-2} \right] \\ &= \left[a_{n-i} \quad b_{n-i} \quad a_{n-i} \quad -b_{n-i} \quad \ldots \quad a_{n-i} \quad -b_{n-i} \right] \end{aligned} \tag{5.3}$$

Where a_n is the sequence in its nth iteration and a_{n-i} is the sequence in (n-i)th iteration, respectively. Equation 5.2 indicates that Golay a_n sequence of length N_{ts} will contain a unique number of shorter a_{n-i} sequence of length N_{ts} /(i+1). Thus for a Golay "*a*" sequence with unknown length N_{ts}, its length can be calculated from the number of short sequence a_{n-i} contained in the main sequence. Thus, assuming detection of the Golay "*a*" sequence from an incoming data stream, both the sequence location and its length can be obtained by first calculating the cross correlation between the sequence a_{n-i} and the received signal as:

$$Z[n] = xcorr\left(R_s, a_{n-i}\right) \tag{5.4}$$

where $Z[n]$ is the cross correlation index, a_{n-i} is the short Golay core and R_s is the received signal. Equation 5.4 can be viewed as the standard frame synchronisation method using Schmild format with the minimum-length TS a_{n-i} as the synchronisation header. When frame synchronisation is performed using minimum length sequence a_{n-i} on TS block with core length larger than a_{n-i}, multiple peaks will be detected as explained in Section 5.4. The first peak of $Z[n]$ will indicate the starting location of the TS block and the number of equally spaced peaks obtained will indicate the length of the TS block. The distance between each peak is equal to twice the length of a_{n-i} as illustrated in Equations 5.2 and 5.3.

However, it can also be seen that in both cases of $i = 1$ and $i = 0$, autocorrelation will only yield a single peak. This ambiguity appears since in both cases the a_n sequence only contains one single a_{n-i} sequence. This can be solved by rearranging the TS block in space and time as:

$$S[k] = \begin{pmatrix} A[k] & B[k] \\ -B^*[k] & A^*[k] \end{pmatrix} \tag{5.5}$$

where $A[k]$ and $B[k]$ are the discrete Fourier transforms of "*a*" and "*b*" Golay sequences, respectively. As "*b*" sequence also contains a number of the a_{n-i} core sequence, the extra peak contribution from the "*b*" sequence in the case $i = 1$ (but not in the case $i = 0$) will help distinguish between these two cases.

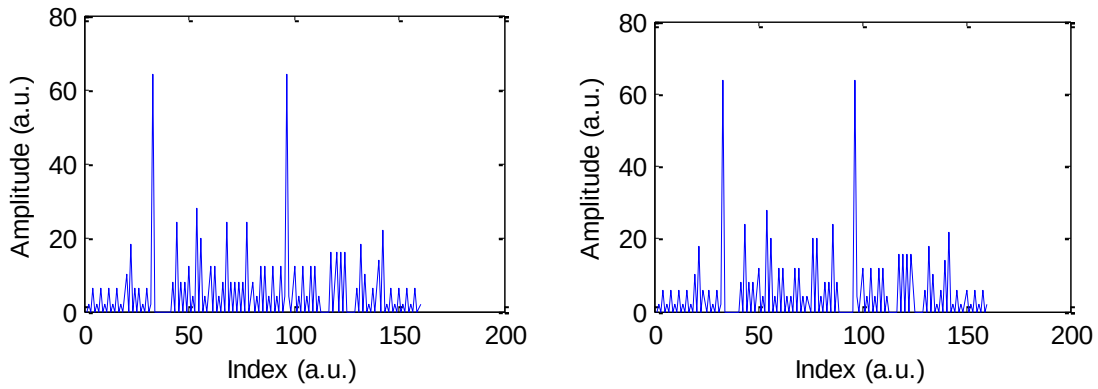

(a) *(b)*

Figure 5.9: Correlation index of (a) xcorr(a_n,a_{n-2}) and (b) xcorr(b_n,a_{n-2}).

Figure 5.9 shows the correlation index of Golay a_{n-i} sequence with full-length sequences a_n and b_n. The length of a_n is 128 symbols and i = 2, resulting in length of 32 symbols for a_{n-2} sequence. Figure 5.9(a) shows the correlation index of $xcorr(a_n,a_{n-2})$ while Figure 5.9(b) shows the correlation index of $xcorr(b_n,a_{n-2})$, respectively. It can be seen that both correlation functions yield two peaks, as both a_n and b_n sequences contain two small sequences a_{n-2} as indicated by Equations 5.2 and 5.3. Thus detection of TS lengths in the case of i = 1 is possible using Equations 5.4 and 5.5. Due to the design of TS block for DA-CE systems, which employ CP blocks to guard the TS from interfering with each other, CP blocks need to be taken into account when rearranging the TS according to Equation 5.5. The distance between peaks can now be either twice the length of core a_{n-i} sequence (peaks found within a sequence) or twice the length N_i of core a_{n-i} sequence plus the length of two CP blocks (peaks found between a_n and b_n sequences).

5.4.2 Simulation Demonstration

5.4.2.1 Effect of Cyclic Prefix

As described in Section 5.4.1, CP blocks are normally needed for guarding the TSs from interfering with each other within the TS block in order to simplify the receiver's CE using DA-CE. However, the use of CP further adds complications to the proposed frame synchronisation method as the distance between peaks can be either $2N_i$ or $(2N_i+2N_{cp})$ where N_i and N_{cp} are the length of the core sequence a_{n-i} and the length of the CP block, respectively. As the CP blocks contain part of the full TSs, they also yield strong resemblance to the small core sequence a_{n-i}. Figure 5.10 shows an autocorrelation index of the proposed TSs with N_{ts} = 64, N_i = 32 and for two different value of N_{cp} = 4 and N_{cp} = 16. It can be seen that with N_{cp} = 16 the CP blocks form a strong resemblance to the core sequence block and thus generate an invalid peak (labelled by the red line in Figure 5.10). The invalid peaks generated by CP blocks are in the middle of two valid ones as expected however the amplitude of this peak will depend on the CP length N_{cp}. Based on recursive construction of Golay sequences, it can be derived that in the case of i = 1, the CP block of b_n sequence and the CP block of a_n sequence form a single a_{n-i} sequence and thus yield a strong autocorrelation peak that appears before the actual second peak.

For the frame synchronisation method to be robust against CP blocks, invalid peak detection must be employed using expected peak distances and expected number of peaks. While the TS length is not known, the length of the CP block must be known for invalid peak detection. The method can then use the CP length information for detection of invalid peaks and ignore these peaks during calculation of TS length. As illustrated in Figure 5.10(a) the distance between the invalid peaks and the peak on the left is approximately 64 symbols, which can lead to detection of the invalid peaks as valid. However as the number of valid peaks is always a multiplication of 2, in the case of less than 4 peaks the distance between two peaks must be $N_{ts} + N_{cp}$ and the correct peaks can be detected by taking CP length into account. It can also be noted that the peak generated from CP blocks is always highest when $N_{cp} = N_i/2$ and $N_{cp} = N_{ts}/4$. As CD is assumed to be compensated in the first stage equalisation, only small blocks of CP are needed. As illustrated in Figure 5.10(b), when the CP length N_{cp} is much smaller than core length N_i ($N_{cp} = 4$), the peak generated from CP blocks is smaller compared to those that are generated from the core sequence a_{n-i}. The invalid peak can then be detected and suppressed without difficulty.

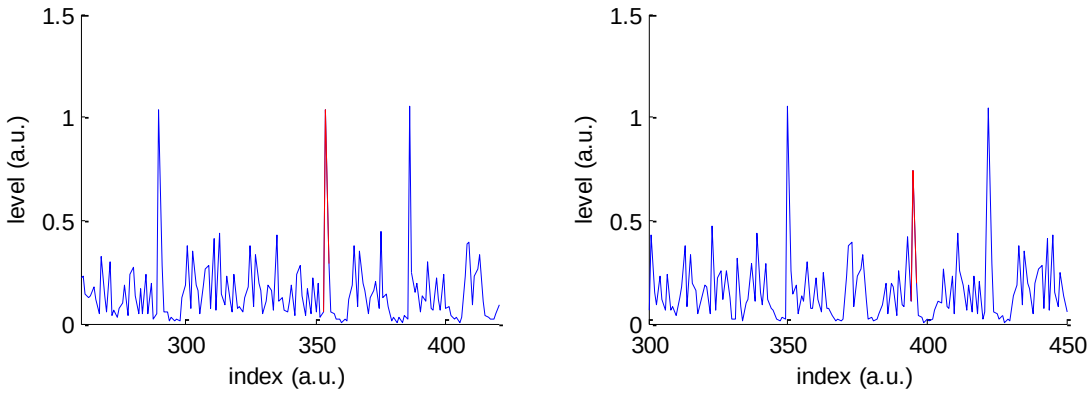

Figure 5.10: Invalid peak (red line) in correlation index for $N_{ts} = 128$, $N_i = 32$ with (a) $N_{cp} = 16$ and (b) $N_{cp} = 4$.

5.4.2.2 Peak to Threshold Ratio

Figure 5.11 shows an example in simulation of Equation 5.4 after 1000-km transmission with $N_{ts} = 128$, $i = 2$, and OSNR = 18 dB and it can be seen that 4 peaks are observed thus both the sequence location and its length can be calculated. Figure 5.12 shows the

peak-to-threshold ratio (PTR), defined as the ratio between the peak level and the maximum correlation index level where the peak does not occur, of the correlation index $Z[n]$ with different a_{n-i} core sequence length under different OSNR. The length of the core sequence cannot be too short as this will cause instability due to the peak being indistinguishable from the rest. It can be seen from Figure 5.12 that at OSNR = 12 dB a core sequence of length N_{ts} = 32 still provides a good peak-to-noise ratio of 1.5. A length of 32 symbols is therefore chosen to be the length of the core sequence a_{n-i}.

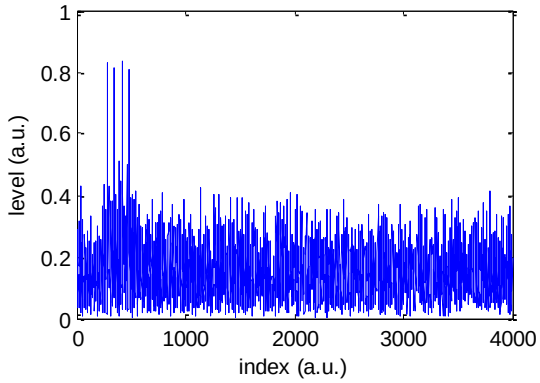

Figure 5.11: Simulated frame synchronisation with TS length detection for N_{ts} = 128 and i = 2.

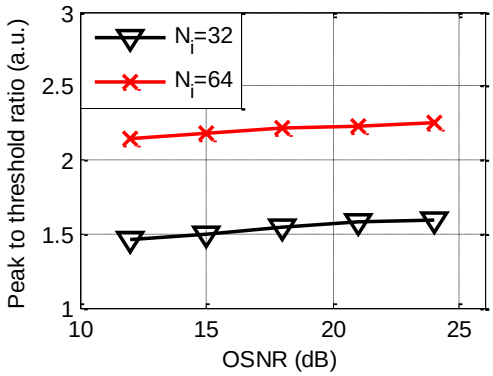

Figure 5.12: Simulated peak to threshold ratio for frame synchronisation with different core sequence lengths.

5.4.2.3 Chromatic Dispersion Tolerance

CD has the effect of "polluting" the signal symbol due to the phase rotation in frequency domain and thus is a primary impairment against recognizing transmitted

symbols. Since the proposed frame synchronisation method is based on finding the TS using autocorrelation, some sensitivity to CD can be expected. Figure 5.13 shows the PTR with respect to CD in simulation for 25 Gbaud system with N_i = 32 symbols. It can be seen that increasing the amount of CD had a significant impact on the proposed frame synchronisation method as the signal is polluted by dispersion. Thus in order for the proposed training scheme to work CD must be compensated during the first stage of a two-stage equalisation process. However, with modern CD estimation techniques and blind CD compensation using overlap frequency domain equalisation (OFDE), most of system bulk CD can be compensated before frame synchronisation, the small remaining amount of CD (residual CD) can be tolerated by the frame synchronisation method.

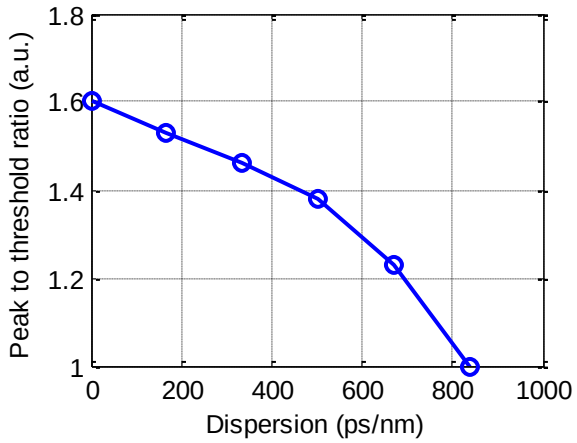

Figure 5.13: Peak to threshold ratio as a function of CD.

5.4.3 Experimental Demonstration

5.4.3.1 Experimental Setup

Figure 5.14 shows the experimental setup for CO systems with DA-CE. The transmitter side consists of one 10-Gbaud arbitrary waveform generator (AWG) and I/Q electrical-to-optical modulator to generate the TS followed by data frame on the X-polarisation and a delay line to emulate the Y-polarisation with a delay time of 27.2 ns. Both polarisations are then multiplexed through the PBC to form the PM optical signal. Due to the structure of this delay line setup, the TSs are modified to allow emulation of space-time coding TS block similar to the structure outlined in Section 3.5.1 of Chapter

3. The maximum TS length N_{ts} for this delay line setup is N_{ts} = 128 symbols with N_{cp} = 4 symbols. The transmission line consists of a recirculating loop with loop timing determining the total transmission length. A transmission length of 1000 km is used for PM-QPSK while a shorter length of 400 km is used for PM-16QAM modulation format due to PM-16QAM format being more sensitive to OSNR. At the receiver, an amplified spontaneous emission (ASE) source is added by cascading two optical amplifiers. The signal is then split into two paths using a coupler with a ratio of 9:1. The 10% path is then fed into an optical spectrum analyser (OSA) for measurement of OSNR while the other path is sent into balanced coherent receivers. The data are then captured using 20-GHz sampling scope for offline DSP. Figure 5.15 shows the DSP procedure which consists of system's CD compensation in frequency domain, frequency offset (FO) compensation, flexible frame synchronisation, CE and data equalisation.

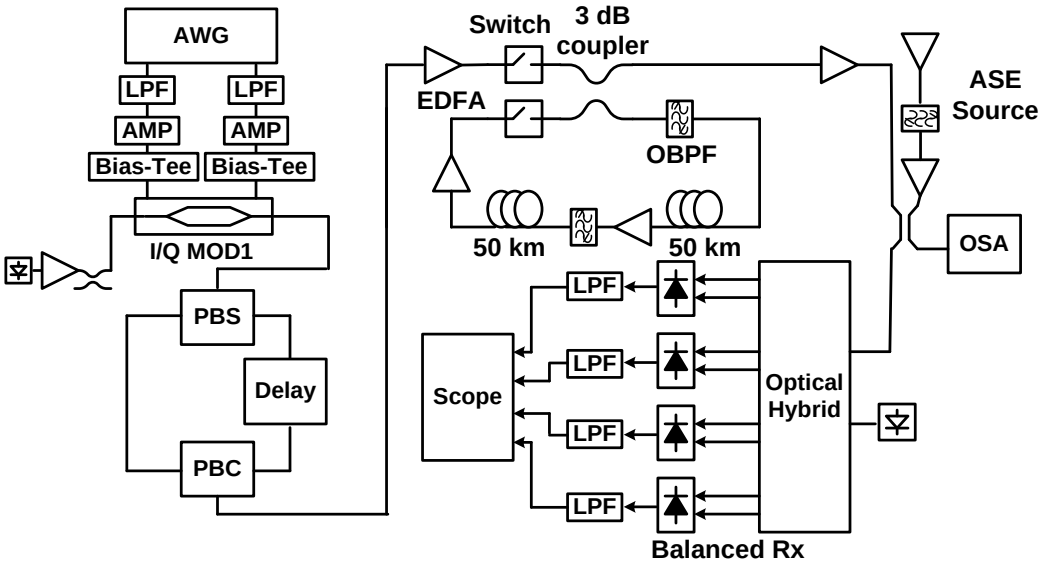

Figure 5.14: Experimental setup

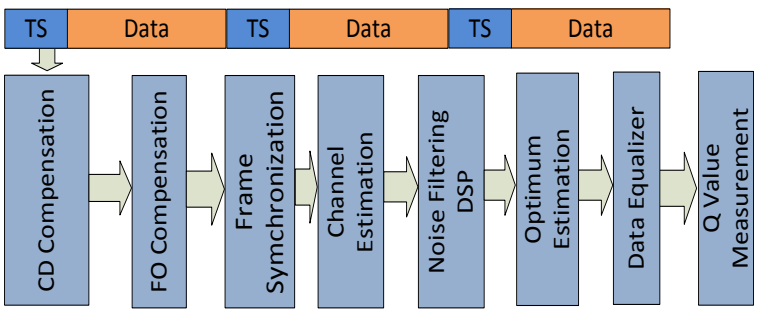

Figure 5.15: Receiver's DSP procedure.

5.4.3.2 Results and Discussion

Figure 5.16 shows the measured Q values for different TSs under different OSNRs with each data point being an average of 100 captures. It can be seen that increasing TS length will improve channel equalisation performance as a result of better estimation accuracy. While increasing the TS length from 32 to 64 symbols results in a significant improvement in Q value of around 0.8 dB, a slightly smaller improvement of around 0.5 dB is observed when increasing TS length from 64 to 128 symbols. 16 QAM modulation format exhibits similar results when increasing the TS length as in the case for QPSK format. While QPSK format can use a wider range of TS length (32-128 symbols) depending on channel condition, 16-QAM format requires a smaller range of TS length (64-128 symbols) in practice due to OSNR and receiver sensitivity limitation. Overall it is clear that there is a trade-off in terms of system performance and total TS length, which in turn affects the overhead ratio and update speed.

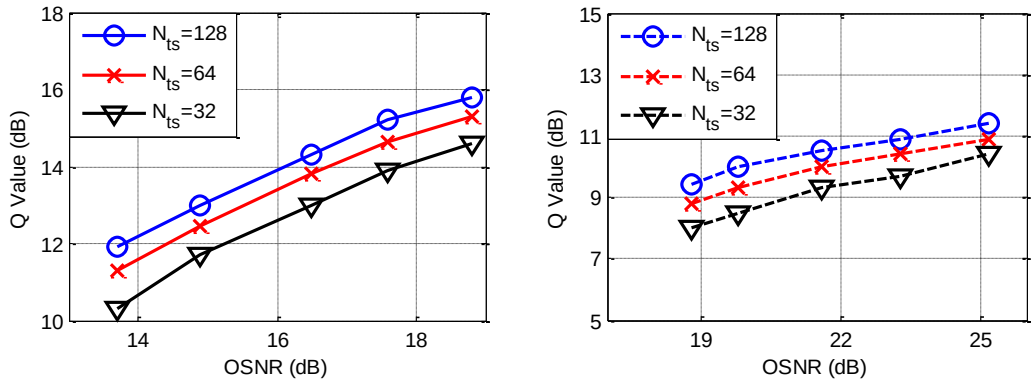

(a) *(b)*

Figure 5.16: Measured Q value of equalised data with different TS lengths for (a) PM-QPSK and (b) PM-16QAM formats.

Figure 5.17 shows the measured peak to noise ratio when using the proposed frame synchronisation method after 1000-km transmission with a core sequence length of 32 symbols for a wide range of OSNR. Each data point is an average of 100 captures with maximum variation plotted as error bar. Adding noise to the system (decreasing OSNR) has an effect of increasing the variation between amplitudes of the detected peaks however it can be seen that for the lowest OSNR of 12 dB the system still maintains a

good average PTR of 1.4 with a minimum PTR of 1.3 which is more than sufficient for determining the location of the TS as well as the length of the TS block. Overall, for CO-SC-FDE systems with two stage equalisation, the proposed frame synchronisation scheme is robust against OSNR and transmission.

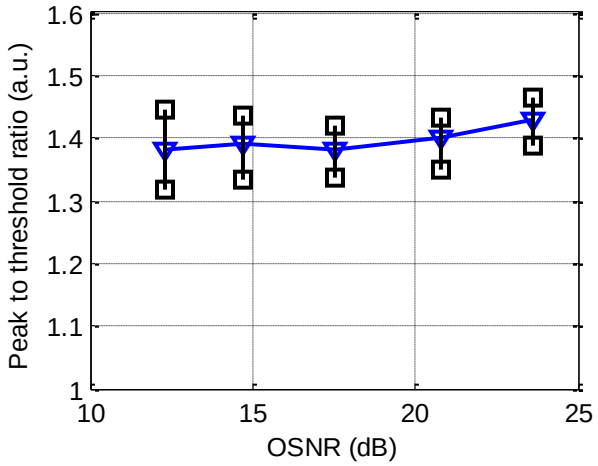

Figure 5.17: Measured peak to noise ratio for frame synchronisation with core sequence length N_{ts} = 32.

5.5 CONCLUSIONS

This chapter presents a comparison of different CE enhancement techniques for CO systems employing DA-CE. Since the raw CE obtained by DA-CE is influenced by noise, enhancement needs to be performed to remove the noise in CEs. This can be performed by repeating the TS block multiple times or by applying a noise filter on the estimated channel transfer matrix. The latter gives similar performance with the added advantage of only utilising a fraction of the time slot required. As CD is compensated in the first stage using OFDE, only a short TS block with small TS length is required for CE in the second stage however increasing the TS lengths will also give better system performance as a results of higher resolution in CE. Thus, for CO-SC systems with DA-CE, there is a trade-off in overhead ratio and system performance. Optimisation of this trade-off is thus desirable in the practical design of DA-CE. Changing the length of TS block with respect to different channel conditions presents a way to optimise the overhead ratio, update speed and channel performance for CO-SC systems with DA-CE.

This chapter also presents a flexible frame synchronisation method for DA CO-SC systems based on Golay sequences. By utilising a small Golay sequence as the synchronisation header, both the location of the TS block and the TS length can be detected. Since the proposed technique utilises the TS block for frame synchronisation, no separate block for frame synchronisation is needed. Only knowledge of the minimum length of TS and the CP length is needed and the TS length can be calculated from the correlation index. This flexibility allows for changing of TS length according to the channel condition in order to optimise overhead ratio or system's update speed. The main drawback of the proposed technique is its degradation in performance with respect to a large value of CD as the training symbols are polluted by CD and cannot be detected reliably using autocorrelation. However as only a small value of CD is presented after first stage CD compensation, this degradation is minimal in practice and does not affect the overall performance of the frame synchronisation technique. The technique is demonstrated in 40-Gb/s PM-QPSK and 80-GB/s coherent PM-16QAM CO-SC systems with good and stable performance with up to 1000-km transmission over a wide range of OSNR. For low values of OSNR, a slight degradation in performance can be observed compared to high OSNR values however this degradation is small and the technique is considered to be robust against OSNR.

5.6 REFERENCES

[1] S. J. Savory, “Digital filters for coherent optical receivers,” *Optics Express*, vol. 16, no. 2, pp. 804-817, Jan. 2008.

[2] K. Roberts, D. Beckett, D. Boertjes, J. Berthold, and C. Laperle, “100G and beyond with digital coherent signal processing,” *IEEE Communications Magazine*, vol. 48, no. 7, pp. 62–69, Aug. 2010.

[3] R. Kudo, T. Kobayashi, K. Ishihara, Y. Takatori, A. Sano, and Y. Miyamoto, "Coherent Optical Single Carrier Transmission Using Overlap Frequrency Domain Equalisation for Long-Haul Optical Systems," *Journal of Lightwave Technology*, vol. 27, no. 16, pp. 3721–3728, Aug. 2009.

[4] M. Kuschnerov, F. N. Hauske, K. Piyawanno, B. Spinnler, M. S. Alfiad, A. Napoli, and B. Lankl, “DSP for Coherent Single-Carrier Receivers,” *Journal of Lightwave Technology*, vol. 27, no. 16, pp. 3614-3622, Aug. 2009.

[5] J. Li, C. Zhao, S. Zhang, F. Zhang, and Z. Chen, "Experimental Demonstration of 120-Gb/s PDM CO-SCFDE Transmission Over 317-km SSMF,” *IEEE Photonics Technology Letters*, vol. 22, no. 24, pp. 1814-1816, Dec. 2010.

[6] J. Li , S. Zhang , F. Zhang and Z. Chen, "Comparison of transmission performances for CO-SCFDE and CO-OFDM systems,” *IEEE Photonics Technology Letters*, vol. 22, no. 14, pp. 1054-1056, Jul. 2010.

[7] M. Kuschnerov, M. Chouayakh, K. Piyawanno, B. Spinnler, E. de Man, P. Kainzmaier, M.S. Alfiad, A. Napoli, and B. Lankl, "Data-aided versus blind single-carrier coherent receivers," *IEEE Photonics Journal*, vol 2, no. 3, pp. 386–403, Jun. 2010.

[8] B. Spinnler, S. Calabro, and M. Kuschnerov, "Pilot-assisted channel estimation methods for coherent receivers," *Optical Fibre Communication Conference OFC'2013,* pp 1-3, paper OW4B-3, Mar. 2013.

[9] A. V. Tran, C. Zhu, C. C. Do, S. Chen, T. Anderson, D. Hewitt, and E. Skafidas, "8×40-Gb/s optical coherent pol-mux single carrier system with frequency domain equalisation and training sequences," *IEEE Photonics Technology Letters*, vol. 24, no. 11, pp. 885–887, Mar. 2012.

[10] R. Elschner, F. Frey, C. Meuer, J. K. Fischer, S. Alreesh, C. Schmidt-Langhorst, L. Molle, T. Tanimura, and C. Schubert, "Experimental demonstration of a format-flexible single-carrier coherent receiver using data-aided digital signal processing," *Optics Express*, vol. 20, no. 27, pp. 28786-28791, Dec. 2012.

[11] C. Zhu, A. Tran, F. Hauske, S. Chen, T. Anderson, and E. Skafidas, "Low-Complexity Fractionally-Spaced Frequency Domain Equalisation with Improved Channel Estimation for Long-Haul Coherent Optical Systems". *Optical Fibre Communication Conference OFC'2013*, pp. OW4B.5, Anaheim, CA, USA, 2013.

[12] R. L. Frank, S. A. Zadoff, and R. Heimiller, "Phase shift pulse codes with good periodic correlation properties," *IRE Transactions on Information Theory*, vol.8, no.6, pp. 381-382, Oct. 1962.

[13] P. Z. Fan, M. Darnell, and B. Honary, "Crosscorrelations of Frank sequences and Chu sequences," *Electronic Letters*, vol. 30, no. 6, pp. 477-478, Mar. 1994.

[14] M. J. Golay, "Complementary series," *IRE Transactions on Information Theory*, vol. 7, no. 2, pp. 82-87, Apr. 1961.

[15] W. H. Holzmann and H. Kharaghani, "A computer search for complex Golay sequences," *Australasian Journal of Combinatorics*, vol. 10, pp. 251-258, Apr. 1994.

[16] R. Craigen, W. H. Holzmann and H. Kharaghani, "Complex Golay sequences: structure and applications," *Discrete mathematics*, vol. 252, no. 1, pp. 73-89, May 2002.

[17] C. Chong and V. Tarokh, "Two construction of 16-QAM Golay complementary sequences," *IEEE International Symposium on Information Theory ISIT*, pp. 240, 2002.

[18] O. Weikert amd U. Zolzer, "Efficient MIMO Channel Estimation with Optimal Training Sequences," *1st Workshop on Commercial MIMO-Components and Systems CMCS' 2007*, Duisburg, Germany, Sep. 2007.

[19] T. M. Schmidl, and D. C. Cox, "Robust frequency and frame synchronisation for OFDM," *IEEE Transactions on Communications*, vol. 45, no. 12, pp. 1613 – 1621, Dec. 1997.

[20] H. Minn, V. K. Bhargava, and K. B. Letaief, "A robust timing and frequency synchronisation for OFDM systems, " *IEEE Transactions on Wireless Communications*, vol. 2, no. 4, pp. 822 – 839, Jul. 2003.

[21] B. Park, H. Cheon, and C. Kang, "A novel timing estimation method for OFDM systems," *IEEE Communications Letters*, vol. 7, no. 5, pp. 239-241, May 2003.

[22] Y. Huang, X. Zhang, and L. Xi, "Modified Synchronisation Scheme for Coherent Optical OFDM Systems," *Journal of Optical Communications and Networking*, vol. 5, no. 6, pp. 584-592, Jun. 2013.

[23] J. M. Groenewald, and B.T. Maharaj, "MIMO channel synchronisation using Golay Complementary Pairs," AFRICON 2007, pp. 1-5, Windhoek, Namibia, 2007.

6 OSNR Estimation Using Low-Bandwidth Receivers for Coherent Optical Systems

6.1 INTRODUCTION

Chapter 3 and 5 presented the use of data-aided (DA) channel estimation (CE) and equalisation in coherent optical (CO) single carrier (SC) systems. The use of training sequences (TSs) enables fast and robust CE processing at the receiver, simple transmitted signal decoding and flexible modulation formats [1]-[3]. System chromatic dispersion (CD) can be estimated using a long block of TSs as presented in Chapter 3 and system optical signal-to-noise ratio (OSNR) can be estimated using the TSs used for CE as presented in Chapter 4. While many other different techniques can be used for OSNR estimation [4]-[7], techniques based on coherent receivers show the most recent research interests [8]-[12]. However, the previously proposed OSNR estimation techniques typically rely on full speed coherent receivers with full sampling speed for data equalisation. While this means that these techniques are practically free of extra required hardware, they can only monitor OSNR at the end receiver where the signals are demodulated and thus are not an ideal solution for distributed monitoring of optical networks. As modern optical networks have evolved to complex multi path with switching instead of simple point to point, different techniques that utilise separate hardware for channel monitoring at network nodes without the need for full speed coherent receiver will be in demand. While cost of coherent receivers does not scale linearly with designed sampling speed, it is expected that low-speed coherent receivers will cost less than their full-speed counterparts for quite some time similar to the cost involved from moving from 40G to 100G technologies [13]. As coherent receiver technology matures, it will be possible to produce coherent receivers with low sampling speeds and low receiver bandwidths at a fraction of the cost of a high-speed coherent

receiver. While these reduced complexity receivers cannot be used for channel equalisation of high-speed optical signals, it is very desirable to use low-cost coherent receivers for distributed optical performance monitoring (OPM) purposes. The low-bandwidth receivers can be used for monitoring at different nodes on the network, for example, at a reconfigurable optical add drop multiplexer (ROADM) site. It is therefore desirable to investigate OPM techniques using separate low-cost coherent receivers.

In this chapter, OSNR estimation method for DA CO-SC systems using low-bandwidth coherent receivers is presented [14]. The technique is based on estimation of spectrum property of the TSs in frequency domain and thus can be adapted to different bandwidth requirements. In Section 6.2, the proposed OSNR estimation technique utilising frequency domain spectrum is presented. Section 6.3 presents simulation demonstration of the proposed method for OSNR estimation using low-bandwidth receivers. Section 6.4 presents experimental demonstration for the proposed estimation method. Finally, the chapter is concluded in Section 6.5.

6.2 DATA-AIDED OSNR ESTIMATION USING LOW-BANDWIDTH COHERENT RECEIVER

Techniques based on coherent receivers typically estimate the signal-to-noise ratio (SNR) of the received signals captured by coherent receivers and translate this quantity into OSNR. While the translation between SNR and OSNR can be done easily by measuring a calibration point and taking reference bandwidth into account as presented in Chapter 4, estimation of SNR will typically require analysing the equalised signal constellation. This in turn requires the optical signal to be captured as full speed for equalisation purpose. In order to utilise a low-bandwidth device for estimation of full-bandwidth signal, the estimator needs to utilise signal information that reside within the receiver bandwidth therefore estimation needs to be performed in frequency domain. For CO orthogonal frequency division multiplexing (OFDM) systems, since this format divides a single high speed stream into multiple low-speed subcarriers and data are modulated in frequency domain, it is trivial that the subcarriers captured within the receiver bandwidth can be used for OSNR estimation purpose and such approach had been demonstrated [15]. However, CO-SC systems with frequency domain equalisation (FDE) modulate data in a single high speed stream and as such it is difficult to estimate

signal's SNR from the frequency spectrum. For CO-SC-FDE systems, a known signal will be required for SNR estimation using the frequency spectrum instead of the signal constellation. CO-SC-FDE systems employing DA-CE utilise TSs for signal processing purposes and the TSs are known thus making it possible to estimate SNR directly from the TSs' frequency spectrum. Optimal sequences such as constant amplitude zero auto correlation (CAZAC) sequences and Golay sequences had been proposed for CO-SC systems with DA-CE [3]. Both sequence types had been demonstrated to provide optimal estimation performance and can be employed in CO-SC systems for CE purpose. However, as one of the main focuses of SC systems is simple transmitter design, TSs with simple signal constellations similar to the actual data are preferable in practice. For this requirement, Golay sequences are better than CAZAC sequences since Golay sequences can be generated at any arbitrary length while still maintain data-like constellation such as quadrature phase shift keying (QPSK) or 16-quadrature amplitude modulation (16QAM). It is therefore desirable to utilise Golay sequences for SNR estimation in CO-SC-FDE systems with DA-CE. The technique for SNR estimation using Golay TSs and spectral property is outlined in the next section.

6.2.1 SNR Estimation Using Golay Spectral Property

As explained in Chapter 3, Golay sequences are a pair of complimentary sequences S_1 and S_2 that satisfy the power spectrum property:

$$G[k] = \left|S_1[k]\right|^2 + \left|S_2[k]\right|^2 = N_{ts} \tag{6.1}$$

where $S_1[k]$ and $S_2[k]$ are the discrete Fourier transforms (DFTs) of the original S_1 and S_2 sequence, respectively, and N_{ts} is a constant related to the length of each sequence. Two sequences are considered complementary if the sum of their power spectrums satisfies Equation 6.1. It can also be seen that in the case of using CAZAC sequences for DA-CE, a pair of CAZAC sequences, with each sequence having a constant power spectrum, also satisfy Golay property. A maximum length sequence (m-sequence), combined with a zero sequence, as designed for DA-CE in [16], can also satisfy Equation 6.1. Thus, approaches based on complementary power spectrums can be generalized for most sequences used for DA-CE. However, compared to CAZAC sequences or PN sequence, Golay sequences offer similar performance but with the added advantage of having simple and length-independent constellation and thus are

more suitable for commercial implementation of CO-SC systems with DA-CE [3]. For 2x2 polarisation-multiplexed (PM) CO-SC systems, four Golay sequences are arranged in a space-time structure followed by the actual data frame as illustrated in Figure 6.1 with S_1 and S_2 being the two orthogonal Golay sequences; S_1^*, S_2^* are the complex conjugate of the original S_1 and S_2 sequences, respectively. To simplify receiver signal processing, cyclic prefix (CP) blocks are added at the beginning and end of each sequence.

Figure 6.1: Golay sequences in PM CO-SC system.

Golay sequences captured at full sampling speed of twice the system baud rate and using a full-bandwidth receiver are first considered for simplification purpose. At the receiver, after signal sampling at the Nyquist rate and following frame synchronisation, the four sequences can be recovered. The received sequences contain the transmitted sequences with linear impairment plus added noise and in the frequency domain, the four received TSs can be expressed as:

$$\begin{pmatrix} R_1[k] & R_2[k] \\ R_3[k] & R_4[k] \end{pmatrix} = H[k] \begin{pmatrix} S_1[k] & S_2[k] \\ -S_2[k]^* & S_1[k]^* \end{pmatrix} + W[k] \tag{6.2}$$

where $H[k]$ is the linear impairment transfer matrix mainly consisting of CD and polarisation-mode dispersion (PMD); $S_1[k]$ and $S_2[k]$ are the DFTs of the original S_1 and S_2 sequences (sampled at Nyquist rate); $R_1[k]$ and $R_2[k]$ are the DFTs of the received Golay sequences S_1 and S_2 at the receiver; and $W[k]$ is the noise spectral density. The noise is further assumed to be Gaussian distributed with zero mean. For application using low-bandwidth receivers, the effect of PMD is small and negligible while CD is an all-pass filter with quadratic phase response in frequency domain and thus does not have effect on complimentary property of Golay codes, which utilise power spectrum. Neglecting the effect of linear impairments, Golay property of the received TSs on the X-polarisation can be expressed as:

$$G[k] = |R_1[k]|^2 + |R_2[k]|^2 = |S_1[k]|^2 + |S_2[k]|^2 + 2|W[k]|^2 + 2\,\mathrm{Re}\left(S_1[k]^* W[k]\right) + 2\,\mathrm{Re}\left(S_2[k]^* W[k]\right) \tag{6.3}$$

where $W[k]$ is the spectral noise density and Re(.) denotes the real part of (.). A similar expression of Equation 6.3 can be derived for signal on the Y-polarisation and has been omitted for clarity purpose. The mean of Equation 6.3 can be expressed as:

$$E\{G[k]\} = E\left\{|S_1[k]|^2 + |S_2[k]|^2\right\} + E\left\{2|W[k]|^2\right\} + E\left\{2\,\mathrm{Re}\left(S_1[k]^* W[k]\right) + 2\,\mathrm{Re}\left(S_2[k]^* W[k]\right)\right\} \tag{6.4}$$

where E{.} indicates the expected value of {.}. Assuming the noise is Gaussian white noise with a mean of zero, Equation 6.4 can be rewritten as:

$$E\{G[k]\} = |S_1|^2 + |S_2|^2 + |W|^2 = 2P_{signal} + 2P_{noise} \tag{6.5}$$

where P_{signal} is the signals' power and P_{noise} denotes the noise power. In theory, the SNR can then be calculated from Equation 6.5. However, as the signal is not fully equalised, the use of Equation 6.5 requires precise estimation of the mean signal power P_{signal} of the captured TSs without any noise component. As estimation of P_{noise} depends on estimation of P_{signal}, error in estimation of P_{signal} will cause large degradation in OSNR estimation performance. In practical coherent receivers, the signal power P_{signal} needs to be estimated and error in estimation of P_{signal} will lead to degradation in SNR estimation performance using Equation 6.5. Thus, instead of estimation of SNR from the mean value, the proposed SNR estimation technique is based on the variance of Equation 6.3. It is noted that the variance of Equation 6.3 can be expressed as:

$$V\{G[k]\} = \left|2\,\mathrm{Re}\left\{(S1 + S2)^* W\right\}\right| \tag{6.6}$$

where V{.} denotes the variance of {,}, |(.)| denotes the absolute value of (.) and (.)* denotes the complex conjugate of (.). Equation 6.6 reduces to zero in the case of no added noise and increases with the noise power and thus can be used for SNR estimation of the signal. Figure 6.2 shows an example in simulation for Equation 6.6 with two different OSNR values using 256-symbol Golay sequences and it can be seen that the change in OSNR value (and hence the change in SNR value) causes changes in

the variation of TS signal spectrum $G[k]$. Thus it is possible to estimate SNR using the TS signal spectrum $G[k]$.

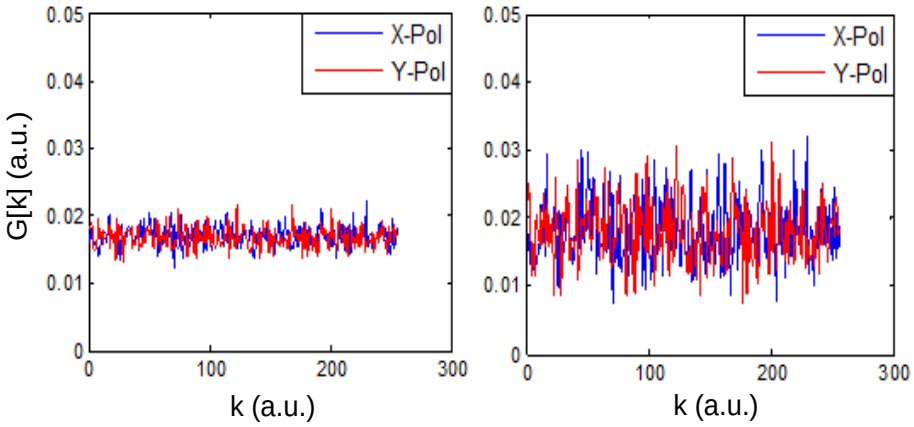

(a) *(b)*

Figure 6.2: Frequency spectrum G[k] of Golay pair on both polarisations with (a) OSNR = 22 dB and (b) OSNR = 12dB.

While it is difficult to solve for SNR from Equation 6.6 analytically, SNR can be estimated from signal spectrum variance by first simulating the spectrum variance for a wide range of SNR values. The results are stored as a pre-defined look-up table for relating signal SNR to the variance of $G[k]$. From Equation 6.6 it can be seen that the increase in signal variance is approximately proportional to the square root of the noise power. To take into account different signal amplitudes captured by the receiver, as well as the inverse relationship between spectrum variance and signals' SNR, the logarithmic variance to mean ratio (VMR_{dB}) can be defined as:

$$VMR_{dB} = -20\log_{10}\left(\frac{V\{G[k]\}}{E\{G[k]\}}\right) \tag{6.7}$$

Figure 6.3 shows the estimated VMR_{dB} as a function of SNR. A relationship between signals' spectrum variance and SNR can be seen. For coherent receivers, as only the signal SNR can be estimated, the calibration line for VMR_{dB} with respect to SNR is calculated using simulation. The results in Figure 6.3 are used as a calibration table for translating from VMR_{dB} to signals' SNR. The system SNR value is then estimated by calculating the variance of the received signal spectrum and then utilising the pre-

defined results for SNR estimation. Finally the OSNR is calculated from the SNR by first measuring the back-to-back SNR value without any extra ASE noise and taking the noise reference bandwidth into account by using the method proposed in [10]-[12].

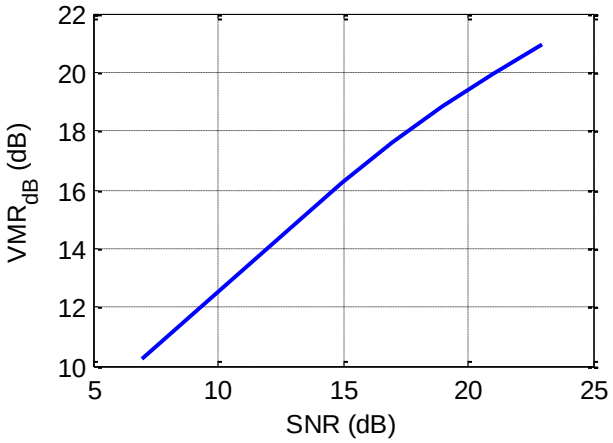

Figure 6.3: VMR_{dB} as a function of signals' SNR.

6.3 Simulation Analysis

Section 6.2 outlined the theory and implementation of the proposed OSNR estimation technique for coherent receivers with low bandwidth and low sampling speed. Since the technique relies on filtered TS signal spectrum, it is desirable to investigate tolerance of the proposed technique with respect to different channel impairments. Estimation performances with different channel impairments are investigated in the next section using computer simulation.

6.3.1 Implementation Using Low-Bandwidth Coherent Receiver

Since the proposed technique utilises spectral property in frequency domain, for SNR estimation using a low sampling speed and low-bandwidth receiver, the SNR is estimated using the estimated spectral components within the receiver's bandwidth. The sampling speed only needs to be approximately twice the bandwidth of the low-speed receiver used for SNR estimation. Figure 6.4 shows an example of a TS spectrum of 10-Gbaud signal filtered by 800-MHz filter and sampled at 2.5 GHz with OSNR = 22 dB in simulation. The spectral components in the right-most region (beyond 800 MHz) are

affected by the filters while the spectral components in the left-most region are affected by the carrier laser peak and laser linewidth. After removing spectral components in these two regions, SNR can be estimated by utilising the remaining spectral components within the monitoring region. The amount of spectral components that fit inside the receiver's bandwidth can be calculated as:

$$N_{spc} = \left\lfloor N_{ts} \frac{B_{rec}}{B_{sys}} \right\rfloor - N_{rmv} \tag{6.8}$$

where N_{spc} is the number of spectral components used for OSNR estimation, N_{ts} is the length of the TS, N_{rmv} = 4 to account for spectral components affected by filters and carrier, B_{rec} is the receiver's bandwidth and B_{sys} is the original's system baud rate. For estimation of OSNR, a minimum of 2 spectral components must remain after removal of other components for reliable calculation of spectrum variance, resulting in a minimum required receiver's bandwidth of 500 MHz for 10-Gbaud system with N_{ts} = 128.

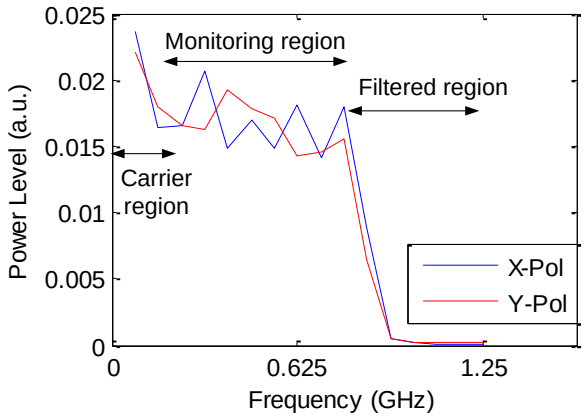

Figure 6.4: Simulated TS frequency spectrum of captured signal and OSNR monitoring region with 800-MHz filter and 2.5-GHz sampling speed.

6.3.2 Frame Synchronisation

Since the proposed technique relies on capturing the TSs for SNR estimation, frame synchronisation is necessary to locate the TS from the captured signal. As the captured signals are filtered using electrical low-pass filters (LPFs) and sampled at low speed, adaptation to full speed frame synchronisation algorithm is needed to locate the filtered

TS. A low-speed version of the sampled autocorrelation algorithm for frame synchronisation is utilised. Frame synchronisation is performed to extract the TSs by first creating a filtered and down-sampled synchronisation header. This is achieved by passing the S_1 sequence (the first sequence of the Golay pair) through a series of digital filters in MATLAB and down-sampling the filtered sequence to match the signal sampling speed. The result is an approximated version of the S_1 sequence filtered by 800-MHz low-pass filter and sampled at 2.5 GS/s, which can be used for frame synchronisation using cross correlation as illustrated in Figure 6.5(a). Figure 6.5(b) shows the correlation index for frame synchronisation using the frame synchronisation method described in Figure 6.5(a) and it can be seen that a synchronisation peak indicating the location of the TS can be observed. Thus by using a filtered sequence, the sequence location in the received signal can be located by the peak in the correlation index.

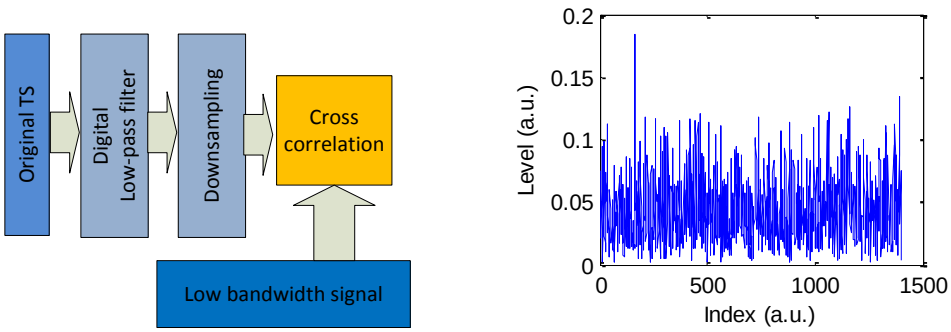

(a) *(b)*

Figure 6.5: (a) Low bandwidth implementation of frame synchronisation and (b) frame synchronisation correlation index.

Since frame synchronisation utilises a low bandwidth version of the sampled autocorrelation algorithm, it can be expected that CD will have an effect on the performance of frame synchronisation in a low-bandwidth receiver. However, as the received signals are low-pass filtered and down-sampled, the effect of CD will be much less significant compared to the case of full-speed signal as illustrated in Chapter 5. The effect of CD and other impairments will be investigated in the next section.

6.3.3 Modulation Formats

For future CO networks, utilisation of higher-order modulation formats will be necessary to achieve better spectral efficiency. The use of DA-CE typically will simplify transition to higher modulation format as a single DSP structure can be used for all types of data modulation. For higher modulation format such as PM-16QAM and PM 64-quadrature amplitude modulation (PM-64QAM), the signal constellation needs to be scaled down to match the range of the digital to analogue converter (DAC). Thus, it is advantageous to utilise QPSK TSs for all square modulation formats (PM-QPSK, PM-16QAM and PM-64QAM) and modulate the TSs using the outer most points of the constellation. While this approach will maximize the TS to noise ratio, the TSs will have significantly more power than the remaining data in case of PM-16QAM and PM-64QAM leading to inaccuracies in OSNR estimation using TSs. In order to utilise TSs for OSNR estimation in higher-order modulation formats, the OSNR estimated from the TSs need to be scaled using a modulation-format dependent scaling factor *k*, similar to the principle of error vector magnitude (EVM) [17]. After estimation of signal SNR using TSs, the modulation format corrections can be applied as:

$$OSNR_{mQAM} = OSNR_{ts} - 10\log_{10}(k) \tag{6.9}$$

where $OSNR_{mQAM}$ denotes the corrected values, $OSNR_{ts}$ denotes estimated OSNR using the TSs. The values of k are k = 1, 9/5, 7/3 for PM-QPSK, PM-16QAM and PM-64QAM, respectively [17]. Using k enables the use of a single type of TSs for different modulation formats. Figure 6.6(a) shows the estimated OSNR values versus true OSNR for different modulation formats using the QPSK Golay sequences. It can be seen that different modulation formats exhibit different results due to the TSs being QPSK. Figure 6.6(b) shows the corrected results when applying the scaling factor and it can be seen that estimation is accurate with all modulation formats. It is also noted that scaling using k is only needed when the TSs are QPSK Golay sequences. In the case of using 16QAM Golay sequences as described in Chapter 4, scaling using k is not necessary as the sequences are already in 16QAM format.

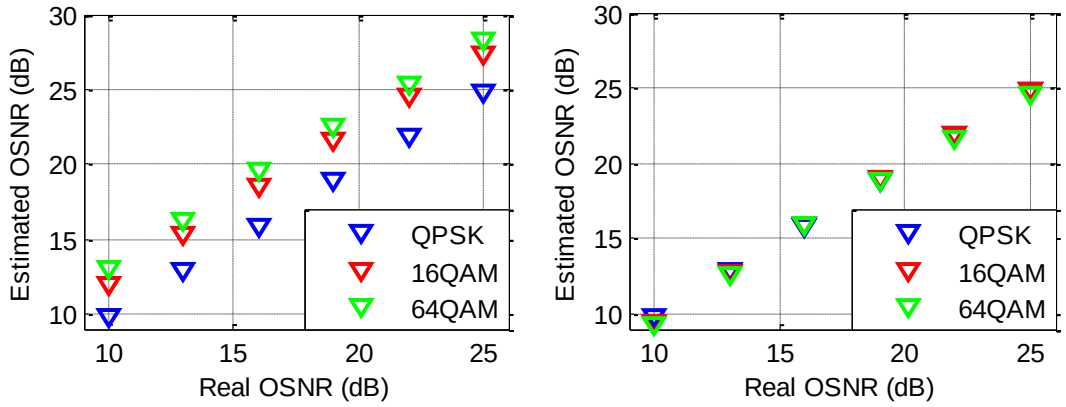

Figure 6.6: Estimated OSNR versus real OSNR for different modulation formats with (a) no correction and (b) modulation format correction.

6.3.4 Chromatic Dispersion

As described in Chapter 3, CD can be described as an all-pass filter with quadratic phase rotation in frequency domain. Since the proposed technique only relies on the complementary power spectrum property of the TSs in frequency domain, it can be seen that the technique is robust against CD as Equation 6.1 will not be affected by CD. However, this condition can only be achieved when the TS length N_{ts} and CP length N_{cp} is sufficiently large to cover the impulse response generated by CD. For practical implementation of DA-CE, the maximum values of N_{ts} and N_{cp} are limited in and thus some degradation is expected when a large amount of CD is accumulated.

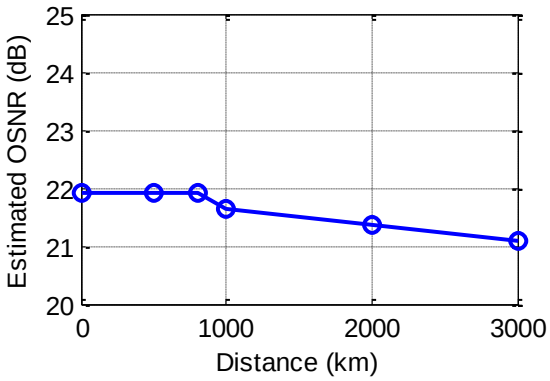

Figure 6.7: Estimated OSNR with respect to transmission distance assuming uncompensated CD for OSNR=22dB.

Figure 6.7 shows the estimated OSNR values at OSNR = 22dB with different amount of CD. It can be seen that when CD is within the tolerance limit then the estimation performance is not affected by CD. However for very large amount of CD the spectrum is distorted resulting in increasing estimation inaccuracy. This degradation is due to insufficient CP symbols that cannot guard the TSs from inter-block interference (IBI) similar to the case of CD estimation with small amount of CP symbols as presented in Chapter 3. For practical implementation of DA-CE when the lengths of TSs and CP blocks are limited, compensation of CD is therefore necessary to prevent degradation in performance due to the effect of very large CD causing IBI between TSs.

Furthermore, CD not only causes degradation in estimation performance due to IBI, but also causes degradation in frame synchronisation method that utilises autocorrelation as the symbols are polluted by CD. Figure 6.8 shows the correlation index of the frame synchronisation method described in Section 6.2.3 after 1000-km transmission with and without CD compensation for 10 Gbaud system with N_{ts} = 128. It can be seen that while only a large amount of CD affects the frequency spectrum, a medium amount of CD will cause the peak in frame synchronisation to become smaller and thus CD causes degradation in frame synchronisation. This effect is similar to the effect of CD on frame synchronisation method that utilises correlation as described in Chapter 5. However, it can be seen that due to the signal being filtered by LPFs the effect of CD is much less severe compared to the case of full bandwidth signal described in Chapter 5. After 1000-km transmission the TSs can still be detected using the timing peak with only a small degradation in peak amplitude. This is expected as CD is proportional to the square of system baud rate and the effect of CD on low-bandwidth signal is very minimal. For a large amount of accumulated CD, while it is necessary to compensate for parts of the accumulated CD to prevent degradation in both estimation performance and frame synchronisation, compensation does not need to be very accurate as the technique is robust against a moderate amount of residual CD. As demonstrated in Figure 6.7, up to 800 km of uncompensated transmission can be tolerated without any degradation in estimation performance.

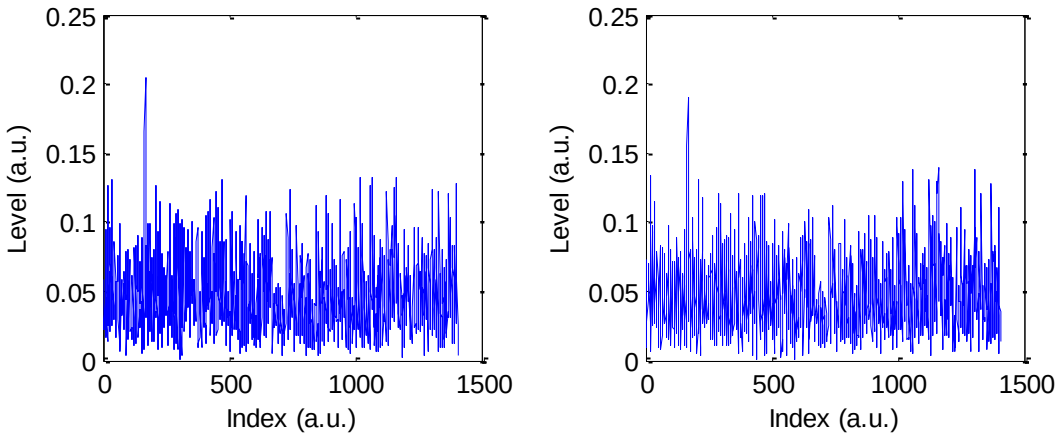

(a) *(b)*

Figure 6.8: Frame synchronisation index using low-bandwidth implementation after 1000-km transmission with (a) CD compensation and (b) no CD compensation.

6.3.5 Polarisation-Mode Dispersion

PMD, characterized by differential group delay (DGD), induces penalty to optical signal by creating a time shift between the two polarisation components of the signal. It is therefore necessary to investigate the effect of PMD on the proposed OSNR estimation technique. Simulations are also carried out to investigate estimation performance with respect to PMD using first-order PMD emulator. Figure 6.9 shows the variance of the frequency spectrum with respect to different DGD values for an OSNR value of 22 dB and a range of DGD from 0 to 120 ps. The LPF bandwidth is set to 800 MHz and the TSs are captured 16 times for OSNR estimation. The estimated value with no DGD (DGD = 0) is set as a calibration point for estimation error measurement and the OSNR estimation error is measured with respect to DGD. It can be seen that, at very high DGD only a very small degradation of approximately 0.05 dB is observed. Similar to the case with CD, PMD is an impairment that scales with the signal bandwidth and will have very small effect on low-bandwidth signals. As the technique utilises a receiver with low bandwidth and low sampling speed, the effect of DGD is expected to be minimal as described in [18]. Therefore it can be concluded that estimation is robust against PMD.

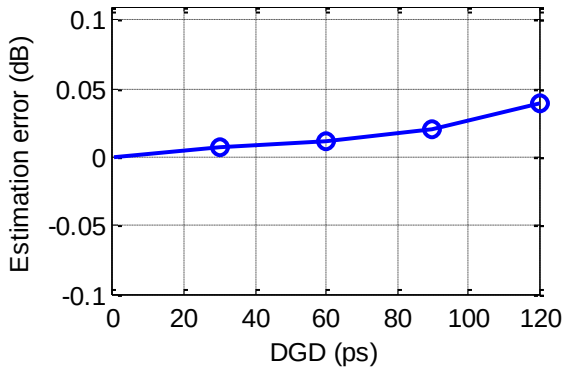

Figure 6.9: Estimation error with DGD.

6.3.6 Polarisation Rotation

Since the proposed technique only relies on the complementary property of the TSs, polarisation rotation could have a detrimental effect on estimation performance. Furthermore, as the TSs are filtered using LPFs and sampled with low sampling speed, blind techniques that can compensate for polarisation rotation is not possible for signal captured with low-bandwidth receiver without some modifications to the techniques. It is therefore necessary to investigate the effect of polarisation rotation on the proposed technique.

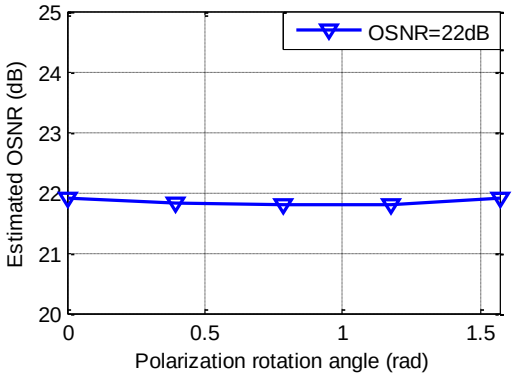

Figure 6.10: Estimated OSNR with different polarisation rotation for OSNR=22dB in simulation.

Figure 6.10 shows the estimated OSNR values for an emulated OSNR value of 22 dB with respect to different polarisation rotation angles in simulation using a polarisation

rotator. It can be seen that, for a wide range of polarisation rotation, the spectral property of Golay sequences can be maintained under different polarisation rotation angles with only a very small amount of distortion. Extra estimation error associated with polarisation rotation is calculated to be approximately 0.15 dB. While some extra penalty is associated with polarisation rotation as the signals are not compensated for this impairment, this penalty is normally small and thus SNR can be estimated without first compensating for polarisation rotation.

6.3.7 Polarisation-Dependent Loss

As presented in Chapter 4, polarisation dependent loss (PDL) causes the two polarisation signals to have different power. The effect of PDL can be modelled in simulation by using the model presented in [19]. PDL generally causes different OSNR values on the two polarisation tributaries and as such estimation of OSNR should reflect the differences caused by PDL.

The proposed OSNR estimation technique is tested against PDL in simulations with different PDL values. For each PDL value, OSNR on each polarisation signal is independently estimated and the resulting OSNR differences between two polarisations are calculated. Figure 6.11 shows the estimated OSNR difference between two polarisation signals and it can be seen that the difference is linearly related to PDL as expected. Performance of the proposed OSNR estimation technique with respect to PDL is similar to the full-bandwidth OSNR estimation technique presented in Chapter 4.

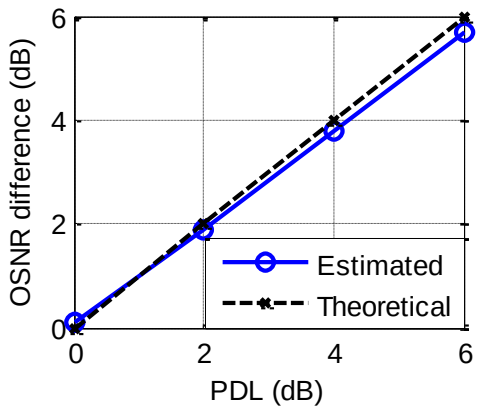

Figure 6.11: Estimation error with PDL.

6.4 EXPERIMENTAL DEMONSTRATION

6.4.1 Experimental Setup

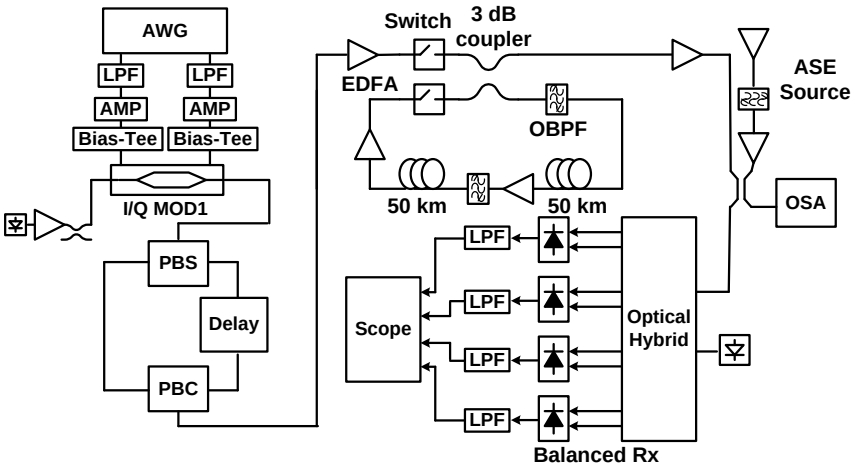

Figure 6.12: Experimental setup.

Figure 6.12 shows the experimental setup for OSNR estimation using a low-bandwidth coherent receiver for CO-SC with DA-CE systems. The TSs are 128-symbol long Golay sequences with 4-symbol CP blocks and the sequence constellations are designed to match the modulation format of the system. For simplicity, QPSK Golay sequences are utilised for PM-QPSK systems and 16-QAM Golay sequences for PM-16QAM systems. The full speed transmitter consists of one arbitrary waveform generator (AWG), low-pass filters (LPFs) and amplifiers (AMPs) to generate the data stream at 10 Gbaud, resulting in PM-QPSK and PM-16QAM system bit rates of 40 Gb/s and 80 Gb/s, respectively. A randomly generated data block is added to the TS block with a training-to-data ratio of 1:99 (1% overhead ratio). The optical signal is split by a polarisation beam splitter (PBS) and a delay line of 27.2 ns is used on one polarisation to emulate the Y-polarisation. The TS block is designed to match this delay line in order to emulate both polarisations of a CO-SC system. The signals on both polarisations are then combined into a single PM optical signal using polarisation beam combiner (PBC), then coupled into a recirculating loop with loop timing determining the total transmission length in order to emulate 1000-km standard single-mode fibre (SSMF) transmission for PM-QPSK systems and 400-km SSMF transmission for PM-16QAM systems. The loop

consists of two spans of 50-km fibre with matched Erbium-doped fibre amplifiers (EDFAs) and optical band-pass filters (OBPF).

At the receiver side, an amplified spontaneous emission (ASE) source consisting of two cascaded EDFAs and one optical band-pass filter is used to control the OSNR level. The optical signal is then split into two paths using a coupler with a ratio of 9:1. The 10% path is fed into an optical spectrum analyser (OSA) to independently measure the OSNR while the other path is fed into a balanced coherent receiver to detect the in phase and quadrature components of the signal. The low-bandwidth receiver is emulated with four 800 MHz electrical LPFs attached to the outputs of standard balanced receivers. The signal is then captured by a 4-channel real-time oscilloscope running at 2.5 GSamples/s for offline processing.

6.4.2 Measurements and Discussions

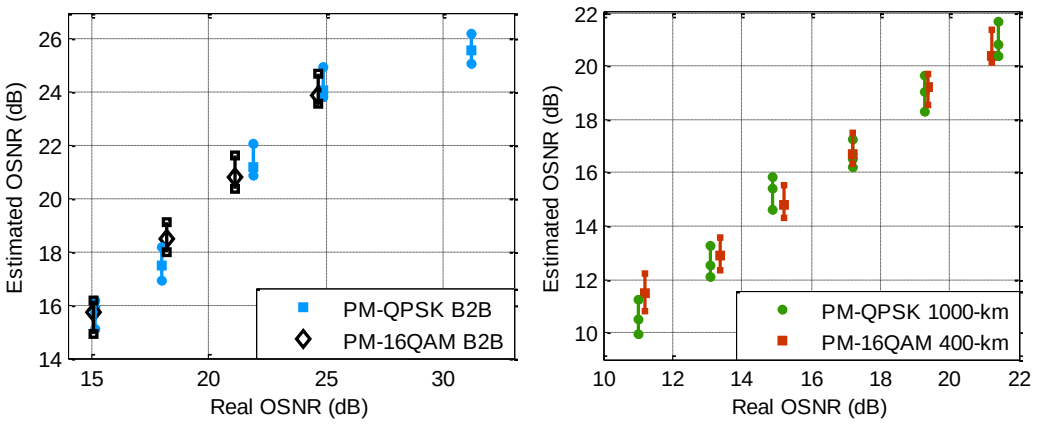

(a) *(b)*

Figure 6.13: Estimated OSNR vs. real OSNR in experiments with 800-MHz filters for (a) back-to-back and (b) after transmission.

Figure 6.13(a) shows the estimated OSNR values with respect to the real OSNR values measured by using the OSA for back-to-back (B2B) transmission in CO-SC systems using PM-QPSK and PM-16QAM modulation formats. The receiver's bandwidth is set at 800 MHz and the four electrical signals are captured at 2.5 GSamples/s. Each data point is an average of 30 captures with each capture consisting of 32 training frames and the maximum deviation in each measurement is plotted as error bars. It can be seen that

for a wide range of OSNR, estimation is accurate with all measurements within 1 dB for both PM-QPSK and PM-16QAM modulation formats. For back-to-back transmission case, high estimation error occurs at very high OSNR due to residual system noise as with most coherent receiver-based techniques [11]. Figure 6.13(b) shows the estimated OSNR values versus real OSNR values measured by the OSA after 1000-km PM-QPSK transmission and 400-km PM-16QAM using the recirculating loop with maximum deviations plotted as error bars and it can be seen that estimation is also accurate for both PM-QPSK and PM-16QAM modulation formats over a wide range of OSNR.

Figure 6.14 shows the root mean squared (RMS) estimation error of the estimated OSNR values with respect to the real OSNR values as a function of the required receiver's bandwidth for 1000-km PM-QPSK transmission. Each data point is also based on 30 captures and the effect of different receiver's bandwidths is emulated by increasing the monitoring region within the required bandwidth of a full bandwidth signal. It can be seen that there is only a slight increase in terms of performance of around 0.1 dB when the receiver's bandwidth increases as the estimator has more samples to work with. Overall it can be concluded that the estimation using low-speed receivers is accurate with errors within 1 dB and is a suitable technique for CO-SC systems employing DA-CE.

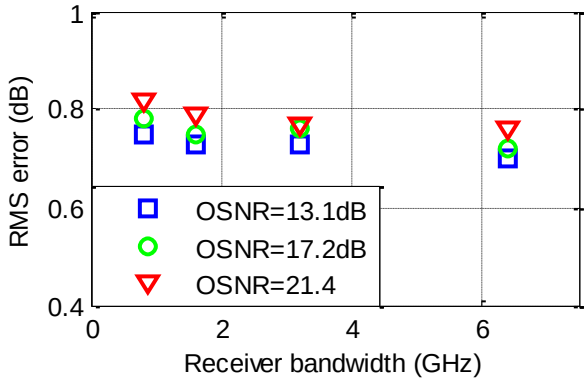

Figure 6.14: RMS estimation error for different receiver's bandwidths for 1000-km PM-QPSK transmission with different OSNR values.

6.5 CONCLUSIONS

This chapter presents an OSNR estimation technique using low-bandwidth receivers with low sampling speed for CO-SC employing DA-CE. By utilising the TSs inserted for CE and capturing these TSs using a low-bandwidth coherent receiver with low sampling speed, SNR can be predicted. Compared to techniques based on full-speed receivers as demonstrated in Chapter 4, the proposed technique has the advantage of being flexible on receiver bandwidth requirement and thus is suitable for reduced speed coherent receiver designed for monitoring purpose. Flexibility in receiver bandwidth requirement is achieved by monitoring the signal spectrum of the received TS instead of constellation of the equalised TSs, as in the case with full-bandwidth receivers. However, as the technique utilises TS spectrum for OSNR estimation purpose, this flexibility in receiver's bandwidth comes with the trade-off of not being compatible with CO-SC systems that utilise blind CE instead of DA-CE.

A small drawback of the proposed technique is the reduced number of samples used for OSNR estimation compared to the case of OSNR estimation using full-bandwidth receivers. Only the spectral components that fit into the monitoring bandwidth can be used for OSNR estimation purpose. In order to overcome the limitation of a reduced number of samples due to the reduced receiver's bandwidth, many frames need to be used before the correct value of SNR can be estimated or a longer core TS length is required. Thus in terms of update speed the proposed technique is slower compared to using full-speed receivers. As OSNR is a slow changing parameter, the slow update speed of the technique can be tolerated.

The technique is demonstrated in experiments, both for 40-Gb/s PM-QPSK and 80-Gb/s PM-16QAM systems, for estimation of a wide range of OSNRs with accuracies within 1 dB after up to 1000-km transmission. The technique is compatible with standard CO-SC systems employing DA-CE and is a promising component in designing future optical communication networks.

6.6 REFERENCES

[1] M. Kuschnerov, M. Chouayakh, K. Piyawanno, B. Spinnler, E. de Man, P. Kainzmaier, M. S. Alfiad, A. Napoli, and B. Lankl, "Data-aided versus blind single carrier coherent receivers," *IEEE Photonics Journal*, vol. 2, no. 3, pp.387-403, Jun. 2010.

[2] B. Spinnler, S. Calabro and M. Kuschnerov, "Pilot-Assisted Channel Estimation Methods for Coherent Receivers," *Optical Fibre Communication Conference OFC'2013*, paper OW4B.3, Anaheim, CA, USA, 2013.

[3] A. V. Tran, C. Zhu, C. C. Do, S. Chen, T. Anderson, D. Hewitt, and E. Skafidas, "8×40-Gb/s optical coherent pol-mux single carrier system with frequency domain equalisation and training sequences," *IEEE Photonics Technology Letters*, vol. 24, no. 11, pp. 885–887, Mar. 2012.

[4] Z. Chen, L. Yan, A. Yi, W. Pan, and B. Luo, "Simultaneous OSNR monitoring for two polarisation tributaries of a PDM signal using a polarisation-diversity nonlinear loop mirror based on FWM," *Journal of Lightwave Technology*, vol. 30, no. 14, pp. 2376-2381, Jul. 2012.

[5] R.Adams, M.Rochette, T.T.Ng, and B.J.Eggleton, "All optical in band OSNR monitoring at 40Gb/s using nonlinear optical loop mirror," *IEEE Photonics Technology Letters*, vol. 18, no. 3, pp. 469–471, Feb. 2006.

[6] M. Petersson, H. Sunnerud, B. Olsson, and M. Karlsson, "Optical performance monitoring using degree of polarisation in presence of polarisation-mode dispersion," *European Conference on Optical Communication ECOC'2004*, paper Tu3.6.2, Stockholm, Sweden, 2004.

[7] G. Lu and L. Chen, "Enhancing the monitoring sensitivity of DOP-based OSNR monitors in high OSNR region using off-centre narrow-band optical filtering," *Optics Express*, vol. 15, no. 3, pp. 823-828, Feb. 2007.

[8] F. Pittala, F. N. Hauske, Y. Ye, N. G. Gonzalez, and I. T. Monroy, "Joint PDL and in-band OSNR monitoring supported by data-aided channel estimation," *Optical Fibre Communication Conference OFC'2012*, paper OW4G, Los Angeles, CA, USA, 2012.

[9] M. S. Faruk, Y. Mori, and K. Kikuchi, "In-Band Estimation of Optical Signal-to-Noise Ratio from Equalised Signals in Digital Coherent Receivers," *IEEE Photonics Journal*, vol. 6, no. 1, pp. 7800109, Feb. 2014.

[10] D. J. Ives, B. C. Thomasen, R. Maher, and S. Savory, "Estimating OSNR of equalised QPSK signals," *European Conference on Optical Communication ECOC'2011*, paper OThH5, Geneva, Switzerland, 2011.

[11] Zhu, A. V. Tran, S. Chen, L. Du, C. Do, T. Anderson, A. Lowery, and E. Skafidas, "Statistical moments-based OSNR monitoring for coherent optical systems," *Optics Express*, vol. 20, no. 16, pp. 17711-17721, Jul. 2012.

[12] M. S. Faruk and K. Kikuchi, "Monitoring of optical signal-to-noise ratio using statistical moments of adaptive-equaliser output in coherent optical receivers," *Opto-Electronics and Communications Conference OECC'2011*, pp. 233–234 , Kaosiung, China, 2011.

[13] A Schmitt, "The Fast Approaching 100G Era," *Infonetics Research*, 2011.

[14] C. Do, C. Zhu, and A.V. Tran, "Data-Aided OSNR estimation using low bandwidth receiver," *IEEE Photonics Technology Letters*, vol. 26, no. 13, pp. 1291-1294, Mar. 2014.

[15] S. Chen, T. Anderson, D. Hewitt, A. V. Tran, C. Zhu, L. B. Du, A. J. Lowery, and E. Skafidas, "Optical performance monitoring for OFDM using low bandwidth coherent receivers," *Optics Express*, vol. 20, no. 27, pp. 28724-28733, Dec. 2012.

[16] J. Li, C. Zhao, S. Zhang, F. Zhang, and Z. Chen, "Experimental Demonstration of 120-Gb/s PDM CO-SCFDE Transmission Over 317-km SSMF," *IEEE Photonics Technology Letters*, vol. 22, no. 24, pp. 1814-1816, Dec. 2010.

[17] R. Schmogrow, B. Nebendahl, M. Winter, A. Josten, D. Hillerkuss, S. Koenig, J. Meyer, M. Dreschmann, M. Huebner, C. Koos, J. Becker, W. Freude, and J. Leuthold, "Error Vector Magnitude as a Performance Measure for Advanced Modulation Formats," *IEEE Photonics Technology Letters*, vol. 24, no. 1, pp. 61-63, Jan. 2012.

[18] C. K. Chan, *Optical Performance Monitoring*, Section 2.3, pp. 26-41, Academic Press, 2010.

[19] T. Duthel, C.R.S. Fludger, J. Geyer, and C. Schulien, 'Impact of Polarisation Dependent Loss on Coherent POLMUX-NRZ-DQPSK" *Optical Fibre Communication Conference OFC'2008*, paper OThU5, San Diego, CA, USA, 2008.

7 DGD Estimation Using Low-Bandwidth Coherent Receivers

7.1 INTRODUCTION

In Chapter 2, a review on channel estimation (CE) techniques for coherent optical (CO) system was presented. For CO single carrier (SC) systems with frequency domain equalisation (FDE), when the signals are captured using full-bandwidth receivers, CE and optical performance monitoring (OPM) can be performed using either blind or data-aided (DA) techniques. For low-bandwidth receivers, most techniques based on blind estimation will not work for CO-SC systems because the signal constellation data figure frame cannot be reconstructed and the spectrum of data signal is typically very noisy. For CO orthogonal frequency division multiplexing (OFDM) systems, however, blind estimation technique is an attractive choice for low-bandwidth receiver applications as some of the subcarriers can be fully preserved within the monitoring bandwidth. In theory, this could enable OPM in a totally blind manner without any extra training sequences (TSs) when CO-OFDM format is utilised with a low-bandwidth receiver. For optical transmission systems with bit rate of 40 Gb/s and beyond, polarisation-mode dispersion (PMD), normally characterised by the differential group delay (DGD), has become a detrimental impact on their speed and performance. Therefore, it is desirable to achieve a cost-effective estimation scheme that can monitor this impairment in order to provide guaranteed service quality, as well as fast reaction for performance degradation [1]-[2]. Several DGD estimation techniques have been proposed for CO-SC systems, including schemes based on measurement of minimum degree of polarisation (DOP) [3]-[4], eye diagram [5]-[6], radio frequency (RF) spectrum analysis [7]-[9], equaliser filter algebraic manipulation [10]-[13] and frequency-resolved state of polarisation (SOP) rotation [14]. On the other hand, research on DGD estimation for optical OFDM systems has not been widely studied. A few proposed schemes for DGD

estimation in CO-OFDM systems [15]-[16] also rely on the captured signal with full bandwidth for DGD estimation. For distributed monitoring of channel impairments, separate monitoring devices are normally preferred and as such estimation schemes that utilise reduced complexity hardwares are more desirable. As coherent receiver technology continues to mature, low-cost receivers with less than full sampling speed and low bandwidth will be made available and these make attractive choices for channel impairment monitoring purposes.

Toward the design of DGD estimation techniques for low-speed coherent receivers, CE using TSs, as designed for DA-CE, provides a solution that can be adapted for both CO-SC-FDE and CO-OFDM systems. Similar to the technique described in Chapter 6, it is possible to estimate the channel transfer functions within the monitor bandwidth using DA-CE and estimate DGD from these transfer functions. While the use of DA technologies can potentially bring the benefits of channel filter-based DGD estimation techniques to both CO-SC-FDE and CO-OFDM systems using low-bandwidth receivers, the use of reduced bandwidth coherent receiver would potentially make DGD estimation using TSs less accurate. While it is not possible to estimate DGD for CO-SC-FDE systems using reduced speed receivers without TSs, CO-OFDM systems possess different spectral characteristics that can be used for DGD estimation using low-bandwidth receivers. Thus it is also desirable to investigate DGD estimation techniques that take advantages of CO-OFDM system characteristics.

In this chapter, DGD estimation technique using TSs with different receiver bandwidths is investigated. Estimation accuracies with respect to receiver bandwidths and TS lengths are presented. A non-data-aided (NDA) DGD estimation scheme designed specifically for CO-OFDM systems is also presented. Compared to DA technique, the proposed NDA DGD estimation method loses compatibility with CO-SC-FDE systems, but gains slightly higher accuracy and improved bandwidth efficiency. The scheme is demonstrated through simulations and experiments to be able to accurately estimate DGD with estimation error of less than 2.5 ps in both back-to-back and after 1000-km standard single-mode fibre (SSMF) transmission.

7.2 DATA-AIDED DGD ESTIMATION

7.2.1 Data-Aided DGD Estimation Using Low-Bandwidth Receivers

Chapter 6 presented DA signal-to-noise ratio (SNR) estimation for low-bandwidth receivers using TSs. It can be seen that the same approach using TSs can be used for CE under low bandwidth and low sampling speed condition. Since DGD can be estimated from the channel transfer functions, in theory the use of TSs enables DGD estimation even when the signals are filtered and under-sampled. For DA-CE using low-bandwidth receivers, the training symbols are designed in time domain similar to the SNR estimation method presented in Chapter 6. Estimation of DGD using DA technique with low-bandwidth receivers is similar to the SNR estimation method presented in Chapter 6 with the only difference being the captured TSs are used for CE with the low-bandwidth receivers. After chromatic dispersion (CD) compensation and frame synchronisation, CE is performed by comparing the received signals to the original TSs using estimation method presented in Chapter 3. In order to adapt CE to low-bandwidth receivers, the original sequences are also passed through a digital low pass filter matched to the bandwidth of the actual receiver in order to obtain low-bandwidth original sequences for CE purpose. From the estimated channel transfer matrix, only the components contained within the receiver bandwidth are utilised. Since DGD can be estimated by measuring the central taps using the method discussed in [12] and these taps are preserved under low-bandwidth CE using TSs, DGD can be estimated using TSs for low-bandwidth receivers. Since DA DGD estimation method relies on extracting DGD information from estimated channel transfer function, it is trivial that the method is totally transparent to modulation formats and can be used for either CO-SC-FDE or CO-OFDM systems. Figure 7.1 shows an example of the phase response of one of the four channel transfer functions (the H_{xx} component) with TS core length N_{ts} = 2048 and receiver's bandwidth = 800 MHz with 2.5-GHz signal sampling speed. It can be seen that while the outer region is affected by the receiver's low pass filters (LPFs), the central region still contains channel information and can be used for DGD estimation purpose.

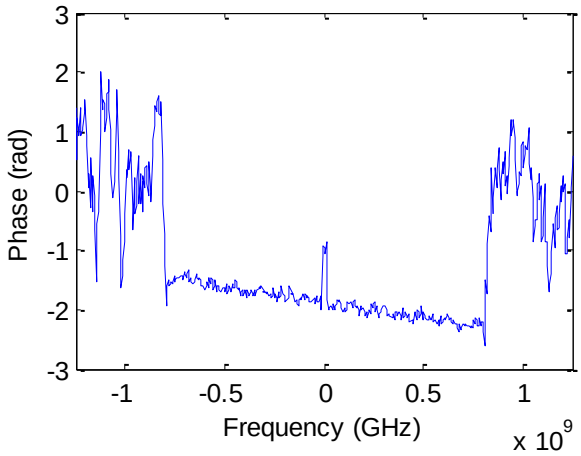

Figure 7.1: Estimated phase response of Hxx with N_{ts} =2048 and filter bandwidth = 800 MHz.

7.2.2 Simulation Results and Discussions

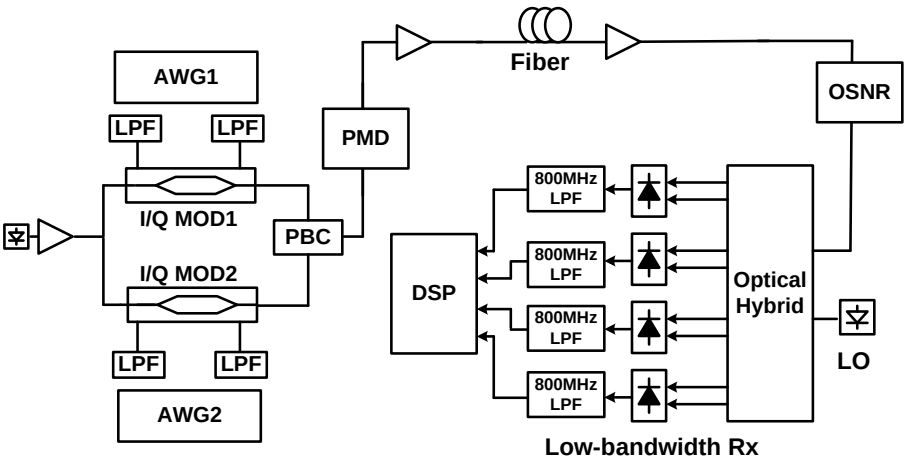

Figure 7.2: Simulation setup for DA DGD estimation with low-bandwidth receivers.

Figure 7.2 shows the simulation setup for DA DGD estimation using low-bandwidth coherent receivers. The transmitter consists of two 10 Gbaud Arbitrary Waveform Generators (AWGs) and optical I/Q modulators to generate the optical signal at rate of 10 Gbaud. In order to adapt DA-CE for low-bandwidth receivers, TSs with longer lengths are needed in order to provide enough resolution within the monitoring bandwidth for DGD estimation. Since the effective receiver bandwidth is reduced by almost 16 times, the TS length N_{ts} needs to be approximately 16 times that of the one

used in full-bandwidth receiver for good estimation accuracy. Thus the TSs are designed using space-time block code (STBC) scheduling as explained in Chapter 3 and the TS core length N_{ts} varies from 128 to 2048 symbols with CP length N_{cp} = 32 symbols. The TSs are inserted into a randomly generated data stream and modulation format is polarisation-multiplexed (PM) quadrature phase shift keying (QPSK) resulting in an effective bit rate of 40 Gb/s. The transmission line is emulated using SSMF with a dispersion parameter of 16.8 ps/nm.km and the transmission distance is set at 1000 km. At the receiver, a PMD emulator is inserted to generate a known amount of DGD with the DGD range set to 0-30 ps for estimation purpose. The optical signal is then filtered using LPFs with a bandwidth of 800 MHz and the sampling rate is reduced to 2.5 GHz. Data are then captured using a balanced coherent receiver and stored for offline processing using MATLAB.

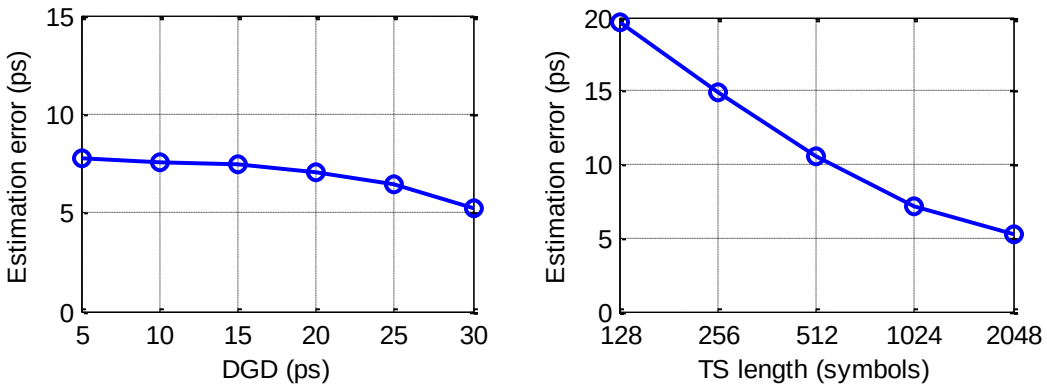

(a) *(b)*

Figure 7.3: Estimation error for DA DGD estimation using low-bandwidth receivers with (a) different DGD values and (b) different lengths of TS with DGD = 30 ps.

Figure 7.3(a) shows the estimation error for DA DGD estimation using a low-bandwidth coherent receiver with TS length N_{ts} = 2048 symbols with different DGD values. It can be seen that DGD can be estimated with moderate estimation error using DA-CE. Figure 7.3(b) shows estimation error as a function of the TS length used for CE for DGD = 30 ps and it can be seen that TSs with very long length are required for accurate estimation of DGD using DA-CE with low-bandwidth receivers. It can be concluded that while DGD estimation using DA-CE is possible even with low-bandwidth

receivers, the bandwidth requirements will pose practical issues for DGD estimation using DA-CE as the TS length needs to be very long in order to make up for the loss due to reduced receiver's bandwidths.

7.3 STOKES VECTOR BASED DGD ESTIMATION

Section 7.2 demonstrated DGD estimation using DA method with low-bandwidth receivers for CO systems. By employing a known training block, CE can be performed even when the signals are filtered with LPFs and DGD can be estimated from the channel transfer matrix. Since the method employs TSs for CE, it can be seen that the method works for both CO-SC-FDE and CO-OFDM systems. However, the primary drawback of DA method is the reduced resolution due to the reduced signal bandwidth and as such estimation error is relatively high if the TS lengths are to be kept reasonably short. Thus it is desirable to investigate alternative methods for DGD estimation using low-bandwidth receivers for CO systems. While it is difficult to develop such method for CO-SC-FDE systems due to the relatively noisy signal spectrum, the special multi-carriers structure of CO-OFDM systems make it possible to develop blind DGD estimation methods using reduced-speed coherent receivers. The NDA DGD estimation method for CO-OFDM systems based on Stokes vectors is presented in this section.

7.3.1 DGD-Induced SOP Rotation

Stokes vectors are three-dimensional (3D) representation of the optical signal electric field. By using Stokes vectors, optical signals on both the X- and Y-polarisations are combined to form a single array of 3D presentation in Stokes space. Thus, many polarisation demodulation schemes can be executed. In order to calculate Stokes vector from the captured data, conversion from Jones vectors to Stokes vectors is performed by applying the following set of equations [17]:

$$S = \begin{pmatrix} s_1 \\ s_2 \\ s_3 \end{pmatrix} = \frac{1}{s_0} \begin{pmatrix} |e_x|^2 - |e_y|^2 \\ 2\,\mathrm{Re}\{e_x^* e_y\} \\ 2\,\mathrm{Im}\{e_x^* e_y\} \end{pmatrix} \tag{7.1}$$

where e_x and e_y are the Jones vectors for the linear *X* and *Y* polarisation states after polarisation beam splitter (PBS); and the Stokes vector component $s_0 = |e_x|^2 + |e_y|^2$ represents the received signal power of two polarisations.

In CO-OFDM systems, due to the data being designed in frequency domain, Stokes vectors can be used to estimate different polarisation properties of the received signals and in turn relate these properties to different impairments for monitoring purposes. Stokes vectors were previously used for polarisation demultiplexing [18]-[20] or modulation format recognition [21]. However, here apply the Stokes vectors are directly applied for DGD estimation purpose. Plotting the Stokes vector on the Poincaré sphere provides a convenient means of characterising properties of OFDM subcarriers without the need for polarisation de-multiplexing and SNR estimation based on characterising single subcarrier's SOP had been demonstrated [22]. While SNR is a frequency independent impairment and estimation of this parameter can be performed on a single OFDM subcarrier with the result being the average result of multiple subcarriers, DGD is normally viewed as a function with respect to frequency. Because different OFDM subcarriers have different locations in the frequency spectrum, DGD will likely induce different changes to different OFDM subcarriers on the Stokes sphere. Thus, characterising this parameter using Stokes vectors will require the use of multiple subcarriers for estimation purpose. For coherent receivers with low sampling speed and low bandwidth requirement, the number of subcarriers used for DGD estimation will be based on the total receiver bandwidth. For DGD estimation using a low-bandwidth coherent receiver, the number of OFDM subcarriers used for DGD estimation can be calculated as:

$$N_{est} = \left\lfloor N_{total} \frac{B_{rec}}{B_{sys}} \right\rfloor \tag{7.2}$$

where N_{est} is the number of OFDM subcarriers used for DGD estimation, N_{total} is the total number of OFDM subcarriers, B_{sys} is the total OFDM system bandwidth, B_{rec} is the bandwidth of the receiver and $\lfloor (.) \rfloor$ denotes the floor function of (.).

As DGD is a function of frequency and is polarisation-dependent, it is expected that DGD will cause different SOPs on different subcarriers, which in turn lead to different

relative positions on the Stokes sphere. Therefore, instead of direct DGD measurement, the proposed DGD estimation scheme measures a slightly different quantity called DGD-induced SOP rotation. Due to the effect of DGD, different OFDM subcarriers will have different average state position on the Stokes sphere, and together the SOP position of these OFDM subcarriers will form DGD-induced traces. DGD-induced SOP rotation is the length of arc trace in Stokes space that is orthogonal to the SOP of the optical signal as shown in Figure 7.4.

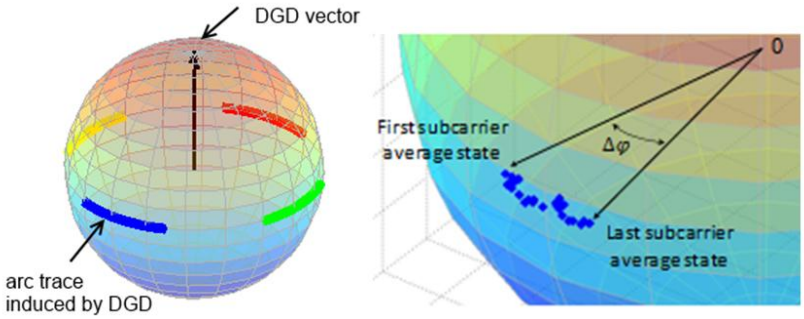

(a) *(b)*

Figure 7.4: Representation of (a) The DGD vector and DGD-induced arc trace on the Poincaré sphere and (b) Zoomed-in arc trace generated by relative position of OFDM subcarriers.

For OFDM systems with each subcarrier modulated in PM-QPSK modulation format, the Stokes vector of OFDM subcarriers generates four traces on the Stokes sphere as illustrated in Figure 7.4. It can be seen that due to DGD, the average state of each subcarrier is different depending on the position of the subcarrier in frequency domain. The first subcarrier average state is defined as the average state of the subcarrier, calculated using Equation 7.1, which is closest to the carrier frequency while the last subcarrier average state is defined as the average state of the furthest subcarrier that is still within the monitoring bandwidth. It is then possible to directly measure the relative position of subcarriers on the Stokes sphere, which is generated by the SOP rotation, in order to determine DGD, as shown in Figure 7.4(b) where each dot represents one average point of the OFDM subcarrier. The traces on the Poincaré sphere form four arcs and the angle between the first and the last subcarrier in each arc approximately represents a DGD-related value. The DGD value is first defined as:

$$\Delta\tau = \frac{\Delta\varphi}{2\pi\Delta f} \tag{7.3}$$

where $\Delta\tau$ is the estimated DGD value, $\Delta\varphi$ is the SOP rotation arc angle caused by DGD in radians between the first and the last subcarriers as illustrated in Figure 7.4(b), and Δf is the frequency span between the first and the last OFDM subcarriers.

Using Equation 7.3, it is possible to estimate DGD by measuring the angle between the first and last subcarrier on each of the four generated arcs and taking the average result for DGD estimation. However, it can be seen that all four traces on the Stokes sphere in Figure 7.4 will follow Equation 7.3 if the input and output DGD vectors are aligned as illustrated in Figure 7.4(a). As DGD is characterised by both input and output vectors and these two can have different positions on the Stokes sphere, further modifications to Equation 7.3 are required in case the input and output DGD vectors are not aligned. Compared to the simple case of having the same input and output DGD vector where all four arcs will be approximately the same length, in the case of different input and output DGD vectors, the four traces will have different lengths and are related by:

$$\Delta\omega = \cos^{-1}\frac{\Delta\varphi_1}{\Delta\varphi_2} \tag{7.4}$$

where $\Delta\omega$ is the angle between the input and output DGD vectors; $\Delta\varphi_1$ and $\Delta\varphi_2$ are the arc angles of the shortest arc and the longest arc respectively.

Figure 7.5 illustrates Equation 7.4 for different values of $\Delta\omega$ with $\Delta\tau$ = 30ps and OSNR = 22dB and it can be seen that the longest arc stays the same while the shortest arc depends on $\Delta\omega$. Thus, in case of different input and output DGD vector positions, DGD can be measured without interference from DGD vector position by utilising only the longest arc, since this arc only depends on the DGD value. While this approach seems to indicate some performance degradation due to the number of samples used for estimation reduced by four times, utilising all four traces is only possible with aligned DGD vectors. In such case, all four traces will be similar which gives similar performance compared to utilising only the longest trace. Thus, in all cases, it is advantageous to estimate DGD from only the longest SOP rotation trace without any performance degradation compared to utilising all four traces.

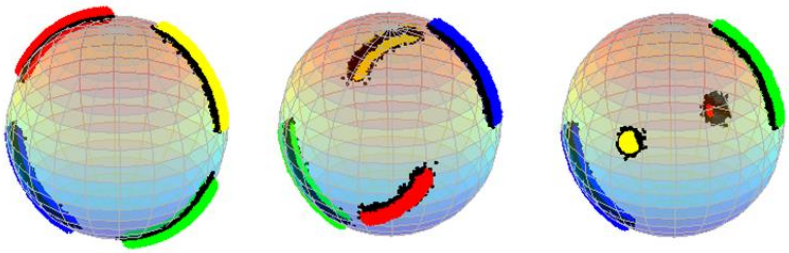

(a) (b) (c)

Figure 7.5: DGD induced SOP traces with (a) Δω=0, (b) Δω=45° and (c) Δω=90°.

7.3.2 Estimation Methods

In order to measure the DGD value from the calculated SOP traces on the Stokes sphere, the length of the traces need to be measured and DGD can be solved from these traces. This section presents two methods for measuring these trace lengths: the first method is by assuming a linear angle model and measuring the trace length by direct angle measurement, while the second method measures the trace length by linear interpolation in two-dimensional space. The merits and drawbacks of each method will be discussed.

7.3.2.1 Point-to-point Measurement

When a low-bandwidth coherent receiver is used, the arc traces in Figure 7.1 are short and mostly linear thus DGD can be estimated by measuring the angle between the first and last subcarriers within the monitoring bandwidth. DGD value can then be estimated from this angle by solving Equation 7.3. This approach is defined as point-to-point angle estimation. For receiver with higher bandwidth and first order DGD effect, the number of subcarriers used for DGD estimation increases, which results in longer SOP traces on the Stokes sphere. As the traces are linear, the DGD value can be solved regardless of the receiver bandwidth. Plus, in general, higher receiver bandwidth can be expected to give better estimation accuracy because the traces are longer which results in fewer errors in angle measurement. Figure 7.6 illustrates the SOP traces for QPSK-modulated PM-QPSK CO-OFDM systems with different receiver bandwidths. It can be seen that the higher the receiver bandwidth, the longer the traces on the Stokes sphere, which allows for easier and more accurate DGD estimation. When the effect of only

first order DGD is considered, direct angle measurement provides a simple method for DGD estimation and can be used for any receiver bandwidth with the expected outcome being that higher receiver bandwidth gives better estimation accuracy as a result of longer traces on the Stokes sphere.

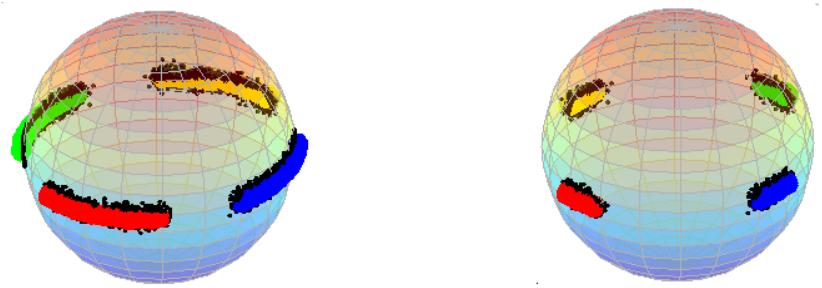

(a) *(b)*

Figure 7.6: SOP traces on Stokes sphere with (a) full bandwidth receiver and (b) low bandwidth receiver.

As the receiver bandwidth increases, the traces will be longer. While this allows for higher estimation accuracy, it also allows different trace shapes that could potentially impact the estimation accuracy of point-to-point estimation approach. For receiver with higher bandwidth, due to the increased number of subcarriers, it is possible to use interpolation to measure the arc length for more precise estimation. Interpolation is particularly more useful for higher bandwidth receivers since higher bandwidth receivers not only generate longer arcs but also suffer from second-order PMD (SOPMD). The effect of second order PMD is most prominent at subcarriers located at high frequency within the signal bandwidth and cause the subcarrier SOP to divert from a single linear line compared to first order DGD, which overall changes the shape of the DGD arc on the Stokes sphere. Figure 7.7 illustrates the effect of SOPMD on the DGD-induced SOP traces generated on the Stokes sphere. Full OFDM receiver bandwidth is used and thus all subcarriers are used for SOP estimation and DGD measurement. It can be seen that without SOPMD the traces will be linear; while with high amount of SOPMD, the traces start to bend at high frequency component resulting in different shapes of the traces. Since direct angle measurement assumes the traces are linear and

only measures the first and last subcarrier positions, this approach will result in degradation in estimation accuracy if the shapes of the traces are no longer linear.

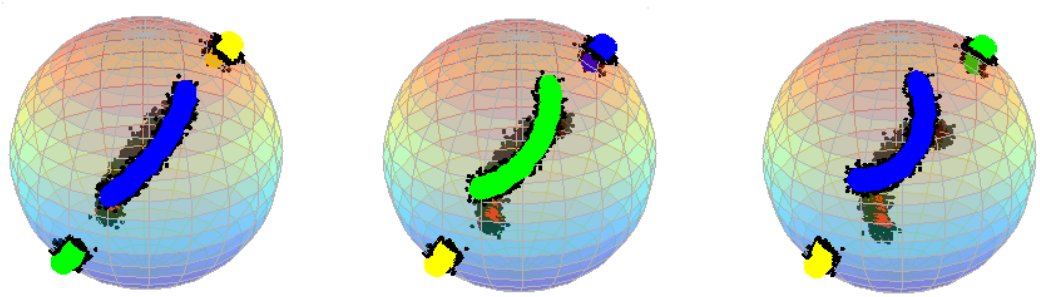

(a) *(b)* *(c)*

Figure 7.7: Second-order PMD effect on Stokes traces with (a) SOPMD = 456 ps^2, (b) SOPMD = 912 ps^2 and (c) SOPMD = 1368 ps^2.

7.3.2.2 Trace Length Interpolation

Since point-to-point estimation assumes the traces being linear, DGD under SOPMD cannot be measured using the angle between the first and last subcarrier as this would lead to incorrect estimation under high level of SOPMD. However, it can be seen from Figure 7.7 that while the trace shapes are different, the trace length stays approximately the same. Thus, it is still possible to measure the length of the SOP traces. Figure 7.8(a) shows the shape of the arc traces for SOPMD = 1368 ps^2 and DGD = 30 ps, and it can be seen that while the longest arc length stays the same, the arc is no longer linear under SOPMD as explained above. Due to the arc being on the surface of the sphere, a simple interpolation method to estimate the length of non-linear SOP traces can be used. By using Equation 7.1, it can be seen that the radius of the Stokes vectors is always a constant. The traces generated by Equation 7.1 are always on the surface of the sphere as a result of radius being constant. Therefore, these traces are only defined by two spherical coordinates namely elevation and rotation. Therefore, the trace length is estimated by first converting Stokes parameter from Cartesian to spherical coordinates and then eliminating the sphere radius parameter to convert the 3-dimensional traces into 2-dimensional plots characterised by rotation and elevation. The data points are then interpolated using least square algorithm and new traces are formed in the 2-dimensional space. DGD value is then measured by estimating the length of the new arc

using integration, and then converting this length to DGD value using the method previously described in Section 7.2.1. Figure 7.8(b) shows an illustration of the interpolation approach for DGD estimation with blue dots representing the actual data points for one trace and the red line representing interpolation of these data points. It can be seen that the arc length by interpolation is longer compared to point-to-point estimation. The new length measured by interpolation is approximately equal to the length of a linear DGD-induced arc in the case without SOPMD and can be used for DGD estimation. Thus, by using Cartesian to spherical conversion and interpolation in 2-dimensional space, accurate length of the traces can be estimated regardless of the trace shape.

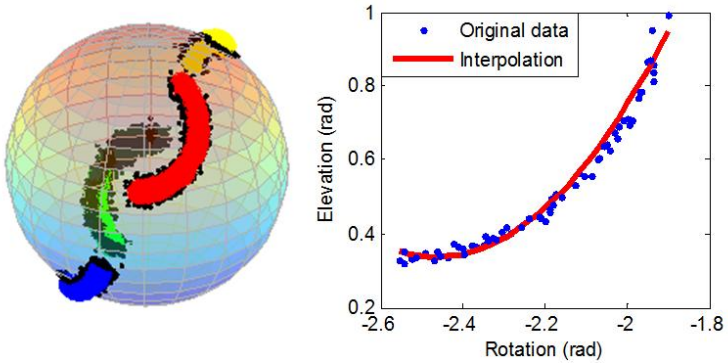

(a) *(b)*

Figure 7.8: (a) SOP traces with SOPMD = 1368 ps^2 and (b) Interpolation of longest trace in 2D plot.

Figure 7.9 shows the shape of the traces for SOPMD with different receiver bandwidth for DGD = 30 ps and SOPMD = 1368 ps^2. Since the traces are generated by calculating the average state of each subcarrier, the length of the traces and their shapes will greatly depend on the number of subcarriers within the receiver bandwidth since these are used for SOP calculation. It can be seen that with full receiver bandwidth then the traces are similar to the ones in Figure 7.7. However, as the receiver bandwidth is reduced then the traces became shorter and mostly reduced to a linear bar even at a very high level of SOPMD. This can be explained as SOPMD having the biggest impact on SOP of subcarriers at high frequency, resulting in the change in trace shapes, which only appear at higher frequency of the full speed signal. For low-bandwidth receivers, only the

subcarriers near the centre frequency are used, which effectively minimise the effect of SOPMD. Thus, for DGD estimation using receivers with low bandwidth and low sampling speed, under a wide DGD and SOPMD conditions it can be expected that interpolation and angle measurement will give similar performance.

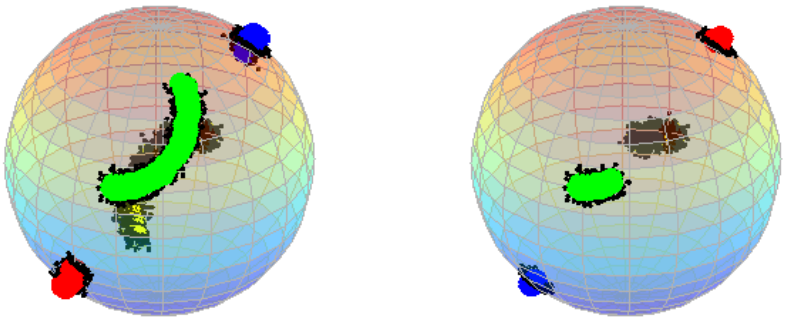

(a) *(b)*

Figure 7.9: SOPMD traces with (a) full-bandwidth receiver and (b) low-bandwidth receiver.

7.4 Simulation Demonstrations

Simulations are carried out in order to investigate the accuracy of the DGD estimation technique described in Section 7.3 for 40-Gb/s coherent OFDM optical systems. Both point-to-point estimation and interpolation methods are studied under different bandwidth requirement and different level of SOPMD. The same simulation setup, described in Section 7.4.1, is used for both methods as their differences only consist of the DSP algorithms. Section 7.4.2 investigates the estimation performance of the proposed DGD estimation techniques and discusses the merits as well as drawbacks of each implementation for NDA DGD estimation purposes.

7.4.1 Simulation Setup

Simulations are carried out using *VPI Transmission Maker 8.7* to evaluate performance of the proposed DGD estimation method for CO-OFDM systems using a setup similar to the one described in Figure 7.2. System baud rate is set to 10 Gbaud and modulation format is PM-QPSK resulting in effective bit rate of 40 Gb/s. Each OFDM frame

consists of 256 subcarriers with cyclic prefix (CP) blocks inserted to resist CD resulting in total OFDM frame of 272 symbols. A PMD emulator is inserted to generate a known amount of DGD with the DGD range set to 0-30 ps for estimation purpose. The transmission distance is emulated using SSMF with a dispersion parameter of 16.8 ps/nm.km and the transmission length is set at 1000 km. Data are then captured using balanced coherent receivers and stored for offline processing using MATLAB. As the proposed technique is designed for receiver with flexible bandwidth requirements, receiver bandwidth is emulated by capturing the OFDM signal in full bandwidth, then only the OFDM subcarriers within the required receiver bandwidth are used to estimate DGD using the method proposed in Section 7.3. Each subcarrier average state is calculated and converted to Stokes parameters using Equation 7.1. Since modulation format is PM-QPSK, SOP of each subcarrier forms 4 clusters on the Stokes sphere. These clusters are recognised by k-means algorithm and their central positions are used as the average state of each subcarrier for DGD estimation purpose.

7.4.2 Estimation Accuracy

The proposed DGD estimation method is verified in computer simulation for estimation accuracy over a wide range of DGD and receiver bandwidths. Performance of the proposed estimation method is measured in terms of root mean squared error (RMS) estimation accuracy. RMS estimation error is used to measure the error in DGD estimation in picoseconds (ps) as a function of actual DGD set by the PMD emulator. For each DGD value, each data point is measured 100 times to ensure estimation performance stability of the proposed method and the errors are calculated as:

$$Error_{rms} = \sqrt{E\left\{\left(DGD_{est} - DGD_{emu}\right)^2\right\}} \tag{7.5}$$

where $Error_{rms}$ denotes the RMS error of the estimation method at a single data point, DGD_{est} is the DGD value estimated using the proposed technique, DGD_{emu} is the actual DGD value sets by the PMD emulator and E{.} denotes the average value of {.} over multiple measurements.

Figure 7.10(a) shows the RMS estimation error for two values of DGD = 20 ps and DGD = 30 ps using first order PMD (DGD only) emulation. The fibre DGD parameter is set to zero to ensure that all DGD values generated are from the PMD emulator and

no extra DGD from the fibre is added. The transmission length is set at 1000-km transmission with a dispersion parameter of 16.8 ps/nm.km and both estimation schemes, direct angle measurement and line interpolation, are tested under different bandwidth requirements emulated by selecting the number of subcarriers that fall within the required monitoring bandwidth. Direct angle measurement calculates DGD values from the positions of the first and last subcarriers only while interpolation is set to linear least square fit to interpolate a straight line from the given data points. It can be seen that both methods perform very similarly to each other over a wide range of bandwidth requirement with a slight performance advantage of using interpolation method compared to point-to-point estimation method. However, this difference is very minimal. This behaviour is expected because first order PMD only contains DGD and the effect is a linear trace in Stokes space as described in Section 7.3. Thus, both direct angle measurement and line interpolation give similar performances. There is also a small trade-off between bandwidth requirement and estimation accuracy with higher bandwidth receivers giving better accuracy. This trade-off can be explained because higher bandwidth receivers use more OFDM subcarriers for estimation, resulting in longer traces on the sphere. This in turn results in a wider angle for better point-to-point estimation accuracy while interpolation method benefits from more number of samples for DGD estimation. However, it can be seen that for bandwidth as low as 800 MHz the estimation schemes are still very accurate with a maximum error of around 2.3 ps.

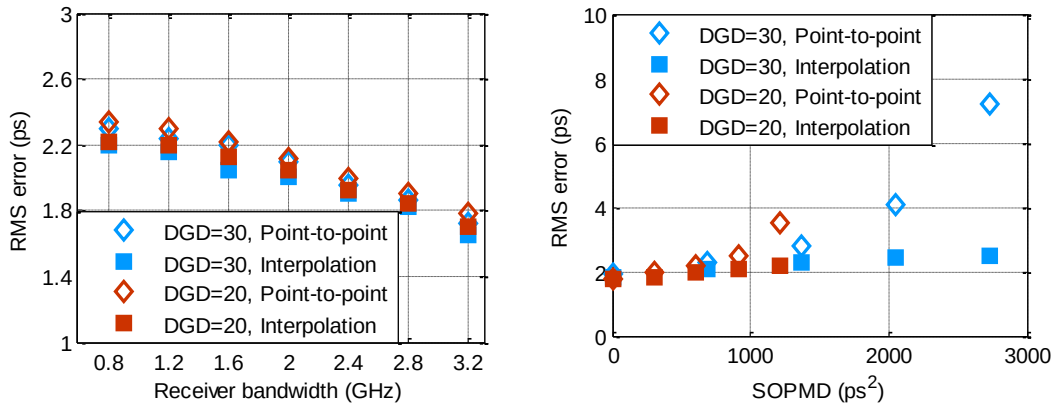

(a) *(b)*

Figure 7.10: Estimation error with (a) different receiver bandwidth and (b) different amount of SOPMD.

The proposed estimation scheme is tested using computer simulation for performance against SOPMD. Two DGD values of 20 ps and 30 ps are used. The Bruyere-Kogelnik model [23] is used for SOPMD generation which consists of polarisation state depolarisation (PSD) and polarisation-dependent chromatic dispersion (PCD). The total amount of SOPMD is calculated as a combination of these two parameters with a standard ratio of 3:7 as suggested by the model. SOPMD range of 0 - 2736 ps^2 and 0 - 1216 ps^2 was chosen for DGD = 30 ps and DGD = 20 ps, respectively. Due to the inclusion of SOPMD, interpolation parameters were set to second order in order to interpolate the data points as a quadratic function. The assumption of the trace being quadratic is valid in general for SOPMD models with a medium to high amount of SOPMD because these models are very similar to the Bruyere-Kogelnik model, which generates quadratic phase response in frequency domain transfer function. Figure 7.10(b) shows the RMS estimation error with different levels of SOPMD after 1000-km transmission using the PMD emulator with SOPMD. It can be seen that under a larger amount of SOPMD, interpolation method is able to estimate DGD with higher accuracy compared to point-to-point angle estimation. This is expected since the traces are no longer linear and point-to-point method suffers degradation as a result. However, this difference can only be observed under high-bandwidth receivers as the traces are long with different shapes. For low-bandwidth receivers, however, the difference between interpolation and point-to-point methods is very minimal even in the case of SOPMD, because the traces are short and mostly linear. In general, interpolation is a superior method compared to direct angle measurement. However, the advantage of interpolation can only be observed under high-bandwidth receivers and the method comes with a trade-off of more complexity. As point-to-point angle measurement has lower complexity, and it should be the method of choice for low-bandwidth monitoring devices while higher bandwidth receivers can use interpolation for more precise estimation.

7.5 EXPERIMENTAL DEMONSTRATIONS

The proposed DGD estimation scheme is demonstrated through experiments in order to verify its performance and consistency with simulation results. Both interpolation and point-to-point estimation methods are tested under different emulated amount of DGD. Section 7.5.1 describes the experimental setup for low-bandwidth receiver DGD

measurement in CO-OFDM systems. The scheme is first tested under a low-bandwidth receiver with low sampling speed in order to verify the validity of the proposed methods. Experimental results and discussion of low-bandwidth DGD estimation for OFDM system are presented in Section 7.5.2. Section 7.5.3 describes the experimental results of the proposed methods for different bandwidth requirements with results for both interpolation and point-to-point estimation presented.

7.5.1 Experimental Setup

Figure 7.11 shows the experimental setup for flexible bandwidth sampling NDA DGD estimation. Randomly generated data bit stream is mapped using PM-QPSK modulation format in frequency domain and then converted to time-domain by the inverse fast Fourier transform (IFFT) operation. The IFFT size is 256 and each consists of 256 subcarriers. Guard intervals are inserted to resist CD and the guard interval length is set to 16 symbols. The total length of OFDM symbol with guard interval is 272 symbols. This length of the guard interval and OFDM symbol is chosen to match the delay time (27.2 ns) of the polarisation multiplexing emulator. The time-domain OFDM signal is uploaded onto an AWG, which produces the analogue signals at 10 Gsymbols/s, resulting in each symbol having a length of 100 ps. The total length of the OFDM symbol with guard interval at 10 Gsymbol/s is therefore 27.2 ns. An optical I/Q modulator directly modulates the OFDM baseband electrical signals to the optical domain in order to form a single-polarisation OFDM signal. The single-polarisation optical OFDM signal from the modulator is evenly split into two polarisation branches through a polarisation-beam splitter (PBS). One branch of this signal is fed to a delay line with delay time tuned to 27.2 ns which is equivalent to one OFDM symbol period. A variable delay line is used in the delayed branch to finely tune the delay accurately equal to one OFDM frame period. The two polarisation branches are subsequently combined by a polarisation-beam combiner (PBC), emulating two independent transmitters on X and Y polarisations with a combined raw data rate of 40 Gb/s. The signal is then coupled into a recirculation loop to emulate transmission distance. The loop consists of 100-km fibre transmission with matched amplifiers and loop timing can be used to achieve a required transmission distance. The transmission distance inside the loop is set to 1000 km which consists of setting the loop timing to 10 times of 100 km. For back-to-back transmission, the signal from PBC is directly connected to the

receiver to emulate back-to-back transmission.

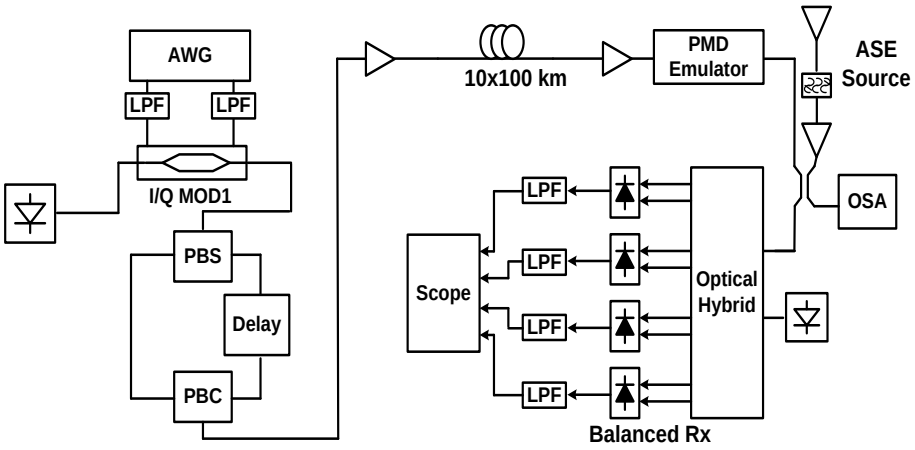

Figure 7.11: Experimental setup.

At the receiver side, an amplified spontaneous emission (ASE) source consisting of two cascaded Erbium-doped fibre amplifiers (EDFAs) and one optical band-pass filter is used to control the optical signal-to-noise ratio (OSNR) level. The ASE-injected signal is then split into two paths using a simple coupler with one path fed to the optical spectrum analyser (OSA) for the measurement of OSNR and the other path fed into the balanced coherent receiver. A PMD emulator (model Fibrepro PE4200) is used to add DGD to the OFDM signal and the control range is from 0 to 30 ps. Four balanced receivers are used to detect the in-phase and quadrature components of the received OFDM signal before sending this signal into a sampling scope. The low-bandwidth receiver is emulated with four 0.8-GHz low-pass electrical filters attached to the outputs of 15-GHz balanced receivers, while full-bandwidth receiver uses four 3.3-GHz low-pass electrical filters. The signals are then captured by a 4-channel real-time oscilloscope with sampling rate depending on the type of filter attached. For low-bandwidth (0.8 GHz) receiver, sampling rate is set at 2.5 GHz while full-bandwidth receiver utilises a sampling rate of 10 GHz. After signal's low pass filtering and sampling, captured data from scope are stored for offline processing using MATLAB.

7.5.2 Low-Bandwidth Receiver Demonstration

Since the coherent receiver used for experiments does not utilise a phase locked loop for frequency synchronisation between the incoming signal and the LO, carrier frequency

offset (FO) compensation is essential to eliminate the inter-subcarrier interference for data processing FFT. As a NDA DGD estimation scheme, this compensation is performed without TSs. The captured OFDM signal is converted to frequency-domain, then the FO between DC and signal carrier is measured and compensated. Frame synchronisation is performed by calculating the Stokes parameters scattering with respect to different frame offset [22] as described in Figure 7.12. For each captured data, an FFT window is slided across different offset values and at each value the Stokes vectors are calculated and the scattering of Stokes parameters is estimated. When the offset value is aligned with the OFDM frame then the scattering on Stokes sphere is minimized. The bottom half of Figure 7.12 shows a zoomed-in period of the frame synchronisation plot, the scattering on Stokes sphere is minimized when the correct offset value is reached.

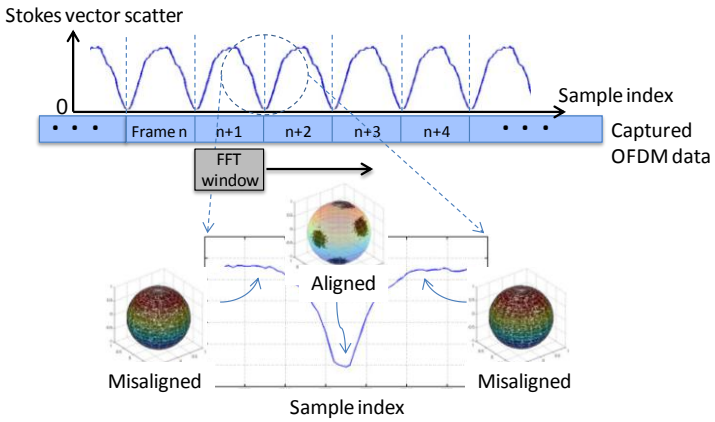

Figure 7.12: Frame synchronisation using Stokes vectors.

In order to verify the validity of the proposed scheme for low-bandwidth receivers with low sampling speed, experiments are first carried out using low-bandwidth receivers emulated by attaching four low pass filters to the full-speed receivers and setting the sampling rate below the required rate of the full-speed signal. Figure 7.13(a) shows the estimated DGD versus actual DGD at back-to-back measurements in 22.5-dB and 12-dB OSNR for PM OFDM signal with four 0.8-GHz low-pass filters using the point-to-point angle measurement method. Each data point in Figure 7.13(a) is an average of 30 captures of data blocks and their maximum DGD estimation deviations are plotted as error bars. It can be seen that for DGD value ranging from 10 ps to 30 ps, performance

of the proposed scheme using point-to-point estimation method is accurate and very close to ideal DGD values for both cases of OSNR = 12 dB and OSNR = 22.5 dB. The largest error is less than 2 ps for this range of DGD values. For low value of DGD, however, the estimation deviation increases to nearly 4.8 ps when the system DGD is close to zero because of the background noise interference on the DGD estimation. When the DGD is set to zero, ideally the average state of each subcarrier should converge to one point resulting in a zero angle and estimated DGD value of 0. However, it can be seen that for the case with no extra DGD, the average points of subcarriers cannot converge to one dot because of system noise. Thus, the angle generated is still considered DGD resulting in large DGD estimation error in small DGD region.

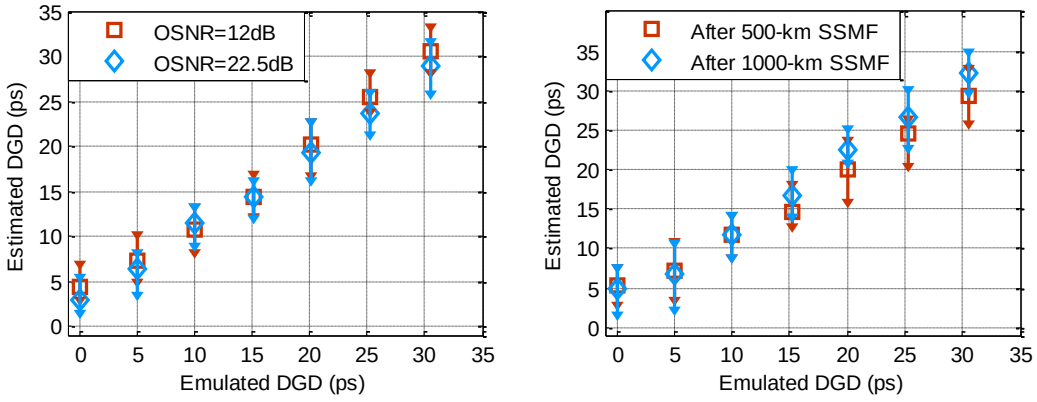

(a) *(b)*

Figure 7.13. Low bandwidth DGD estimation for (a) back-to-back and (b) after 500-km and 1000-km transmission.

The estimation scheme is tested for 500-km and 1000-km transmission to further evaluate its performance in the presence of CD and a large amount of ASE noise. As fibre will introduce extra DGD to the systems, this DGD will be added to the amount generated by the PMD emulator and resulting in a total system DGD larger than the values generated using the PMD emulator. Thus, it is necessary to measure this background DGD value in order to analyse the performance of the proposed DGD estimation methods. An Adaptif A2000 optical component analyser is used before the main experiments to measure the DGD parameter of a single fibre loop for background DGD compensation. The fibre DGD parameter measured by the analyser is 0.092

$ps/\sqrt{km}$ after averaging 20 measurements. With this parameter the background DGD is 2.9 ps for the 1000-km transmission using recirculation loop and 2.1 ps for the case of 500-km transmission. Figure 7.13(b) demonstrates the two estimated DGD curves after background DGD compensation for 1000-km and 500-km transmission. It can be seen that estimation for 500-km transmission is accurate and close to theoretical value if the emulated DGD is larger than 10 ps. The increased errors from 0~10-ps region are caused by the accumulated ASE noise as explained in the last paragraph. The estimated DGD values for 1000-km transmission are around 2.3-ps larger than the true values for the DGD between 5 ps and 30 ps. This is caused by the much more accumulated ASE noise and imperfections of the recirculation loop. The 5-ps offset at zero is due to the residual noise after averaging.

Figure 7.14(a) shows the estimated DGD values with respect to emulated DGD after 1000-km transmission with 800-MHz receiver using both point-to-point and interpolation method and it can be seen that both methods perform similarly with slightly less variation in estimation for interpolation method. For different receiver bandwidths, as previously illustrated in Section 7.3.2 assuming the right sampling rate of approximately 2 times the receiver bandwidth for CO-OFDM systems, different receiver bandwidth requirements effectively mean different numbers of subcarriers used for estimation purpose. Thus, different receiver bandwidths are emulated by capturing the signals in full-bandwidth receiver, then for each receiver bandwidth value, only a number of subcarriers that fit inside the required bandwidth are used for estimation purposes. This in turn results in different trace lengths and different estimation accuracies for different receiver bandwidths. Figure 7.14(b) shows the RMS estimation error as a function of the receiver bandwidth emulated by selecting the amount of OFDM subcarriers used for estimation. Transmission distance is 1000 km and the estimation offset after transmission is taken into account for RMS calculation. It can be seen that there is an increase in performance accuracy of around 0.8 ps between the lowest receiver bandwidth of 0.8 GHz and full bandwidth at 3.3 GHz. This behaviour is consistent with theory and simulation since for the same amount of DGD, the SOP traces are longer in higher bandwidth receivers. As a result, this enables more precise estimation. The accuracy of using the interpolation method is about 0.1 ps better compared to the point-to-point estimation method under full-bandwidth receivers. Thus,

the relative relationship between these two methods is consistent with simulation results. Both interpolation and point-to-point methods achieve very similar performance under a wide range of receiver bandwidths. This is expected as the traces for DGD are linear and the estimation accuracy is more limited by the system OSNR.

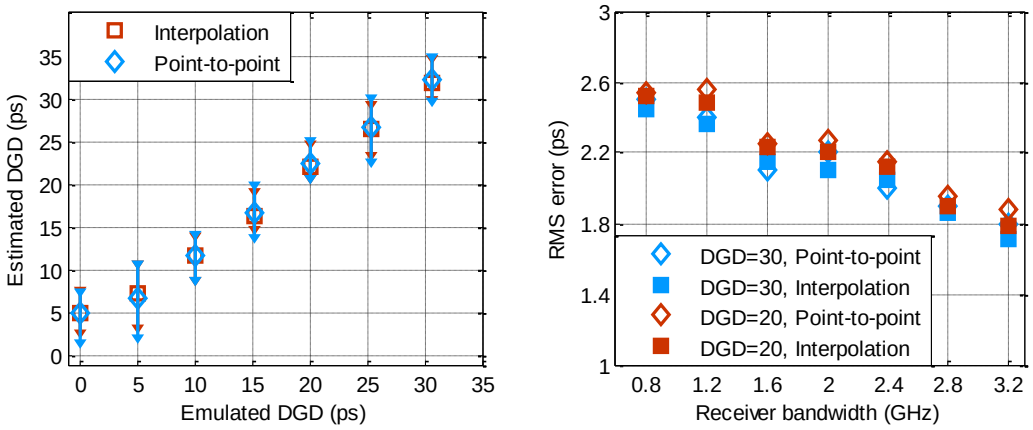

(a) *(b)*

Figure 7.14: (a) Estimated DGD between interpolation and point-to-point after 1000-km transmission and (b) estimation error as a function of receiver bandwidth.

7.6 CONCLUSIONS

This chapter presents DA and NDA DGD estimation methods for CO-OFDM systems with flexible receiver bandwidth requirements. As DA-CE techniques utilise TSs for CE, it is possible to utilise DA technique for DGD estimation under low-bandwidth coherent receivers for both CO-SC-FDE and CO- OFDM systems. While DA DGD estimation is modulation format independent and can work for both SC-FDE and OFDM systems, the use of low-bandwidth receivers effectively reduces the number of filter taps used for DGD estimation. On the other hand, the special structure of OFDM modulation format, namely the design of multiple subcarriers within the receiver bandwidth, makes it possible to extract only a few subcarriers for estimation using less than full speed coherent receivers. Compared to CO-SC systems, in which full speed signal is required for blind CE and DGD estimation by reading channel filter taps, the design of CO-OFDM makes it possible to fully recover subcarriers that are contained

within a defined bandwidth for channel DGD estimation purposes. This enables NDA DGD estimation using low-bandwidth coherent receivers with low sampling speed.

The NDA DGD estimation method presented in Section 7.3 is based on filtering a small number of OFDM subcarriers and evaluating their SOPs using Stokes vectors. By using Stokes vectors, DGD can be directly estimated from the subcarriers without demultiplexing OFDM signal. Due to the effect of DGD, different OFDM subcarriers will generate different SOP positions on the Stokes sphere and together, these form traces with length related to DGD. Two measurement methods are used for measuring DGD from the DGD-induced traces: point-to-point measurement which measures the angle between the first and last subcarriers on the Stokes sphere and interpolation which estimates the length of the traces generated by DGD using least square fit. For estimation without SOPMD effect, the two methods perform similarly, and estimations are accurate. For DGD estimation with added SOPMD, the interpolation method has better performance under full-bandwidth receivers as the shapes of the traces are not linear and interpolation is required for accurate estimation of the trace lengths. However, under low-bandwidth receivers, the effect of SOPMD is minimal, which enables the use of either point-to-point measurement or interpolation method. The Stokes vector DGD estimation method is shown to be slightly more accurate compared to DA DGD estimation by CE. Thus, for the proposed DGD estimation method, the trade-off in being OFDM specific is made up with higher estimation accuracy and the totally blind nature thus does not require any TSs.

The proposed Stokes vectors based DGD estimation methods are demonstrated in experiments for 40-Gb/s QPSK OFDM system with up to 1000-km transmission using 800-MHz receiver. For DGD higher than 15-ps average, estimation after 500-km transmission is accurate with zero mean, and after 1000-km transmission estimation error is around 2.6 ps with mean error of 2.3 ps. The method is found to be most accurate when there is a sufficient amount of DGD and this DGD range is found to be above 10 ps. At low to zero DGD value, the error is larger due to system noise still being interpreted as DGD values. For DGD values beyond 10 ps, estimation is accurate for both back-to-back and 1000-km transmission.

7.7 REFERENCES

[1] D.C. Kilper, R. Bach, D. J. Blumenthal, D. Einstein, T. Landolsi, L. Ostar, M. Preiss, and A.E. Willner, "Optical performance monitoring," *Journal of Lightwave Technology*, vol. 22, no. 1, pp. 294–304, Jan. 2004.

[2] Y. C. Chung, "Optical performance monitoring techniques; current status and future challenge," *European Conference on Optical Communications ECOC'2008,* pp. W.E.1.D.1, Brussels, Belgium, 2008.

[3] H. Rosenfeldt, R. Ulrich, E. Brinkmeyer, U. Feiste, C. Schubert, J. Berger, R. Ludwig, H. G. Weber, and A. Ehrhardt, "Feedforward approach for automatic PMD compensation at 80 Gbit/s over 45 km installed single mode fiber," *European Conference on Optical Communications ECOC'2001*, pp. 68-69, 2001.

[4] S. R. M. R. M. Nezam, J E. McGeehen, and A E. Willner, "Measuring Component DGD by using Polarised ASE Noise and Monitoring the Degree of Polarisation," *Optical Fibre Communication Conference OFC'2003,* pp. TuK2, Atlanta, Georgia, USA, 2003.

[5] F. Buchali, S. Lanne, J.P. Thiery, W. Baumert, and H. Bulow, "Fast eye monitoring for 10 Gbit/s and its application for optical PMD compensation," *Optical Fibre Communication Conference OFC'2001*, pp. TuP5, Anaheim, CA, USA, 2001.

[6] Y. Benlachtar, R. I. Killey, P. Bayvel, and M. Scopes, "Novel Eye Monitoring Technique for Detection of First Order PMD," *Conference on Lasers and Electro-Optics*, Baltimore, Maryland, May 2005.

[7] G. Ishikawa and H. Ooi, "Polarisation-mode dispersion sensitivity and monitoring in 40-Gbit/s OTDM and 10-Gbit/s NRZ transmission experiments," *Optical Fibre Communication Conference OFC'1998*, paper WC5, San Jose, 1998.

[8] R. Noe, D. Sandel, M. Yoshida-Dierolf, S. Hinz, C. Glinhener, C. Scheerer, A. Schopflin, G. Fischer, "Polarisation mode dispersion compensation at 20 Gb/s with fibre-based distributed equaliser," *Electronics Letters*, vol. 34, pp. 2421-2422, 1998.

[9] J. H. Lee and Y. C. Chung, "Optimisation of Monitoring Bandwidth for PMD Monitoring Technique Based on RF Spectrum Analysis," *Optical Fibre Communication Conference OFC'2005*, paper OME24, USA, Mar 2005.

[10] M. S. Faruk, Y. Mori, C. Zhang, K. Igarashi, and K. Kikuchi, "Multi-impairment monitoring from adaptive finite-impulse-response filters in a digital coherent receiver," *Optics Express*, vol. 18, no. 26, pp. 26929-26936, Dec. 2010.

[11] C. C. Do, A. V. Tran, C. Zhu, S. Chen, L. B. Du, T. Anderson, A. J. Lowery, and E. Skafidas, "PMD monitoring in 16-QAM coherent optical system using Golay sequences," *Opto-Electronics and Communications Conference OECC'2012*, paper 6B3-5, Busan, Korea, 2012.

[12] F. Pittala, F. N. Hauske, Y. Ye, N. Gonzalez, and I. Monroy, "Fast and robust CD and DGD estimation based on data-aided channel estimation," *International Conference on Transparent Optical Networks ICTON 2011*, pp. 1-4, Stockholm, Sweden, 2011.

[13] F. N. Hauske, J. Geyer, M. Kuschnerov, K. Piyawanno, T. Duthel, C. Fludger, D. van den Borne, E. Schmidt, B. Spinnler, H. de Waardt, and B. Lankl, "Optical performance monitoring from FIR filter coefficients in coherent receivers," *Optical Fibre Communication Conference OFC'2008*, paper OThW2, San Diego, CA, USA, 2008.

[14] G. W. Lu, C. Xie, Y. C. Ku, L. K. Chen, and C. K. Chan, "Enhanced PMD monitoring with frequency-resolved SOP rotation by self phase modulation," *IEEE Photonics Technology Letters*, vol. 16, no. 9, pp. 2180–2182, Sep. 2004.

[15] X. Yi, W. Shieh, Y. Ma, Y. Tang, and G. J. Pendock, "Experimental demonstration of optical performance monitoring in coherent optical OFDM systems," *Optical Fibre Communication Conference OFC'2008*, pp. OThW3, San Diego, USA, 2008.

[16] M. Mayrock and H. Haunstein, "Monitoring of linear and nonlinear signal distortion in coherent

optical OFDM transmission," *Journal of Lightwave Technology*, vol. 27, no. 16, pp. 3560–3566, Aug. 2009.

[17] C. Brosseau, *Fundamentals of polarised light: A statistical optics approach* , Chapter 4, John Wiley & Sons, 1998.

[18] B. Szafraniec, B. Nebendahl, and T. Marshall, "Polarisation demultiplexing in Stokes space," *Optics Express*, vol. 18, no. 17, pp. 17928-17939, Aug. 2010.

[19] Z. Yu, X. Yi, Q. Yang, M. Luo, J. Zhang, L. Chen, and K. Qiu, "Polarisation demultiplexing in Stokes space for coherentoptical PDM-OFDM," *Optics Express*, vol. 21, no. 2, pp. 3885–3890, Feb. 2013.

[20] P. Serena, A. Ghazisaeidi, and A. Bononi, "A new fast and blind cross-polarisation modulation digital compensator," *European Coference and Exhibition on Optical Communications ECOC'2012*, paper We.1.A.5, Amsterdam, Netherlands, 2012.

[21] R. Borkowshi, D. Zibar, A. Caballero, V. Arlunno, and I. T. Monroy, "Stokes Space-Based Optical Modulation Format Recognition for Digital Coherent Receivers," *IEEE Photonics Technology Letters*, vol. 25, no. 21, pp. 2129-2132, Nov. 2013.

[22] S. Chen, T. Anderson, D. Hewitt, A. Tran, C. Zhu, L. Du, A.J. Lowery, and E. Skafidas, "Optical performance monitoring for OFDM using low bandwidth coherent receivers," *Optics Express*, vol. 20, no. 27, pp. 28724-28733, Dec. 2012.

8 Conclusions

8.1 THESIS OVERVIEW

This thesis had investigated two important aspects of coherent optical (CO) networks: the use of full-bandwidth coherent receivers for channel parameter estimation and optical performance monitoring (OPM) and the use of low-bandwidth coherent receivers for distributed OPM of the entire optical network. Technologies for channel estimation (CE) based on training sequences (TSs) have been designed, analysed and demonstrated. TSs for data-aided (DA) digital signal processing (DSP) at the receiver end are used to ensure a simple and robust DSP structure that can be employed for all modulation and carrier formats including orthogonal frequency division multiplexing (OFDM) and single carrier (SC) systems. The use of Golay sequences ensures compatibility with commercial modulator due to the binary structure while the special spectrum property will ensure optimal estimation performance for CE and monitoring purposes. DA and blind channel performance monitoring methods for low-bandwidth receivers are also proposed and demonstrated. Compared to methods designed for full-bandwidth receivers, these methods provide a solution for distributed monitoring of CO networks using receivers with reduced cost and hardware requirements. Combined with full-bandwidth receiver methods, the low-bandwidth methods enable the design of next-generation CO networks with fast and robust CE, powerful performance monitoring at the receiver end, as well as distributed monitoring of the entire networks using hardware with reduced cost.

In Chapter 2, a literature survey of different CE techniques for CO systems was presented. Techniques for channel equalisation were presented and discussed. Typical design of CO systems involves a two stage process where the first stage typically

consists of chromatic dispersion (CD) compensation and the second stage consists of adaptive equalisation either by blind or DA method. Since knowledge of system CD is required for the first stage compensation, different technologies used for estimation of CD, were compared and discussed. DA technology for CD estimation is found to be very attractive due to the simple DSP structure design, and fast and robust estimation performance. For system CD, as this parameter is only needed to be estimated once, this significantly reduces the impact of using long TSs for dispersion estimation making TSs very ideal for system CD estimation. Furthermore, the use of TSs enables the monitoring/estimation technique to be modulation format independent and thus the same technique can also be used for CE for multiple modulation formats including polarisation multiplexed (PM) quadrature phase shift keying (QPSK), 16-quadrature amplitude modulation (16QAM) and also OFDM. From the CE performed by the TSs, equalisation can be performed in frequency domain in a fast and effective way. This chapter also presented a review of different implementations of DA-CE for receiver's DSP. The result is a trade-off between system performance and overhead ratio and thus making changing the overhead ratio a very desirable approach. This chapter also presented a review of various OPM techniques which are also of great importance in the design of next generation optical networks. These techniques are designed for estimation of system optical signal-to-noise ratio (OSNR), as well as system differential group delay (DGD) as these two parameters can change during system operation and need to be monitored. For CO-SC systems with frequency domain equalisation (FDE), schemes based on TSs are of great interest as the same binary type TSs used for CE can also be used for channel monitoring purposes. For CO-OFDM systems, as the modulated data are designed in frequency domain, blind performance monitoring is of great interest as CO-OFDM exhibits special characteristics in frequency domain.

In Chapter 3, a novel system CD estimation method based on TSs was presented. In order to estimate system CD, long TSs are required to cover the impulse response required for accurate CE. However the use of traditional CAZAC-Chu sequences makes generation of long sequences difficult due to the complex constellation. Two types of long TSs, both having binary constellation for easy commercial integration, were proposed namely Golay sequences and quantised CAZAC-Chu sequences. The design of these two types of TSs for PM-QPSK and PM-16QAM modulation formats, as well

as dispersion estimation method based on sending TSs were presented. Theory on the relationship between total system dispersion and required TS length was also presented and discussed. The method was demonstrated in both computer simulation and experiments with accurate and robust estimation performance for up to 2000-km standard single-mode fibre (SSMF) transmission. Estimation performances of both types of sequences are similar to the traditional ideal CAZAC sequences while the binary constellation formats ensure easy integration of the proposed TSs for CD estimation. Single-stage and two-stage dispersion estimation methods based on TSs were also presented, analysed and demonstrated. The results indicate high accuracy with less than 5% in estimation error for single-stage estimation and less than 1% in estimation error for two-stage dispersion estimation. As the required accuracy depends on the amount of dispersion in the system and this information is readily available after the first stage of estimation, depending on the total dispersion, single-stage or two-stage CD estimation can be employed. The proposed system CD estimation method can be employed in CO networks for estimation of system link dispersion at system start up and this value can be saved for subsequent CD compensation using overlap-cut method.

A novel OSNR estimation technique based on TSs was presented in Chapter 4. After CD estimation and compensation using techniques provided in Chapter 3, the proposed technique utilises TSs for CE of residual impairments, approximate a noise-free estimation of the channel transfer functions through receiver signal processing, then self-equalises the TSs for OSNR monitoring purpose. Two methods using available digital noise filters were proposed namely utilising the moving average filter (MAF) and using the time-domain nulling filter (TDNF). The performance as well as optimisation of these filters for DA OSNR estimation were presented and discussed. The method's tolerance to CD and timing offset (TO), assuming zero compensation of these two parameters within the method's DSP, was also discussed. The DA OSNR estimation method was demonstrated through simulation and experiments for both PM-QPSK and PM-16QAM CO-SC systems. Results indicate robust performance against residual CD, TO, polarisation-mode dispersion (PMD) and polarisation independent loss (PDL). Estimation performances were demonstrated to be high and accurate with estimation error of approximately 0.7 dB for using both filter types and both filters gave similar estimation performances.

Chapter 5 presented the use of TSs for CE and equalisation in a two stage approach. CD is compensated in the first stage and TSs are used for CE in the second stage. The relationship between estimation performance and the length of TSs is confirmed. The use of long TSs is desirable in case of maximum estimation performance while the use of short TSs is desirable in case minimum overhead is required. A new flexible timing synchronisation method based on Golay sequences was presented. The technique is based on finding the number of small Golay sequences in the received signal and can be used to detect the length of total transmitted sequences. Experimental demonstration of the technique shows robust performance against different level of OSNR.

In Chapter 6, a DA OSNR estimation technique for CO-SC systems using low-bandwidth receiver was presented. Compared to the technique proposed in Chapter 4, this technique only requires receivers with low bandwidth and low sampling speed. The required receiver bandwidth is only a fraction of the full speed signal bandwidth and thus making the technique desirable for distributed monitoring of CO-SC networks. The same TSs used for DA-CE in full speed systems are re-used for OSNR estimation after low bandwidth capturing and sampled at low speed. The technique was demonstrated for CO-SC systems with DA-CE with accurate estimation within 1 dB for both PM-QPSK and PM-16QAM systems.

Chapter 7 presented the use of low-bandwidth receivers for DGD estimation for CO systems. While estimation of DGD using DA-CE is well known in literatures, due to the reduced bandwidth requirements of the receiver, DGD estimation using DA-CE method shows inaccurate results and requires long TSs. A new non-data-aided (NDA) DGD estimation technique for CO-OFDM systems using low-bandwidth receivers was presented. The technique is specific to CO-OFDM systems and thus is not applicable to CO-SC-FDE. However, the full utilisation of OFDM specific features enables accurate estimation of DGD even while low-bandwidth receivers are used.

8.2 DIRECTIONS FOR FUTURE WORK

Several techniques for CE in CO systems and OPM were presented in this thesis. There are several other topics related to CO systems that were not pursued due to the breadth of the thesis. These topics however, warrant further investigations.

8.2.1 Space Division Multiplexing

The format of CO systems investigated in the thesis is polarisation multiplexed (PM). As demand for bandwidth continues to rise and PM systems reaching the efficiency limit, systems that are capable of higher transmission efficiency such as space division multiplexing (SDM) CO systems are required. SDM can be implemented on top of PM using multi-mode [1]-[2] or multi-core [3]-[4] fibre and these technologies will become more attractive and CE techniques for these systems will warrant further investigations. The use of DA-CE for SDM optical systems is very attractive as traditional NDA-CE could suffer more degradation due to SDM systems having more sources. Further investigation on OPM for SDM systems will also be necessary as new techniques need to be developed for these types of optical transmissions. As SDM will potentially have much more complex transfer characteristics compared to PM standard systems, further techniques for DA-CE will be required. The current DA-CE technique in this thesis utilises a 2x2 multiple-input multiple-output (MIMO) transmission model. In order to employ DA-CE with SDM, higher-order channel transmission models such as 4x4 or 6x6 MIMO need to be used and the TSs will need to be redesigned for these models. Other CE technique for system CD, OSNR, DGD will also need to be modified for SDM. The experiments of this kind would involve designing efficient training structures for estimation of channel transfer matrix with size larger than 2x2, and transmission experiments with either multi-mode or multi-core fibre SDM systems.

8.2.2 Non-linear Noise Compensation

Another direction for future research is the identification of non-linear noise in CO systems. Compensation of non-linear noise will allow CO systems to operate at much higher power without running into degradation issues caused by non-linear noise. While digital back propagation [5] can compensate for non-linear noise, the technique is computationally intensive and alternative techniques that are based on TSs for non-

linear noise compensation will need to be investigated. While compensation of nonlinear impairments can be performed by attaching a pilot tone to the signal [6]-[7], an approach based on TSs will be more desirable as it utilises the same TSs employed for DA-CE. Beside the properties demonstrated in this thesis, the proposed TSs can be further developed to contain extra special pattern used to identify the non-linear noise. The pattern identified by the TSs can be used to initialise a tracking algorithm that compensates for subsequent nonlinear noise in the actual data-frame. Two algorithms will need to be developed for this purpose. The first algorithm will examine the specially designed TSs for non-linear noise and the second algorithm will be capable of tracking the data pattern and compensating for nonlinearity in the actual data provided by the first one. Simulation and experimental study can be conducted for this purpose.

8.2.3 OPM using Direct-Detection Receivers

The techniques demonstrated in Chapters 6 and 7 are based on a low-bandwidth coherent receiver and further investigations on reduced complexity devices for OPM purposes will be a promising research direction. Further investigations can be based on using low-bandwidth direct detection receivers for OPM. DA-CE technique is a very promising part of OPM using further reduced complexity receivers as there are many known information in the sequences that can be used for channel impairment estimation purposes. Sending known sequences in a full bandwidth system could potentially simplify the estimation of channel impairments using simple low cost, direct detection receivers. While only a part of the sequences can be recovered using direct detection, comparing this information with the known sequences can reveal many impairments accumulated during transmission. The experimental study for this research would be similar to the one presented in Chapter 6, but with a direct detection receiver and a new estimation algorithm will need to be developed.

Estimation of other impairments such as polarisation-dependent loss (PDL) and second-order polarisation-mode dispersion (SOPMD) had also been demonstrated in literatures for standard coherent detection [8], [9]. However, the move to further reduced-complexity receivers such as direct detection will potentially make estimation of these impairments a much more required feature. New techniques for estimation of OSNR, DGD, PDL, and SOPMD will need to be developed for direct detection scheme and a

unified algorithm to estimate all these impairments from the captured signal will be much more preferable.

A different research direction of OPM using direct detection receivers would be in direct detection OFDM (DD-OFDM) [10]. DD-OFDM has been proposed as a very strong candidate for high speed transmission with short reach distance and the use of OPM techniques based on direct detection receivers will benefit DD-OFDM as the techniques can be executed directly during the DSP procedure at the receiver together with data decoding. While TSs can be used for both DD-SC-FDE and DD-OFDM systems, the special structure of OFDM, inherited by DD-OFDM, will likely enable different blind OPM techniques similar to the DGD estimation technique demonstrated in Chapter 7.

8.3 REFERENCES

[1] A. Li, A. A. Amin, X. Chen, and W. Shieh, "Transmission of 107-Gb/s mode and polarisation multiplexed CO-OFDM signal over a two-mode fibre," *Optics Express*, vol. 19, no.9, pp. 8808-8814, Apr. 2011.

[2] A. Li, A. A. Amin, X. Chen, S. Chen, G. Gao, and W. Shieh, "Reception of Dual-Spatial-Mode CO-OFDM Signal Over a Two-Mode Fibre," *Journal of Lightwave Technology*, vol. 30, no. 4, pp. 634-640, Feb. 2012.

[3] M. Koshiba, K. Saitoh, K. Takenaga, and S. Matsuo, "Multi-core fibre design and analysis: coupled-mode theory and coupled-power theory," *Optics Express*, vol. 19, no. 26, pp. B102-B111, Dec. 2011.

[4] T. Hayashi, T. Sasaki, E. Sasaoka, K. Saitoh, and M. Koshiba, "Physical interpretation of intercore crosstalk in multicore fibre: effects of macrobend, structure fluctuation, and microbend," *Optics Express*, vol. 21, no. 5, pp. 5401-5412, Mar. 2013.

[5] E. Ip and J. M. Kahn, "Compensation of Dispersion and Nonlinear Impairments Using Digital Backpropagation," *Journal of Lightwave Technology*, vol. 26, no. 20, pp. 3416-3425, Oct. 2008.

[6] T. Kobayashi, A. Sano, A. Matsuura, Y. Miyamoto, and K. Ishihara, "Nonlinear Tolerant Spectrally-Efficient Transmission Using PDM 64-QAM Single Carrier FDM With Digital Pilot-Tone," *Journal of Lightwave Technology*, vol. 30, no. 24, pp. 3805-3815, Dec. 2012.

[7] S. L. Jansen, I. Morita, T.C.W. Schenk, N. Takeda, and H. Tanaka, "Coherent optical 25.8-Gb/s OFDM transmission over 4160-km SSMF," *Journal of Lightwave Technology*, vol. 26, no. 1, pp. 6–15, Jan. 2008.

[8] M. S. Faruk, Y. Mori, C. Zhang, K. Igarashi, and K. Kikuchi, "Multi-impairment monitoring from adaptive finite-impulse-response filters in a digital coherent receiver," *Optics Express*, vol 18, no. 26, Dec. 2010.

[9] F. N. Hauske, M. Kuschnerov, K. Piyawanno, B. Spinnler, E. D. Schmidt, and B. Lankl, "DGD estimation from FIR filter taps in presence of higher order PMD," *European Conference on*

Optical Communication ECOC'2008, pp. 1-2, Sep. 2008.

[10] L. Mehedy, M. Bakaul, A. Nirmalathas, and E. Skafidas, "OFDM versus single carrier towards spectrally efficient 100 Gb/s transmission with direct detection," *IEEE/OSA Journal of Optical Communications and Networking*, vol. 4, no. 10, pp. 779-789, Oct. 2012.

Appendix A: Acronyms

ACSPW	Auto-correlation of the Signal Power Waveform
ASE	Amplified Spontaneous Emission
CD	Chromatic Dispersion
CE	Channel Estimation
CO	Coherent Optical
CP	Cyclic Prefix
DA	Data-Aided
DCF	Dispersion Compensation Fibre
DSP	Digital Signal Processing
FDE	Frequency Domain Equalisation
NDA	Non-Data-Aided
OFDM	Orthogonal Frequency Division Multiplexing
OFDE	Overlap Frequency Domain Equalisation
PBC	Polarisation Beam Combiner
PMD	Polarisation-mode dispersion
SC	Single Carrier
TDE	Time Domain Equalisation
IDFT	Inverse discrete Fourier transform
DFT	Discrete Fourier Transform
FFT	Fast Fourier Transform
IFFT	Inverse Fast Fourier Transform
PAPR	Peak-to-Average Power Ratio
LMS	Least Mean Square
DFE	Decision Feedback Equaliser

STBC	Space-time block code
OPM	Optical Performance Monitoring
SNR	Signal-to-Noise Ratio
OSNR	Optical Signal-to-Noise Ratio
PM	Polarisation-multiplexed
BPSK	Binary Phase Shift Keying
QPSK	Quadrature Phase Shift Keying
8PSK	8-Phase Shift Keying
16QAM	16-Quadrature Amplitude Modulation
64QAM	64-Quadrature Amplitude Modulation
SSMF	Standard Single-mode Fibre
IBI	Inter-block Interference
FO	Frequency Offset
LO	Local Oscillator
DGD	Differential Group Delay
EDFA	Erbium-doped Fibre Amplifier
FIR	Finite Impulse Response
RGI	Reduced Guard Interval
ISI	Inter-symbol Interference
MMSE	Minimum Mean Square Error
CAZAC	Constant Amplitude Zero Autocorrelation
MP	Minimum-phase
PDL	Polarisation-dependent Loss
OBPF	Optical Band-pass Filter
TS	Training Sequences
MAF	Moving Average Filter
TDNF	Time Domain Nulling Filter
DAC	Digital-to-Analogue Converter
ACF	Autocorrelation Function
DOP	Degree of Polarisation
PBS	Polarisation Beam Splitter
HLNF	Highly Non-linear fibre
XPM	Cross-phase Modulation

OSA	Optical Spectrum Analyser
EVM	Error Vector Magnitude
NRZ	Non-Return-to-Zero
NOLM	Non-linear Optical Loop Mirror
AWG	Arbitrary Waveform Generator
RMS	Root Mean Squared
MIMO	Multiple-input Multiple-output
TO	Timing Offset
DAML	Data-Aided Maximum Likelihood
OOK	ON-Off Keying
PSK	Phase Shift Keying
3D	Three-Dimensional